UNIVERSITY OF SOUTHAMPTON

FACULTY OF ENVIROMENTAL AND LIFE SCIENCES

Geography and Environmental Science

Volume 1 of 1

Earth Observation for Quantifying Urban Growth and its Application to Sustainable City Development

by

Andrew Charles MacLachlan

ORCID ID: 0000-0003-0356-1623

Thesis for the degree of Doctor of Philosophy

September 2018

UNIVERSITY OF SOUTHAMPTON

ABSTRACT

FACULTY OF ENVIRONMENTAL AND LIFE SCIENCES

Geography and Environmental Science

Thesis for the degree of Doctor of Philosophy

Earth Observation for Quantifying Urban Growth and its Application to Sustainable City Development

Andrew Charles MacLachlan

Urban areas are predicted to triple by 2030 in accommodating 68% of the global population, with anthropogenic landscape modifications to impervious surfaces established as a critical driving force in local and global climate change. Accurate temporal monitoring of urban expansion and subsequent environmental issues are essential for ensuring the future sustainability of our cities. In particular the urban heat island effect is considered one of the major problems posed to humans in the 21st century associated with detrimental health impacts and increased energy demand, emissions, water output and economic expenditure. Yet, alongside a uniform modelling omission from global climate models, mitigation of the urban heat island effect lacks a global standardised framework, representative data for modelling impacts, and robust academic outputs for policy incorporation. These limitations are precluding effective data-informed governance.

This thesis presents a holistic policy-applicable approach for accurately monitoring and sustainably planning (re)development in relation to metropolitan and local level urban temperature dynamics. This is achieved through generating land cover maps from Earth observation data using a temporally consistent methodology with refinements to urban estimates based upon comparison to high resolution imagery. Variations between changes in land cover and land surface temperature are determined at the metropolitan level to aid sustainable urban growth plans. Temperature is then minimised at the local level through a modelling approach to optimally place vegetation with a proposed new development. The application area for this thesis is the Perth Metropolitan Region in Western Australia which has experienced sustained outward, non-strategic and low density expansion in response to booming natural resource sector. The presented methodology makes progress to aligning urban heat island mitigation efforts with global targets including the United Nation's Sustainable Development Goals and New Urban

Agenda, providing a reproducible method, transferable to other global metropolitan regions to improve sustainable city planning.

Table of Contents

Table of Tables

Table of Tables

Table of Figures

Table of Figures

Academic Thesis: Declaration of Authorship

I, Andrew Charles MacLachlan

declare that this thesis and the work presented in it are my own and has been generated by me as the result of my own original research.

Earth Observation for Quantifying Urban Growth and its Application to Sustainable City Development

I confirm that:

1. This work was done wholly or mainly while in candidature for a research degree at this University;
2. Where any part of this thesis has previously been submitted for a degree or any other qualification at this University or any other institution, this has been clearly stated;
3. Where I have consulted the published work of others, this is always clearly attributed;
4. Where I have quoted from the work of others, the source is always given. With the exception of such quotations, this thesis is entirely my own work;
5. I have acknowledged all main sources of help;
6. Where the thesis is based on work done by myself jointly with others, I have made clear exactly what was done by others and what I have contributed myself;
7. Parts of this work have been published as:

MacLachlan, A., Biggs, E., Roberts, G. and Boruff, B., 2017. Urban growth dynamics in Perth, Western Australia: using applied remote sensing for sustainable future planning. *Land*, *6*(1), p.9. [open access].

MacLachlan, A., Biggs, E., Roberts, G. and Boruff, B., 2017. Classified Earth observation data between 1990 and 2015 for the Perth Metropolitan Region, Western Australia using the Import Vector Machine algorithm, PANGAEA, https://doi.org/10.1594/PANGAEA.871017 [data]. [open access].

MacLachlan, A., Roberts, G., Biggs, E. and Boruff, B., 2017. Subpixel land-cover classification for improved urban area estimates using Landsat. *International Journal of Remote Sensing*, *38*(20), pp.5763-5792. [open access].

MacLachlan, A., Biggs, E., Roberts, G. and Boruff, B., 2017. Urbanisation-Induced Land Cover Temperature Dynamics for Sustainable Future Urban Heat Island Mitigation. *Urban Science*, *1*(4), p.38. [open access].

MacLachlan, A., Biggs, E., Roberts, G. and Boruff, B., 2018. Earth Observation for Sustainable City Planning. [submitted to Global Environmental Change].

Smith, A., MacLachlan, A., Haworth, B., Biggs, E. and Maginn, P., 2018. Demonstrating the global potential of a high-resolution spatiotemporal population modelling framework. *International Journal of Geographical Information Science* [under review].

In all jointly published work presented in this thesis Andrew MacLachlan was responsible for sourcing data, liaising with planning authorities, devising methodological approaches, all analysis and producing and revising manuscript drafts. Dr Biggs and Dr Roberts contributed ideas, comments and data in a supervisory capacity based on their own expertise throughout the research. Dr Boruff supported the research in similar manner through an advisory role at the University of Western Australia. Author attribution statements for each individual paper are presented below, providing specific details into Andrew MacLachlan's responsibilities and the supervisory and advisory support supplied by Dr Biggs, Dr Roberts and Dr Boruff. All authors declare no completing interests.

Author attribution statements

Chapter 4, paper 1a

Chapter 4 corresponds to the publication:

MacLachlan, A., Biggs, E., Roberts, G. and Boruff, B., 2017. Urban growth dynamics in Perth, Western Australia: using applied remote sensing for sustainable future planning. *Land*, *6*(1), p.1-14.

Andrew MacLachlan liaised with and obtained data from the Western Australian Department of Planning, analysed all data and produced manuscript drafts. The co-authors assisted in guiding the overall research objectives, provided methodological advice and revised manuscript text in a supervisor capacity. In particular Dr Biggs contributed valuable figure and policy recommendations whilst Dr Roberts ensured valid data normalisation suggesting analysis found in the supplementary material, section 4.7.

Chapter 4, paper 1b

The data produced using the methodology described in Paper 1a (main body of chapter 4) corresponds to the publication:

MacLachlan, A., Biggs, E., Roberts, G. and Boruff, B., 2017. Classified Earth observation data between 1990 and 2015 for the Perth Metropolitan Region, Western Australia using the Import Vector Machine algorithm, PANGAEA, https://doi.org/10.1594/PANGAEA.871017.

Andrew MacLachlan produced and formatted the data for publication, with methodological advice from co-authors in a supervisory capacity.

Chapter 5, paper 2

Chapter 5 corresponds to the publication:

MacLachlan, A., Roberts, G., Biggs, E. and Boruff, B., 2017. Subpixel land-cover classification for improved urban area estimates using Landsat. *International Journal of Remote Sensing*, *38*(20), pp.5763-5792.

Andrew MacLachlan was responsible for designing the methodology, processing all data and producing manuscript drafts. Co-authors agreed upon and guided the research questions, provided access to high resolution aerial data, gave methodological and practical advice and reviewed manuscript drafts in a supervisory capacity. More specifically, Dr Boruff provided high resolution data, with Dr Roberts advising Andrew MacLachlan on the best Object Based Image classification procedures.

Chapter 6, paper 3

Chapter 6 corresponds to the publication:

MacLachlan, A., Biggs, E., Roberts, G. and Boruff, B., 2017. Urbanisation-Induced Land Cover Temperature Dynamics for Sustainable Future Urban Heat Island Mitigation. *Urban Science*, *1*(4), pp.1-21.

Andrew MacLachlan designed the methodological procedure, processed and analysed all data and produced manuscript drafts. The co-authors assisted in guiding research objectives and provided valuable advice and manuscript comments in a supervisory capacity. Dr Biggs critically commented on policy applications and data output, especially Figure 6-8 that was selected for the Journal Issue front cover. Dr Roberts provided practical methodological advice and assisted in selecting appropriate data for figures and tables presented throughout the paper.

Chapter 7, paper 4

Chapter 7 corresponds to the pending publication:

Academic Thesis: Declaration of Authorship

MacLachlan, A., Biggs, E., Roberts, G. and Boruff, B., 2018. Earth Observation for Sustainable City Planning [submitted to Global Environmental Change].

Andrew MacLachlan identified and processed all data required used within the modelling methodology, produced figures, liaised with the City of Fremantle and drafted all versions of the manuscript. Co-authors guided the overall objectives ensuring linkage to previous work whilst also providing critical feedback in a supervisory capacity. Dr Biggs ensured policy relevance and critically commented on produced figures. Dr Roberts contributed ideas throughout and reviewed the final draft manuscript alongside Dr Boruff.

Signed: [signature removed from digital version]

Date: 14/09/2018

Andrew MacLachlan

As a supervisor for this postgraduate student I certify that the authorship attribution statements above are true and accurate.

Signed: [signature removed from digital version]

Date: 14/09/2018

Dr Biggs

As a supervisor for this postgraduate student I certify that the authorship attribution statements above are true and accurate.

Signed: [signature removed from digital version]

Date: 14/09/2018

Dr Roberts

Acknowledgements

Personal

I wish to sincerely thank both my supervisors Dr Biggs and Dr Roberts alongside my advisor Dr Boruff for their advice, contributions and enthusiasm throughout this thesis. Specifically, Dr Biggs continuously challenged how developed methodologies were applicable in applied planning terms, complemented by Dr Roberts who would challenge more technical aspects of the research and Dr Boruff who would often question the applicability to the bigger, global picture. Combined they have been a simply fantastic supervisory team that have undoubtedly developed my overall research skills. Beyond the methodological and technical aspects of the project the team have consistently encouraged me, provided numerous further opportunities and promoted both my work and I. I am extremely grateful the time all three academics have invested in me and for how much I have learnt from them over the last four years.

I also thank those not officially involved with this thesis but have nonetheless contributed in ways they were probably unaware of. This is especially true of all those I have cycled with, taking my mind away from research, subsequently feeling refreshed and often having methodological breakthroughs. Similarly (soon to be Drs) Luke Brown and Micheline Campbell for their friendship, advice and support through the rollercoaster of emotions during the project. I thank Amelia Vincent for her unrelenting encouragement and empathy over the last four years. Finally I wish to thank my parents, Valerie and Angus MacLachlan, for their continued encouragement and investment throughout my entire education.

Funding and data access

This work was supported by the Economic and Social Research Council (ESRC) [grant number ES/J500161/1] and the University of Southampton School of Geography and Environmental Science, with institutional visit funding support from the University of Southampton via the World University Network (WUN) researcher mobility programme and Study Abroad department. Appreciation is shown to the University of Western Australia (UWA) and the UWA School of Agriculture and Environment for supporting grant and visa applications alongside hosting institutional visits. Access to Urban Monitor high resolution data over the Perth Metropolitan Region was provided in part through the National Environmental Science Program, Clean Air and Urban Landscapes Hub. I would like to respectively thank the United States Geological Survey (USGS) and Goddard Space Flight Center for continuing to supply free Landsat and Moderate

Acknowledgements

Resolution Imaging Spectroradiometer (MODIS) data used throughout this project. I also express gratitude to Western Australia Department of Planning (WAPC), in particular Matt Devlin and Lisl van Aarde for urban estimate data and supplementary planning information used within chapter 4. In a similar theme the City of Fremantle, especially Mayor Brad Pettitt, Paul Garbett, Marcel Maron and Gavin Giles who provided valuable localised operational planning insights used to inform analysis in chapter 7. I also extend further thanks to the ESRC, School of Geography and Environmental Science and University of Southampton for the numerous free training sessions and qualifications on offer that have enhanced my research outputs, professional development and overall doctorate experience. Finally I wish to thank my mother and late father for continuing to support my education and providing funds for research equipment and field visits.

Definitions and Abbreviations

All definitions and abbreviations are re-defined at the start of each chapter due to the extensive use within throughout the Earth observation discipline and subsequently within this thesis.

AATSR: Advanced Along-Track Scanning Radiometer

ABS: Australian Bureau of Statistics

ANN: Artificial Neural Networks

AOT: Aerosol Optical Thickness

API: Application Interface

ARCSI: Atmospheric Radiometric Calibration of Satellite Imagery

ASGS: Australian Statistical Geography Standard

ASTER: Advanced Spaceborne Thermal Emission Reflection Radiometer

AUD: Australian Dollar

AWS: Amazon Web Service

BE: Bare Earth

BLHI: Boundary Layer Heat Island

BOM: Bureau of Meteorology

BP: Back-Propagation

BRDF: Bidirectional Reflection Distribution Function

C40 CCLG: C40 Cities Climate Leadership Group

CBD: Central Business District

CCI: Climate Change Initiative

CLHI: Canopy Layer Heat Island

CMSA: Consolidated Metropolitan Statistical Area

CPI: City Prosperity Index

CRC-LCL: Cooperative Research Centre-Low Carbon Living

CRF: City Resilience Framework

CSIRO: Commonwealth Scientific and Industrial Research Organisation

CV: Coefficient of Variation

CVAR: Canonical Variate Analysis with Rational polynomials

DEM: Digital Elevation Model

DSM: Digital Surface Model

DT: Decision Trees

ECMEF: European Centre for Medium-range Weather Forecasts

EnMAP: Environmental Mapping and Analysis Program

ENVI: ENvironment for Visualizing Images

EO: Earth Observation

ERP: Estimated Residential Population

ESA: European Space Agency

ETM+: Enhanced Thematic Mapper Plus

F: Forest

G: Grassland

GCC: Global Climate Change

GCCSA: Greater Capital City Statistical Areas

GCPs: Ground Control Points

GDP: Gross Domestic Product

GEM: Ground Elevation Model

GHG: Green House Gas

GLS: Global Land Survey

GSP: Gross State Product

IBI: Index-based Built-up Index

IDL: Interactive Data Language

IVM: Import Vector Machine

L1T: Level 1 Terrain-corrected data

L8SR: Landsat 8 Surface Reflectance algorithm

LAI: Leaf Area Index

LaSRC: Landsat 8 Surface Reflectance Code

LEDPAS: Landsat Ecosystem Disturbance Adaptive Processing System

LGA: Local Government Area

LiDAR: Light Detection and Ranging

LST: Land Surface Temperature

LULC: Land Use Land Cover

MESMA: Multiple Endmember Spectral Mixture Analysis

MIR: Mid-Infrared

ML: Maximum Likelihood

MLAs: Machine Learning Algorithms

MLP: Multi-Layer Perceptron

MNDWI: Modified Normalized Difference Water Index

MODIS: Moderate Resolution Imaging Spectroradiometer

MRDA: Metropolitan Redevelopment Authority

MRS: Metropolitan Region Scheme

MSA: Metropolitan Statistical Area

NDBI: Normalized Difference Built-up Index

NDSV: Normalised Difference Spectral Vector

NDVI: Normalised Difference Vegetation Index

NDWI: Normalized Difference Water Index

NIR: Near-Infrared

OA: Output Areas

OBIA: Object Based Image Analysis

OLI: Operational Land Imager

ONS: Office for National Statistics

OOB: Out Of Bag

PEP: Pessimistic Error Pruning

PGE16: Product Generation Executives

PMR: Perth Metropolitan Region

PMSA: Primary Metropolitan Statistical Area

QGIS: Quantum Geographical Information Systems

QLD: Queensland

R: Radiance

REM: Relative Elevation Model

RF: Random Forests

RMSE: Root Mean Square Error

ROI: Regions of Interest

SA1-4: Statistical Areas Level 1-4, increasing numbers between 1 and 4 represent larger geographic areas

SAVI: Soil Adjusted Vegetation Index

SDGs: Sustainable Development Goals

SEVIRI: Spinning Enhanced Visible and Infrared Imager

SHI: Surface Heat Island

SMA: Spectral Mixture Analysis

SNPP: Suomi National Polar-orbiting Partnership

SOLWEIG: Solar and LongWave Environmental Irradiance Geometry

SOS: Section of State

SOSR: Section of State Range

SRS: Subiaco Redevelopment Scheme

SUA: Significant Urban Area

SUHI: Surface Urban Heat Island

SUHII: Surface Urban Heat Island Intensity

SVF: Sky View Factor

SVM: Support Vector Machine

T: Temperature

TB: TeraByte

TIR: Thermal-Infrared

TM: Thematic Mapper

TOA: Top Of Atmosphere

U: Urban

UA: Urbanised Area

UAV: Unmanned Aerial Vehicle

UBL: Urban Boundary Layer

UC: Urban Centre, in relation to the Australian Bureau of statistics urban definitions

UC: Urban Cluster, in relation to the USA census Bureau urban definitions

UCL: Urban Canopy Layer, in reference to heat island categories

UCL: Urban Centres and Localities, in reference to census bureau urban definition

UH: High Urban albedo

UHI: Urban Heat Island

UHII: Urban Heat Island Intensity

UK: United Kingdom

UL: Low Urban albedo, in relation to land cover

UL: Urban Locality, in relation to the Australian Bureau of statistics urban definitions

UMEP: Urban Multi-scale Environmental Predictor

UN: United Nations

USA: United States of America

UWA: University of Western Australia

VIIRS: Visible Infrared Imaging Radiometer Suite

V-I-S: Vegetation, Impervious and Soil

VIS: Visible

WA: Western Australia

WAPC: Western Australian Planning Commission

WATCH: Water and Global Change

WEASEL+MUSE: Word ExtrAction for time SEries cLassification + MUltivariate Symbols and dErivatives

WFD: WATCH Forcing Data

WFDEI: WATCH Forcing Data methodology applied to ERA-interim data

WUN: World University Network

Chapter 1 Introduction

1.1 An expanding urban area

Urban areas only cover 0.5% of Earth's terrestrial surface and yet are one of the fastest growing land use types on a per area basis (Gashu and Egziabher, 2018; Powell et al., 2007; Sexton et al., 2013). Population growth is fuelling urbanisation with 55% of the planet's 7.6 billion people residing in urban areas in 2018, and which is expected to accommodate up to 68% of the global population by 2050 as a result of an estimated additional 2.5 billion people (Powell and Roberts, 2010; Sexton et al., 2013; Sharifi and Lehmann, 2014; United Nations, 2018). Land use and land cover change represent the main driving force in global environmental change, especially anthropogenic modifications from vegetated to impervious surface material, through which water does not infiltrate (Sundarakumar et al., 2012; Tan et al., 2009; Verburg et al., 2015). In order to accommodate the expected increase in population, urban area is predicted to triple by 2030 based on current trends, increasing total global coverage to 0.9% of Earth's terrestrial surface (2000 baseline of 652,825 km^2) (Seto et al., 2012).

Urban growth, defined as the sum of the increase in developed land between two or more time periods, was traditionally thought of as an intrinsic process and metric of economic success (Sundarakumar et al., 2012). However, the benefits have now been carefully evaluated in conjunction with any adverse social, economic and environmental impacts. For example, continued outward expansion exponentially decreases resource efficiency due to vast infrastructural requirements, additional commuting time and household transportation expenditure (Batty et al., 2003; Downs, 2005). The alteration of natural land to impervious surfaces frequently induces the Urban Heat Island (UHI) effect whereby man-made urban areas obtain comparatively higher atmospheric and surface temperature than rural areas; the UHI effect is considered one of the major environmental problems posed to humans in the 21st century (Rizwan et al., 2008). In conjunction with expanding global urban areas and population growth the extent and magnitude of the UHI will continue to grow (Zhang et al., 2013). Furthermore, urbanisation can lead to income-based neighbourhood segregation which exacerbates social and ethnic divisions (Batty et al., 2003), and coupled with the UHI effect can result in sociodemographic-driven healthcare implications during heatwaves (Gronlund et al., 2015; Yu et al., 2010). Whilst urban expansion can generate benefits, accurate and timely information on the characteristics and associated impacts of urban expansion are critical for assessing current and future needs regarding urban growth and developing policy priorities for inclusive and sustainable [socioeconomic and environmental] development, as reflected in recent

global initiatives e.g. the United Nations (UN) New Urban Agenda (UN-Habitat III, 2017), City Resilience Framework (CRF) (ARUP and The Rockefeller Foundation, 2015) and 2030 Sustainable Development Goals (SDGs) (Osborn et al., 2015). **The overall aim of this research is to demonstrate the application of EO data in quantifying urban growth and its impact on the UHI in order to illustrate its potential for informing both global and metropolitan sustainable city development goals.**

1.2 Defining urban area

The term 'urban area' is surrounded by conceptual vagueness, with definitions varying based on discipline origin e.g. academia, census bureaus and metropolitan development agencies (Bennett, 2001). Weeks (2010) defined 'urban' as a characteristic of place whereby a spatially concentrated population are organised around non-agricultural activities. This definition is composed of (i) population size, (ii) land area, (iii) population density, and (iv) economic and social organisation. However, due to increased population movement towards traditional urban centres and subsequent outward expansion, the urban-rural divide is becoming difficult to differentiate (United Nations, Department of Economic and Social Affairs, 2014; United Nations, 2016; Weeks, 2010). In an effort to mitigate the increasing pressure from rural-urban migration on city expansion and metropolitan services developing countries have initiated schemes to attract urban infrastructure to previously considered rural areas (Weeks, 2010). For example, the Vietnamese government initiated side-line productions with the slogan "leaving the land without leaving the village" (Rigg, 1998; Weeks, 2010). Similarly, China's Special Economic Zones (SEZs), offering corporations economic incentives, attempted to resolve socio-economic problems associated with the centrally administrated system whilst also importing a foreign knowledge base (Kam Ng and Tang, 2004). In 1980 the city of Shenzhen was designated as China's first SEZ, originally considered a tiny rural town located at the northern edge of Hong Kong with a population of only 0.3 million. By 2000 SEZ status resulted in a 23 fold population increase to an estimated 7 million (Kam Ng and Tang, 2004; Zhou et al., 2016). Nevertheless it is difficult to exactly determine at what point in time Schenzen's status changed from rural to urban due to the multitude of possible factors that could be considered (e.g. population, land area or economic organisation).

Statistical bureaus define urban in various ways to ensure data availability for specific applications. For example, the Australian Bureau of Statistics (ABS) currently provide five definitions of urban area based upon differing Statistical Areas (SA) levels of collection. Due to the complexity of the ABS urban definitions they are summarised in Figure 1-1 (ABS, 2017). One important consideration within this framework is that the Greater Capital City Statistical Areas (GCCSAs) have only been in force since the 2011 census, replacing the statistical divisions that

previously covered the greater metropolitan area, often referred to as the metropolitan region of each capital city constrained by Local Government Areas (LGA); consequently no previous census data is available for the complete GCCSAs (ABS, 2017).

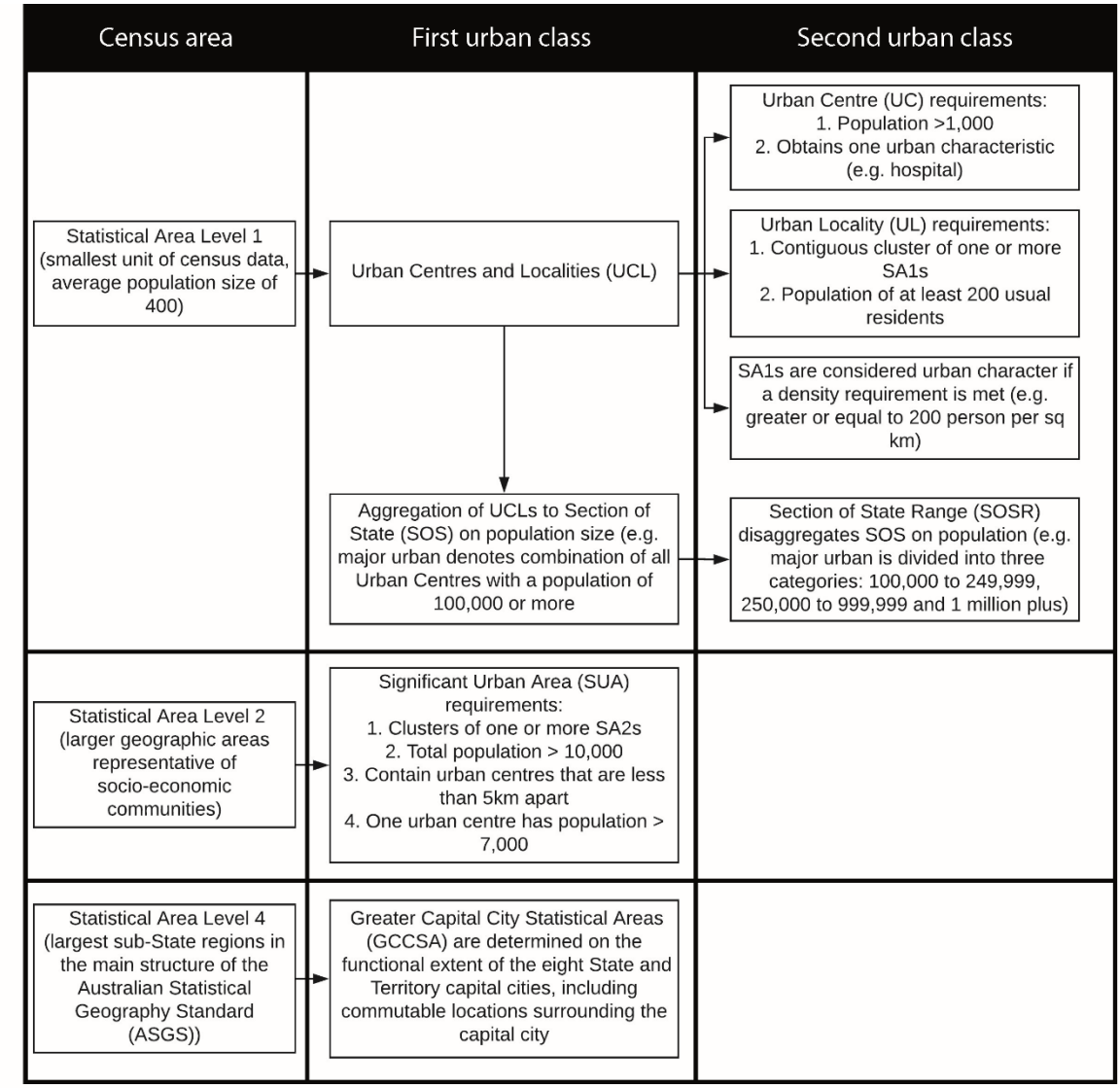

Figure 1-1. Varying urban definitions associated with different datasets produced by the Australian Bureau of Statistics (ABS). Adapted from ABS (2017).

Similarly the United States of America (USA) Census Bureau provides further urban definition variation (Figure 1-2). The USA Census Bureau base urban categorisation on census blocks, tracts, cities and counties. Census blocks are the smallest geographic census area, established from visible features such as roads, property boundaries and rivers. Census tracts are representative of neighbourhoods as defined by the Census Bureau, generally obtaining between 2,500 and 8,000 people, with boundaries also defined on visible features. Cities and associated spatial boundaries

are defined in legislation by the city government whilst Counties are based upon geographic, political and administrative subdivision of a State (U.S. Census Bureau, 2018).

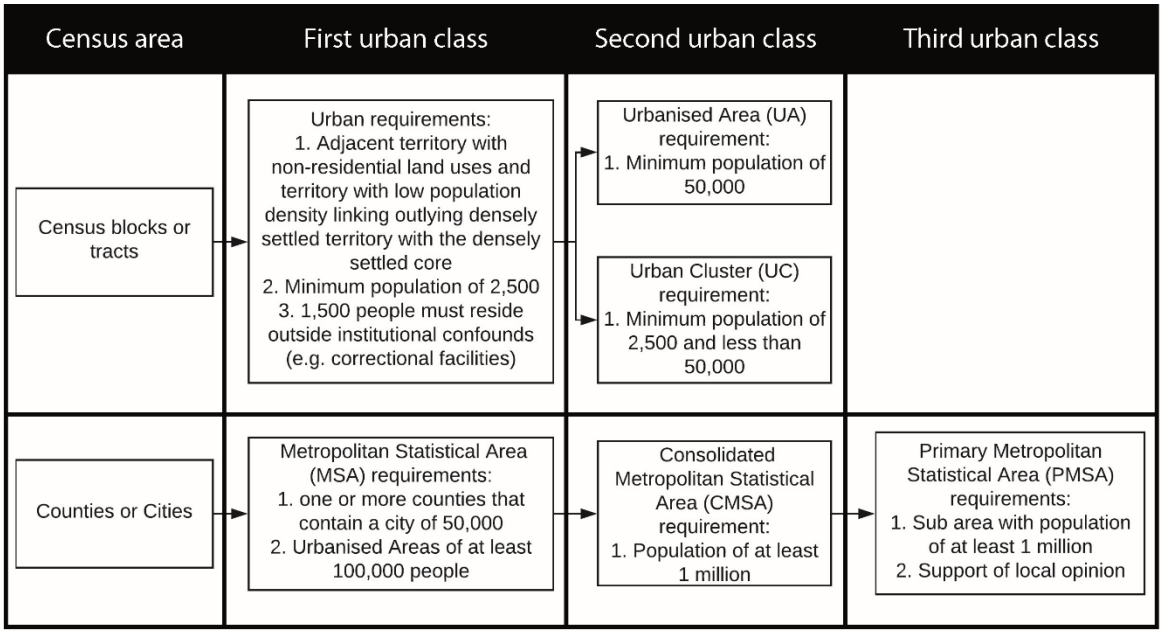

Figure 1-2. Varying urban definitions associated with different datasets produced by the United States of America (USA) Census Bureau. Adapted from U.S. Census Bureau (2018).

In contrast the United Kingdom (UK) Office for National Statistics (ONS) rather more simplistically define urban as settlements with a population of 10,000 or more residents. Settlements are established from a grid of hectare cells (100m x 100m) over England and Wales, with residential properties inferred from Royal Mail's (UK's postal service) postcode address file assigned to cells. Residential density for a set of increasing radii surrounding each cell is calculated and compared to defined standards assigning each cell to a settlement type (e.g. village, town, urban fringe). Census Output Areas (OA), the smallest level of census data are combined with the classified cell output and defined urban if both classed as a settlement and obtaining a population of 10,000 or more (Bibby and Brindley, 2013).

These contrasting urban definitions and associated data are based upon local governments and organisations being able to best identify features that differentiate urban and rural (Brockerhoff, 2000). Nevertheless individual country specific approaches hinder cross country comparison and accurate global estimates due to the multitude of differing factors that are considered in determining urban extent.

Urban development strategies that outline future development and sustainability targets are frequently provided by metropolitan development agencies such as the Spatial Development Strategy For London (Mayor of London, 2016a), Perth's Directions 2031 (Western Australian Planning Commission, 2010a) and Johannesburg's Spatial Development Framework 2040 (City of Johannesburg Metropolitan Municipality, 2016). These documents often fail to definitively define the term urban, generating inconsistencies throughout national agencies. In the case of Perth, Western Australia (WA), initial urban estimates only covered the Perth Metropolitan Region (PMR) based upon cadastral land parcel valuations, with later estimates considering spatial modelling, multiple urban categories and the larger spatial extent of the Perth GCSSA (Western Australian Planning Commission, 2010a). Consequently, whilst the spatial extent of the defined metropolitan region or GCCSA will align with the ABS extents, urban estimations are derived from differing metrics.

The main overall limitation of the aforementioned classifications pertains to the assumption of a dichotomous urban and rural divide. However, due to the wide variations in urban designation, the UN Population Division (1950) originally proposed an urban-rural continuum (Weeks, 2010). Nevertheless, of the 228 countries for which the UN compiles data, around half define urban extent based on administrative boundaries, 51 use population size or density, 39 implement financial metrics, 22 have no definition and 8 define all (e.g. Singapore) or none (e.g. Polynesian countries) as urban (Brockerhoff, 2000). A lack of consistent national and international urban definitions precludes scientifically valid comparisons (Brockerhoff, 2000).

The advent of remote sensing provides an alternative approach for mapping urban areas. Sensors on board satellites provide consistent and reliable collection of data that when combined with approaches for classification can determine urban extent over time based upon unique and specific land cover characteristics. For this research urban is defined as a determinant of urban land cover as calculated from the spectral reflectance properties of temporally consistent user defined areas (termed Regions Of Interest (ROIs)) from satellite Earth Observation (EO) sensors: Landsat 5 Thematic Mapper (TM), and Landsat 8 Operational Land Imager (OLI). The reflected radiation monitored in each spectral band was combined in producing unique surface reflectance spectral signature for the ROIs subsequently matched to other similar pixels through classification methodologies. Due to the heterogeneity of urban areas and spectral confusion of classification methodologies associated with spectrally similar land cover classes (e.g. bare earth and urban) urban land cover was classified as either high or low urban albedo (Chen et al., 2014). The former represents surfaces with higher solar reflectivity (e.g. concrete) usually found in city centres whilst the latter denotes lower solar reflectivity (e.g. asphalt) commonly used in residential developments (Yang et al., 2015).

In this sense urban area depicts land cover representing the biophysical attributes of Earth's surface as opposed to land use that defines the human purpose or intent applied to the biophysical attributes (Lambin et al., 2001). Whilst this definition excludes population, economic and social organisation factors, it provides the longest temporal record of land cover derived from a replicable and temporally consistent methodology appropriate in determining further environmental relationships such as the association with temperature; important for planning (sustainable) development. Within this research development refers to an expansion of urban area based upon a change in land cover whilst sustainable is defined as actions causing minimal (or no) damage to the environment and humans enabling long-term continuation aligning with the UN's combined sustainable development definition of development "that meets the needs of the present without compromising the ability of future generations to meet their own needs" (Brundtland, 1987, p.41).

1.3 Types of urban expansion

1.3.1 Urban growth

Within scientific literature urban growth is often conceptualised using a form of geographic data resulting in three main categories considering the relationship to existing urban areas, namely infill, expansion and outlying, with outlying obtaining three further sub categories of isolated, linear branch and clustered branch (Wilson et al., 2003; Yuan et al., 2005) (Figure 1-3). Infill growth is defined by the (re)development of a small land tract surrounded by urban land cover. Often characterised by the conversion of a non-developed area (e.g. 30 m^2) to an urban surface with at least 40% of the surrounding area that is also defined as developed, usually occurring in areas of existing infrastructure (Bhatta, 2010; Wilson et al., 2003). Expansion growth constitutes conversion of non-developed area to developed, whilst being surrounded by no more than 40% existing developed area (Bhatta, 2010; Wilson et al., 2003). The overall limiting factor of these characterisations pertains to the assumption of conversion from non-developed land (known as a greenfield site), when other urban land cover could be converted from dormant use (e.g. wasteland or abandoned facilities, known as a brownfield site) to a form infill development. However, this type of conversion is difficult to determine without land use information accompanying geographic data. Outlying growth occurs beyond the existing developed area, in the isolated form it is characterised by one or several developed areas surrounded by minimal developed land. The linear branch form refers to a new linear development (e.g. roads) that are surrounded by non-developed areas. Finally the clustered branch form identifies large compact developments that are neither isolated nor linear in nature (Wilson et al., 2003).

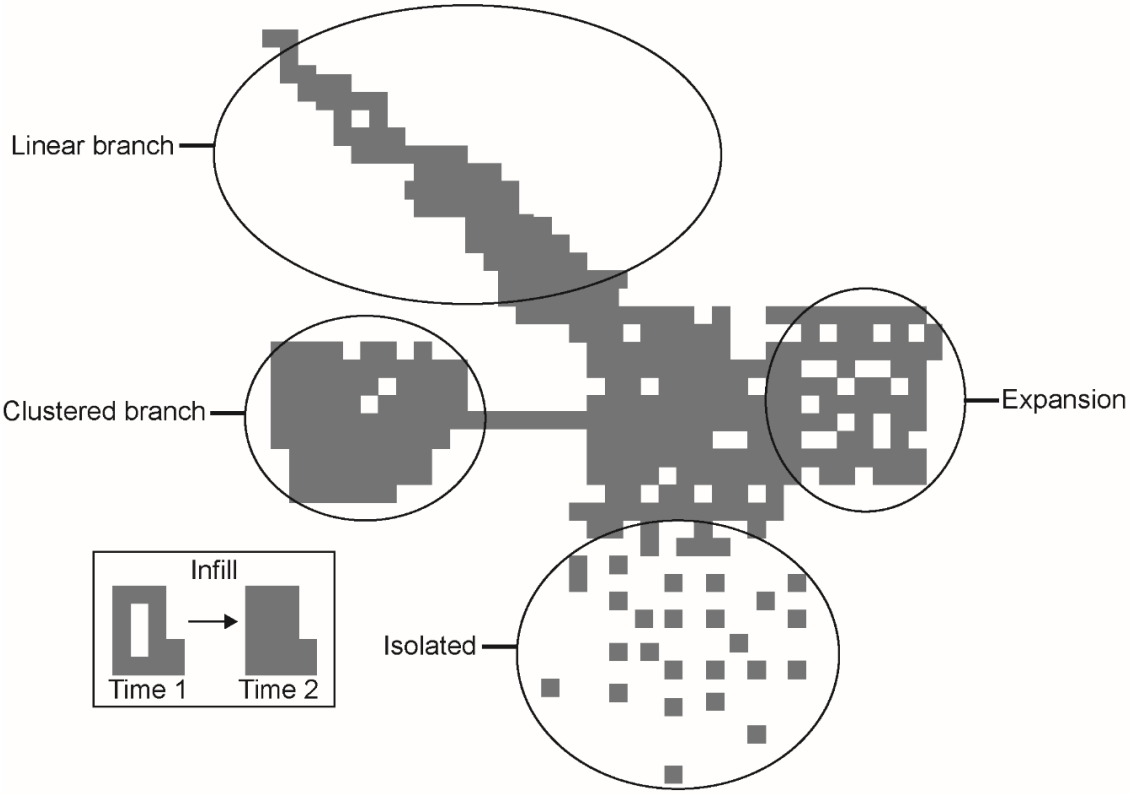

Figure 1-3. Forms of urban growth as defined by scientific literature. Adapted from Bhatta (2010).

In contrast to academic literature, previously presented metropolitan level policy documents in section 1.2 stipulate infill targets and aspirations but often omit urban growth definitions providing no further subcategories (e.g. Perth and London) or vague definitions (e.g. Johannesburg) that are difficult to quantitatively assess. For example, the Johannesburg Metropolitan Municipality specified a linear future development scenario defined based on concentration of population and jobs along extensive transit corridors, but lack a measureable metric that would provide adequate monitoring. Whilst the Western Australian Planning Commission (WAPC) aim to achieve 47% of future development as infill by 2050, monitoring considered zoned and not necessarily developed industrial, commercial and residential land use defined as infill or greenfield based upon residential density above or below an unspecified threshold using census data (Western Australian Planning Commission, 2016a). In Australia, census data is collected every 5 years, restricting temporal monitoring of development and assuming that changes in density across a range of land use types that may not yet be developed is an accurate representation of infill development (Western Australian Planning Commission, 2016a). The vagueness associated with current policy definitions initiates difficulties for local governments in meeting specified targets and in the provision of policy-focused methodologies to accurately monitor urban development.

1.3.2 Urban sprawl

The expansion of low density suburbs into previously rural areas creates exurbs, urban or suburban areas and raises the notion of urban sprawl (Sun et al., 2013; Yuan et al., 2005). Currently there is no universally accepted definition of urban sprawl, with multiple studies using urban growth, urban sprawl, peri-urbanisation and exurban development interchangeably without providing definitive definitions (Schneider, 2012; Schneider and Mertes, 2014; Suarez-Rubio et al., 2012; Xian et al., 2012). Whilst Yuan et al. (2005) highlighted the requirement of an undeveloped land buffer between established area and new development, Castrence et al. (2014) simply stated urbanisation is a loss of open space and agricultural land that leads to urban sprawl. In terms of previously considered metropolitan policy documentation only Johannesburg provided a definitive sprawl definition revolving around dispersed over focused developed forms, whereas Perth's implied low density, greenfield detached housing dwellings located on the urban fringe and London's suggested development beyond the greenbelt. Consequently in a similar theme to urban growth, policy orientated urban sprawl ambiguity produces difficulties for both local governments and researchers in monitoring and identifying solutions when the very concepts aren't defined by metropolitan agencies.

Defining urban sprawl as a concept has highlighted ambiguity and conceptual vagueness (Bennett, 2001; Bhatta, 2010; Bhatta et al., 2010). Galster et al. (2001) undertook an extensive evaluation of sprawl within the literature that revealed sprawl can be alternatively or simultaneously referred to as patterns of land use, processes of land development, causes of land use behaviours and consequences of land use behaviours (Bhatta, 2010; Bhatta et al., 2010; Galster et al., 2001). Furthermore, to add to the complexity, sprawl is also referred to as a noun and a verb. As a noun it signifies a condition representing an urban area at a particular time, whereas when used as a verb it defines a stage or process of development (Bhatta, 2010; Galster et al., 2001). Whilst a definitive definition of sprawl is contested, a general academic consensus exists that urban sprawl is characterised by unplanned and uneven pattern of growth resulting in inefficient resource utilisation (Bhatta, 2010; Bhatta et al., 2010; Sun et al., 2013), which is the definition followed in this research.

1.3.3 Urban growth and sprawl in Earth observation

It is important to establish that every type of urban growth should not be considered sprawl (Bhatta, 2010). Whilst the notion of sprawl attracts a negative connotation in terms of environmental and societal impacts, types of urban growth such as infill development are considered resolutions to urban sprawl. Consequently, sprawl should not be used interchangeably

with urban growth and must be considered as its own separate entity. However, within EO studies this is often unfeasible due to similarities of materials and geometries that compose both urban sprawl and urban growth being indiscernible using medium resolution EO imagery. Therefore the majority of studies focus on monitoring urban growth as a holistic concept (which could encompass sprawl) as being the change in developed land between two or more time periods (e.g. Luo et al., 2014; Schneider and Mertes, 2014; Sexton et al., 2013; Song et al., 2016).

1.4 The urban heat island effect

1.4.1 Introduction

One of the main environmental impacts of urbanisation is the UHI effect, whereby urban areas obtain comparatively higher atmospheric and surface temperatures than surrounding rural areas (Cai et al., 2016; Howard, 1988; Hu and Brunsell, 2015; Voogt and Oke, 2003; Xie and Zhou, 2015). The modification of land cover properties as a result of urbanisation has been identified as the most extreme cumulative effect of land cover change, permanently influencing atmospheric energy exchange and altering local and regional climate change (Cai et al., 2016; Howard, 1988; Hu et al., 2015; Voogt and Oke, 2003; Xie and Zhou, 2015). Thus, UHIs are considered one of the major problems posed to humans in the 21st century, with the importance of understanding heat risk highlighted by extreme temperatures overtaking flooding and rising to the third highest cause of global disaster mortality (11.3%) between 2006 and 2015, behind only earthquakes (51.2%) and storms (24.9%) (Centre for Research on the Epidemiology of Disaster and the United Nations Office for Disaster Risk Reduction, 2016).

1.4.2 Urban heat island theory

The UHI phenomena is created through a shift in energy balance toward sensible heat over latent heat. The former represents heat exchanged by a body that changes temperature (e.g. conduction, convection or advection) whilst the latter is defined as energy released or absorbed by a body (e.g. evapotranspiration) (Sexton et al., 2013; Wong et al., 2013). The creation of UHIs is the result of two major factors: an increased spatial coverage of dark surfaces and the absence or removal of vegetation (Frumkin, 2002; Voogt, 2004). Dark urban surfaces obtain a low albedo (albedo being the fraction of shortwave radiation reflected from an object, in comparison to natural surfaces). Consequently, impervious surfaces (such as asphalt and concrete) absorb and retain a large proportion of the shortwave radiation during the daytime, reemitting this energy as long wave energy (or sensible heat) during the day (based on surface properties) and particularly at night (Zhao et al., 2016). However, due to the three dimensional structural arrangement of

modern cities, a low Sky View Factor (SVF), defined as the ratio of radiation received (or emitted) by a planar surface to the radiation emitted (or received) by the entire hemispheric environment, frequently precludes efficient heat dispersion (Abutaleb et al., 2015; Frumkin, 2002; Kalnay and Cai, 2003; Lindberg and Grimmond, 2010; Sharifi and Lehmann, 2014; Voogt, 2004; Watson and Johnson, 1987; Zhao et al., 2016). The absence or removal of vegetation reduces solar radiation blocking to urban surfaces which inhibits heat emittance, diminishing evapotranspiration that cools the atmosphere through ambient heat dissipation (Frumkin, 2002). Further factors including air speed, cloud cover, cyclic solar radiation, building material type and anthropogenic energy sources can exacerbate this phenomena in a temporary (e.g. weather patterns) or more permanent (e.g. built environment) manner (Rizwan et al., 2008; Sheng et al., 2015).

Contributing UHI factors are commonly described through the energy balance equation whereby net radiation, defined as the balance between incoming and outgoing energy at the top of the atmosphere equates to the sum of sensible heat (energy heating the air), latent heat (energy used for evaporation) and surface conductive heat (energy heating the ground) fluxes. When applying the energy balance equation to UHI concepts sensible heat is representative of building thermal properties, latent heat is a function of vegetation coverage and surface conductive heat is dependent on surface albedo. Recent iterations have also included anthropogenic heat sources, representative of systems that emit heat such as air-conditioning and automobiles combined with net radiation equating to the sum of surface, latent and conductive heat fluxes (Arnfield, 2003).

1.4.3 Urban heat island categories

This section describes UHI categories and temporal forms, enabling appropriate terminology inclusion when discussing monitoring approaches leading to identification of current research and policy issues in relation to global and metropolitan sustainable city development goals, the latter part of the overall thesis aim.

1.4.4 Heat island layers

The UHI concept can be decomposed into three subcategories: the Boundary Layer Heat Island (BLHI), the Canopy Layer Heat Island (CLHI) and the Surface Heat Island (SHI) (Figure 1-4). BLHI and CLHI refer to warming of the urban atmosphere, with SHI indicating urban surface heat (Fabrizi et al., 2010; Voogt, 2004). The UCL and SHI are both located within the Urban Boundary Layer (UCL), extending up to around 1 km or more above the surface during daytime and shrinking to around hundreds of meters or less at night. The UCL is the layer of air closet to city surfaces

and extending upwards to average tree or building height, whilst the SHI depicts the temperature Earth's surface as seen from above (Schwarz et al., 2012).

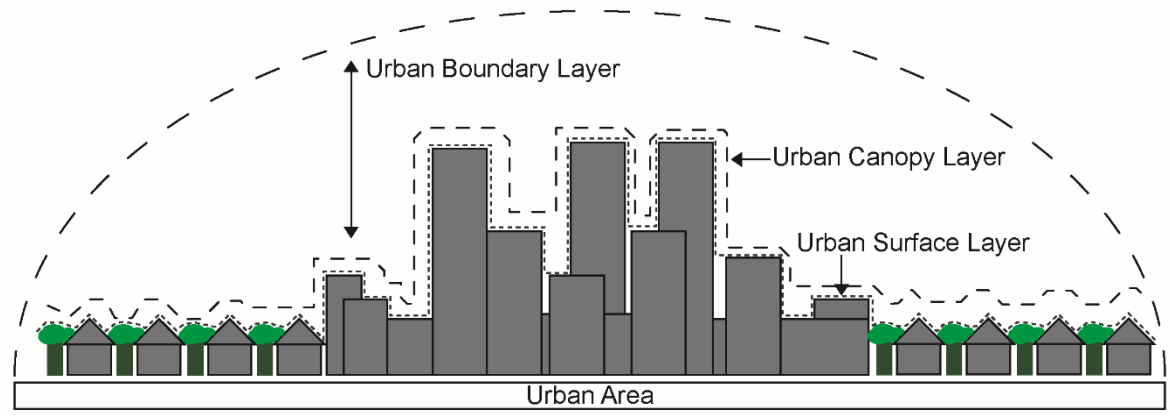

Figure 1-4. The main Urban Heat Island (UHI) components of the urban atmosphere. Adapted from Voogt (2004) and the USA Environmental Protection Agency (2008).

1.4.5 Heat island temporal form

Two different temporal forms of UHI exist: daytime and nighttime. Daytime UHI is largely driven by solar radiation and the thermal properties of urban surface materials, compared to nighttime UHI which is predominately controlled by the release of solar energy trapped during the day and additional anthropogenic energy sources (Zhao et al., 2016). Consequently, the temporal alteration of heat source generates two unique urban heat island profiles, daytime and nighttime. No clear consensus exists within the literature when identifying whether surface UHIs of the day (Cheval and Dumitrescu, 2014; Sun et al., 2015; Tran et al., 2006; USA Environment Protection Agency, 2008; Weng et al., 2004) or night (Fabrizi et al., 2010; Kenward et al., 2014; Sheng et al., 2015; Zhou et al., 2015) are more intense, with differences being based upon geographic location.

1.5 Urban heat island impacts

Elevated temperatures resulting from UHIs have been associated with detrimental health consequences (Goggins et al., 2012; Michelozzi et al., 2009; Tan et al., 2010), increased energy requirements (Santamouris et al., 2015), heightened emissions and economic expenditure (AECOM Australia, 2012; Frumkin, 2002; USA Environment Protection Agency, 2008). The following sections outline the effects of the UHI in terms of social, environmental and economic impacts.

1.5.1 Social impacts

The direct effect of heat on populations was first explored by Buechley et al. (1972), who established an exponential increase in the mortality rate relative to maximum temperature (Tan et al., 2010). Typically skin receives 5-10% of inactive cardiac output, during heat stress this can rise to between 50 and 70%. Consequently in order to maintain healthy blood pressure cardiac yield must be increased generating additional tension on the heart (Wong et al., 2013). Heat-related illnesses ensue if heat gain cannot be dissipated through physiological or thermoregulatory processes (Loughnan et al., 2013). Thus health issues can range from mild to life-threatening and commonly pertain to the cardiovascular and respiratory systems, including heat syncope or fainting, heat edema or swelling, heat tetany or hyperventilation (Basu and Samet, 2002; Frumkin, 2002; Loughnan et al., 2013). Excess heart strain can further exacerbate underlying conditions (e.g. ischemic heart disease and respiratory illnesses) or the health of vulnerable groups (e.g. elderly, high population density residents or high rise living residents) (Buchin et al., 2015; Tomlinson et al., 2011). The impact of the UHI effect on health is frequently presented in relation to respiratory hospital admissions and changes in mortality (Lowe, 2016; Michelozzi et al., 2009). For example, population adjusted excess mortality rates during the 1998 Shanghai heatwave were estimated at 27.3 per 100,000 within the urban area compared to only 7 per 100,000 in the exurban districts (Tan et al., 2010). In Hong Kong a 1 °C rise in temperature above 29 °C was associated with a 4.1% increase in mortality in areas with a high UHI intensity, compared to only a 0.7% in areas with a low UHI intensity (Goggins et al., 2012). Whilst in six ‘‘Mediterranean’’ (Barcelona, Ljubljana, Milan, Rome, Turin, and Valencia) and six ‘‘North-Continental’’ (Budapest, Dublin, London, Paris, Stockholm, and Zurich) cities a 2.1% and 1.2% increase in respiratory admissions was respectively observed across all age groups, increasing to 4.5% and 3.1% in the 75 plus age category (Michelozzi et al., 2009).

1.5.2 Environmental impacts

In terms of energy usage, for each degree of ambient temperature rise the increase in peak electricity load has been estimated between 0.45 and 4.6%, corresponding to around 21 W per degree rise per person (Santamouris et al., 2015). This is particularly problematic in countries where the majority of energy originates from fossil fuel combustion (e.g. Australia and USA). The increased energy requirement can elevate air pollutants such as sulphur dioxide (SO_2), nitrogen oxides (SO_x), particulate matter (PM), carbon monoxide (CO) and mercury (Hg) all of which are considered harmful to human health (Frumkin, 2002; USA Environment Protection Agency, 2008). For example, using data across 25 USA communities, a rise of 10 $\mu g/m^3$ in two day average $PM_{2.5}$

(particles with a diameter of less than 2.5 μm) mass concentration was associated with a 0.74% increase in non-accidental deaths (Franklin et al., 2008).

1.5.3 Economic impacts

The collective impacts of the UHI were quantitatively estimated in the first ever economic assessment undertaken by the City of Melbourne (2012), with the annual UHI cost estimated at AUD 300 million. This was composed of costs associated with factors and services including health, transport, energy, anti-social behaviour, tree maintenance and animal care and mortality (AECOM Australia, 2012). Of these categories increased health costs dominated (AUD 282 million) overall expenditure, due to the dangers associated with extreme temperatures on human life and subsequent predicted mortality rise. The established impacts associated with the UHI highlight the importance of effective mitigation measures. However, recent research has estimated the impact of the UHI could increase the percentage of Gross Domestic Product (GDP) lost by 0.71% (in 2050) and 1.04% (in 2100) for the low Green House Gas (GHG) scenario and 0.80% (in 2050) and 1.79% (in 2100) under the very high GHG scenario due to exclusion from Global Climate Change (GCC) scenarios (Estrada et al., 2017). As a result the UHI effect has been included in updated international polices such as the Sendai Framework for Disaster Risk Reduction (UNISDR, 2015), SDGs (Osborn et al., 2015) and CRF (ARUP and The Rockefeller Foundation, 2015), yet these policies currently lack any methodological approach for UHI monitoring. **Consequently, it is of vital importance to develop effective data-driven mitigation measures and planning policies to ensure the future sustainability of our cities.**

Chapter 2 Monitoring urban growth and the urban heat island effect using Earth observation

2.1 Introduction

Chapter 1 outlined the concepts and issues of poorly planned urban development and the Urban Heat Island (UHI) effect. Chapter 2 builds upon this base knowledge through discussing current monitoring approaches and associated limitations that are addressed within this thesis.

2.2 Monitoring land cover change

Land cover data can be collected using traditional field surveys, however, for expansive urban metropolitan areas these are often unfeasible due to the required funding, person hours, strategic planning and annual replication for complete temporal and spatial coverage. As a result, data derived from field surveys is often incomplete, spatially aggregated, and temporally and geographically limited. Comparatively, satellite remote sensing enables efficient extraction of geographic land cover changes with considerable cost reductions in a timely and synoptic manner (Powell et al., 2007; Yuan et al., 2005). This is achieved through classification of unique surface reflectance signatures per pixel, being the fraction of incoming solar radiation reflected by the Earth's surface over a defined area (e.g. 30 m^2) into predefined land cover classes.

Classifying an Earth Observation (EO) image in determining land cover change can be summarised by three main steps: preprocessing, classification and output evaluation. The majority of recent research advancements focus on classification, with comparatively fewer and more established methods for preprocessing and output evaluation. Three main image analysis approaches exist for extracting land cover estimates from EO data: classification algorithms, spectral indices and data-fusion approaches. Classification algorithms assign one or more user-defined land cover classes to a pixel in the digital image. For example, GlobeLand30 provided global land cover estimates divided into 10 classes, namely water bodies, wetland, artificial surfaces, cultivated land, snow/ice, forest, shrubland, grassland, bare earth and tundra from Landsat data with an overall accuracy exceeding 80% (Chen et al., 2015). However, the difficulties of extracting built-up areas is a known issue within the remote sensing community, resultant from spectral similarities between natural surface materials such as bare soil and man-made materials such as impervious surfaces leading to spectral confusion during classification (Herold et al., 2002; Lu et al., 2011; Varshney and Rajesh, 2014). New per-pixel spectral indices, such as the Normalized Difference

Built-up Index (NDBI) (Zha et al., 2003), provide an alternative approach in determining the presence of a sole land cover class (e.g. urban), with a user-determined threshold establishing the value at which a pixel is assigned to the land cover type (Angiuli and Trianni, 2013; Xu, 2008; Zha et al., 2003). However, Schneider (2012) suggested analysis must move beyond mere consideration of spectral information to the temporal, spatial or polarimetric domain in order to resolve misclassification, particularly in an urban environment. In this sense, additional variables are obtained or computed and appended to original imagery for classification algorithm accuracy improvement. In the following sections an overview of preprocessing and output evaluation is provided, with a comprehensive literature review of current classification methodologies.

2.2.1 Image preprocessing

Image preprocessing entails correction for noise unattributed to surface reflectance, such as radiometric (atmospheric), geometric (image projection) and topographic (physical features) errors (Hansen and Loveland, 2012). Satellite data results in images experiencing differing radiometric conditions defined as the sensitivity of the sensor to incoming reflectance, due to variations in atmospheric conditions, solar illumination, sensor calibration, view angle and soil and vegetation changes (Du et al., 2002; Yang and Lo, 2000). Similarly, geometric misalignment and slope orientation in relation to incoming solar radiation can result in inconsistences when undertaking scene classification and thematic evaluation (Richter et al., 2009). The majority of studies exploring land use and land cover change have implemented medium spatial resolution (30 m) Landsat imagery, obtaining the longest, free temporal image repository of consistent medium spatial resolution data, with a temporal resolution of 16 days (Bagan and Yamagata, 2012a; Kressler and Steinnocher, 2001; Lu et al., 2011; Sexton et al., 2013; Sundarakumar et al., 2012; Tan et al., 2009).

Landsat data are distributed as a surface reflectance product achieved through the Landsat Ecosystem Disturbance Adaptive Processing System (LEDPAS) and the Landsat 8 Surface Reflectance algorithm (L8SR) otherwise known as the Landsat 8 Surface Reflectance Code (LaSRC) for correction of atmospheric conditions (Hansen and Loveland, 2012; USGS, 2015). The former corrects for atmospheric effects using the Second Simulation of a Satellite Signal in the Solar Spectrum (6S) radiative transfer model, whilst the latter implements an internally developed algorithm (Hansen and Loveland, 2012; USGS, 2015). Additional processing to Level 1 Terrain-corrected data (L1T) corrects for both geometric and topographic errors using ground control points and a Digital Elevation Model (DEM) from the Global Land Survey (GLS) 2000 data set (Hansen and Loveland 2012). However, owing to the requirement of several parameters (i.e. Aerosol Optical Thickness (AOT), ozone and air temperature) for surface reflectance derivation

assumptions or models of values are often implemented (Ju et al., 2012). Consequently, for removal of remaining post-atmospheric correction noise such as the brightening effect of cloud or darkening of cloud shadow, Sexton et al. (2013) put forward the notion of image standardisation based on pre-defined band specific values and subsequent normalisation for reduced inter-annual surface reflectance values. When classifying EO imagery over multiple years this approach permits the use of a single classification model as opposed to individual classification for each time point considered.

2.2.2 Image classification

Holistic image classification is achieved through a supervised or unsupervised methodology. In a supervised classification the user selects sample pixels termed Regions of Interest (ROI) that are representative of predefined land cover classes. ROIs are then input to a classification algorithm that identifies pixels with similar reflectance values to each provided land cover class for entire image classification. During an unsupervised classification an algorithm automatically separates image pixels into clusters obtaining similar spectral characteristics, with only a user defined number of classes. Owing to the majority of recent literature focusing on supervised classifiers due to the complexity and size of datasets this review shall be limited to supervised methodologies (Schneider, 2012).

2.2.3 Recent classification methodologies

Classifier selection is dependent on the nature of input data and desired output, defined as parametric or nonparametric. Parametric algorithms make assumptions regarding ROIs selected for training, such as a Gaussian distribution, whereas nonparametric algorithms do not make this assumption (Donnay and Unwin, 2001; Jensen, 2005). Popular traditional nonparametric classification algorithms include density slicing, parallepiped, minimum distance to mean, and nearest-neighbour, with Maximum Likelihood (ML) the most widely utilised parametric classifier (Jensen, 2005).

2.2.3.1 Maximum likelihood

The ML classification is based on Bayes' Theorem of decision making. It assigns each pixel to the most probable user-defined land cover class, rather than the minimum distance, through considering both the variances and covariances of class signatures (Atkinson and Lewis, 2000; Jensen, 2005). The ML algorithm permits specification of prior classification probability information (i.e. expected frequency of classes per scene). However, in reality, information of this sort is rarely available, with the majority of ML applications assuming equal class probability per

scene and assigning land cover classification to pixels based upon the highest probability. The advantage of the ML classifier pertains to assignment based on probability often used in determining land cover (Fuller et al., 1994).

2.2.3.2 Spectral mixture analysis

More recently, parametric Spectral Mixture Analysis (SMA) and subsequently machine learning or 'expert systems' have been implemented to solve classification problems (Jensen, 2005; Okujeni et al., 2014). SMA considers the selection of spectrally unique endmembers, with image data being assigned the most appropriate match (Powell et al., 2007). It is based on the assumption that reflectance measured at each pixel is represented by the linear sum of endmembers weighted by the associated endmember fraction. In standard SMA a set number of representative endmembers, commonly between two and five, are extracted, with the entire image being modelled on their spectral characteristics (Powell et al., 2007). Endmember extraction normally revolves around identification of spectral extremes (e.g. Adams, 1995). However, selection of a limited number of extreme endmembers results in an inability to adequately represent the high spectral heterogeneity of the urban landscape (Powell et al., 2007). Consequently endmembers may not fully represent image spectral variability or a pixel may be modelled by endmembers that do not represent materials within its field of view. Both factors result in a reduction of classification accuracy (Powell et al., 2007). Due to being an original approach that could consider multiple endmembers whilst improving accuracy of ML and minimum distance approaches SMA has been used in establishing Vegetation-Impervious surface-Soil (V-I-S) fractions (Phinn et al., 2002) and analysing impervious surface distributions (Wu and Murray, 2003).

2.2.3.3 Multiple endmember spectral mixture analysis

Multiple Endmember Spectral Mixture Analysis (MESMA) extends this methodology through permitting the number and type of endmembers to alter on a per pixel basis attempting to represent the inherent spectral variability within land cover types over the entire image as a linear combination of constituent components (Okujeni et al., 2015, 2013; Powell et al., 2007; Weng and Pu, 2013). Mixture models are iteratively calculated for each pixel, comparing all possible endmember formulations, deriving the fit between measured and modelled signals. The model obtaining the lowest Root Mean Square Error (RMSE) is designated to the pixel (Okujeni et al., 2013). For each land cover class the MESMA library should obtain sufficient spectra to competently represent spectral variability. However, as the overall number of endmembers increases computational efficiency exponentially decreases. Thus, the endmember library should remain adequately small to maximise computational efficiency, whilst obtaining land cover spectral diversity within selected spectra (Powell et al., 2007). Due to the advantages of multiple

endmember selection MESMA has been implemented in classifying land cover (Franke et al., 2009) and mapping forest fire burn severity levels (Quintano et al., 2013).

2.2.3.4 Machine learning algorithms

In contrast, Machine Learning Algorithms (MLAs) use an automated inductive approach for identification of patterns in data (Cracknell and Reading, 2014). The majority of research focusing on MLAs surrounds the predication of land cover from multi-spectral or hyperspectral surface reflectance measurements (Angiuli and Trianni, 2013; Braun et al., 2012; Rodriguez-Galiano et al., 2012; Schneider, 2012). MLA classification is derived by a discrimination function $y = f(x)$, with inputs expressed as vectors d of the form $(x_1, x_2, \dots, x_d)$, where y is a definitive set of c class labels $(y_1, y_2, \dots, y_c)$. Using instances of x and y supervised machine learning trains the classification model, mapping image data to defined classes (Cracknell and Reading, 2014). Popular MLAs include Artificial Neural Networks (ANNs), Random Forests (RFs) and Support Vector Machines (SVMs).

2.2.3.4.1 Artificial neural network

Nonparametric ANNs are an interconnected group of nodes that use mathematical methods to process information in a self-adaptive system, attempting to 'mimic' a human brain (Bhatta, 2010; Hu and Weng, 2009). The Multi-Layer Perceptron (MLP) feed forward network is the most popular ANN; obtaining three layers - one input, one hidden and one output layer - each comprising of several nodes (artificial neurons). The input layer represents the original image, with each band representing one node. Classification is undertaken in the hidden layer, with results presented in the output layer. The learning ability originates from the learning algorithm, with the most popular being Back-Propagation (BP) otherwise known as delta rules (Hu and Weng, 2009). Learning is achieved through node weight assignment, with training samples input into the model. If the difference between the produced results and test sample is larger than the initial threshold, weights are altered for difference minimisation. The process is iterated until a pre-defined accuracy level is obtained or maximum iterations reached and a classified land cover output is produced (Candade and Dixon, 2004; Cracknell and Reading, 2014; Hu and Weng, 2009). ANNs have been widely used due to their robustness and ability to learn complex patterns, successfully implemented in ship detection (Tang et al., 2015), tree detection (Malek et al., 2014) and land use classification (Cheng and Han, 2016; Hu and Weng, 2009; Pacifici et al., 2009).

2.2.3.4.2 Random forest

RFs are a nonparametric ensemble learning method that implement a majority vote system to predict classes based on data partition from multiple Decision Trees (DT) (Breiman, 2001;

Cracknell and Reading, 2014). Multiple trees are created, using a random subset of input features to reduce generalisation error, with the end user specifying the number of trees to be developed and number of features at each node. Each tree implements a bagging sample permitting growth based on differing training subsets, with a search across a random selection of input variables for derivation of a split per node (Cracknell and Reading, 2014; Gislason et al., 2006; Rodriguez-Galiano et al., 2012). Bagging facilitates training data creation through randomly resampling the original dataset, with each selected subset for tree growth containing a proportion of the training dataset. Samples not selected are input to the Out Of Bag subset (OOB). OOB samples not utilised for tree training can be classified by the tree for performance evaluation (Rodriguez-Galiano et al., 2012). DT design requires the determination of an attribute section and pruning method. The random forest classifier implements the Gini Index as the attribute selector method, measuring the impurity of an attribute compared to classes (Pal, 2005). DT can be constrained through a termination criterion threshold limiting growth size and therefore overfitting, termed pre-pruning. Additionally post-pruning techniques permit overall performance evaluation, due to being pruned with validation data. However, Breiman (1999) suggested that whilst the number of trees increases the generalisation error always converges without overfitting due to the Strong Law of Large Numbers, which states that the average results obtained from a large number of trials (or trees) should be near the expected value and will become closer with the more trials performed (Rodriguez-Galiano et al., 2012). Thus, for classification, each tree within the RF inputs a vote for the most popular class, with the output classification determined by the majority of tree votes (Gislason et al., 2006). RF are advantageous over other ensemble classification methodologies such as boosting and bagging through an improved methodological process and less intensive computational requirement being used in instances to classify: land cover (Gislason et al., 2006) and tree species (Immitzer et al., 2012).

2.2.3.4.3 Support vector machine

The nonparametric SVM classifier identifies an optimal maximum margin separating hyperplane, dividing the dataset into the predefined number of classes, with points on the margins termed support vectors (Braun et al., 2012; Foody and Mathur, 2006, 2004; Mountrakis et al., 2011; Qian et al., 2014; Vapnik and Chervonenkis, 1971). The underlying benefit of SVM is known as structural risk minimisation, whereby SVMs are able to minimise error on unseen data without prior assumptions made on the data probability distribution (Mountrakis et al., 2011). SVMs are linear binary classifiers assigning participant pixels into one of two possibilities. However, remote sensing derived land covers are often not linearly separable due to cluster overlap. Consequently implementation of soft margin and kernel methods aid inseparability through transforming data into high dimensional feature spaces (Euclidean or Hilbert) utilising non-linear functions to

identify linear solutions (Braun et al., 2012; Mountrakis et al., 2011). In order to prevent over fitting SVM implements a two-dimensional grid search using stratified crossvalidation to search for the kernel (g) and regularisation parameter (C); (g) defines the width of the Gaussian kernel function whilst (C) controls training data and decision boundary maximisation plus margin errors (Zhu and Hastie, 2005). For derivation of more than two land cover classes additional methodological processes are required, common methods include one-against-all, one-against-one and directed acyclic graph SVM, whereby the binary nature of SVM is iterated in differing formants to derive the appropriate land cover classification (Chih-Wei et al., 2008; Mountrakis et al., 2011). SVMs are one of the most prominent and effective MLA due to structural risk minimisation applied to a variety of applications including land cover change detection (De Morsier et al., 2013), airport detection (Tao et al., 2011) and road extraction (Cheng and Han, 2016; Das et al., 2011).

2.2.4 Comparison of recent classification methodologies

Image classification accuracy is dependent on the selected classification methodology and the choice of internal parameters (Huang et al., 2002; Watanachaturaporn et al., 2008). Due to the parametric nature of the ML classifier it can often fail to represent land cover that might be multimodal, thus in certain circumstances ML has been outperformed by alternative classification algorithms (Melgani and Bruzzone, 2004; Mountrakis et al., 2011; Otukei and Blaschke, 2010; Watanachaturaporn et al., 2008). Similarly MESMA classification can be inefficient owing to additional computational demands associated with an increasing numbers of endmembers which often precludes selection and is consequently considered a more traditional method when compared to MLAs (Okujeni et al., 2015; Ram and Wang, 2013). In a comparison of ML, DT (e.g. RF), ANN and SVM classifiers, Watanachaturaporn et al. (2008) and Kotsiantis et al. (2006) found the SVM classifier to produce optimal accuracy. Similarly Huang et al. (2002) found SVMs obtain a higher accuracy than ML, DTs and ANNs indicating that the superior performance of SVM is attributed to the derivation of an optimal separating hyperplane (Foody and Mathur, 2006, 2004; Huang et al., 2002; Mountrakis et al., 2011). Whilst no single MLA can uniformly outperform all other MLAs across all data sets, in terms of overall accuracy the majority of literature preferences implementation of SVM due to its self-adaptability, efficient learning speed and limited training data requirements (Kotsiantis et al., 2006; Mountrakis et al., 2011).

2.2.5 Image spectral combinations

The reliable and accurate identification and extraction of built-up areas from medium resolution EO imagery (e.g. Landsat) is a known issue within the remote sensing community; originating from

spectral heterogeneity of urban surfaces often resulting in spectral confusion during image classification (Herold et al., 2002; Lu et al., 2011; Varshney and Rajesh, 2014). Consequently new spectral indices, which in the most part do not require classification have been postulated as an alternative and more computational efficient approach.

Zha et al. (2003) proposed a built up index termed the Normalized Difference Built-up Index (NDBI) algorithm for identification of built up regions using the reflective bands: Red, Near-Infrared (NIR) and Mid-Infrared (MIR). NDBI makes the assumption that built up area has a high spectral reflectance in the MIR compared to the NIR. However, MIR vegetated spectral response can increase above NIR under drier conditions (Gao, 1996; Xu, 2008). Thus, Zha et al. (2003) implemented the Normalised Difference Vegetation Index (NDVI) to filter noise arising from vegetation. Nevertheless Xu (2008) stated that sole use of original spectral bands for construction of a built-up land index is inappropriate due to the composition of complex spectral features.

Consequently Xu (2008) followed the methodological framework of Ridd (1995), that the spatial composition of urban areas can be decomposed into Vegetation-Impervious surface-Soil creating the V-I-S model with the inclusion of water, grouping the urban area into: built up land, vegetation and open water (Ridd, 1995). Three indices of NDBI, the Soil Adjusted Vegetation Index (SAVI) and Modified Normalized Difference Water Index (MNDWI) represented the land cover categories respectively. MNDWI modifies the Normalized Difference Water Index (NDWI) through selection of the MIR band in place of the NIR band, remediating built up land noise for open water selection. SAVI was preferenced over NDVI due to greater sensitivity in detecting vegetation in low-plant covered regions such as urban areas, estimated to work with plant cover as low as 15% compared to NDVI at 30% (Xu, 2008). Aforementioned indices extracting unique features were then combined in the Index-based Built-up Index (IBI). However, the intrinsic issue of IBI pertains to selection of an appropriate user defined correction value for SAVI ranging from 0 for high plant densities to 1 for low plant densities. Furthermore complete land cover is assumed to be adequately modelled from built land, vegetation and water. Thus, analysis has resulted in urban area remaining mixed with bare earth, requiring additional polygon layers defining the urban region from an unspecified source to filter erroneous built up land for definitive extraction (Stathakis et al., 2012; Sun et al., 2015; Xu, 2008; Zha et al., 2003). Additionally, the nature of determining appropriate singular threshold values over heterogeneous urbans fails in global practicality and has the potential for the introduction of localised errors impacting reliability (Xu, 2008).

In contrast to the threshold approach presented by Xu (2008), Angiuli and Trianni (2013) proposed the Normalised Difference Spectral Vector (NDSV). Due to multiple indices presented

throughout literature NDSV attempts a simultaneous merge for the production of intrinsically normalised globally consistent data whilst reducing ambiguities associated within individual indexes (Angiuli and Trianni, 2013; Patel et al., 2015). NDSV computes all possible indices through the combination of all bands. Thus, with 6 Landsat bands a total of 30 indexes are generated, but due to the symmetry of definition, 15 are negative representations of other indexes (Angiuli and Trianni, 2013; Patel et al., 2015). NDSV creates a normalised signature per pixel and is subsequently classified. Nevertheless, any index is founded upon assumptions, for example, NDVI is based on the rationale that green plants absorb solar radiation in the photosynthetically active radiation spectral region (400 – 700 nm) and reflect radiation in the NIR region. Therefore NDVI is usually highly correlated with Leaf Area Index (LAI) and has found to be sensitive to canopy background variations such as soil visible through the canopy (Jensen, 2009). Consequently NDVI can be unsatisfactory, especially when mapping senesced vegetation owing to reduced absorption in the visible bands and reflection in the NIR band (Jensen, 2005). This methodology also fails to directly extract urban extents owing to the requirement of a classification model.

2.2.6 Data fusion methodologies

Recent data fusion methodologies combine additional or computed data to existing spectral bands in order to improve classification accuracy (Rodriguez-Galiano et al., 2012). Popular approaches can be categorised into spatial, temporal and polarimetric domains extracting additional information from texture, temporal composites and radar respectively. The following sections outline and compare these procedures, determining current research trends and establishing the most appropriate methodological approach in quantifying the temporal urban growth section of the overall thesis aim.

2.2.6.1 Spatial domain

Texture analysis provides a representation of the visual characteristics of an image permitting incorporation of spatial information into image (e.g. Landsat) classification found to produce more accurate classifications of heterogeneous land covers such as urban (Møller-Jensen et al., 2005; Rodriguez-Galiano et al., 2012; Zhou and Troy, 2008). Co-occurrence texture measures such as mean, variance, homogeneity, contrast, dissimilarity, entropy, second moment and correlation are computed using a moving rectangular window surrounding a central pixel. Nevertheless, an overarching issue pertains to window size; it must be large enough to capture variance, yet small enough to represent homogenous land cover (Møller-Jensen et al., 2005). Consequently, the window-based approach tends to smooth boundaries between discrete land cover types determined from medium-coarse resolution imagery, with the appropriate window size being

difficult to discern and a rectangular window not necessarily representative of real land coverage (Møller-Jensen et al., 2005). Very high resolution (< 1 m) surface reflectance imagery, Light Detection and Ranging (LiDAR) and stereo imagery such as that procured during Perth's Urban Monitoring project and the State of Indiana's strategic plan can overcome these limitations, but are associated with high financial outlay and often infrequent repeat collections that currently preclude extensive temporal monitoring (e.g. 15 years) (Caccetta et al., 2012; The State of Indiana, 2017).

2.2.6.2 Temporal domain

Annual and multi-seasonal temporal image composites increase class spectral separability through stacking imagery from multiple dates into a single image (Bhatta, 2010; Castrence et al., 2014; Schneider, 2012; Sexton et al., 2013; Yuan et al., 2005; Zhu et al., 2012). This follows the logic that natural surfaces obtain a type of cyclical pattern resulting from changes in the proportion of land cover (e.g. mixtures of vegetation, soil and water) based on the time of year (Jensen, 2005). However, when natural surfaces are replaced with impervious structures the fluctuation will cease owing to the conversion to built-up land cover generally being unidirectional, identifiable from a multi-temporal signature in spectral space (Castrence et al., 2014). Regardless, the premise of this method is founded upon the assumption that limited or no change will have occurred within a complete temporal period of stacked imagery. Ideally, each variable used in classification should enable additional refinement for improved accuracy. Nevertheless, due to the number of bands within the multi-temporal image composite high variable correlation may be prevalent (Bhatta, 2010; Zhu et al., 2012). Redundancy can be overcome through principal component transformation, with components containing significant variance selected for classification (Bhatta, 2010). Whilst Zhu et al. (2012) acknowledged this issue through investigating the effect of increasing variables during classification they concluded that although some variables contribute relatively little, the trend is straightforward; more independent data results in higher classification accuracy.

2.2.6.3 Polarimetric domain

Synthetic Aperture Radar (SAR) data are playing an increasingly important role in remote sensing owing to all weather operational ability (Zhu et al., 2012). Although SAR images over urban areas provide low quality images due to problems associated with radar imaging in such an environment (i.e. multiple bouncing, layover and shadowing), SAR texture measures can provide valuable information in discerning urban areas (Dell'Acqua et al., 2003; Zhu et al., 2012). Isolated scattering of residential areas and crowded backscatters of inner city high density areas permit classification refinement, thus textural measures such as those descried within the spatial domain

can aid identification of alternative urban forms (Zhu et al., 2012). However, the lack of freely available SAR data that temporally coincides with other satellite imagery (e.g. Landsat) frequently precludes extensive use.

2.2.7 Output evaluation

Accuracy assessment of classified data is key to ensure effective and appropriate data usage. Accuracy can be determined through visual inspection, non-site specific analysis, difference imaging, error budgeting and quantitative assessments (Congalton, 2001). Visual inspection is often the first step of assessment in ensuring the production of a valid output, but does not provide numerical quantification. Non-site specific analysis and difference imaging compare classified output between an alternative data source for a small spatial area and complete image respectively, providing a spatial component to map error. However, these methods fail in determining the accuracy of each individual land cover class, presented as difference in area estimates and difference images. Error budgeting estimates the total error of a project workflow based on analyst attributed values, combined in an error index (Congalton, 2001). Whilst this assists in determining and assessing data input, user and methodological error potential it fails in end user classification output accuracy estimation. A quantitative accuracy assessment is imperative in order to accurately report any modelled urban growth estimates, often omitted from values provided in metropolitan planning documents. An error matrix is the most common quantitative evaluation of classified remotely sensed data (Foody and Mathur, 2004; Friedl et al., 2010; Van de Voorde et al., 2011; Watanachaturaporn et al., 2008). An error matrix is a square array comparing the number of sample units correctly determined by the classifier in relation to a data source (e.g. original image or Google Earth) per land cover category. Outputs include (i) user's accuracy defined as the fraction of correctly classified pixels relative to all others classified as a particular land cover, (ii) producer's accuracy defined as the fraction of correctly classified pixels compared to ground truth data, and (iii) overall accuracy that represents the combined fraction of correctly classified pixels across all land cover types (Congalton, 2001). Quantitative accuracy metrics of this sort permit appropriate use of land cover products and parameterisation of further analysis that expands upon the classified output such as recent Urban Heat Island (UHI) studies that combine land cover data and satellite derived temperature.

2.2.8 Classification methodological conclusion

Mapping urban areas remains a complex challenge owing to the complex variation of materials and geometries that compose the urban environment and contribute to mixed spectral signatures (Schneider, 2012). Methodologies employed for extraction of urban areas from satellite imagery

are diverse and often location dependent, with no current standardised best practice for urban monitoring. Throughout the literature spectral, spatial, temporal and polarimetric data have been used in differing formulations for urban area extraction.

Due to the limited past record of complete SAR data, required temporal analysis observed within academic and metropolitan studies (e.g. 15 years) is often unfeasible. Additionally, spectral analysis can be seasonally dependent, whilst spatial analysis can remove underlying trends through data smoothing and poor representation of real land cover due to a definitive rectangular moving window. Generation of unique multi-temporal spectral signatures increases the amount of independent data available for classification but the underlying assumption of minimal change between composited images is made. Due to these limitations, EO data is typically classified as standalone data (e.g. surface reflectance) by classification algorithms discussed in section 2.2.3. However, these methodologies have been found to significantly over or underestimate urban area by between 50-60% in complex landscapes such as the urban-rural frontier (Lu et al., 2011; Wu and Murray, 2003). **Improving our ability to map urban area is currently an essential challenge due to the potential for classified land cover products to inform decision making such as determining future development strategies and informing further environmental analysis and policies** (Bagan and Yamagata, 2014; Hepinstall-Cymerman et al., 2013; Miller and Small, 2003; Schneider et al., 2005).

2.3 Monitoring urban heat islands

Two forms of temperature affecting urban areas are frequently monitored in relation to an expanding urban area; air temperature and Land Surface Temperature (LST). The former often pertains to traditional meterological monitoring, whereas the latter is based on thermal measurements made from EO data. The following sections describe these two methodological approaches.

2.3.1 Traditional urban heat island methodologies

Air temperature represents Urban Canopy Layer (UCL) temperature; directly impacting human comfort and public health, monitored from static weather stations (Guo et al., 2014). For example, Shanghai's heatwave excess mortality rates (Tan et al., 2010), Hong Kong's UHI-mortality association (Goggins et al., 2012) and Melbourne's UHI economic assessment (AECOM Australia, 2012) used differenced temperature data from meteorological stations in rural and urban geographical locations to determine the UHI Intensity (UHII) (Tan et al., 2010). To account for the spatial variation in the UHI effect, the temperature measurements from weather stations

are often spatially interpolated. The accuracy of the interpolated dataset can be dependent on the type of interpolation method, the number of points available and distance between them (Hattis et al., 2012). **Consequently, whilst studies using point-based meteorological data provide a broad city scale view of the UHI, they are impractical for targeted mitigative planning actions (e.g. urban greening) due to the limited number of meteorological stations in many areas.**

2.3.2 Remotely sensed land surface temperature

EO data overcomes the limitations of point based methods through providing near global coverage of LST on a per pixel basis using instruments that measure in thermal spectral wavebands. LST measurements are widely used to quantify the impact of land cover type on the Surface Heat Island (SHI), often related to air temperature in the same location, resulting in the term Surface Urban Heat Island (SUHI) (Schwarz et al., 2012; Voogt and Oke, 2003). In the context of characterising the UHI, LST is typically used, as opposed to air temperature due to the additional parameters required to compute air temperature such as surface properties, atmospheric conditions and solar angles that must be incorporated, assuming data availability during satellite overpass.

Due to their advantages in monitoring temperature, satellite instruments including the Moderate Resolution Imaging Spectroradiometer (MODIS) (Wang et al., 2015), Landsat Thematic Mapper (TM) (Jimenez-Munoz et al., 2014; Rinner and Hussain, 2011; Sobrino et al., 2004), the geostationary Spinning Enhanced Visible and Infrared Imager (SEVIRI) (Blasi et al., 2016) and the Advanced Along-Track Scanning Radiometer (AATSR) (Fabrizi et al., 2010) have been used to monitor LST and the UHI effect. Nevertheless, current methodologies frequently fail in planning practicality due to the static temporal nature through consideration of limited (two or less) EO temperature images (Li et al., 2011; Tomlinson et al., 2011) alongside aggregation to broad land cover types or use of singular metrics such as the UHII (Cao et al., 2010; Imhoff et al., 2010; Zhou et al., 2016). For example Li et al. (2011) used temperature extracted from two Landsat images captured in March and July 2001 to infer the effects of landscape composition and configuration on the UHI in Shanghai. Whilst their results produced strong correlations between LST and landscape metrics, selection of single images obtained during spring (March) and summer (July) disregard the temporal component of LST (e.g. the complete annual temperature cycle) and fail to account for potential abnormalities in temperature on selected days (e.g. heatwaves) (Li et al., 2011).

Similarly, whilst Zhou et al. (2016) explored the spatio-temporal trends of the UHI throughout China using daily MODIS LST between 2003 and 2016, their analysis was restricted to comparison

of the UHII using land cover data from only 2005 and 2010. The use of two classified land cover images restricted UHI analysis through the assumption of unchanged urban area between 2003-2007 (for the 2005 image) and 2008-2012 (for the 2010 image). Land cover changes within these timeframes had the potential to produce erroneous results alongside sole output of the UHII that precludes quantification of changes in land cover associated with temperature for targeted policy remediation (Zhou et al., 2016). **Consequently, research must adapt to consider the needs and requirements of metropolitan development frameworks in order to assist in more sustainable future metropolitan development.**

2.3.3 Localised temperature mitigation

In response to the UHI effect and updated international policies outlined in section 1.5 a variety of localised mitigation measures have ensued, categorised into voluntary and policy themes. The former represents demonstrative projects and incentives such as Sacramento's Tree Foundation providing free shade trees to Sacramento residents (USA Environmental Protection Agency, 2013). The latter incorporates the UHI into metropolitan frameworks such as Perth and Peel @3.5million (Western Australian Planning Commission, 2015a), The London Plan (Mayor of London, 2016a) and Johannesburg's Spatial Development Framework 2040 (City of Johannesburg Metropolitan Municipality, 2016). **However, these policies frequently fail in planning practicality through lacking any specific methodological requirement.** Consequently local governments have incorporated quantifiable policy requirements such as Seattle's Green Factor specifying minimum vegetation requirements, yet lacking placement guidelines that could result in sub-optimal locations (USA Environmental Protection Agency, 2013). Other local governments such as the City of Perth and Fremantle have initiated EO informed Urban Forest programmes to maintain and increase vegetation coverage (City of Fremantle, 2017; City of Perth, 2006). However, due to the lack of scientifically applied UHI mitigation studies and devolution of targets to local governments, varied, inconsistent and aggregated block scale LST methodologies provide the potential to misinform vegetation placement (City of Fremantle, 2017; City of Perth, 2006). The majority of academic literature implementing remotely sensed data analysing the UHI effect uses medium-low resolution satellite imagery (e.g. MODIS, 1 km and Landsat, 30 m), inappropriate for very small scale, localised UHI mitigation decisions. It is therefore imperative to provide policy-relatable methodologies in order to facilitate scientifically-valid decision making in ensuring the sustainability of our cities.

Chapter 3 Research aim and objectives

This short chapter outlines the overall research aim and objectives of this thesis. The aim of this research is to demonstrate the application of Earth Observation (EO) data in quantifying urban growth and its impact on the Urban Heat Island (UHI) in order to illustrate its potential for informing both global and metropolitan sustainable city development goals. In achieving this aim the research objectives are extracted from current themes and gaps, presented both in the main thesis introduction and in each paper style chapter. This is divided across the four paper style chapters each addressing their own objectives:

1. Provide a remotely sensed spatio-temporal assessment (paper 1a, chapter 4) and associated methodology (paper 1b, chapter 4) of change in urban area across the Perth Metropolitan Region (PMR) using a consistent methodology.
2. Develop an approach to remediate frequent over (or under) estimation of urban area classified from medium resolution satellite imagery through comparison to very high resolution aerial imagery — paper 2, chapter 5.
3. Investigate the spatio-temporal UHI characteristics at the sub-metropolitan level using a per pixel approach through (a) determining the complexities of the UHI effect and (b) deriving associations between land cover and temperature change at the intra-urban scale — paper 3, chapter 6.
4. Establish an operational methodology for evidence-based urban planning to optimise localised UHI mitigation through the use of EO data and open source spatial temperature models — paper 4, chapter 7.

3.1 Study site

This section provides an introduction and overview to the PMR in Western Australia (WA), the study site used throughout this thesis in achieving the objectives and overall aim. The City of Perth is the State Capital of WA and has undergone dramatic urban and population growth accredited to Australia's natural resources boom commencing around the start of the 21st century. Mining and petroleum exports dominate WA's export products attributing 95% of export earnings between 2010 and 2011, with sales rising from AUD 4.7 billion in 1996 to a peak of AUD 121.6 billion mid-2013 (Department of Mines and Petroleum, 2015). The majority of the urban growth has been identified as sprawling, outward and low-density by the Western Australian Planning Commission (WAPC) (Western Australian Planning Commission, 2015a). This is representative of the 'Australian dream' comprising of detached living within a green suburb on

greenfield urban-fringe sites (Dhakal, 2014; Western Australian Planning Commission, 2015a). Consequently in comparison to other Australian state capitals Perth was Australia's fastest growing city (in terms of population) between 2007 and 2014 whilst only obtaining a maximum population density of only 3,662 people per square kilometre (Melbourne 10,827; Sydney 14,747) (ABS, 2015, 2011; Kennewell and Shaw, 2008). The pressures from this extensive low density and outward expansion has induced non-strategic and car centric development that has the potential to degrade social and environmental systems such as amenity servicing efficiency and habitat loss (Dhakal, 2014; Downs, 2005; Turner et al., 2010). The guide for the long term (2050) development of Perth specifies that future land rezoning must be the result of strategic urban planning as opposed to individual requests (Western Australian Planning Commission, 2015a). However, current urban monitoring within the PMR is based upon unrepresentative (e.g. land value information) and temporally varied data. Thus, owing to PMR's vast and rapid expansion alongside a globally diverse range of urban characteristics (e.g. compact central business district, older residential areas and new suburban developments) it provides a timely and relevant example to develop innovative solutions in determining temporally consistent urban area models whilst remediating frequently reported over (or under) urban estimation from medium resolution imagery.

In a similar theme under the sustainability key strategy within the long term development guide, recently devised metropolitan and local temperature mitigation plans use limited and/or aggregated data which could misguide remedial actions (Western Australian Planning Commission, 2012). Based on the lack of global investigation into the causes and consequences of the metropolitan and local UHI effect alongside Perth's large scale conversion of natural to impervious surfaces it provides a unique and globally important case study in resolving current limitations of expanding urban areas and their association to temperature. More specific information pertinent to each objective can be found within each paper style chapter, with further contextual study area information provided in chapter 4.

3.2 Thesis structure and methodological outline

This thesis is composed of nine chapters including two introduction chapters, this aim and objectives chapter, four chapters presented in the form of scientific journal articles aligning with the 'three-paper' format PhD submission, a discussion and final conclusion chapter. Each paper style chapter is taken from a published or submitted journal article, with minor editing to ensure consistency throughout the thesis. Whilst each paper explores unique research aims, Figure 3-1 outlines inter-linkages between the collective papers forming a coherent body of novel research

contributions. Specifically temporal land cover data produced within the first paper is used within paper 2 and 3, with analysis from paper 3 informing paper 4 (Figure 3-2).

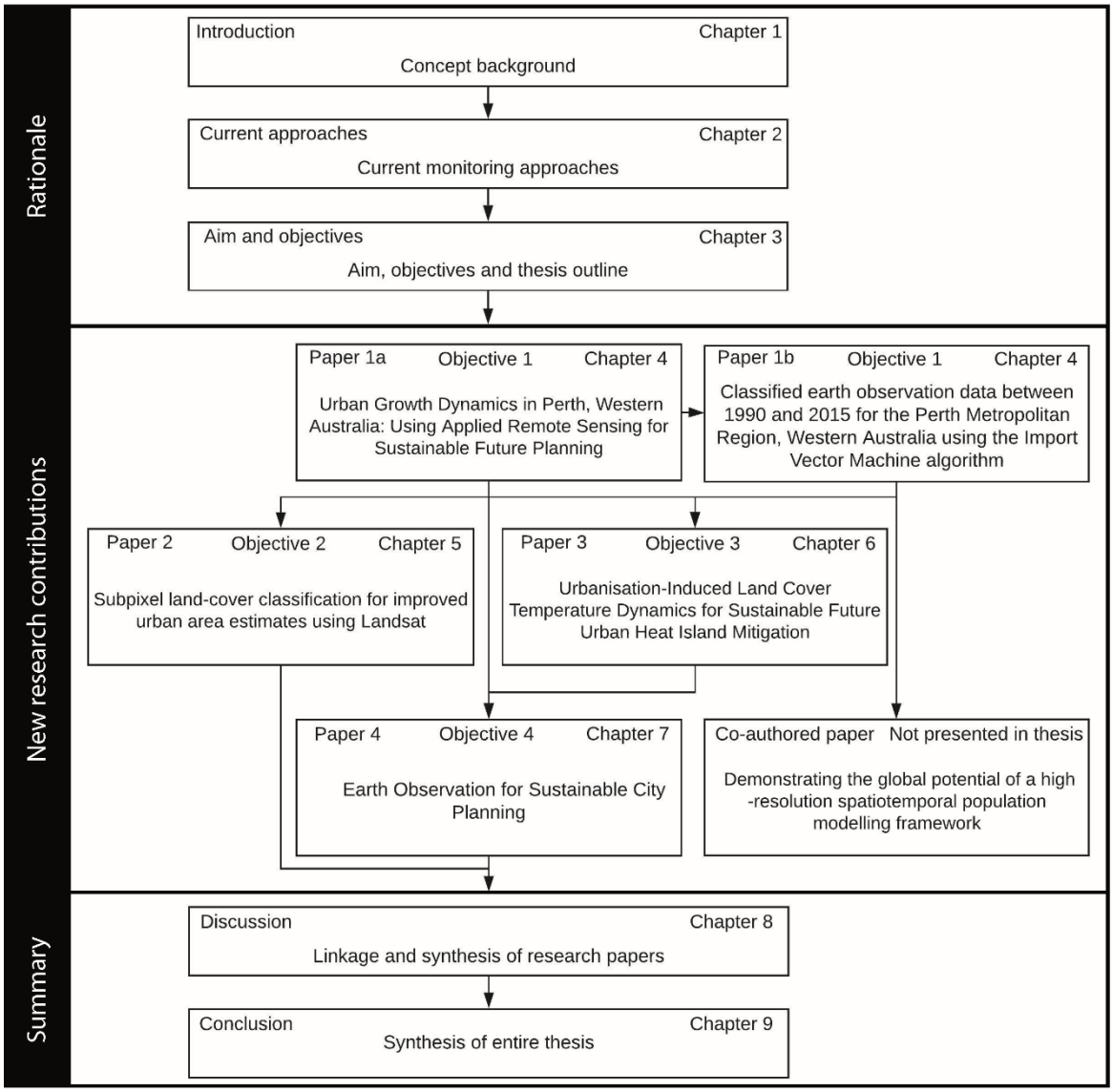

Figure 3-1. Outline of general thesis structure and paper linkages.

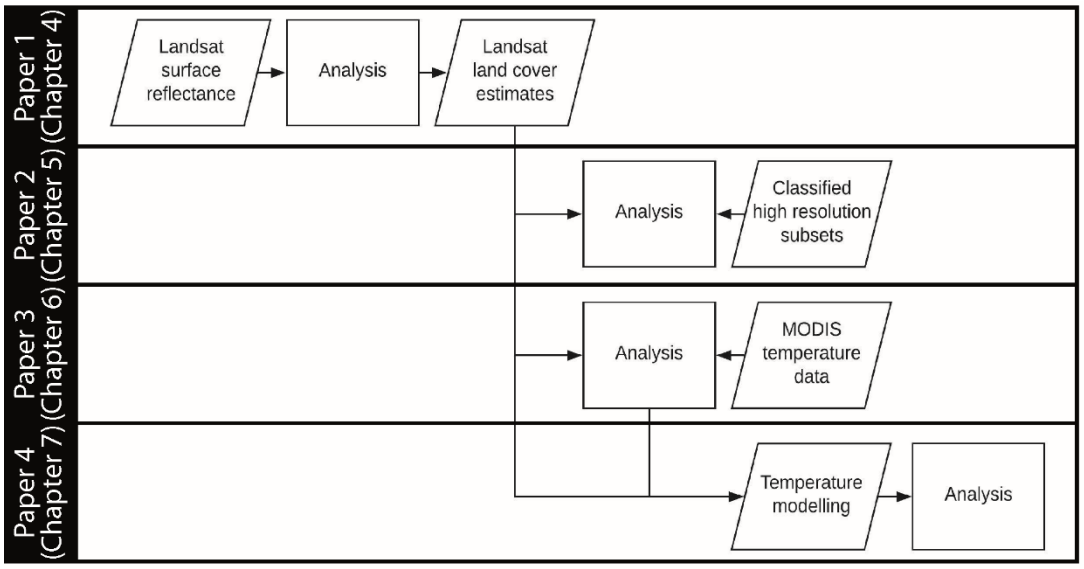

Figure 3-2. Data flow and linkage throughout papers presented in thesis.

Following this thesis introduction and literature review chapter 4 provides an applied example into using EO data for monitoring urban expansion in the city of Perth, WA. The implications of a rapidly expanding urban area are discussed and EO derived estimates are compared to those provided by the WAPC based upon temporally varied methodologies. This study provides the first EO temporal examination of land cover within Perth from normalised satellite imagery highlighting the applicability of EO data in accurate urban quantification for sustainable targeted planning practices and addressing the first thesis objective.

Building on the work in chapter 4, chapter 5 further analyses classified hard and sub-pixel 2007 land cover data in relation to classified high resolution (20 cm) aerial imagery. The hard classification refers to the dominant land cover within each Landsat pixel, whilst the sub-pixel classification represents the probability of a pixel containing a classification value. High resolution imagery was classified using Object Based Image Analysis (OBIA) and aggregated to Landsat pixels (30 m) producing the percentage of land cover and identification of the dominant land cover class per Landsat pixel area. Firstly, the two hard land cover datasets were compared, identifying overestimation from the Landsat classification. Addressing errors of this nature are essential owing to EO land cover data being used to influence policy decisions. Overestimation was remediated through the implementation of novel spatially explicit regression model approach between the high resolution percentage urban per Landsat pixel and the Landsat sub-pixel data that improved urban land cover estimations from medium resolution imagery, achieving the second thesis objective.

Chapter 6 uses 2003 and 2013 classified land cover data produced in chapter 4 alongside temperature data from the MODIS Terra sensor. The methodology overcomes current limitations

of UHI studies such as use of temporally static land cover, assumption of urban homogeneity and disregard of a spatial component through global indices, inappropriate for policy incorporation. Land cover estimates were aggregated to MODIS resolution (1 km) producing the percentage of land cover per MODIS pixel for both 2003 and 2013. The dominant land cover change per MODIS pixel was identified and associated with the difference in temperature between 2003 and 2013. Consequently the presented novel analysis established ideal future land rezoning in relation to temperature change, accomplishing the third thesis objective.

Chapter 7 draws upon chapter 6 analysis in demonstrating an improved localised UHI mitigation approach. Current global, metropolitan and localised mitigation policies and strategies often fail in planning practicality through a lack of specificities or inappropriate data use. Chapter 7 demonstrates the power of EO data and spatial modelling in reducing localised temperature for a proposed redevelopment in the City of Fremantle, WA through optimum vegetation placement using a scientifically valid and policy integratable approach, advancing current policy and academic mitigation attempts, aligning with the final objective of this thesis.

Chapter 8 critically discusses the research significance, methodological transferability, global applicability, current critical challenges and future research potential.

Chapter 9 provides a summary of the key findings of the thesis in relation to the overall thesis aim.

Chapter 4 Urban growth dynamics in Perth, Western Australia: using applied remote sensing for sustainable future planning

4.1 Abstract

Earth observation data can provide valuable assessments for monitoring the spatial extent of (un)sustainable urban growth of the world's cities to better inform planning policy in reducing associated economic, social and environmental costs. Western Australia has witnessed rapid economic expansion since the turn of the century founded upon extensive natural resource extraction. Thus, Perth, the state capital of Western Australia, has encountered significant population and urban growth in response to the booming state economy. However, the recent economic slowdown resulted in the largest decrease in natural resource values that Western Australia has ever experienced. Here, we present multi-temporal urban expansion statistics from 1990 to 2015 for Perth, derived from Landsat imagery. Current urban estimates used for future development plans and progress monitoring of infill and density targets are based upon aggregated census data and metrics unrepresentative of actual land cover change, underestimating overall urban area. Earth observation provides a temporally consistent methodology, identifying areal urban area at higher spatial and temporal resolution than current estimates. Our results indicate that the spatial extent of the Perth Metropolitan Region has increased 45% between 1990 and 2015, over 320 km^2. We highlight the applicability of Earth observation data in accurately quantifying urban area for sustainable targeted planning practices.

4.2 Introduction

Over the last 15 years, Perth has experienced exponential economic growth with Gross State Product (GSP) increasing 218% (ABS, 2015). Originally labelled as the 'Cinderella State' due to its remote location and perceived neglect from the rest of Australia, Western Australia (WA) has experienced sustained discovery and extraction of natural resources since the beginning of the 21st century (Kennewell and Shaw, 2008). In response to a growing resource sector, the city of Perth has undergone extensive urban expansion at what Dhakal (2014) identified as an unsustainable rate. To this end, the Western Australian Planning Commission (WAPC) identified that Perth's urban footprint has increased from 631 km^2 to 870 km^2 in the 10 years between 2002 and 2012 (Western Australian Planning Commission, 2010a, 2015a). However, these figures

should be considered with caution as data used in early estimates represent land parcel (Cadastral) valuations only (provided by the Western Australian Value General's Office), with later estimates (from 2009) based on multiple urban zoning classifications, and more recently (from 2010) spatial modelling taking into account land valuation and zoning (Western Australian Planning Commission, 2010b, 2009). The use of varied data and methods impacts confidence in the ability of the Commission's estimates to represent actual change in urban extent, especially when urban zoning information includes land identified for growth but not necessarily developed. Such inconsistencies could have potential to misinform future development decisions. Consequently, here we present a spatiotemporal assessment of change in areal urban growth based upon medium resolution remote sensing through a single classification model. This provides the first accurate depiction of urban expansion for one of the world's fastest growing cities—Perth, WA. We present our findings and discuss the implications of more accurately classified urban extents in facilitating scientifically evidence-based adaptive and targeted planning policies to help reduce environmental and socio-economic consequences of poorly planned development.

4.2.1 Earth observation for monitoring urban change

Mapping the spatial extent and temporal profile of urban growth from medium resolution satellite imagery facilitates a consistent, detailed characterisation of the actual urban footprint of a city (Angiuli and Trianni, 2013; Bagan and Yamagata, 2012b). Other conventional spatial datasets such as Cadastral data provide information on freehold and Crown land parcel boundaries including attributes such as ownership and value for a singular temporal period (Thompson, 2015). However, attributed data for a singular year provides an ineffective portrayal of actual parcel land cover and temporal change. Thus, the methods and results presented in this study provide foundational information for the development of planning regulations that ensure sustainable growth of our cities, particularly in the reduction of environmental risks from ever-increasing expansion along the wildland–urban interface (Turner et al., 2010). Specifically, Earth Observation (EO) data allows spatially detailed identification of locations where (un)sustainable urban growth is occurring which enables expansion limits to be imposed through targeted policies (Bettencourt and West, 2010). In this theme, Schneider et al. (2005) determined the spatial distribution of development zones from 1978 to 2002 in Chengdu, Sichuan province, China in response to the Go West policy of the 1990s, aimed at economically boosting the West of the country. Whilst the policy was successful in raising Gross Domestic Product (GDP) levels, urbanisation concurrently increased, generating issues of urban management, including service, infrastructure and resource deficiency. Their results indicated spatial clustering, specialisation of

land use and peri urban development (not considered by the original policy) which were subsequently used to tailor policy in remediating issues, facilitating sustainable future urban development (Patino and Duque, 2013; Schneider et al., 2005). Similarly, Hepinstall-Cymerman et al. (2013) used classified Landsat data to monitor urban growth in regards to imposed growth boundaries in the Central Puget Sound, Washington, United States of America. Surprisingly, more new development occurred outside the growth boundaries than inside within their last time period, illustrating the ineffectiveness of the imposed policy leading to economic and ecological consequences, including a loss of avian diversity in native forest species (Hepinstall-Cymerman et al., 2013; Hepinstall et al., 2008). These studies highlight the potential effectiveness of EO data in consistently monitoring the spatiotemporal dynamics of urban development for applied policy outcomes and ensuring sustainable future planning decisions, for which such outputs are unachievable from traditional datasets.

4.2.2 The case of Perth

Perth's dramatic urban expansion can be attributed to Australia's minerals and energy boom commencing at the turn of the century. Queensland (QLD) and WA were at the forefront of the boom contributing the largest proportion of the nation's resources output, valued at 3.3% of GDP (ABS, 2015). In WA, mining and petroleum extraction dominate exports, peaking at 95% of the state's export earnings between 2010 and 2011 (Department of Mines and Petroleum, 2015). The increase in extraction was predominantly attributable to greater demand for raw materials from China, resulting in steady growth of the WA mineral and petroleum industry from AUD 4.7 billion in 1996 to a peak of AUD 121.6 billion mid-2013. However, in 2009, a 10.3% reduction in the overall value of mineral and petroleum resources resulted from falling commodity prices and the 2007–2009 global financial crisis (Department of Mines and Petroleum, 2015). Again in 2012, a further 9% reduction in resource value was observed as uncertainty in global economic conditions increased (Department of Mines and Petroleum, 2015). The largest decline to date occurred between 2014 and 2015, with an additional 22% reduction in the value of mineral and petroleum resources as a result of surplus capacity, decreased demand, and decline in the value of the Australian dollar (Department of Mines and Petroleum, 2015). The temporal trend in resource value indicates a stagnation and decline since late 2013 (Figure 4-1).

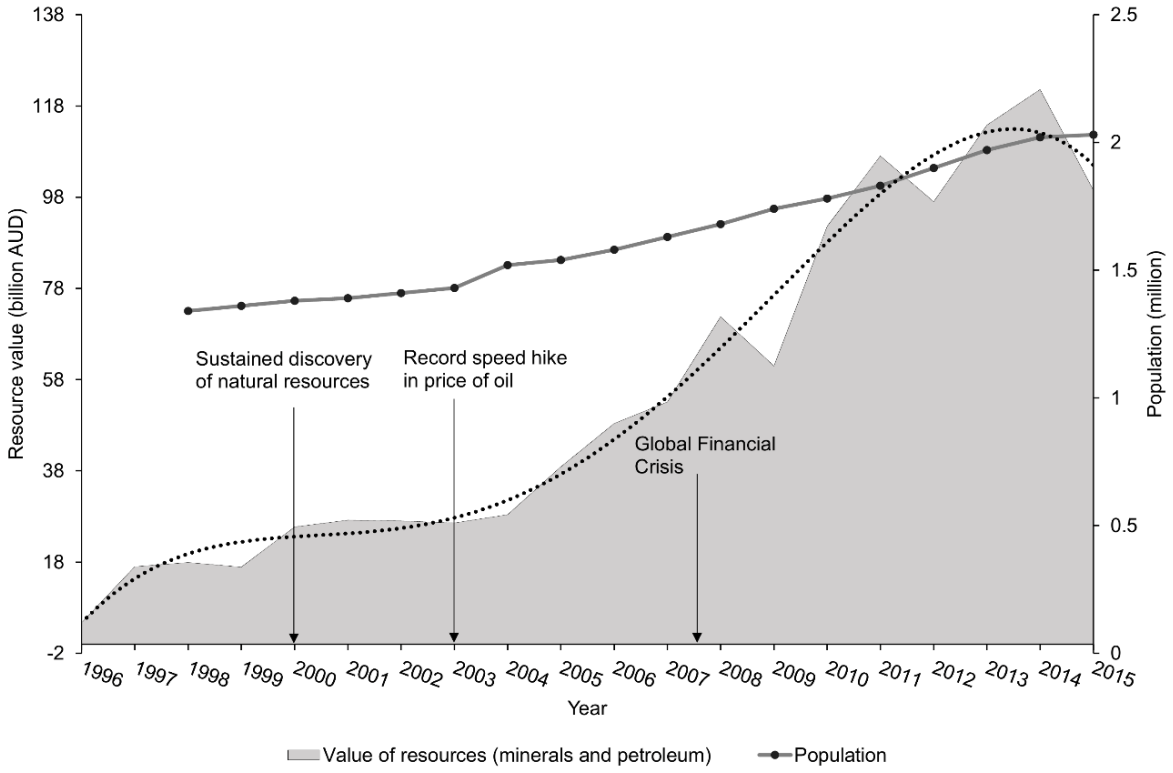

Figure 4-1. Timeline of natural resource value (based on Department of Mines and Petroleum annual reports) fitted with a fourth order polynomial trend line and population (based on Australian Bureau of Statistics data) also indicating key milestones.

Perth is described as one of the most isolated cities in the world (pop. > 1 million) and was Australia's fastest growing metropolis between 2007 and 2014; however, subsequent to a decline in natural resource value, a slowdown in population expansion soon followed (Figure 4-1) (Kennewell and Shaw, 2008). As a result, 2015 population statistics highlight the lowest population increase since records began with a 0.5% increase from the previous year (ABS, 2015; Kennewell and Shaw, 2008). In comparison to other Australian state capitals, based on the Australian Bureau of Statistics (ABS) 2011 population grid, Perth exhibits a relatively sparse spatial distribution of population with a maximum population density of only 3662 people per square kilometre (Melbourne 10,827; Sydney 14,747). Such low density population has generated high demand for dispersed housing, amenities and services, and has influenced changes to Perth's land use patterns in a non-strategic, "lot-by-lot fashion" based on a car-dependent lifestyle (Dhakal, 2014). Anthropogenic modifications of the landscape from vegetation cover to human-made impervious surfaces represent a critical driving force in both local and global environmental change (Kalnay and Cai, 2003; Vitousek et al., 1997). For example, abrupt, poorly planned and uncontrolled urban expansion can lead to environmental impacts which degrade ecological

systems including habitat fragmentation and socio-economic issues that deteriorate efficiency of amenity provisioning, both of which can exacerbate localised climate change (Downs, 2005; Turner et al., 2010). Identifying impacts of Land Use and Land Cover (LULC) change on socio-ecological systems is vital for future sustainable urban development; as reflected in the "sustainable cities and communities" 2030 sustainable development goal and the effective land use planning criteria of the City Resilience Framework (CRF) (ARUP and The Rockefeller Foundation, 2015; Vitousek et al., 1997). It is essential for Perth to adapt current practices of outward suburban expansion to achieve more sustainable urban growth and become city-smart for accommodating the predicted additional half a million new residents by 2031, which will result in an overall population exceeding 2.2 million (Western Australian Planning Commission, 2010a).

4.3 Materials and methods

4.3.1 Data preprocessing

EO data have been extensively used to monitor the sustainability of urban areas (Li et al., 2015; Song et al., 2016). However, accurate identification and temporal monitoring of urban land is frequently precluded due to the coarse resolution (300 m–1 km) of a number of commonly used remotely sensed datasets including nighttime lights (1 km) and the Moderate Resolution Imaging Spectroradiometer (MODIS) land cover product (0.083°) (Potere et al., 2009; Song et al., 2016). Whilst 30 m resolution data (e.g. Landsat) are more suitable to detect nuances of urban development the majority of studies and classified products which have used these finer resolution products implement large temporal windows, negating the possibility of detailed temporal urban characterisation (e.g. GlobeLand30, Hu et al., 2015; Masek et al., 2000; Suarez-Rubio et al., 2012; Van de Voorde et al., 2011; Xian et al., 2012). This research provides the first comprehensive temporal evolution analysis quantifying land cover change and associated urban expansion for the Perth Metropolitan Region (PMR) using 30 m Landsat imagery, the longest temporal record of medium spatial resolution imagery, for seven sequential time snapshots between 1990 and 2015.

Cloud free imagery was acquired in or close to the month of July for 1990, 2000, 2003, 2005, 2007, 2013 and 2015. Analysis of imagery acquired from WA winter season coincided with peak green-up which provided the greatest contrast between spectrally similar surfaces (e.g. bare earth and urban) (Herold et al., 2002; Lu et al., 2011; Varshney and Rajesh, 2014). Imagery date selection was founded upon the strong positive relationship between Australian soil moisture (related to rainfall) and the Normalised Difference Vegetation Index (NDVI) (Chen et al., 2014),

which exhibits an approximate one month lag between peak soil moisture and peak NDVI (Chen et al., 2014).

Productive photosynthesising plants use energy in the visible red (VIS) portion of the electromagnetic spectrum whilst reflecting in the near-infrared (NIR) region. NDVI ((NIR -VIS)/(NIR + VIS)) is a representative measure of growth allowing for the identification of green, healthy vegetation (Chen et al., 2014; Myneni et al., 1997; Piao et al., 2011), as illustrative of Southwest WA's winter months. A total of 14 images from Landsat 5 Thematic Mapper (TM) (eight images), Landsat 7 Enhanced Thematic Mapper Plus (ETM+) (two images) and Landsat 8 Operational Land Imager (OLI) (four images) were acquired for the specified years. Seamless images were produced based on Voroni diagrams that locate the bisector between images; adjacent edges were identified as seamlines constraining effective mosaic polygons that specify inclusion pixels for the final mosaicked product, permitting less visible boundaries through blending overlapping pixels (Pan et al., 2009). Mosaicked images were subsequently clipped to the original PMR study area boundary.

The atmospherically corrected Landsat data used in this study were obtained from the Landsat Ecosystem Disturbance Adaptive Processing System (LEDAPS) and the Landsat 8 Surface Reflectance (L8SR) algorithm (Hansen and Loveland, 2012; USGS, 2015). Some inherent residual noise remained, for example, due to the differences in modelled atmospheric correction parameters (Ju et al., 2012). To correct for this, surface reflectance values were standardised as:

$$p_{i,b} = \frac{p_{x,b}}{max_b} \tag{4.1}$$

where $p_{i,b}$ is the standardised pixel value i, from band b based on the original surface reflectance x, standardised through division of a priori specific upper reflectance limit for each band $(\max b)$: 0.1 (blue; 0.48 µm), 0.11 (green; 0.56 µm), 0.12 (red; 0.66 µm), 0.225 (near-infrared; 0.84 µm), 0.205 (shortwave-infrared; 1.65 µm), 0.150 (shortwave-infrared 2; 2.22 µm) (Sexton et al., 2013). Standardised values were then normalised per pixel j through cross band sum division:

$$p_{j,b} = \frac{p_{i,b}}{\sum_i p_{i,b}} \tag{4.2}$$

where $\sum_i p_{i,b}$ is the sum of each standardised pixel across all bands (Sexton et al., 2013). Normalised Landsat data obtained a statistically significant reduction of spectral variation per land cover class within (inter) and between (intra) each image (see Supplementary Figure 4-5).

4.3.2 Data classification

The normalised Landsat imagery was classified using the Import Vector Machine (IVM) which builds upon the popular Support Vector Machine (SVM) methodology (Roscher et al., 2012). In order to obtain the optimum classification, the IVM algorithm explores all possible subsets of training data for optimal selection (termed import vectors) which are derived through successively adding training data samples until a given convergence criterion is met (Roscher et al., 2012). Data samples are selected according to their contribution to the classification solution. However, a pure forward system is unable to remove import vectors that become obsolete after addition of other vectors. Therefore the implemented version of IVM utilised here is a hybrid forward/backward strategy that adds import vectors whilst concurrently testing if they can be removed in each step, thus leading to a sparse and more accurate solution (Roscher et al., 2012). Furthermore, the IVM selects data points from the entire distribution resulting in a smoother decision boundary which is based on the optimal separating hyperplane in multidimensional space compared to that of SVM algorithms (Braun et al., 2012). The benefits of the IVM algorithm have resulted in this approach being successfully applied in a number of studies (e.g. Braun et al., 2012, 2011; Roscher et al., 2010; Suess et al., 2014) due to its accuracy and performance advantages over alternative methodologies including SVM and the traditional Maximum Likelihood (ML) classifier (Braun et al., 2011; Roscher et al., 2010).

Model training samples were selected using the July 2005 Landsat 5 TM image coinciding with the month post maximum rainfall of all considered Landsat 5 TM and 7 ETM+ to facilitate optimum spectral seperability (Chen et al., 2014). Land cover was defined as high albedo urban (e.g. concrete), low albedo urban (e.g. asphalt) or other. Two urban classes were initially identified in order to reduce confusion between spectrally similarly classes (e.g. urban and bare earth) being merged post-classification to represent complete urban coverage (Hu and Weng, 2009). For each class, 250 pixels were randomly selected as training data, which is consistent with Foody and Mathur (2006) and Pal and Mather (2003) (see supplementary section 4.7.2). Training data parametrised the IVM algorithm, creating a classification model of spectral profiles that are compared to Landsat spectral profiles for classification. The classification model was then applied to all Landsat 5 TM and Landsat 7 ETM+ images obtaining similar spectral wavebands, considered to be equivalent (Flood, 2014). However, due to Landsat 8 OLI sampling different spectral regions, a new classification model was developed using the same training areas, as these were deemed to remain representative of the land cover, but with Landsat 8 OLI spectral wavebands (Flood, 2014; Roy et al., 2016). Validation was performed through an accuracy assessment based on an independent dataset (Google Earth high resolution imagery) consistent with Landsat acquisition months following previously published methods (e.g. Bagan and Yamagata, 2014; Cunningham et

al., 2015; Dorais and Cardille, 2011; Song et al., 2016; Sun et al., 2015; Zhu and Woodcock, 2014). For each land use category, 50 pixels per class per year were visually identified and classified based on the majority land cover within the coincident Landsat pixel from Google Earth imagery for the available years 2000, 2003, 2005, 2007, 2013 and 2015 consistent with recommended land cover accuracy sample size of Congalton (2001).

4.4 Results

The spatial footprint of PMR development has increased 48.61% between 1990 and 2015, over 320 km^2 (Figure 4-2 and Figure 4-3), with a 40.56% increase occurring since 2000. The classification accuracy assessment indicates an average overall accuracy of 81.06% and Kappa Coefficient of 0.73 being comparable to other studies (e.g. Bagan and Yamagata, 2014; Gislason et al., 2006; Luo et al., 2014; Sundarakumar et al., 2012) (see Supplementary Table 4-1 and Supplementary Table 4-2). Urban expansion mirrors population increase and as population growth has slowed, urban development has concurrently exhibited a levelling trend compared to expansion previously observed (Figure 4-3).

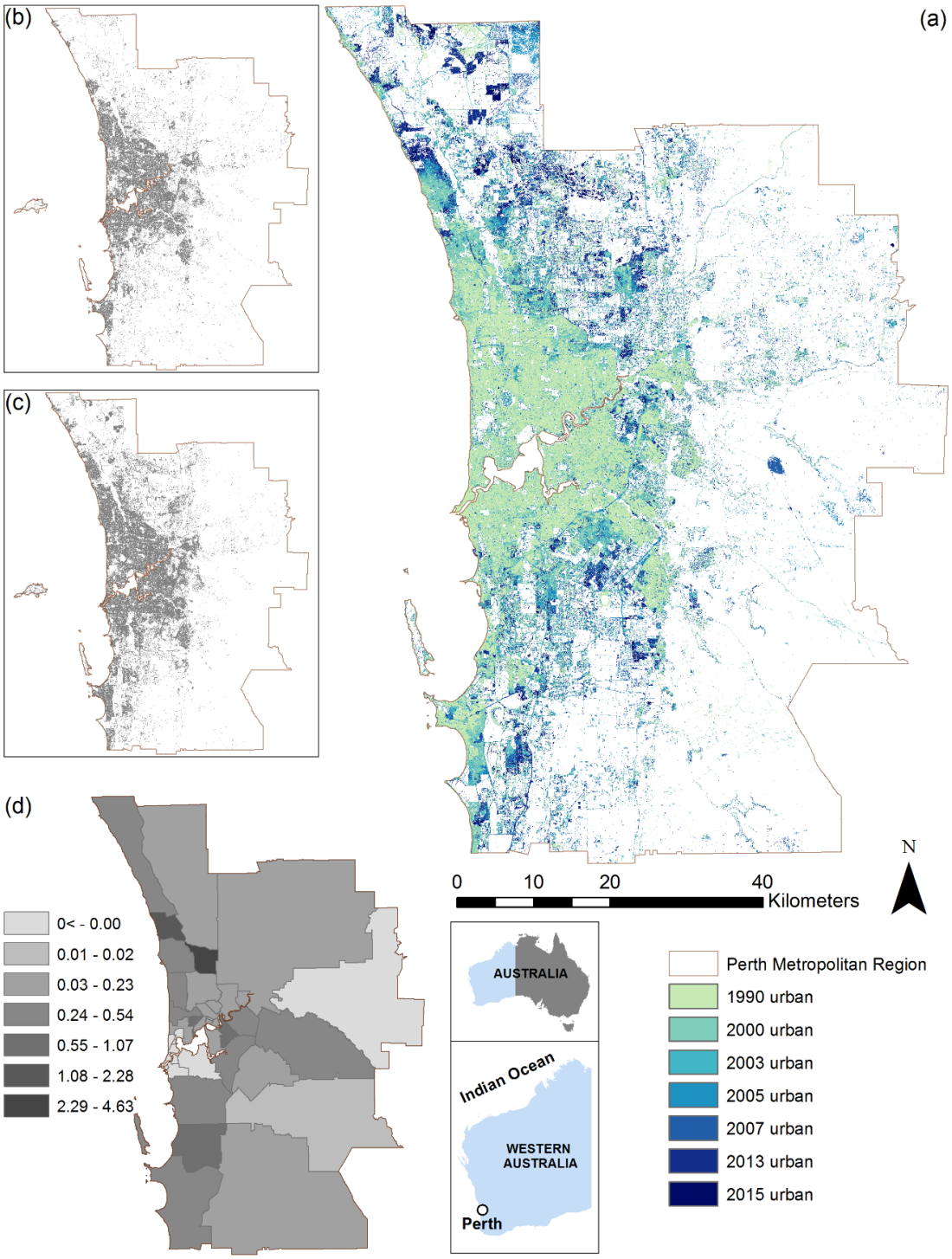

Figure 4-2. Urban expansion within the Perth Metropolitan Region (PMR) between 1990 and 2015. Vast urban growth has been observed in PMR with graduating colours exhibiting outward expansion (a); (b) and (c) exhibit static snapshots of urban extent from 2000 (b) and 2015 (c); whilst (d) depicts percentage of urban change per subnational administrative boundary (Local Government Area (LGA)).

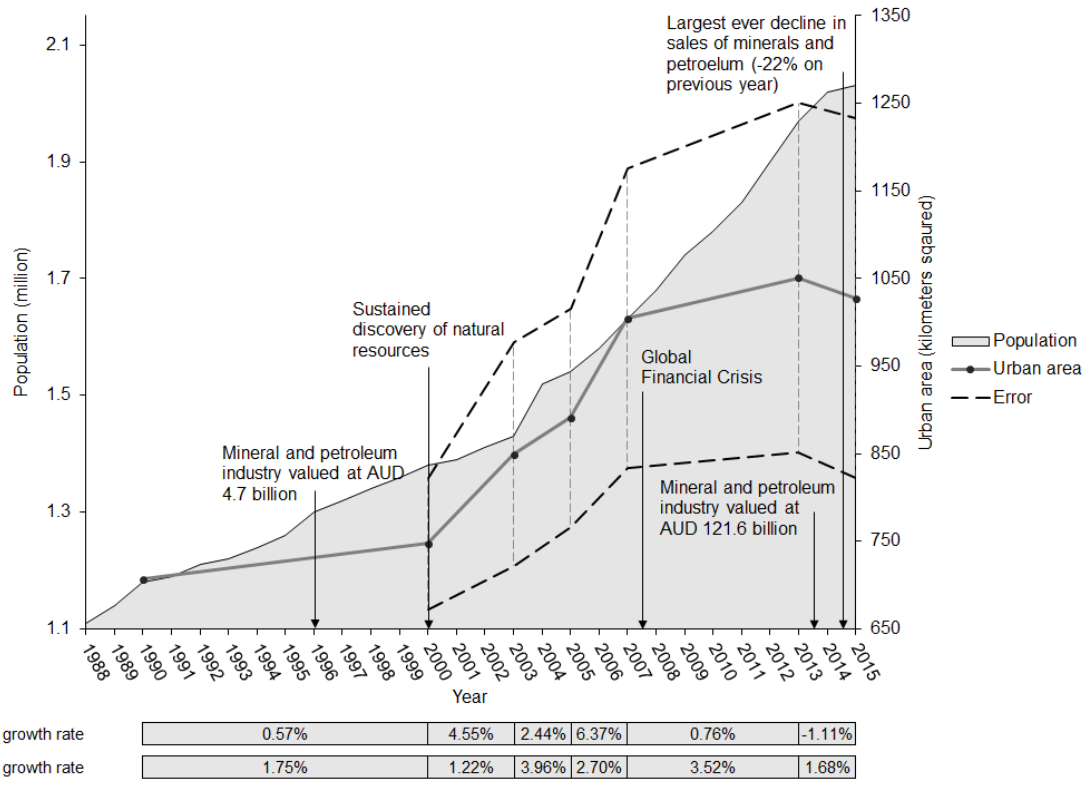

Figure 4-3. Time line of urban expansion in kilometers squared derived from Earth observation data with associated classification error derived from validation data (points indicating classified image years). Alongside population data in millions per year since 1988 (based on Australian Bureau of Statistics data, 2015 data is projected) with key natural resource milestones indicated, and average annual urban and average annual population growth rate indicated between classified image years.

WAPC's urban estimates of the PMR from Directions 2031 (the strategic plan for the Perth and Peel region) were provided for comparison to those produced within this study (Western Australian Planning Commission, 2010a). WAPC's estimates note an expansion from 637 km^2 to 813 km^2 between 2001 and 2012. Our results indicate an expansion of 747.41 km^2 to 1050.57 km^2 from 2000 to 2013 illustrating an overall underestimation by WAPC figures (Figure 4-4). Within suburban areas surrounding the two major cities in the metropolitan region, Perth and Fremantle, WAPC's estimates underrepresent the amount of urban area derived from EO, being more pronounced in 2013 than 2000. The Local Government Area (LGA) of Stirling South Eastern (LGA outlines displayed in Supplementary Figure 4-6) represented the maximum overestimation in 2013 urban area with 34.47% (2000: 9.95%) additional urban area per km^2 of LGA established on a difference of 2.89 km^2, 41.91% (2000: 0.83 km^2, 14.99%) between EO data and WAPC's estimates. Outer Northern and Southern LGA WAPC urban values were consistently underestimated, with

the LGA of Belmont representing the maximum underestimation of percent per km^2 of LGA in 2013 with 23.62% (2000: 12.60%) due to a difference of 9.37 km^2, 40.39% (2000: 5.00 km^2, 26.46%). Prior to 2009, WAPC's estimates were solely based upon land parcel valuations from the Western Australian Value General's Office, consequently valuation thresholds designating land to urban may have been inappropriately applied to outer suburban LGAs, where land might be developed but less valuable than central LGAs.

For urban estimates post 2005, two urban land zones, urban and urban deferred, are used within the Perth Metropolitan Region Scheme (MRS), the division of the State Planning Policy Framework applicable to the PMR, pursuant to the Planning and Development Act (2005) that inform recent WAPC land parcel based estimates (Western Australian Planning Commission, 2016b, 2010c). Urban land refers to locations where activities in line with urban development are permitted, but not necessarily constructed (e.g. housing and commercial use) whilst urban deferred represents land suitable for future development with remaining planning, servicing or environmental issues (Western Australian Planning Commission, 2016a, 2010c). For land to be assigned urban deferred, it must obtain characteristics of the urban zone including being able to provide essential services, a logical progression of development, and able to satisfy regional requirements (e.g. roads and open spaces). The 2012 WAPC estimates were derived from stock of land zoned urban or urban deferred, cadastral land plot and value information, conditional subdivision approvals, and ongoing regional rezoning and subdivisions (Western Australian Planning Commission, 2012). Similarly to 2000, valuation data may misrepresent suburban urban land cover resulting in overestimation. Inclusion of additional variables that are unrepresentative of actual land cover change (e.g. rezoning and conditional approvals) could exacerbate differences between WAPC and EO derived urban estimates (Figure 4-4 (b)), leading to the potential confounding of errors in WAPC estimates.

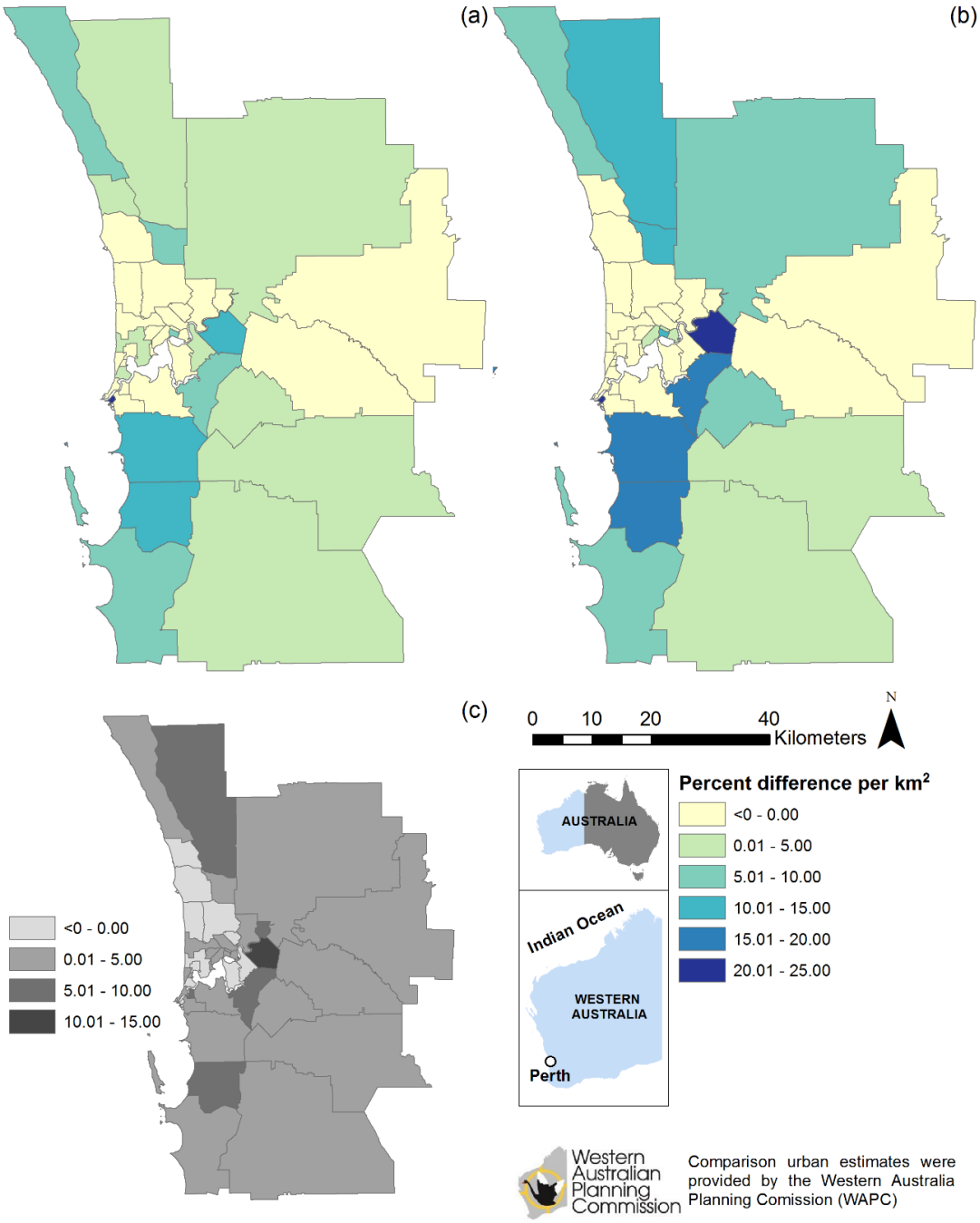

Figure 4-4. Percentage differences relative to local government area size, permitting a change metric standardised by Local Government Area (LGA) area between Earth Observation (EO) and the Western Australian Planning Commission's (WAPC) urban estimates for (a) 2000 (EO) and 2001 (WAPC) and (b) 2012 (WAPC) and 2013 (EO), whilst (c) depicts the percentage difference in the relative urban rate of change (km^2 per LGA area) between 2000 and 2013 (EO) and 2001 and 2012 (WAPC). Positive values indicate underestimation by WAPC whilst negative values represent overestimation by WAPC.

4.5 Discussion

WA state government planning documentation states that the majority of new development within the PMR has occurred as low-density suburban growth, responding to consumer preferences and market forces (Western Australian Planning Commission, 2015a). Additionally, sustainable policy objectives suggest that new development should be managed and focused on current communities, making the most efficient use of existing urban areas (Western Australian Planning Commission, 2010a, 2015a). Planning policy research has highlighted issues of outward urban expansion as being costly in economic, environmental and social terms based on dispersed service requirements, habitat fragmentation and neighbourhood segregation (Downs, 2005). Thus, urban expansion in the PMR may result in further economic, social and environmental costs associated with servicing and maintaining low-density lifestyles, owing to the rapid outward urban growth estimates between 2000 and 2007 (Downs, 2005; Turner et al., 2010).

In contrast, the witnessed slowdown of urban growth, population and natural resource value since 2013 indicates the possibility that the 'boom' of previous years has reached a turning point. Stagnation of urban growth implies that issues associated with spatially distributed urban areas might be contained to the current urban extent. Nevertheless, it is conceivable that prosperous future economic circumstances could initiate growth at a rate previously observed, and that the economic slowdown might be a temporary hiatus responding to current economic conditions (Perry and Rowe, 2014). For example, in 2014–2015, WA continued to attract the largest proportion of state mineral exploration expenditure at 58%, with QLD (the second ranked stated) obtaining only 20% (Department of Mines and Petroleum, 2015). Furthermore, as of September 2015, WA had an estimated AUD 171 billion in mineral and petroleum projects under construction, with a further AUD 110 billion allocated for future expansion (Department of Mines and Petroleum, 2015). Comparatively, during the peak (mid-2013) in terms of total sales, WA only had an estimated AUD 160 billion worth of projects under construction and a further AUD 108 billion for future development (Department of Mines and Petroleum, 2015). Whilst 2014–2015 observed the greatest decline in total sales of resources, sustained investment and improved global economics could reinvigorate the industry and reinitiate urban expansion within the PMR.

Future development (urban and urban deferred) is guided by Directions 2031 amending the MRS and local planning schemes (Western Australian Planning Commission, 2015b, 2015c, 2015d, 2015e, 2010a). WAPC aims to achieve 47% of future development as infill and a 50% increase in average residential density by 2050 of 10 dwellings per urban zoned hectare and 15 per new urban zoned hectare (Western Australian Planning Commission, 2010a). In monitoring progress towards the infill target, zoned development land within the PMR is considered, including

residential, industrial and commercial land uses (Western Australian Planning Commission, 2015a). Densities are defined as infill or greenfield if above or below an undocumented residential threshold from census data (Western Australian Planning Commission, 2016a). Initial results from Delivering Directions 2031, 2014 report indicate the requirement of a significant increase in infill development if the above targets are to be met (Western Australian Planning Commission, 2014). Similarly, average residential density monitoring has been achieved with land valuation data (from the Valuer General's Office) for major activity centres, being unrepresentative of actual density change and providing an incomplete metropolitan comparison (Western Australian Planning Commission, 2014). Inclusion of EO data would permit quantitative evidence of urban expansion, infill and density at a higher spatial and temporal frequency than current census based estimates. This would facilitate credible, evidence-based efficient targeted action founded upon improved representative urban area, insuring infill and density attainment. In this theme, Schneider et al. (2005) and Hepinstall-Cymerman et al. (2013) used spatial metrics (e.g. urban area mean patch size) based on classified Landsat data in either pre-defined census units (Hepinstall-Cymerman et al., 2013) or development corridors (Schneider et al., 2005) to monitor development type (infill or expansion) over time for adapting inappropriate static urban development policy. Using EO derived land cover data in this manner aids in understanding dynamics of the urban environment through monitoring, planning and mitigating land use changes that impact natural assets and increase vulnerability of city systems (Hepinstall-Cymerman et al., 2013; Miller and Small, 2003; Patino and Duque, 2013). Information of this sort aligns with criteria of the CRF in improving city resilience from effective land use planning, possible at lower expense and higher temporal frequencies than in situ measurements (ARUP and The Rockefeller Foundation, 2015).

The universal methodology implemented within this research lends itself to credibly inform policy in a similar manner in other global cities through monitoring urban expansion in order to identify rapid, unsustainable development. For example, Jakarta, obtaining the world's second largest urban area with a population of 28 million, has yet to have any quantitative urban area delineation (Pravitasari et al., 2015; Seto et al., 2011). Identification of actual urban growth in developing cities is vital to city planners, environment managers and policy makers due to the difference between planned growth and actual growth (Patino and Duque, 2013). Such information could be of critical importance for regulating urban expansion due to extreme poverty and high level of risk to environmental hazards, such as that posed from flooding (Marfai et al., 2014; Suryahadi and Sumarto, 2003). EO data presents many opportunities for added value within urban planning policy, and additional analyses could be pursued into specific human-induced environmental issues, such as detecting thermal changes in the urban environment for

planning issues associated with urban heat islands (e.g. cooling provisions) and their impact on human health (e.g. air quality).

4.6 Recommendations

Consistent and accurate LULC estimates are a vital aspect of sustainable urban development throughout the world, especially considering the predicted additional 2.5 billion city dwellers by 2050. LULC models that require agents that are representative of land use decisions can often fail in practicality due to the difficulty in quantifying driving forces of change and multi-level relationships. Models of this nature are also temporally independent, with each annual iteration implementing new data or data not representative of actual LULC change. EO data provides a replicable detailed representation of the complete urban extent requiring no additional data. The use and application of EO data reported within this paper highlights several improvements to WAPC policy for consistent urban area estimations with associated accuracy measures. Therefore it is recommended that planning authorities, such as WAPC, integrate EO data to achieve the following: (1) provide scientific urban estimates based on a temporally consistent model within future regional structure plans, metropolitan region and local planning schemes; (2) monitor infill development at a higher temporal frequency than census years for policy targeting to meet key goals; (3) monitor urban density through areal urban expansion compared to current metrics using land valuations; and (4) restrict development based on temporal urban analysis that degrades amenity efficiency and ecological systems whilst promoting development in locations to maximise efficiency and long-term sustainability. Additional EO datasets (e.g. finer resolution Sentinel 2 satellite imagery or aerial imagery) could be used to refine planning decisions based on areas of concern identified from Landsat. For example, finer spatial resolution datasets could facilitate enhanced feature extraction, optimising sustainable planning decisions through the identification of candidate infill sites. EO data of this nature provides an essential tool for timely planning policy that is adaptive to changes in urban landscape to mitigate socio-environmental issues associated with poorly planned urban areas for the future sustainability of our cities.

4.7 Supplementary material

This supplementary material section supports the main chapter and thesis through providing further detail into the summarised methods and results, pertaining to three concepts, namely the: standardisation and normalisation methodology, accuracy assessment and locations of Local Government Areas (LGAs). In the first instance a statistical comparison between the original un-corrected and corrected imagery is provided to highlight the reduction in inter and intra-year

variance for land cover types demonstrating the validity of a single classification model for multiple years of imagery. Whilst key overall accuracy metrics are provided within the main chapter this supplement provides additional measures for each classified image for appropriate contextualisation if used by other researchers (accessible online). Similarly, Supplementary Figure 4-6 supports Figure 4-4 and text comparing estimates produced within the main chapter to that of the Western Australian Planning Commission (WAPC) through visually identifying the LGAs. A short discussion surrounding other considered approaches and a list of data used within the chapter are also provided to demonstrate the entirety of analytical process.

4.7.1 Standardisation and normalisation

The non-urban land cover class was composed of four classes defined based on existing literature (e.g. Feyisa et al., 2016; Hu and Weng, 2009; Schneider, 2012) and study area characteristics. These classes were forest, water, grassland and bare earth. Grassland and forest were also merged to create a single vegetation class. A complete set of land cover classes enabled examination of statistical differences generated from normalisation (Supplementary Figure 4-5). The Coefficient of Variation (CV) statistic was calculated to describe the amount of variability relative to the mean spectral reflectance of the post classification datasets (Brown, 1998). The CV was calculated for pre- and post-normalisation datasets for both intra-year class reflectance, which describes the variability within each class per year, and the inter-year reflectance, which describes the variability of each class across all imagery dates. Post-normalised Landsat data exhibited statistically significant lower inter- and intra-CV with $T = 0$, $Z = -2.154$, $p = 0.016$, $r = -0.359$ and $T = 0$, $Z = -2.418$, $p = 0.008$ $r = -0.373$, respectively. The test statistic (T) was obtained from dataset differencing (pre- minus post-processed images), representing the lowest value of the sum of positive ranks (values increased) or negative ranks (values decreased). Hence, $T = 0$ dictates that post-processed data consistently obtained a lower value than pre-processed imagery, statistically significant at $p < 0.05$ (Field, 2009). Therefore, reduced intra and inter year variance facilitates more appropriate one model classification for Landsat 5 TM and Landsat 7 ETM+ and another for Landsat 8 OLI.

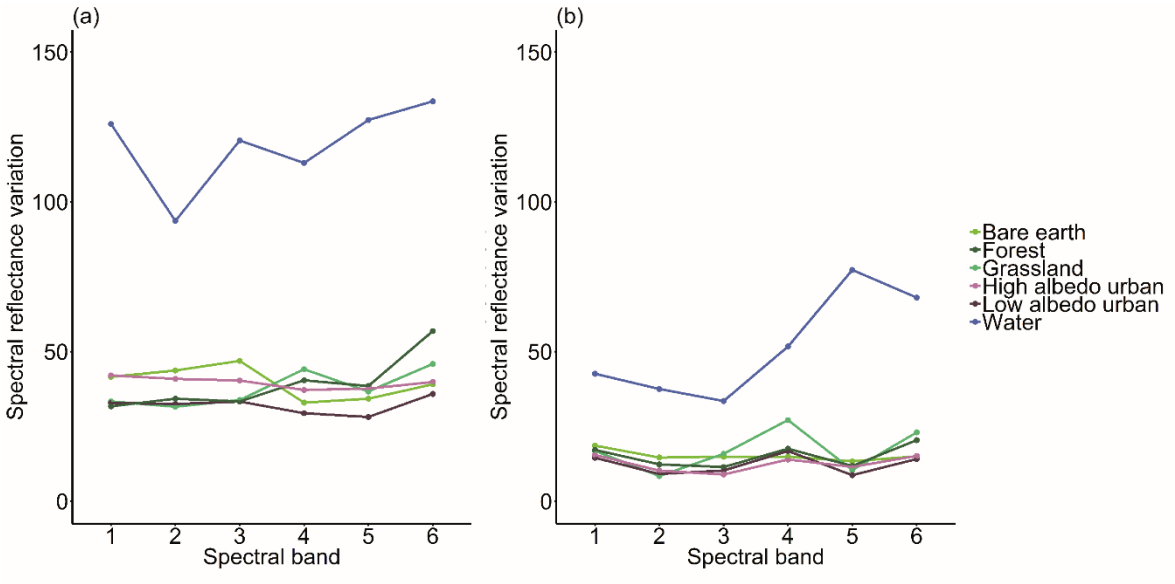

Supplementary Figure 4-5. Inter year classification reflectance variation categorised by classified output for each spectral band for: pre (a) and post (b) normalisation correction.

4.7.2 Accuracy assessment

For each land use category, 50 random pixels per class per year were visually identified and classified based on the majority land cover within the coincident Landsat pixel from Google Earth imagery for the available years: 2000, 2003, 2005, 2007, 2013 and 2015 (Congalton, 2001). Both user's accuracy (fraction of correctly classified pixels relative to all others classified as a particular land cover), producer's accuracy (fraction of correctly classified pixels compared to ground truth data) and associated Kappa coefficients were consistently high except for the producer accuracy of bare earth which has an average accuracy of 53.33% (Supplementary Table 4-1 and Supplementary Table 4-2). This is due to the known spectral similarities between bare earth and impervious surfaces, and water and shadow which resulted in spectral confusion during classification (Feyisa et al., 2016; Herold et al., 2002; Lu et al., 2011; Sawaya et al., 2003; Varshney and Rajesh, 2014).

Supplementary Table 4-1. Classification accuracy and associated Kappa Coefficient per year of classified Landsat.

Year	Accuracy (%)	Kappa Coefficient
2000	82.33	0.75
2003	80.33	0.72
2005	82.00	0.74
2007	84.00	0.78
2013	79.00	0.70
2015	78.67	0.70
Average	81.06	0.73

Supplementary Table 4-2. Producer's and User's accuracy per year of classified Landsat imagery.

Producer Accuracy	Bare Earth	Vegetation	Urban	Water
2000	56.00	96.00	90.00	66.00
2003	50.00	97.00	85.00	68.00
2005	52.00	98.00	86.00	72.00
2007	48.00	98.00	83.00	94.00
2013	52.00	99.00	81.00	62.00
2015	62.00	99.00	80.00	52.00
Average	53.33	97.83	84.17	69.00
User Accuracy	**Bare Earth**	**Vegetation**	**Urban**	**Water**
2000	84.85	76.80	84.11	94.29
2003	69.44	76.98	83.33	94.44
2005	81.25	78.40	81.13	97.30
2007	68.57	80.33	87.37	97.92
2013	68.42	73.88	83.51	100.00
2015	75.61	73.88	83.33	89.66
Average	74.69	76.71	83.80	95.60

4.7.3 Local government areas

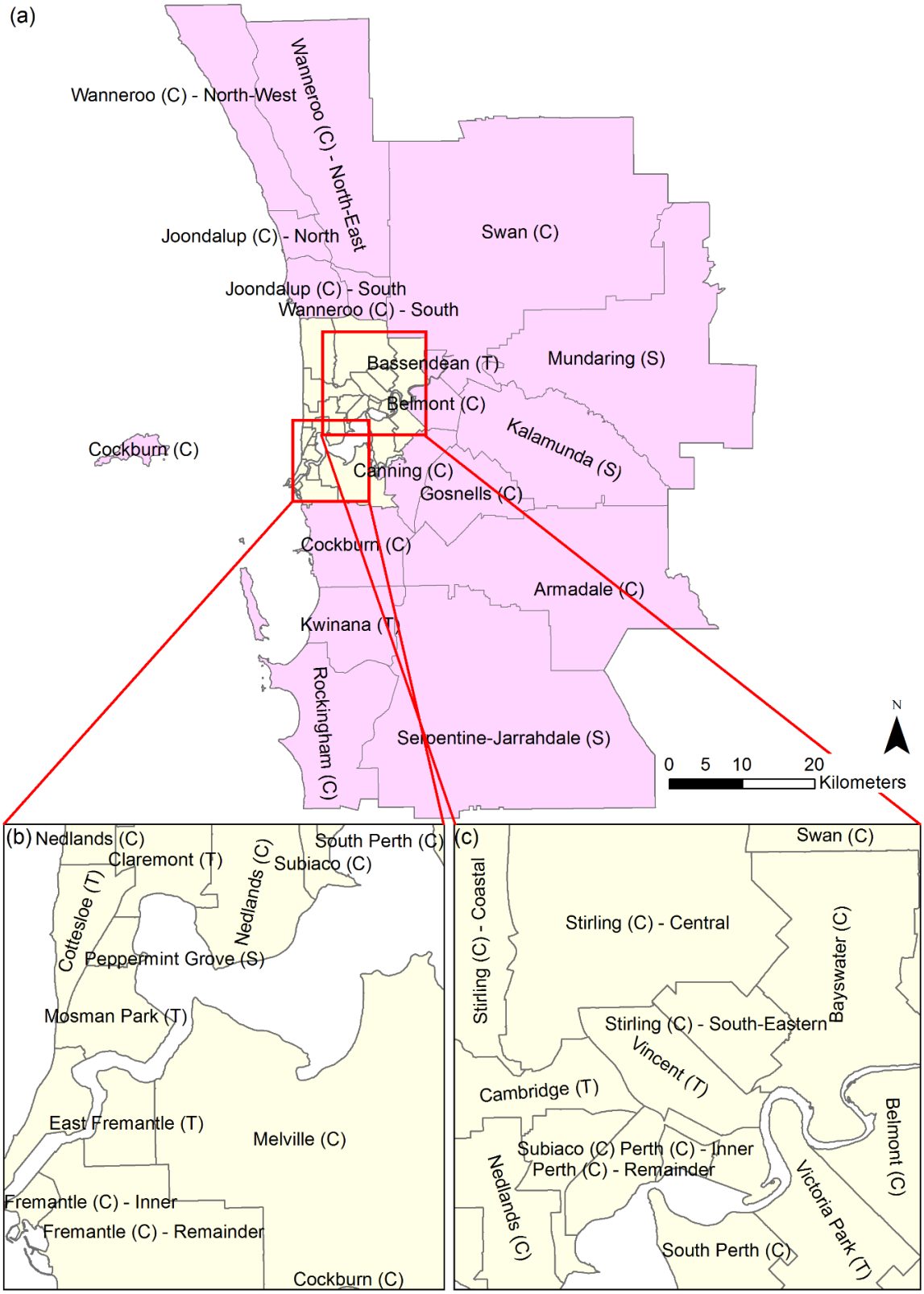

Supplementary Figure 4-6. Local Government Areas (LGAs) located in Perth Metropolitan Region (a); with (b) exhibiting LGAs South and West of the Swan River and (c) LGAs North and East of the Swan River.

4.7.4 Other considered data and approaches

In classifying the Landsat data a multitude of alternative approaches were attempted before arriving at one detailed within the main chapter. These included the use of different pre-processing data methodologies, classifiers and data combinations. Originally raw uncorrected (digital number) Landsat data was corrected using the Atmospheric Radiometric Calibration of Satellite Imagery (ARCSI) tool that makes use of the Py6S radiative transfer model (Bunting, 2017). However, due to the lack of availability of a number of required model parameters Landsat surface reflectance data was preferenced for consistency and repeatability. Numerous other classifiers and data combinations were tested including Support Vector Machines (SVMs) (Mountrakis et al., 2011), Multiple Endmember Analysis (MESMA) (Powell and Roberts, 2008), spectral indices such as the Normalised Difference Spectral Vector (NDSV) (Angiuli and Trianni, 2013) and classification of multi-temporal Landsat surface reflectance composites (Castrence et al., 2014). Nevertheless these were all found to produce unfavourable results in comparison to the presented approach or were unable to compute sub-pixel estimates (required within further chapters). Further information and discussion on these approaches is provided within section 2.2.

In a similar theme alternative data sources were considered and tested for classification validation such as GlobeLand30 (Chen et al., 2015) and the European Space Agency's (ESA) Climate Change Initiative (CCI) annual global land cover (300 m) time series (1992-2015) (European Space Agency, 2017). However, these products are constrained by limited temporal frequency (e.g. GlobeLand30), inadequate resolution (e.g. CCI), their own internal errors (e.g. based upon an accuracy assessment) and selection of global reference data that could fail to represent the land cover heterogeneity within the Perth Metropolitan Region. Consequently this prior work and reasoning guided the analysis undertaken in chapter 4.

4.7.5 Chapter data list

This section provides an overview of the data presented and analysed within this chapter.

Supplementary Table 4-3. Summary of the data, sources and applications used within chapter 4.

Data	Source	Application
Annual population data	Australian Bureau of Statistics	Contextual information
Annual natural resources value	The Government of Western Australia, Department of Mines and Petroleum annual reports	Contextual information
Landsat surface reflectance data, path 112 and 113, row 82 **Dates and paths** 1990: 14/04 (path 112), 7/05 (path 113) 2000: 23/08 (path 112), 1/10 (path 113) 2005: 12/07 (path 112), 19/07 (path 113) 2007: 6/10 (path 112), 9/07 (path 113) 2013: 22/10 (path 112), 13/10 (path 113) 2015: 9/08 (path 112), 17/09 (path 113) **Sensors** Landsat 5 TM: 1990, 2003, 2005, 2007 Landsat 7 ETM+: 2000 Landsat 8 OLI: 2013, 2015	United States Geological Survey Earth Explorer system	Land cover analysis
High resolution data (read only)	Google Earth	Accuracy assessment
Comparison urban estimates	Western Australian Planning Commission	Comparison to the Commission's estimates
Spatial boundary outlines	Australian Bureau of Statistics	Comparison to the Commission's estimates

4.8 Associated published data

The classified Landsat data presented within this chapter are archived at the Pangaea open access data publisher for Earth and Environmental Science: https://doi.pangaea.de/10.1594/PANGAEA.871017. The following is taken from the abstract associated with the published data set.

This dataset represents land cover for 7 sequential snapshots (1990, 2000, 2003, 2005, 2007, 2013 and 2015) over the Perth Metropolitan Region (PMR), Western Australia (WA) derived from medium resolution Landsat data. Cloud free imagery was acquired in or close to the month of July coinciding with WA's winter months coinciding with peak green-up facilitating the greatest contrast between spectrally similar surfaces (e.g. bare earth and urban). Imagery was first standardised and normalised to remove inherent residual noise (e.g. differences in modelled atmospheric correction parameters) whilst permitting classification of all imagery based upon a single classification model. The model was computed from the 2005 image representing the month post maximum rainfall of all considered imagery associated with peak greenness and maximum spectral separability. Classification of the normalised data was achieved with the Import Vector Machine (IVM) algorithm following a hybrid forward/backward strategy that adds import vectors whilst continuously testing validity in each step, producing a sparse and more accurate classification solution. Classified land cover data is provided in raster format (.tif) and divided into the classes: bare earth (1), grassland (2), low urban albedo (e.g. asphalt (3)), water (4), forest (5) and high urban albedo (e.g. concrete (6)). Please see MacLachlan et al. (2017a) for further details.

Chapter 5 Subpixel land cover classification for improved urban area estimates using Landsat

5.1 Abstract

Urban areas are Earth's fastest growing land use that impact hydrological and ecological systems and the surface energy balance. The identification and extraction of accurate spatial information relating to urban areas is essential for future sustainable city planning owing to its importance within global environmental change and human-environment interactions. However, monitoring urban expansion using medium resolution (30-250 m) imagery remains challenging due to the variety of surface materials that contribute to measured reflectance resulting in spectrally mixed pixels. This research integrates high spatial resolution orthophotos and Landsat imagery to identify differences across a range of diverse urban subsets within the rapidly expanding Perth Metropolitan Region, Western Australia. Results indicate that calibrating Landsat derived sub-pixel land cover estimates with correction values (calculated from spatially explicit comparisons of sub-pixel Landsat values to classified high resolution data which accounts for over (under) estimations of Landsat) reduces moderate resolution urban area over (under) estimates by on average 55.08% for the Perth Metropolitan Region. This approach can be applied to other urban areas globally through use of frequently available and/or low cost high spatial resolution imagery (e.g. using Google Earth). This will improve urban growth estimations to help monitor and measure change whilst providing metrics to facilitate sustainable urban development targets within cities around the world.

5.2 Introduction

Urban areas are estimated to cover only 0.5% of Earth's surface yet are one of the fastest growing land use per area basis (Bettencourt and West, 2010; Schneider et al., 2010, 2009). Population growth has resulted in increased urbanisation with 54% of the planet's seven billion people in 2014 residing in urban areas with an additional 2.5 billion urban dwellers projected by 2050, whilst concurrently increasing the proportion of world's urban population to 66% (Powell et al., 2007; Powell and Roberts, 2010; Sexton et al., 2013; Sharifi and Lehmann, 2014; Song et al., 2016; United Nations, Department of Economic and Social Affairs, 2014). Alteration of natural land cover to anthropogenic impervious surfaces has been identified as the most extreme cumulative effect of land cover change, generating numerous socio-economic consequences including: amenity provision efficiency, ecological degradation and the Urban Heat Island (UHI) effect (Cai et

al., 2016; Howard, 1988; Hu and Brunsell, 2015; Xie and Zhou, 2015). Accurate information on urban land use and land cover is therefore imperative for monitoring expansion and planning policy targeting for future sustainable development of our cities (Bettencourt and West, 2010; Wu and Murray, 2003). Earth Observation (EO) enables consistent, detailed characterisation of the actual urban footprint of a city having been mapped and monitored using remotely sensed data at a range of spatial and temporal scales for associated implications (Akbari et al., 2003; Friedl et al., 2002; Imhoff et al., 1997; Schneider et al., 2010; Sexton et al., 2013). However, accurate and consistent monitoring of urban land cover is frequently precluded by coarse spatial (e.g. 1 km Moderate Resolution Imaging Spectroradiometer (MODIS) land cover product) and temporal (e.g. 2000 and 2010 GlobeLand30 product) resolution of such datasets (Lu et al., 2014; Song et al., 2016).

Urban mapping remains challenging due to the heterogeneity of surface materials and surface structure which contributes to pixel surface reflectance that are often difficult to disentangle (Herold et al., 2002; Lu et al., 2011; Schneider, 2012; Varshney and Rajesh, 2014). When delineating urban land cover from remotely sensed data, spatial resolution is considered the most important factor which provides increased visibility of discrete surface features (e.g. buildings) and greater pixel homogeneity over medium to coarse spatial resolution satellite imagery (e.g. Landsat and MODIS) (Myint et al., 2011). Nevertheless, high spatial resolution data often lack temporal acquisition consistency (e.g. airborne orthophotos) or are expensive to purchase (e.g. commercial satellite imagery). Consequently, in order to best monitor urban land use and land cover change, datasets must have an adequate spatial and temporal resolution to discern change. In this regard, data from the Landsat series of satellites provides the longest time-series of consistent, medium spatial resolution imagery that has been extensively applied to urban area mapping (Powell et al., 2007; Schneider and Mertes, 2014; Song et al., 2016; Sundarakumar et al., 2012; Wilson et al., 2003; Yuan et al., 2005).

Accurate quantification of anthropogenic landscape modification is of critical importance due to associated environmental, anthropogenic and climatic impacts (Kalnay and Cai, 2003). Urban estimates from Landsat data have been used within global biogeochemistry and climate models (Zhu and Woodcock, 2014), further scientific studies such as UHI investigations (Hu et al., 2015) and targeted urban development policies (Hepinstall-Cymerman et al., 2013; Schneider et al., 2005). Whilst comparative studies (e.g. Li et al., 2014) have shown marginal holistic image accuracy difference between algorithm selection on per-pixel Landsat classification assuming sufficient training data. Traditional per-pixel methods, such as the maximum likelihood classifier (discussed in supplementary section 5.9.1), have been found to significantly over or underestimate urban area from Landsat data (Lu et al., 2011; Wu and Murray, 2003). Addressing

this error is important when accurate classifications are required for monitoring change in land use patterns whereby calculations of urban extent can influence decision-making (e.g. policy for sustainable urban development) (Bagan and Yamagata, 2014; Hepinstall-Cymerman et al., 2013; Miller and Small, 2003; Schneider et al., 2005).

Due to the heterogeneity of urban areas, sub-pixel classification methodologies have been increasingly applied to medium spatial resolution data to more accurately represent the mixture of land covers within a pixel (Lu et al., 2011; Lu and Weng, 2006; Powell and Roberts, 2008; Wang et al., 2013; Weng and Pu, 2013). This has been achieved through variations of Spectral Mixture Analysis (SMA) where a set number of representative endmembers, frequently following the Vegetation, Impervious and Soil (V-I-S) framework, are used to model the entire image based on their spectral characteristics (Powell et al., 2007; Ridd, 1995). However, endmembers may not fully represent image spectral variability or a pixel may be modelled by endmembers that do not represent materials within its field of view resulting in an inability to adequately portray the high spectral heterogeneity of the urban landscape (Powell et al., 2007). Support Vector Machine (SVM) spectral unmixing attempts to resolve this issue through consideration of a large number of training pixels which provides preferential accuracy in comparison to SMA although high dimensional data and large training samples can hinder its performance (Wang et al., 2013).

Comparatively the novel sub and hard pixel Import Vector Machine (IVM) classifier permits simultaneous multi-class comparison whilst continuously testing training samples for validity providing a more accurate solution (Roscher et al., 2012). IVM has been found to consistently outperform decision trees, artificial neural networks and maximum likelihood algorithms (Huang et al., 2002; Kotsiantis et al., 2006; Watanachaturaporn et al., 2008), with preferential (Braun et al., 2012) and comparable results to SVM (Roscher et al., 2010). However, due to the heterogeneity of urban areas it is important to calibrate these sub-pixel approaches against high spatial resolution data that capture the diverse characteristics found within urban environments (Lu et al., 2011). Perth, Western Australia (WA) is characterised by extensive urban diversity, surpassing all other major Australian and United States cities in terms of suburban development (Kelly et al., 2011; U.S. Department of Commerce, 2013). It therefore provides a suitable case study for assessing the ability of Landsat to map urban development, which is a pre-requisite for appropriate policy incorporation. This paper describes an approach to map the urban extent of the Perth Metropolitan Region (PMR) using an IVM classifier applied to medium spatial resolution imagery. The impact of sub-pixel land cover heterogeneity is investigated by comparing the urban area estimates to those derived from very high spatial resolution (20 cm) imagery. An innovative, spatially explicit correction to account for over (or under) estimation of urban area is derived which improves the urban land cover estimates from medium resolution imagery.

5.3 Study area

The PMR (Figure 5-1 (a)), WA has experienced sustained urban development since the 21st century in response to a rapidly growing resource sector (Kennewell and Shaw, 2008). The majority of recent urban growth within the PMR has transpired as outward low-density development resulting in a maximum population density of 3,662 km^2 which is 33.45% and 24.83% lower than Melbourne (10,827) and Sydney (14,747) respectively (ABS, 2015; Western Australian Planning Commission, 2015a). The notion of the 'Australian dream', depicted as detached living in a green suburb, is most pronounced in Perth (Western Australian Planning Commission, 2013a). As a result 79% of the current housing is detached, compared to 62% in Sydney, 72% in Melbourne and a national average of 74% (Kelly et al., 2011; Western Australian Planning Commission, 2013b). Globally, Australia surpasses other developed countries in terms of detached suburban living with England having 42% of housing as either detached or semi-detached (Department for Communities and Local Government, 2015). Similarly only 64.2% of United States of America (USA) housing stock is detached, with Perth eclipsing all of the major 25 USA metropolitan areas in terms of detached housing (U.S. Department of Commerce, 2013). Low population density and outward expansion witnessed in Perth has generated high demand for dispersed amenities and services in a non-strategic, "lot-by-lot fashion" (Dhakal, 2014). Suburbanisation of this nature has been identified as unsustainable due to impacts on ecological systems (e.g. habitat fragmentation) and socio-economic issues (e.g. amenity provisioning costs), with accurate urban area identification essential for sustainable future planning and maximum resource efficiency, particularly in Perth owing to its globally high suburbanisation and distributed population (Western Australian Planning Commission, 2013a).

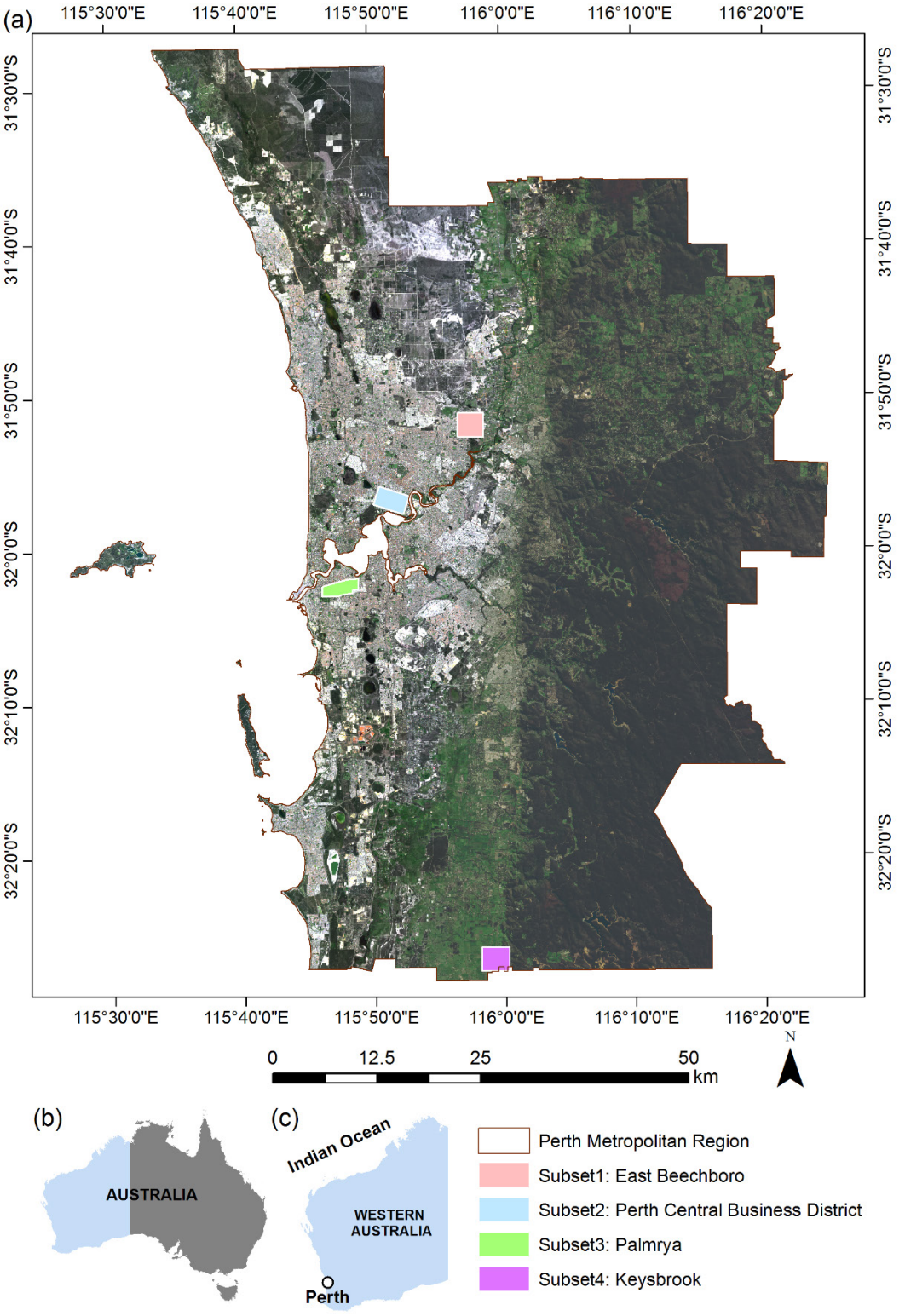

Figure 5-1. Landsat 8 Operational Land Imager (OLI) true colour image mosaic of the Perth Metropolitan Region (9 August 2015 [path 112] and 17 September 2015 [path 113]). The locations of the high spatial resolution aerial image subsets are indicated by coloured overlays (a), with Western Australia identified in (b) and Perth city (c).

Therefore, the PMR provides a globally diverse range of urban characteristics (e.g. compact urban central business district, older residential areas and new suburban developments) facilitating broad dataset comparison opportunities between Landsat and high spatial resolution urban area estimates. The high spatial resolution data identifies the complexity of these suburban and urban areas, which is obscured in medium and coarse spatial resolution datasets. This permits the extraction of individual features such as buildings, roads and vegetation that compose the urban environment and which are represented as a spectrally mixed pixel in Landsat imagery (illustrated in Figure 5-2) (Myint et al., 2011).

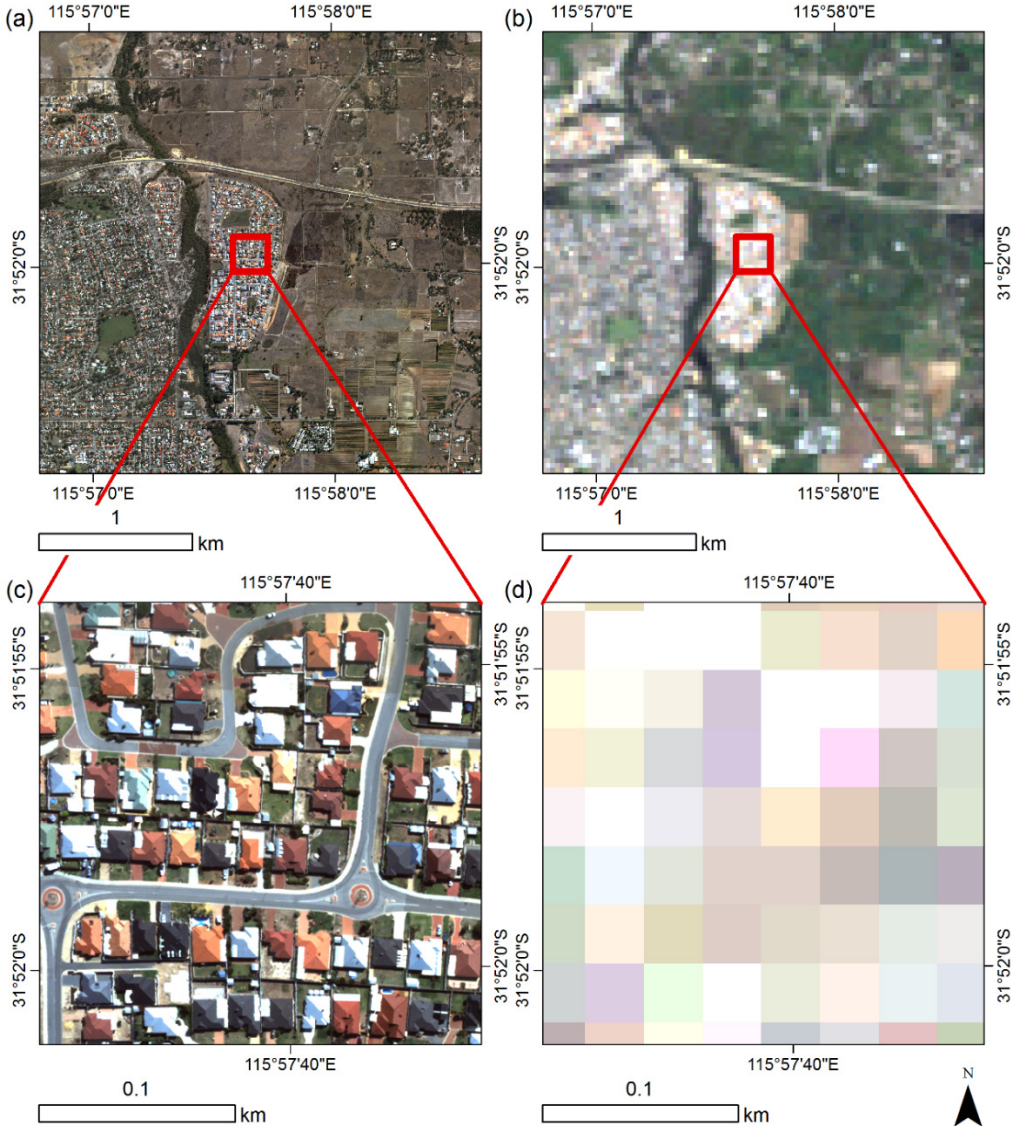

Figure 5-2. Comparison of true colour high spatial resolution data (a) (acquired from 14 March 2007) and Landsat surface reflectance (b) (acquired on 6 October 2007 [path 112]), highlighting the spatial detail captured by high-resolution imagery (c) and the same areas as observed by Landsat (d) for the subset East Beechboro used within this study.

Definitive feature detection from high resolution data can assist in refining urban area estimates produced from moderate spatial resolution satellite imagery (Lu et al., 2011; Wu and Murray, 2003). More accurate satellite derived urban area estimates are imperative for ensuring appropriate data use for policy and environmental variable applications in order to mitigate the consequences of unsustainable urban development. This aligns with the criteria of effective land use planning within the City Resilience Framework (CRF) which is designed to improve city resilience (ARUP and The Rockefeller Foundation, 2015).

5.4 Data

5.4.1 Landsat data

Cloud free Landsat scenes were obtained for 2007 from Landsat 5 Thematic Mapper (TM), coinciding with high resolution orthophotos (described in section 5.4.2). Imagery were acquired within winter months (9 July 2007 for path 113 and 6 October 2007 for path 112) corresponding with peak vegetation green-up which limits issues concerning the spectral separation between senescent vegetation, bare earth and some impervious surfaces (Chen et al., 2014; Feyisa et al., 2016). Landsat imagery was processed to standard terrain correction (Level 1T), geometrically and topographically corrected using Ground Control Points (GCPs) and a Digital Elevation Model (DEM) from the Global Land Survey 2000 dataset (Hansen and Loveland, 2012). Landsat 5 TM surface reflectance values were derived from the Landsat Ecosystem Disturbance Adaptive Processing System (LEDPAS) (Hansen and Loveland, 2012; Masek et al., 2006) which corrects for atmospheric effects using the Second Simulation of a Satellite Signal in the Solar Spectrum (6S) radiative transfer model (Vermote et al., 1997).

5.4.2 High spatial resolution airborne imagery

Radiometrically calibrated multispectral red (0.58-0.77 µm), green (0.48-0.63 µm), blue (0.41 µm - 0.54 µm) and near-infrared (0.69-1.00 µm) orthophotos were acquired over 19 cloud free days commencing on 14 March 2007 as part of the Perth and Peel Urban Monitor Programme (Caccetta et al., 2012). Aerial imagery, obtained between 10:00 and 14:00 to reduce shadow effects, were captured using a Microsoft UltraCAM-D at a height of 1300m resulting in a spatial resolution of 20 cm. Forward and side frame overlap of 60% and 30% respectively permitted automatic Digital Surface Model (DSM) extraction using geometric control points provided by WA's land information authority (Landgate). Extraction of ground points exclusively representing terrain variations facilitated derivation of a Ground Elevation Model (GEM) which, when

subtracted from the DSM, generated a Relative Elevation Model (REM), depicting elevation relative to ground points.

Spatial and temporal inconsistencies in reflectance can arise from atmospheric scattering and absorption; instrument noise and Bidirectional Reflection Distribution Function (BRDF) effects. The latter describes the systematic variation in reflectance across an image due to differences in view and illumination angles and which is dependent on the surface 3D structure (Collings et al., 2011). The orthophotos were provided as a surface reflectance product, corrected for multiplicative and additive errors over frames (e.g. instrument noise and atmospheric effects) and within frame viewing and illumination geometry (Caccetta et al., 2012; Collings et al., 2011). Image preprocessing consisted of two steps. Firstly, a combined BRDF and atmospheric correction procedure was applied to retrieve surface reflectance for each image acquisition. Linear BRDF model parameters from the Li Sparse reciprocal kernel (Wanner et al., 1995) were used to correct for BRDF effects. Atmospheric perturbations were corrected by assuming that the obtained digital number represented the relative reflectance affected by spatially dependent multiplicative and additive terms. These combined steps generated an internally consistent mosaicked dataset. 'True' surface reflectance was estimated through fitting global offset and gain values to replicate laboratory measured calibration targets based on the assumption that relative reflectance requires a linear transformation to true reflectance (Collings et al., 2011).

5.5 Methodology

5.5.1 Landsat preprocessing

The two Landsat scenes covering the study area were combined to form a seamless image mosaic following the methodology of Pan et al. (2009). Voroni diagrams were created on the bisector between images with adjacent edges defined as seamlines, identifying effective mosaic polygons that specify pixels from each image to include in the final mosaic, facilitating less visible boundaries through blending of overlapping pixels (Pan et al., 2009) (Figure 5-1 (a)). Due to remaining residual noise in the mosaicked imagery caused by factors such as the brightening effect of thin clouds and atmospheric correction differences, surface reflectance values were standardised following the approach identified by Sexton et al. (2013):

$$p_{i,b} = \frac{p_{x,b}}{max_b} \tag{5.1}$$

where $p_{i,b}$ is the standardised pixel value i, from band b based on the original surface reflectance x, standardised through division by a waveband specific upper reflectance limit which are: 0.10

(blue; 0.48µm), 0.11 (green; 0.56µm), 0.12 (red; 0.66µm), 0.23 (near-infrared; 0.84µm), 0.21 (shortwave-infrared; 1.65µm), 0.15 (shortwave-infrared 2; 2.22µm). The standardised values ($p_{i,b}$) were then normalised against the summed band standardised values:

$$p_{j,b} = \frac{p_{i,b}}{\sum_i p_{i,b}} \tag{5.2}$$

where $\sum_i p_{i,b}$ is the sum of each standardised pixel across all bands (Sexton et al., 2013). This approach has been found to satisfactorily reduce variations generated from inherent residual noise across mosaicked imagery, for example due to differences in modelled atmospheric parameters within the LEDAPS algorithm (Luo et al., 2014; Sexton et al., 2013) (Figure 5-3 (a)). Statistical assessment of image radiometric normalisation provided in MacLachlan et al. (2017a) found that the post-processed Landsat data exhibited significantly lower inter and intra Coefficient of Variation (CV) when compared to the pre-processed data.

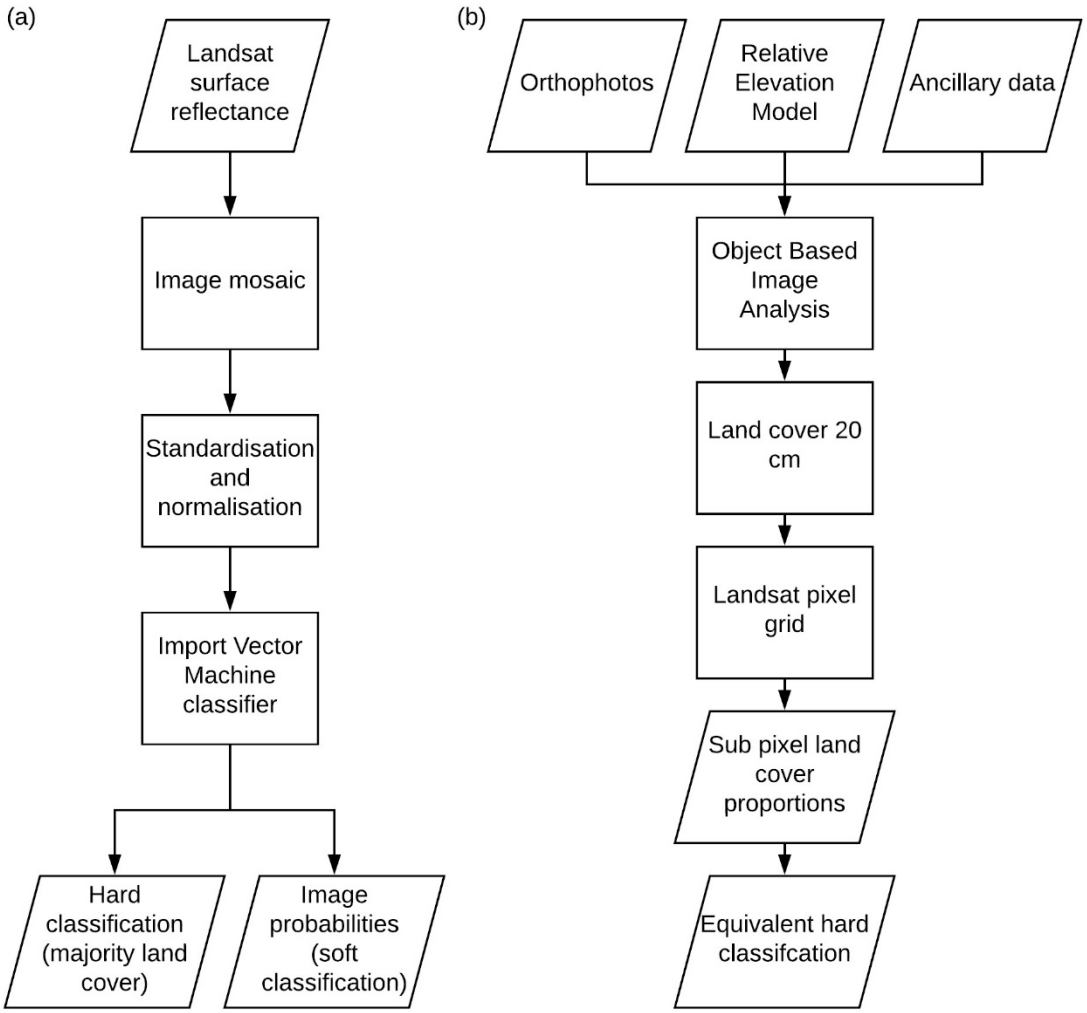

Figure 5-3. Summary of classification procedures for (a) Landsat and (b) high-resolution orthophoto data.

5.5.2 Landsat classification

The 2007 Landsat data was classified as a time series of data for seven sequential periods between 1990 and 2015 using an IVM classifier produced in MacLachlan et al. (2017a). The method uses a hybrid strategy which assesses whether new samples (termed import vectors) can be removed in each forward step in order to provide a smoother decision boundary which ideally leads to a more accurate solution (Roscher et al., 2012). Samples are selected based on how much their incorporation decreases the objective function to minimise the decision boundary to form the optimal separating hyperplane between overlapping clusters (e.g. land cover types) in spectral feature space (Mountrakis et al., 2011; Roscher et al., 2012; Zhu and Hastie, 2005). IVM generates two outputs, a soft (sub-pixel) dataset which defines the probability of a pixel containing a given classification value (e.g. land cover type) and a traditional 'hardened' classified dataset (Braun et

al., 2012). Training samples were collected from the 12th and 19th July 2005 Landsat 5 TM image composite, coinciding with peak vegetation greenness which provides the greatest spectral separability between vegetated and non-vegetated surfaces (Chen et al., 2014; Feyisa et al., 2016). Six land cover types were defined based on existing literature (e.g. Feyisa et al., 2016; Hu and Weng, 2009; Schneider, 2012) and scene analysis which are high reflectance urban (e.g. concrete), low reflectance urban (e.g. asphalt), forest, water, grassland and bare earth. Two urban land cover classes are specified to reduce spectral confusion between spectrally similarly classes (e.g. urban and bare earth) (Hu and Weng, 2009). For each land cover type, 250 pixels were randomly identified from across the image for training the IVM classifier which follows the approach used by Foody and Mather (2006) and Pal and Mather (2003). The IVM algorithm is parameterised using the training data that generates a classification model consisting of spectral profiles for each land cover type, which are then matched to the Landsat mosaic during classification.

The resulting per-pixel (hardened) classification indicates that the total urban extent of the PMR has increased 45.32% (sub-pixel estimate of 32.96%) between 1990 (hardened estimate 706.88 km^2, sub-pixel estimate 736.93 km^2) and 2015 (hardened estimate 1027.22 km^2, sub-pixel estimate 979.84 km^2) (MacLachlan et al., 2017a). This can be broken down into low reflectance urban cover expanding from a hardened value of 592.83 km^2 (sub-pixel estimate 668.46 km^2) to 839.00 km^2 (sub-pixel estimate 850.87 km^2) and high reflectance urban cover increasing from a hardened value of 114.05 km^2 (sub-pixel estimate 135.32 km^2) to 188.20 km^2 (sub-pixel estimate 214.06 km^2) across the same temporal period.

5.5.3 Google Earth Landsat accuracy assessment

Google Earth imagery consistent with the Landsat acquisition date was used to assess the accuracy of the hardened Landsat classification following previously published methods (e.g. Bagan and Yamagata, 2014; Cunningham et al., 2015; Dorais and Cardille, 2011; Song et al., 2016; Sun et al., 2015; Zhu and Woodcock, 2014). Using the Google Earth imagery, 300 random locations (50 per land cover class) within the PMR which were visually identified and compared to the classified land cover data, consistent with recommended land cover accuracy sample size of Congalton (2001) (Song et al., 2016). The 2007 Landsat classification obtained an accuracy of 84.00% and a Kappa Coefficient of 0.78. Urban land cover estimates had a producer's accuracy of 83.00% and user's accuracy of 87.37%. MacLachlan et al. (2017a) provide a full breakdown of urban temporal change and associated accuracy for all imagery in the Landsat time series (1990-2015), with the Landsat classification data available from the pangaea open access publisher (DOI: 10.1594/PANGAEA.871017) (MacLachlan et al., 2017b).

5.5.4 Aerial image classification

Urban areas are complex, heterogeneous environments which are challenging to classify even when using high spatial resolution multi-spectral imagery (Lu et al., 2011; Varshney and Rajesh, 2014). Within urban areas, traditional moderate and coarse spatial resolution pixel based classification methods present multiple challenges due to the land surface spatial heterogeneity and the spectral similarity between urban and non-urban materials (Myint et al., 2011). To characterise the influence of spatial resolution on the ability to map urban areas, high spatial resolution multispectral ortho-imagery (20 cm) were classified into the four broad land cover types. To reduce data processing requirements, four 3 km^2 subsets were chosen that are representative of the land cover composition and spatial heterogeneity found within Perth (Figure 5-1 (a)). These subsets are an out of town development area (East Beechboro), the Central Business District (CBD), an older suburban area (Palmrya, Melville) and a largely vegetated region (Keysbrook). Using the high spatial resolution multispectral imagery and a relative elevation model, an Object Based Image Analysis (OBIA) method was applied to classify each subset into vegetation, urban, bare earth and water (Figure 5-3 (b)). OBIA methods are often applied to high spatial resolution imagery as they include spatial, textural and spectral information to classify the scene (Myint et al., 2011). Incorporating surface elevation measurements into urban classifications has been found to improve building (urban) extraction accuracy (Aguilar et al., 2012; Poznanska et al., 2013). Surface elevation estimates and Normalised Difference Vegetation Index (NDVI) data provided additional urban classification parameters, with refinement (e.g. additions and alterations) made based on object spatial, spectral and textural properties. Unlike the Landsat imagery, the airborne imagery were collected during the late dry season when the grass was senescent which resulted in textural and spectral similarity between bare earth and roads. To mitigate the impact of potential misclassification between these features, Landgate road and, where appropriate, rail vector datasets were used for identification of coincident image objects for urban assignment.

Table 5-1. The percentage of different land-cover types within the classified high spatial resolution subsets (Figure 5-1).

Subset	Vegetation (%)	Urban (%)	Bare earth (%)	Water (%)
East Beechboro	81.00	16.56	2.37	0.07
CBD	33.33	65.66	0.91	0.10
Palmrya	57.29	42.21	0.42	0.08
Keysbrook	97.36	0.90	1.56	0.18

5.5.5 Dataset comparison and Landsat refinement

In order to compare the orthophoto and Landsat land cover classifications, the two urban (high and low reflectance) and two vegetation (woodland and grassland) Landsat land cover classes were merged so that both land cover classifications contained four identical classes. To facilitate comparison between the high spatial resolution orthophoto-derived classification and the Landsat classification, the orthophoto land cover data is aggregated to Landsat spatial resolution to provide a 'soft' and a 'hard' land cover dataset. To create the soft 30 m^2 orthophoto-derived classification, each resampled 30 m^2 pixel area contains the proportion of each land cover type within it (Lu et al., 2011) (Figure 5-3 (b)). This dataset was subsequently 'hardened' by assigning the pixel land cover type according to the dominant land cover found within the 30 m^2 area.

The comparison methodology is to firstly compare the per-pixel (i.e. hardened) Landsat land cover classification with the aggregated (30 m^2) orthoimage classification. Misclassified Landsat pixels are assessed further to establish the conditions that lead to erroneous classification using the sub-pixel proportion information (i.e. soft classification datasets). The latter are also used to identify a spatially explicit correction model to improve urban area estimates from moderate spatial resolution imagery.

5.6 Results

5.6.1 Orthophoto and Landsat land cover comparison

A comparison is conducted between the orthophoto land cover classification, aggregated to 30 m^2 spatial resolution using the majority land cover, and the IVM 'hardened' Landsat classification. At its native spatial resolution (20 cm; Figure 5-4 ((a-d)(i))), the orthophoto land cover classification (Figure 5-4 ((a-d)(ii))) captures the land cover spatial heterogeneity found within each region and highlights the difference in the spatial structure between these regions.

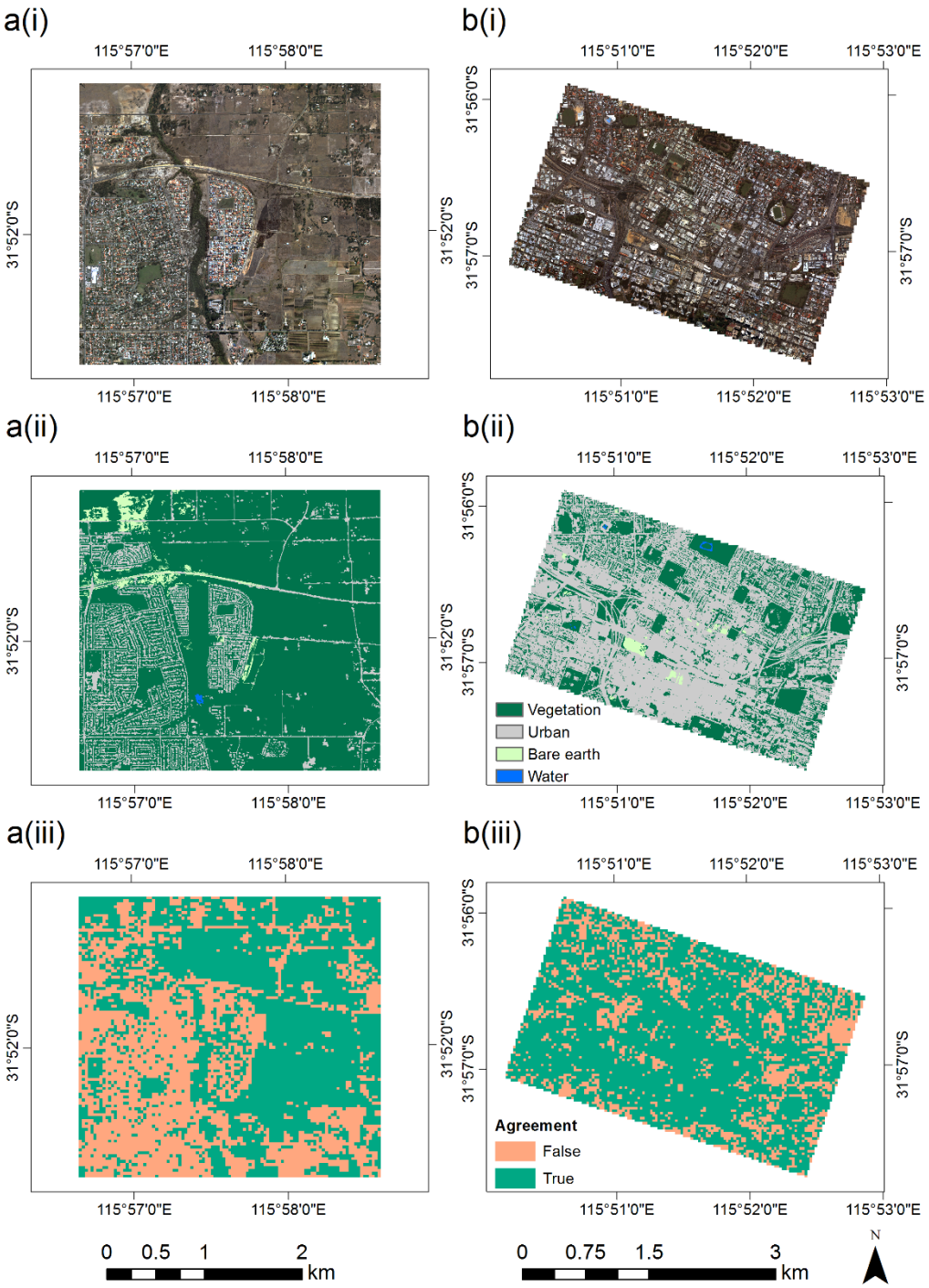
a(i)
b(i)
a(ii)
b(ii)
a(iii)
b(iii)
115°57'0"E
115°58'0"E
115°51'0"E
115°52'0"E
115°53'0"E
31°52'0"S
31°56'0"S
31°57'0"S
Vegetation
Urban
Bare earth
Water
Agreement
False
True
0 0.5 1 2 km
0 0.75 1.5 3 km
N

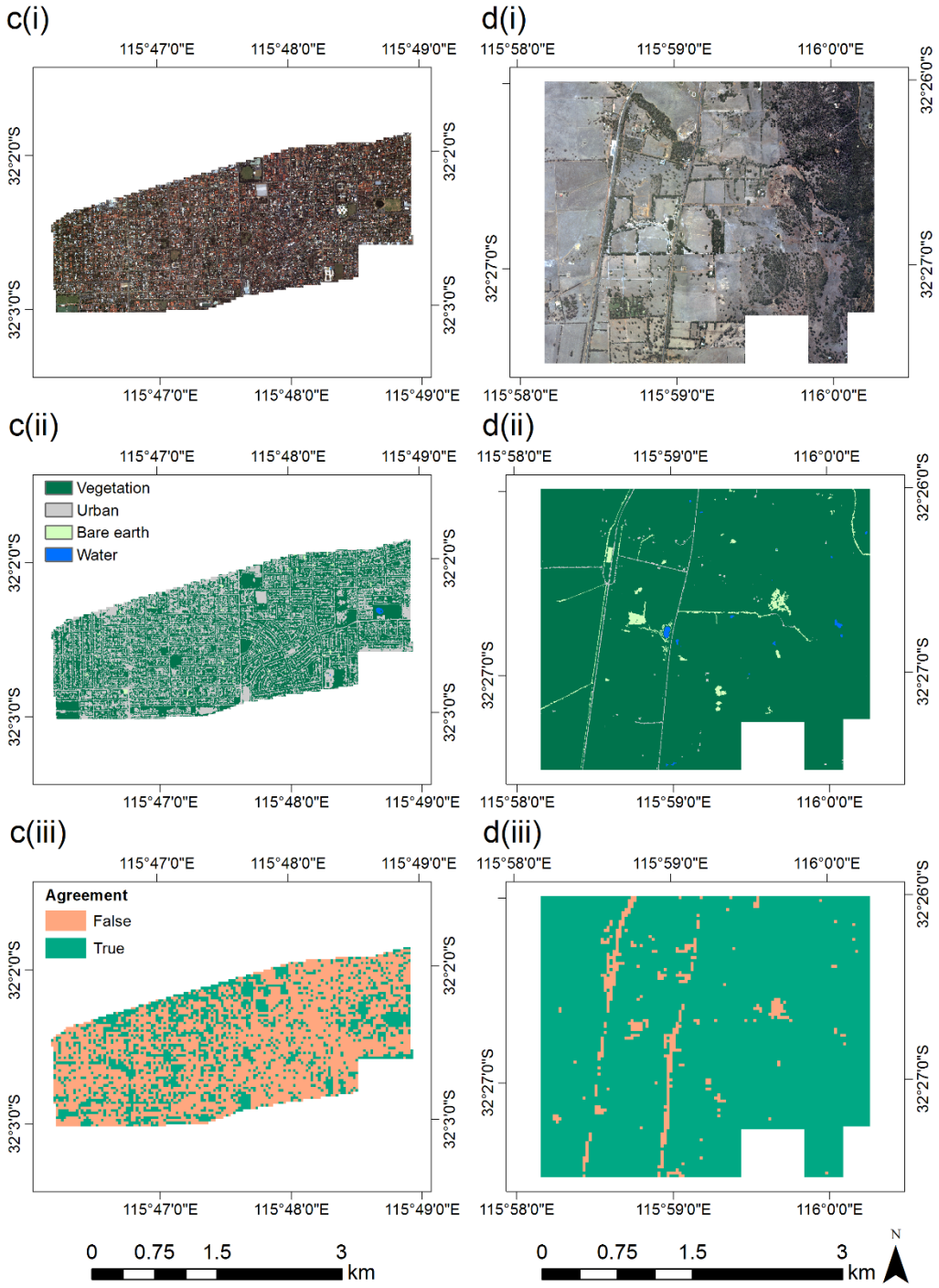

Figure 5-4. (i) High spatial resolution true colour orthophotos, (ii) land-cover maps, and (iii) the agreement between the orthophoto classification resampled to 30 m^2 and the Landsat classification for: (a) an out of town development area (East Beechboro), (b) old inner city urban area (central business district), (c) older suburban area (Palmrya, Melville), and (d) predominantly vegetated site (Keysbrook). In (iii), areas depicted as 'true' indicate those 30 m^2 pixels where the orthophoto land-cover type, based on the dominant land cover in the 30 m^2 area, and Landsat land-cover type are in agreement.

A comparison is carried out between the orthophoto land cover classification, aggregated to 30 m^2 spatial resolution, and the 'hardened' Landsat classification. Figure 5-4 (iii) illustrates the spatial agreement between these datasets and highlights those pixels where the same land cover type (true) has been assigned to a pixel in both classifications. The areas which are more homogeneous at Landsat's spatial resolution, such as the CBD (urban, Figure 5-4 (b)) and Keysbrook (vegetation, Figure 5-4 (d)), have greater level of agreement (73.14% and 95.68% respectively). In contrast, the more heterogeneous subsets (East Beechboro and Palmrya, Figure 5-4 (a and c)), have much lower levels of agreement (56.09% and 32.03% respectively). The differences in agreement result from the sub-pixel heterogeneity at 30 m^2 spatial resolution. Table 5-2 shows the percentage of Landsat pixels which contain >50% of a given land-cover for each subset region.

Table 5-2. The percentage of pixels which contain >50% of a given land-cover type in each region.

Subset	Vegetation (%)	Urban (%)	Bare earth (%)	Water (%)
East Beechboro	87.57	9.84	1.89	0.06
CBD	26.14	72.81	0.74	0.05
Palmrya	66.71	32.33	0.21	0.07
Keysbrook	98.90	0.05	0.88	0.11

To investigate the influence of sub-pixel heterogeneity on the ability of Landsat to identify the pixel land cover type, the classification accuracy is determined as a function of the percentage of urban area within each Landsat pixel for all four subsets (Figure 5-5). The urban percentage cover within each Landsat pixel is derived from the orthophoto land cover classification which has been aggregated to 30 m^2 and which provides the proportion of each land cover within each pixel. The accuracy of the hardened Landsat classification was determined through comparison against the 'hardened' (e.g. aggregated to 30 m^2) orthophoto land cover classification where the per-pixel land cover type was determined based on the land cover type with the greatest sub-pixel proportion. Figure 5-5 indicates that the hardened Landsat classification results in a relatively high accuracy, with an average of 85.40% (excluding Keysbrook), for pixels containing >50% urban land cover (according to the high spatial resolution land cover classification). In the subsets of East Beechboro, the CBD and Palmrya, the overall Landsat classification accuracy drastically declines to 1.99-6.21% when urban land cover within a 30 m^2 pixel area decreases to 40-50%. The classification accuracy then increases with decreasing sub-pixel urban cover which is particularly

evident with Landsat pixels containing 0-10% urban cover. Keysbrook, on the other hand, is a largely vegetated region and exhibits lower accuracy with increasing urban land cover.

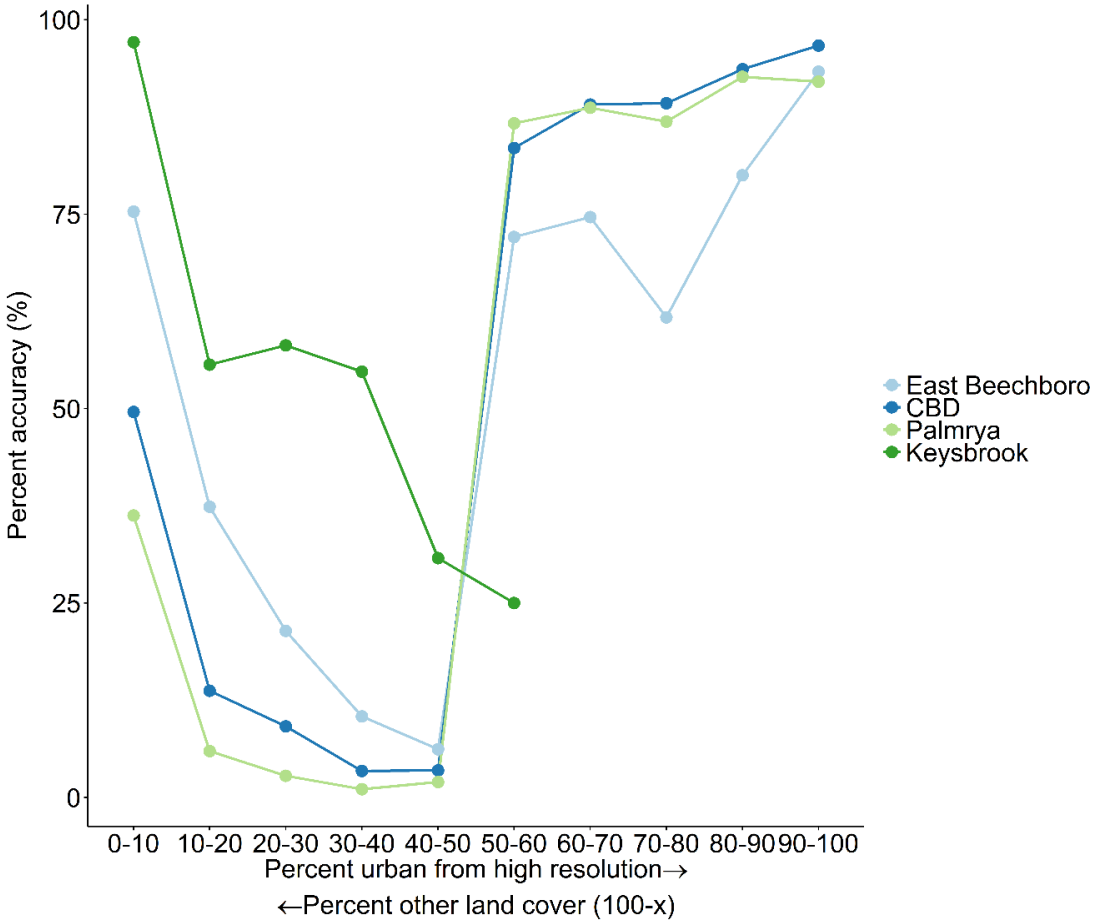

Figure 5-5. Landsat classification accuracy as a function of the percentage urban cover within Landsat image pixels (as derived from the high spatial resolution land-cover data set) for each of the four subsets. In the Keysbrook subset, no Landsat pixels contained >60% urban land cover.

In order to understand the counter-intuitive behaviour of such as rapid decrease in classification accuracy in pixels which contain between 40-50% urban area (Figure 5-5), an analysis of the percentage of pixels classified as a given land cover type is presented. To do so, all pixels containing different ranges in urban percentage cover (e.g. 0-10%, 20-30% etc) were identified using the high spatial resolution land cover dataset. The total percentage of each land cover type was calculated for all pixels that contained urban percentage cover within each range urban percentage cover (e.g. 0-10%, 20-30% etc) using hardened IVM Landsat land cover dataset and

the aggregated high spatial resolution land cover dataset (i.e. defined by the dominant land cover type within a 30 m^2 pixel area).

Figure 5-6 illustrates the percentage of pixels identified as a given land cover type as indicated by the hardened Landsat land cover dataset and the hardened high spatial resolution orthophoto land cover dataset for pixels which contain differing percentage urban cover (e.g. 0-10%) derived using the original high spatial resolution orthophoto land cover classification for the East Beechboro subset. This area was selected as it is an intermediate area in terms of land cover heterogeneity (Figure 5-2 and Figure 5-4 (a)). The results indicate that the hardened Landsat classification consistently overestimates urban land cover when compared to the 'hardened' high spatial resolution classification which has been aggregated to 30 m^2 based on the dominate land cover within the Landsat pixel area for pixels with 10-50% urban defined by high resolution data. Table 5-3 and Figure 5-7 illustrates the sub-pixel (30 m^2) percentage urban land cover for East Beechboro with the original reflectance imagery for this area shown in Figure 5-2. The hardened high spatial resolution land cover dataset (left bar in each plot (Figure 5-6)) indicates that pixels containing <50% urban land cover are largely dominated by vegetation. In contrast, Landsat largely identifies these pixels as being either urban or vegetated to differing extents and more correctly identifies pixels with 0-10% urban land cover as being predominantly vegetated. For example, pixels containing 40-50% urban area are correctly identified as being vegetated (98.45% of pixels within this range) by the hardened high spatial resolution land cover dataset since these pixels contain on average 54.72% vegetation, 44.83% urban and 0.45% bare earth. In contrast, the hardened Landsat land cover dataset identifies 5.65% of pixels containing 40-50% urban cover as being vegetation, 74.28% being urban and 20.07% being bare earth. As the percentage of urban land cover decreases, the overall accuracy of the hardened Landsat classification increases due to the increase in Landsat vegetation cover which increases from 5.65% (40-50% urban cover) to 75.41% (0-10% urban cover). The results are similar for the other regional subsets. The rapid decrease in accuracy between 40-50% and 50-60% (Figure 5-5) appears extreme as the subset regions are dominated by vegetation and urban land cover (Table 5-1) which results in the aggregated 30 m^2 pixels being assigned to vegetation when the percentage urban cover is <50% (Figure 5-6 (a-e)) or urban when the percentage urban cover is >50% (Figure 5-6 (f-j)).

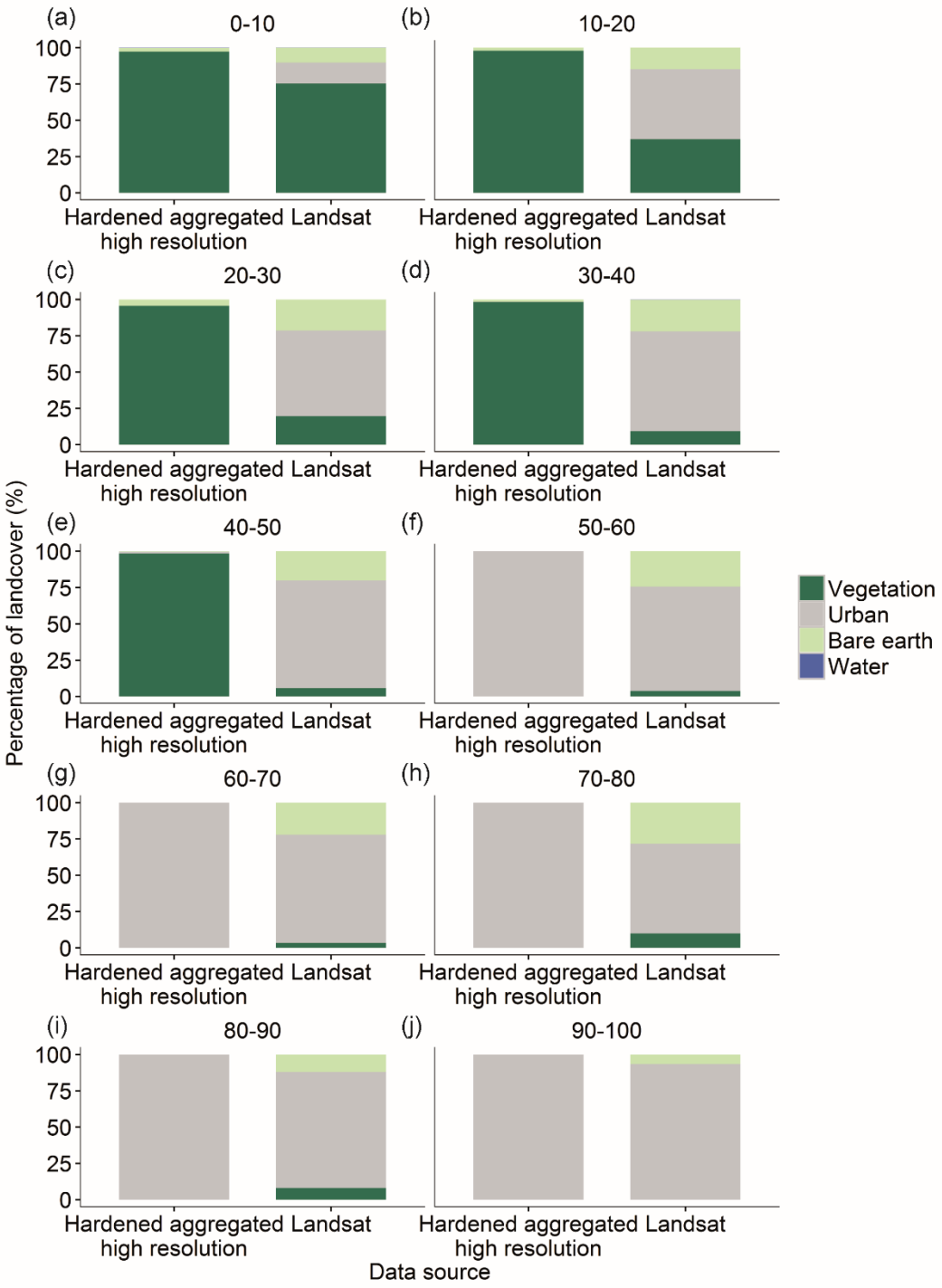

Figure 5-6. Land-cover type disaggregation for urban land cover (according to the orthophoto imagery) Landsat pixels in East Beechboro. The left axis indicates the total percentage cover of a given land-cover type using all of the pixels within a given range of urban percentage cover range for: (a) 0–10%, (b) 10–20%, (c) 20–30%, (d) 30–40%, (e) 40–50%, (f) 50–60%, (g) 60–70%, (h) 70–80%, (i) 80–90%, and (j) 90–100%. For each percentage urban land-cover graph, the left bar illustrates the overall percentage of pixels from the hardened high spatial resolution classification identified as a given land types whilst the right bar indicates the percentage of hardened Landsat pixels mapped as a given land-cover type.

Table 5-3. Urban area estimates (km^2) from high spatial resolution orthophoto land cover data for each subset and those from the corresponding hard and soft IVM Landsat classification. The overestimation of urban area by the hardened Landsat land cover classification is evident.

Subset	**High resolution urban area (km^2)**	**Percentage cover of subset area (%)**	**Landsat urban area (km^2)**	**Percentage cover of subset area (%)**	**Percent difference to high resolution (%)**	**Landsat urban area sub-pixel (km^2)**	**Percentage cover of subset area (%)**	**Percent difference to high resolution (%)**
East Beechboro	1.47	16.56	3.22	36.21	118.66	3.12	35.06	111.69
CBD	5.58	65.66	7.28	85.71	30.54	6.78	79.85	21.62
Palmrya	2.70	42.21	5.50	85.94	103.60	4.90	76.55	81.42
Keysbrook	0.08	0.90	0.28	3.17	252.22	0.39	3.30	266.26

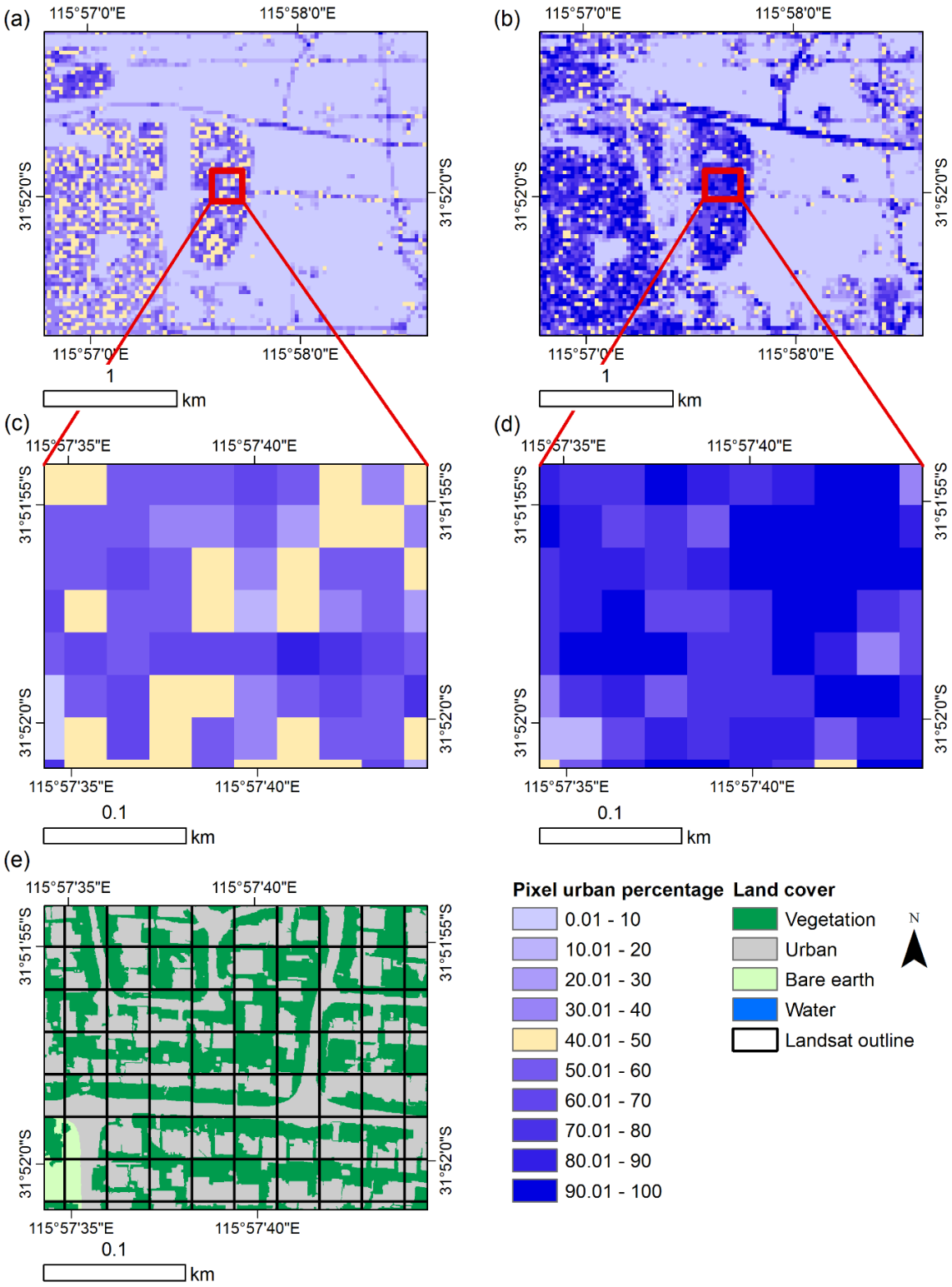

Figure 5-7. Comparison of percentage urban area aggregated to 30 m^2 from high-resolution data (a) and IVM 'soft' Landsat classification (b) highlighting the (overestimation) between the high (c) and moderate (d) spatial resolution estimates for the East Beechboro subset. The classified high spatial resolution data are shown in (e) with the moderate spatial resolution grid (30 m^2) overlaid for context (e).

The results in Figure 5-6 suggest that the spectral data used to train the IVM classification (discussed in section 5.5.2) contained spectrally 'mixed' pixels resulting in land cover type misclassification. To investigate this, the spectral reflectance from Landsat pixels containing 20-30% urban cover for the Palmrya subset, which had the lowest overall agreement and which were identified as being mostly vegetated by the hardened high spatial resolution land cover dataset, are extracted and compared to the spectral reflectance profiles used to train the IVM classification algorithm. Figure 5-8 indicates that there are strong similarities between the average spectral reflectance profile used to train the IVM classification algorithm and the average spectral profile of the misclassified pixels. This suggests that the IVM classification algorithm is accurately representing the Landsat pixel spectral reflectance properties but that the training data used to develop the classification model contained a high proportion of mixed pixels.

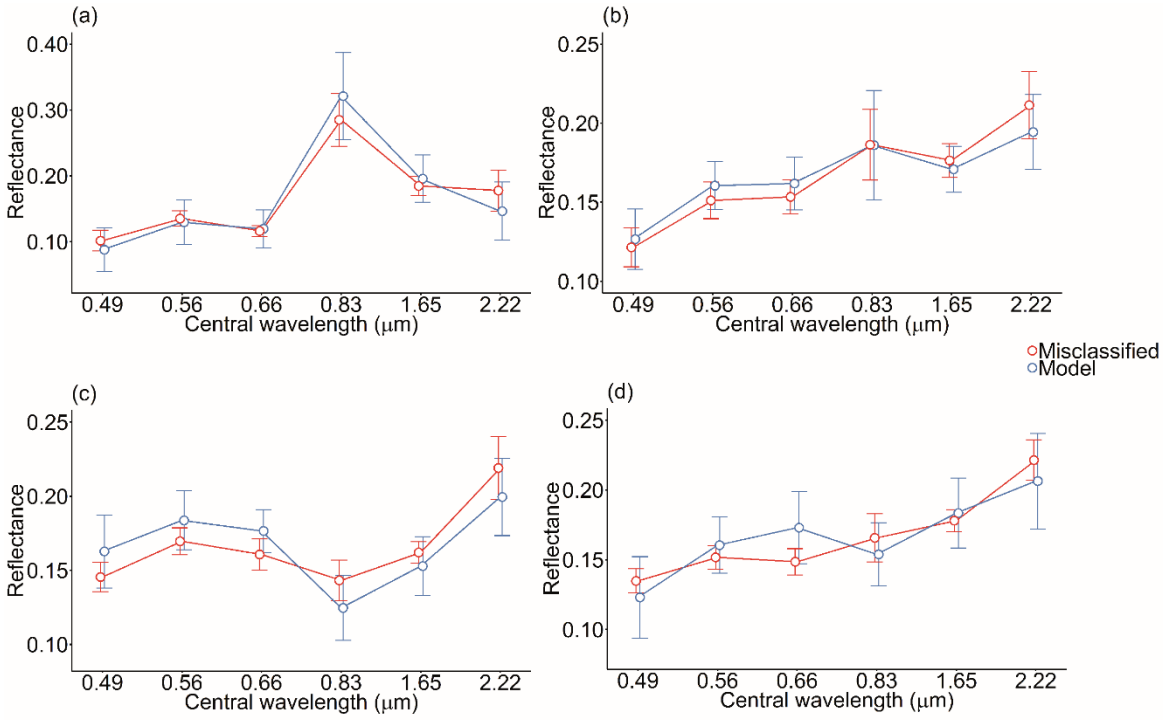

Figure 5-8. Average spectral reflectance profile for misclassified pixels (red) from the Palmrya subset for pixels containing 20–30% urban cover compared to the average spectral reflectance profile of pixels used to train the IVM classification algorithm (blue). For (a) forest, (b) low urban reflectance, (c) high urban reflectance, and (d) bare earth. The error bars show the standard deviation.

Pure (i.e. homogeneous) pixels are conventionally selected to train classification models (e.g. Weng and Pu, 2013) but these are inherently difficult to identify in urban areas owing to the

multitude of land covers within a Landsat pixel area. Using the high spatial resolution classification, the percentage of pure pixels, defined here as those containing between 90-100% of a single land cover type, were identified (Table 5-4). It is evident that some regions contain a high percentage of pure pixels for a given land cover type, such as vegetation in Keysbrook (92.05%), but that other land cover types within a region typically have much lower percentages of pure pixels. Pure urban pixels are particularly limited in all subset regions. Whilst the CBD subset obtains a high percentage of pure urban pixels (28.77%) these are predominately urban areas with high spectral reflectance (e.g. concrete), differing from subsets with urban areas which have urban areas with both high and low spectral reflectance (e.g. East Beechboro; Figure 5-2).

Table 5-4. Percentage of 'pure' pixels (defined here as comprising 90-100% of given landcover within a Landsat pixel area) from the high spatial resolution imagery.

Subset	Vegetation (%)	Urban (%)	Bare earth (%)	Water (%)
East Beechboro	53.93	0.15	0.34	0.03
CBD	8.98	28.77	0.35	0.00
Palmrya	5.80	2.13	0.00	0.01
Keysbrook	92.05	0.00	0.00	0.00

5.6.2 Comparison between Landsat and high spatial resolution impervious surface estimates

Landsat data have been widely applied to map impervious surface area in order to assess its effects on: urban growth dynamics (Masek et al., 2000), the UHI effect (Hu et al., 2015) and surface run-off (Weng, 2001). Figure 5-6 indicates that the 'hardened' Landsat IVM classification overestimates urban land cover, particularly for pixels containing <50% urban area. The IVM classifier also provides a 'soft' land cover dataset that quantifies the sub-pixel land cover proportions.

Here we investigate the utility of the sub-pixel Landsat urban land cover estimates by comparing them to those derived from the high spatial resolution land cover dataset (20 cm) which is used to provide the actual land cover proportion within each 30 m^2 pixel area. Urban area estimates from each of the four subsets (Figure 5-1 (a)) were spatially averaged over different size spatial windows (30 × 30 m, 90 × 90 m, 150 × 150 m and 210 × 210 m) in order to account for any errors resulting from pixel heterogeneity, spatial misregistration, residual atmospheric and BRDF effects and phenological differences (Ghimire et al., 2010; Ju et al., 2012; Liang et al., 2001; Lu et al., 2011; Maiersperger et al., 2013) that may increase the uncertainty in estimating land cover

proportions (Lu et al., 2011; Sexton et al., 2013). Comparison of impervious surface proportions at 30 m^2, for example the CBD subset (Figure 5-9), reiterates the overestimation of urban area at 30 m^2 spatial resolution, with a clustering of values toward the upper percentage boundaries associated with lower urban area estimates from the high spatial resolution classification. When neighbourhood averaging is applied, the agreement in urban area typically improves with increasing window size although the subset specific bias remains consistent (Table 5-5). It is also evident that urban area is still overestimated with decreasing urban sub-pixel proportion even when utilising the sub-pixel IVM Landsat classification results.

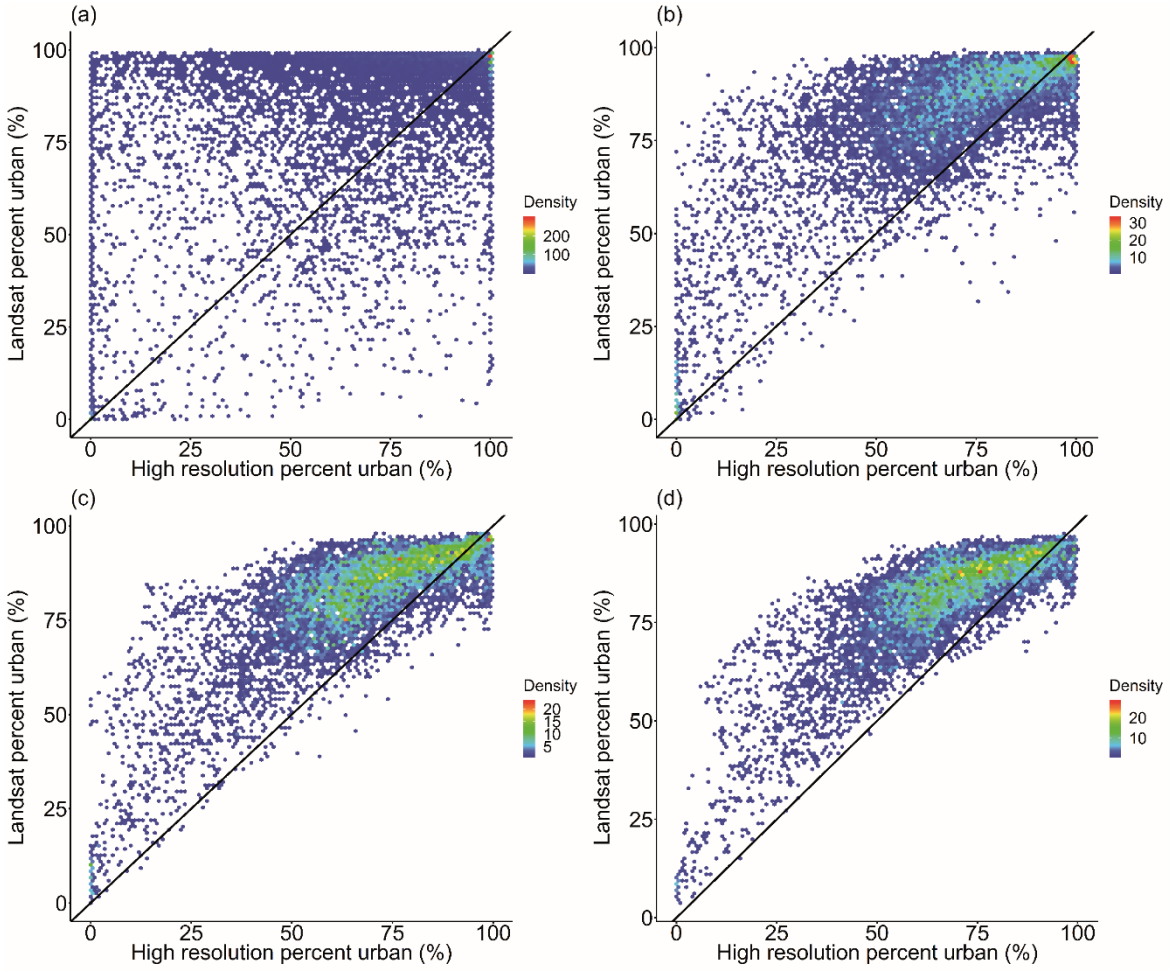

Figure 5-9. Relationship between the sub-pixel urban area percentage cover estimated from the IVM sub-pixel Landsat classification and the high spatial resolution orthophoto classification in the Central Business District (CBD) subset for (a) 30 × 30 m window, (b) 90 × 90 m window, (c) 150 × 150 m window, and (d) 210 × 210 m window.

Table 5-5. Comparison between high (20 cm^2) and moderate (30 m^2) spatial resolution sub-pixel impervious surface estimates considering differing kernel sizes over four subsets (Figure 5-1) within the PMR.

Subset	Kernel size (m)	R^2	Scatter	Bias	Root Mean Square Error (RMSE)
East Beechboro	30×30	0.41*	26.65	18.68	32.54
	90×90	0.68*	16.95	18.66	25.21
	150×150	0.75*	14.11	18.71	23.44
	210×210	0.80*	12.52	18.74	22.54
CBD	30×30	0.26*	28.41	14.38	31.84
	90×90	0.53*	16.65	14.37	22.00
	150×150	0.61*	13.18	14.38	19.51
	210×210	0.66*	11.30	14.36	18.28
Palmrya	30×30	0.04*	26.65	34.54	43.62
	90×90	0.16*	13.56	34.61	37.17
	150×150	0.19*	10.15	34.64	36.10
	210×210	0.17*	8.45	34.67	35.69
Keysbrook	30×30	0.24*	11.85	2.51	12.11
	90×90	0.52*	7.47	2.51	7.88
	150×150	0.60*	5.89	2.50	6.40
	210×210	0.63*	4.98	2.50	5.57

5.6.3 Refining Landsat estimations using high spatial resolution data

Sub-pixel land cover heterogeneity influences Landsat urban area overestimation which must be considered in order to reduce the bias and improve Landsat derived urban area estimation (Herold et al., 2002; Lu et al., 2011; Schneider, 2012; Varshney and Rajesh, 2014). The complexity and diversity of urban areas identified here from high spatial resolution data, with biases ranging from -2.50% to -34.67%, highlights the inappropriateness of applying a single model to adjust the moderate spatial resolution urban area estimates in a metropolitan region (e.g. Lu et al., 2011). The Landsat sub-pixel urban areas estimates from all four subsets were stratified based on the Landsat sub-pixel derived urban area and calibrated against the percentage of urban area from the high spatial resolution classification within each moderate spatial resolution pixel area. Both datasets were averaged at the neighbourhood level using a 210 × 210m window as this provided the best overall relationship (Table 5-5). Stratification of Landsat sub-pixel urban estimates into divisions of 10%, consistent with previous results, were selected to develop (using 50% of the data) and test (remaining 50% of the data) regression models to improve the dataset agreement (Lu et al., 2011).

The applied spatially explicit models reduced the bias and Root Mean Square Error (RMSE) between the predicted (moderate spatial resolution) and observed (high spatial resolution) estimates (Table 5-6). It is evident from Table 5-6 that the adjustment made to the Landsat urban area estimates reduced the overestimation difference of urban area by between 34.38% and 80.67%, with the largest improvement found within Keysbrook. Whilst the corrected Landsat urban area estimates still overestimates the urban area compared to the high spatial resolution dataset the corrected moderate spatial resolution urban area reduces moderate resolution urban area over (under) estimation by on average 55.08% in comparison to the high spatial resolution dataset reducing the average overestimation from 11.86 km^2 per subset to just 0.09 km^2 (Table 5-6). In the case of this study area, this approach is appropriate for producing more accurate urban area statistics. Due to the frequently reported over and under estimation of land cover estimates by moderate spatial resolution data this approach can refine urban estimates for planning development policies that may inform decision makers (Hepinstall-Cymerman et al., 2013; Schneider et al., 2005; Zhu and Woodcock, 2014). However, the derived correction values are not globally applicable since the spatial structure and makeup of urban and suburban areas varies regionally, nationally and globally. Nevertheless the methodology implemented here could be replicated to produce localised correction values from other sources of high resolution imagery (e.g. digitisation of Google Earth imagery) to calibrate urban area estimates from moderate spatial resolution data.

Table 5-6. Comparison between calibrated moderate (30 m^2) and high (20 cm^2) resolution sub-pixel impervious surface estimates with a kernel size of 210m. * = statistically significant relationship (p<0.05).

Subset	R^2	Bias	Root Mean Square Error (RMSE)	High resolution urban (km^2)	Uncorrected Landsat urban (km^2)	Uncorrected percent difference to high resolution (%)	Corrected Landsat urban (km^2)	Corrected percent difference to high resolution (%)
East Beechboro	0.84*	1.54	6.76	2.49	5.32	72.47	2.72	8.83
CBD	0.52*	-7.12	14.61	12.26	15.36	22.45	10.88	-11.93
Palmrya	0.12*	7.43	12.53	6.92	12.48	57.32	8.10	15.71
Keysbrook	0.62*	0.37	1.38	0.13	0.50	115.96	0.19	35.29

5.7 Discussion

Refined urban estimates are vital in ensuring suitable sustainable and strategic planning decisions are implemented (Bettencourt and West, 2010; Wu and Murray, 2003). The hybrid spatial resolution approach applied here to estimate urban area was necessary due to the difficulty in accurately estimating urban area using a traditional per-pixel classification methods. This was due to a combination of the sensors moderate (30 m^2) spatial resolution, land surface heterogeneity and the selection of 'mixed' pixels for use in training the classification algorithm. The overall classification accuracy, determined using Google Earth imagery, was on average 84.00%, which is similar to that found in other studies, albeit for different urban areas (e.g. Bagan and Yamagata, 2014; Gislason et al., 2006; Luo et al., 2014; Sundarakumar et al., 2012).

Closer examination of the moderate spatial resolution classification results using a higher resolution dataset indicates that when urban land cover within a 30 m^2 area decreases to 40-50% (based on high spatial resolution classification) the Landsat classification accuracy decreased from 85.40% to between 1.99 and 6.21%. This resulted from the Landsat classification overestimating urban area in comparison to high spatial resolution data (Figure 5-5) which more correctly identified these pixels as containing a greater per-pixel proportion of vegetation. Pixels containing 40-50% urban cover, contained on average 54.50% vegetation cover excluding Keysbrook. The dominance of vegetation and urban land covers in the regional subset, when ascribed to a 30 m^2 pixel area based on the majority land cover, results in a rapid change in classification accuracy. Strong spectral similarities between training data and misclassified pixels (Figure 5-8) suggests that the spectral reflectance observations used to train the classification algorithm contained spectrally mixed pixels. The average percentage urban area within a moderate spatial resolution pixel area derived from the high resolution data was 16.56%, 65.66%, 42.21% and 0.90% for East Beechboro, CBD, Palmyra and Keysbrook respectively. The percentage of 'pure' pixels, defined as those containing over 90% urban land cover, was 28.77% for the CBD but <2.50% for the suburban regional subsets. This highlights the difficulty in selecting pure pixels at moderate spatial resolution and in accurately disentangling mixed spectral reflectance's without the aid of high spatial resolution data. Overestimation of urban extent was most prominent in Keysbrook, where vegetation dominates the subset (97.36%, Table 5-1). In this instance, Landsat derived urban area corresponded to 0.28 km^2 compared to 0.08 km^2 from high spatial resolution classification; a difference of only 0.20 km^2 but which equates to 251.74%. In terms of total area difference, the East Beechboro and the CBD Landsat subsets were found to contain 1.75 km^2 and 1.70 km^2 more urbanised area, whilst Palmyra data overestimated urban area by 2.79 km^2 compared to the high spatial resolution equivalent due to its suburban nature and associated pixel heterogeneity (Figure 5-4).

Spatially averaging the Landsat and orthophoto land cover classifications, to account for potential errors in the datasets (Ghimire et al., 2010), improved their relationship although Landsat still overestimated urban area with differing bias per subset. Over (under) estimation of urban land from Landsat estimations could result in an under (over) prediction on further environmental variables (e.g. UHI) or policy applications. Multiple studies have used classified per-pixel moderate spatial resolution data to influence policy changes through monitoring urban growth (e.g. Hepinstall-Cymerman et al., 2013; Schneider et al., 2005). However, per-pixel methodologies fail to address the issue of mixed pixels, which, as shown here, can result in overestimation of urban area (average: 126.25%, equivalent to 57.58 km^2 within the PMR) (Lu et al., 2011). Sub-pixel methods attempt to remedy this issue, but have been found to inaccurately separate impervious land cover from other land cover types resulting in poor representation of impervious surface area (Lu et al., 2011). Consequently over estimation of urban area may have resulted in sub-optimal policies that fail to maximise resource and amenity efficiency (Downs, 2005; Turner et al., 2010).

Calibrating Landsat urban estimates using high spatial resolution data reduces the bias, RMSE and improves urban area estimation. However, the range of bias values across subsets of differing urban land cover characteristic highlights the inappropriateness of a single regression model due to pixel heterogeneity influencing overestimation (Lu et al., 2011). Spatially explicit models, as presented here, permit varying moderate spatial resolution refinement by considering the influence of surface heterogeneity. Whilst the limited availability of low cost high spatial resolution data can preclude analysis of this type, subset digitisation of Google Earth or Unmanned Aerial Vehicle (UAV) imagery may provide a suitable alternative for calibrating Landsat data for improved urban area estimates. Enhanced estimates of urban area would facilitate planning policies which avoid potential environmental and socio-economic consequences of urban development than can result from policies based on over (or under) predicted urban area (ARUP and The Rockefeller Foundation, 2015). For example, classified Landsat data was used to identify spatial clustering, peri urban development and specialisation of land use in Chengdu, Sichuan province not considered by China's original 1990 Go West policy, aimed at economically boosting the West of the country. Results were used to reform policy and remediate issues of urban management including: service, infrastructure and resource deficiencies (Schneider et al., 2005). However, traditional Landsat classification may over (or under) estimate urban area and result in ineffective planning, environmental and policy decisions (Miller and Small, 2003; Pravitasari et al., 2015). Therefore classified sub-pixel data alongside high spatial resolution imagery (e.g. UAV, Google Earth, high spatial resolution aerial or satellite imagery) as presented here can refine urban estimates facilitating improved decision making whilst maximising often

limited financial resources. This is especially important in developing countries in regards to directing urban development and resources based on factors including: poverty, environmental hazards (e.g. flooding) and current amenity centres (Marfai et al., 2014; Suryahadi and Sumarto, 2003).

5.8 Conclusion

Landsat imagery from 2007 was used to map the urban extent within the PMR using an IVM classifier which provides both a per-pixel and a sub-pixel classified datasets. The 2007 Landsat classification overall average accuracy was 84.00% with associated Kappa coefficient of 0.78. Comparison between the Landsat per-pixel urban area and urban area estimates obtained from a high spatial resolution (20 cm) orthophoto-derived classification indicates that the moderate spatial resolution classification overestimates urban extent by 126.25 % on average, which is equivalent to 57.58 km^2 in the study area. Similarly, when the high spatial resolution urban area estimates are compared to those derived using a sub-pixel Landsat classification, the latter still overestimates urban extent by 120.25%.

Accurately quantifying urban expansion within the PMR due to the large population growth over the last decade is important in order to make the efficient use of current resources and to avoid additional amenity, environmental and health expenditure that can impact sprawling cities. Landsat data provides the longest time series of medium spatial resolution imagery to map and monitor urban area. However, the reported over and underestimation inhibits accurate quantification of urbanised land cover which increases uncertainty within global climate models, environmental studies and targeted urban planning policy. Neighbourhood averaging, to account for potential errors in the datasets, improved the agreement between the two datasets but Landsat sub-pixel overestimation still remained. The broad differences in bias between the difference subsets indicates that a single regression model is inappropriate to heterogeneous urban land cover estimates. Therefore, the moderate spatial resolution urban area estimates were corrected using spatially explicit regression models which, on average, across the four subsets reduced the bias and RMSE by 17.02 km^2 and 6.65 km^2 respectively, whilst reducing moderate resolution urban area over (under) estimation by 55.08%

Current and future EO satellites that provide complimentary data with enhanced spatial, spectral and temporal resolution, such as Sentinel-2, may further reduce over or under estimation of urban area experienced by moderate spatial resolution sensors such as Landsat. Similarly, high spatial resolution satellite sensors, such as Worldview-3, are able to remediate discrepancies by capturing the fine spatial detail of urban environments but their cost and small swath limit their

widespread application. This might change with companies, such as Planet, which are launching large numbers of small micro-satellites that provide high spatial resolution data more frequently. Accurate urban land cover and land use mapping is essential in understanding the impact of urban expansion on, for example, social-ecological systems and human-health and will improve future sustainable planning of our cities.

5.9 Supplementary material

This supplementary material sections supports the main chapter and thesis through providing a review surrounding classifier selection, pertinent to the selection of the Import Vector Machine (IVM) classifier implemented in generating the classified Landsat image used within the chapter. A short discussion surrounding other considered approaches and a list of data used within the chapter are also provided to demonstrate the entirety of analytical process.

5.9.1 Classification methodologies

Currently two main image analysis techniques exist for urban mapping: spectral indices and classification algorithms. Spectral indices such as the Normalised Difference Built-up Index (NDBI) have been used to delineate urban areas from non-urban (Zha et al., 2003). NDBI identifies built up regions using a ratio of the shortwave-infrared (SWIR) and near infrared (NIR) wavebands and assumes that built up areas have higher SWIR reflectance (Xu, 2008). In comparison to ground truth observations, NDBI-derived classification from Landsat Thematic Mapper (TM) over Nanjing, China was found to result in an overall accuracy of 92.6% (Zha et al., 2003). However, due to the heterogeneous nature of urban environments, the identification of built up areas by thresholding a spectral index is not always reliable (Xu, 2008).

The Impervious Build-up Index (IBI) attempts to mitigate for this by using a combination of a number of thematic indices namely: NDBI, the Soil Adjusted Vegetation Index (SAVI) and the Modified Normalised Difference Water Index (MNDWI) (Xu, 2008). The index amplifies the identification of built up land through the inclusion of ancillary information on the presence of bare surfaces (SAVI) and water bodies (MNDWI) resulting in positive values for pixels identified as being urban (Xu, 2008). Nevertheless, urban areas often remain an inseperable mix of impervious and bare earth surfaces which require additional post-processing to delineate (Stathakis et al., 2012; Sun et al., 2015; Zha et al., 2003).

In the second instance, classification algorithms are defined as parametric (e.g. Maximum Likelihood (ML)) or nonparametric (e.g. Decision Trees (DT)), depending on whether training samples can be represented by a Gaussian probability density function (Donnay and Unwin, 2001;

Jensen, 2005). Maximum Likelihood accounts for the variance-covariance within class distributions and has been implemented for monitoring land cover change and to derive sub-pixel proportions (Atkinson et al., 1997; Shalaby and Tateishi, 2007). However, due to the parametric assumption of multivariate normal data, the ML classifier can often fail to represent land cover that might be multimodal (Melgani and Bruzzone, 2004; Mountrakis et al., 2011; Otukei and Blaschke, 2010). An example of this issue is illustrated in semi-arid locations, such as grasslands, which are sensitive to precipitation timing and volume that can result in differing multimodal spectral-temporal profiles (Friedl et al., 2002). A decision tree methodology was utilised to generate the United States of America National Land Cover Database 2001 (NLCD 2001) resulting in a nonparametric approach able to handle continuous and nominal data, interpretable classification rules and swift application (Homer et al., 2004). Nevertheless, DTs can be negatively affected by pruning methods, for example Pessimistic Error Pruning (PEP) introduces a continuity correction value, within error estimation on no theoretical basis, resulting in under or over pruning (Esposito et al., 1997; Otukei and Blaschke, 2010; Pal and Mather, 2003).

More recently, Machine Learning Algorithms (MLA) or 'expert systems' (e.g. Support Vector Machine (SVM)) have been implemented for image classification (Jensen, 2005; Okujeni et al., 2014) using an automated inductive approach for identification of patterns in data (Cracknell and Reading, 2014). SVM is a nonparametric binary statistical learning methodology that separates a dataset into example classes (training data) based on a decision boundary, or hyperplane, with an aim to minimise misclassification. The optimal maximum margin separating hyperplane divides the data into a predefined number of classes, with points on the margins termed 'support vectors' (Foody and Mathur, 2006, 2004). The underlying benefit of SVM pertains to structural risk minimisation, whereby SVMs are able to minimise error on unseen data without prior assumptions on the distribution (Mountrakis et al., 2011; Vapnik and Chervonenkis, 1971). SVMs are linear binary classifiers which, when deriving more than two classes, require implementation of an additional process, either a one-against-all or one-against-one analysis. One-against-all solves for the multiple optimisation problem, which separates one class from the remaining classes. Comparatively one-against-one combines multiple classifiers and performs pair-wise comparisons using a 'voting' process to assign a pixel to a land cover class, based on the class assigned the most votes (Chih-Wei et al., 2008; Mountrakis et al., 2011; Pal and Mather, 2005). Within SVMs implementation of soft margin and kernel methods aid separability through the introduction of additional variables that ignore hyperplane outliers and transform data into high dimensional feature spaces (Euclidean or Hilbert) utilising non-linear functions to identify linear solutions respectively (Braun et al., 2012; Cortes and Vapnik, 1995; Melgani and Bruzzone, 2004; Mountrakis et al., 2011).

SVMs have been extensively used for classification purposes, due to their ability to ignore inherent image errors and to avoid overfitting (Foody and Mathur, 2006; Mountrakis et al., 2011). SVMs have obtained broad applicability for land cover classification using data from a multitude of sensors such as HyMAP (Camps-Valls et al., 2004), Advanced Spaceborne Thermal Emission and Reflection Radiometer (ASTER) (Zhu and Blumberg, 2002) and Landsat (Knorn et al., 2009) producing classification results with accuracies between 85% and 95%.

5.9.2 Other considered data and approaches

In proposing the research within this chapter multiple other datasets were considered in replace of Landsat. These included: GlobeLand30 (classified Landsat data for 2000 and 2010) (Chen et al., 2015), the European Space Agency's (ESA) Climate Change Initiative (CCI) annual global land cover (300 m) time series (1992-2015) (European Space Agency, 2017) and yearly MODIS land cover products (500 m or 0.05°) (Friedl et al., 2002). Nevertheless these products are constrained by: resolution, temporal frequency, collection dates to closely match the high resolution imagery and global accuracy assessments that might fail to represent the Perth Metropolitan Region. Additionally, using data produced within chapter 4 enabled greater flow throughout the thesis.

Similarly, other datasets under consideration in replace of the high resolution orthophotos included that from Google Earth (through digitisation) and digital elevation data from Geoscience Australia (5 metre resolution) (Geoscience Australia, 2015). However, the potential for analyst error alongside lower resolution elevation data could have potentially exacerbated errors within the classification process. Consequently, object based image analysis of the high resolution orthophotos was selected as it provided a repeatable approach with minimal subjectivity (Myint et al., 2011).

5.9.3 Chapter data list

This section provides an overview of the data presented and analysed within this chapter.

Supplementary Table 5-7. Summary of the data, sources and applications used within chapter 5.

Data	Source	Application
Classified Landsat land cover data (including sub pixel estimates) from 2007 **Raw data information (2 images)** Landsat 5 TM, 6/10 (path 112), 9/07 (path 113), row 82	Chapter 4 or (MacLachlan et al., 2017b)	Comparison to high resolution urban estimates
High resolution (20cm) orthophotos comprised of four spectral bands, digital surface and elevation models **Sensor** Microsoft UltraCAM-D **Collection dates** 19 could free days from 14/03/2007	Australian Commonwealth Scientific and Industrial Research Organisation Perth and Peel Urban Monitoring Programme	To compare classified high resolution data to that of Landsat in order to remediate Landsat's overestimation
Railway and road vector data	Landgate	Classification of the high resolution imagery

Chapter 6 Urbanisation-induced land cover temperature dynamics for sustainable future urban heat island mitigation

6.1 Abstract

Urban land cover is one of the fastest global growing land cover types which permanently alters land surface properties and atmospheric interactions, often initiating an urban heat island effect. Urbanisation comprises a number of land cover changes within metropolitan regions. However, these complexities have been somewhat neglected in temperature analysis studies of the urban heat island effect, whereby over-simplification ignores the heterogeneity of urban surfaces and associated land surface temperature dynamics. Accurate spatial information pertaining to these land cover change – temperature relationships across space is essential for policy integration regarding future sustainable city planning to mitigate urban heat impacts. Through a multi-sensor approach, this research disentangles the complex spatial heterogeneous variations between changes in land cover (Landsat data) and land surface temperature (MODIS data), to understand the urban heat island effect dynamics in greater detail for appropriate policy integration. The application area is the rapidly expanding Perth Metropolitan Region in Western Australia. Results indicate that land cover change from forest to urban is associated with the greatest annual daytime and nighttime temperature change of 0.40 °C and 0.88 °C respectively. Conversely, change from grassland to urban minimises temperature change at 0.16 °C and 0.77 °C for annual daytime and nighttime temperature respectively. These findings are important to consider for proposed developments of the city as such detail is not currently considered in the urban growth plans for the Perth Metropolitan Region. The novel intra-urban research approach presented can be applied to other global metropolitan regions to facilitate future transition towards sustainable cities, whereby urban heat impacts can be better managed through optimised land use planning, moving cities towards alignment with the 2030 sustainable development goals and the City Resilience Framework.

6.2 Introduction

Rapid global urbanisation has resulted in more than half of the world's population (54.5% in 2016) currently residing in cities and this is expected to increase by 2.5 billion by 2050 or 66% of the world's population (United Nations, Department of Economic and Social Affairs, 2014; United

Nations, 2016). To accommodate the large increase in urban population, the urban area is expected to triple by 2030 based on current trends (2000 baseline of 652,825 km^2) increasing global urban area from 0.5 to 0.9% of total land area (Angel et al., 2011; Seto et al., 2012; Zhou et al., 2016). Urbanisation of natural land is recognised as the most extreme cumulative effect of land cover change which leads to a multitude of socio-economic and physical consequences that include amenity provision efficiency, ecological degradation and the Urban Heat Island (UHI) effect (Cai et al., 2016; Howard, 1988; Hu and Brunsell, 2015; MacLachlan et al., 2017a; Xie and Zhou, 2015).

The UHI effect is considered one of the major problems posed to humans in the 21st century; urbanisation is permanently altering the atmospheric energy exchange and modifying local and regional climate, negatively influencing city sustainability and liveability (Revi et al., 2014; Rizwan et al., 2008). The UHI is defined by increased atmospheric and surface temperatures over surfaces covered by manmade urban materials (e.g. asphalt) which have modified the thermal bulk properties (heat capacity and thermal conductivity) and surface radiative properties (albedo and emissivity) compared to that experienced by natural surfaces such as vegetation and bare soil. UHIs are characterised into three categories: Surface Urban Heat Island (SUHI), Canopy Layer Heat Island (CLHI) and Boundary Layer Heat Island (BLHI). SUHI refers to the relative heat of urban surfaces compared to surrounding areas, whilst CLHI and BLHI denote atmospheric warming from the surface to mean building height (CLHI) and above the canopy layer (BLHI) (Schwarz et al., 2012; Yuan and Bauer, 2007). The higher temperatures experienced over urban areas, described as the UHI effect, have been associated with adverse health impacts (Goggins et al., 2012; Smargiassi et al., 2009), increased energy consumption and emissions (Lowe, 2016), water usage escalation (Guhathakurta and Gober, 2007), and economic expenditure (AECOM Australia, 2012). For example, Goggins et al. (2012) found that in Hong Kong a 1 °C rise in temperature above 29 °C was associated with a 4.1% increase in mortality within areas obtaining a high UHI, in comparison to a 0.7% increase in locations with a low UHI. Consequently, global cities including London (Mayor of London, 2016b), New York (Mayor Bill de Blasio, 2014) and Tokyo (Governor of Tokyo, 2008) have introduced development standards to mitigate exacerbation of the UHI effect, aligned with the C40 Cities Climate Leadership Group's (C40 CCLG) guide for cool cities, as a critical facet in managing city environmental risk (C40 Cities, 2018; C40 Cities and ARUP, 2011).

The magnitude of the UHI effect varies both spatially and temporally. For example, northern cities of the United States of America (USA) (e.g. Washington, DC) were found to require less energy (net benefit) due to additional warming from urban surfaces mitigating past energy consumption as a result of colder climates. Contrastingly, southern cities (e.g. Dallas) utilised more energy (net deficit) as a consequence of UHI within warmer climates (Lowe, 2016). Similarly, research from

Romanian (Cheval and Dumitrescu, 2014), Chinese (Hu et al., 2015) and Asian cities (Tran et al., 2006) established more pronounced daytime SUHIs, whilst Italian (Fabrizi et al., 2010), other Chinese (Sheng et al., 2015; Zhou et al., 2015) and USA (Kenward et al., 2014) cities established both more distinct nighttime surface and atmospheric UHIs. Identifying the localised spatio-temporal impacts of urban expansion on the UHI effect is therefore essential to help prevent further socio-ecological impacts and inform targeted policies for sustainable future development (ARUP and The Rockefeller Foundation, 2015; Bhatta, 2010; Lowe, 2016; Osborn et al., 2015).

One approach to assess the impact of urban and rural land cover on the magnitude of the UHI is the use of in-situ ground observations (e.g. weather station data) of air temperature (Earl et al., 2016; Gallo and Xian, 2014; Giorgio et al., 2017; Guo et al., 2014; Hattis et al., 2012; Knight et al., 2010; Tan et al., 2010). For example, the city of Melbourne analysed temperature differences between one Central Business District (CBD) and three non CBD weather stations in determining a UHI effect and associated socio-economic impacts across the city (AECOM Australia, 2012). However, in-situ ground observations such as weather stations preclude collection of comprehensive temperature data over highly heterogeneous urban areas negating targeted policy application (e.g. Earl et al., 2016; Gallo and Xian, 2014; Guo et al., 2014; Hu and Brunsell, 2015; Tan et al., 2010). Over the last two decades, Earth Observation (EO) has provided a key tool in monitoring Land Surface Temperature (LST) using instruments that contain thermal spectral wavebands such as: the Moderate Resolution Imaging Spectroradiometer (MODIS; Terra and Aqua) (e.g. Wang et al., 2015), Landsat Thematic Mapper (TM) (e.g. Jimenez-Munoz et al., 2014; Rinner and Hussain, 2011; Sobrino et al., 2004), the geostationary Spinning Enhanced Visible and Infrared Imager (SEVIRI) (e.g. Blasi et al., 2016) and the Advanced Along-Track Scanning Radiometer (AATSR) (e.g. Fabrizi et al., 2010). An advantage of satellites is their capability for near global coverage, high temporal and moderate spatial resolution that resolve point-based data generalisations and interpolative processing (e.g. Hattis et al., 2012). Urban areas affect both air temperature and LST. Air temperature represents the urban canopy layer whereas LST pertains to the association of land-cover types with the Surface Heat Island (SHI), depicting the SUHI (Schwarz et al., 2012). To derive air temperature from LST additional factors including surface properties, atmospheric conditions and solar angles are incorporated to calculations (assuming local data is available during satellite overpass) (Hu and Brunsell, 2015; Kim and Han, 2013). Therefore, temperature directly extracted from satellite imagery enables universal comparison, averting issues associated with scaling to air temperature over large spatial extents, typically used within UHI studies (Fabrizi et al., 2010; Hu and Brunsell, 2015; Hu et al., 2015; Imhoff et al., 2010; Zhou et al., 2015).

Previous EO and traditional studies have considered cross-sectional (temporally static land cover map) or longitudinal (temporally dynamic series of land cover maps) homogenous urban land cover areas in relation to surface temperature, yet such research has limitations. Cross-sectional studies either ignore the temporal component of urbanisation on LST (Li et al., 2011; Tomlinson et al., 2012) or assume a consistent urban area over the study period (Cao et al., 2010; Imhoff et al., 2010; Zhou et al., 2016). Longitudinal studies classify land cover over multiple periods but often disregard valuable spatial information through comparison of global temperature indices (e.g. the Urban Heat Island Intensity (UHII)) across years and do not quantify changes in land cover that are associated with temperature change (Kikon et al., 2016; Zhang et al., 2013; Zhao et al., 2017; Zhou et al., 2015, 2014). Transformation of land during urbanisation encompasses a broad range of changes within metropolitan regions which are frequently excluded from temperature analysis, and this needs consideration to address the aforementioned limitations. For example, whilst Xie et al. (2012) and Hu et al. (2015) identified urban to represent the greatest increase in land cover, their analysis focused on the difference between averaged land cover temperatures producing singular metropolitan values that is unable to identify which land cover change induced the greatest temperature change. Exclusion of the holistic impact of land cover change on temperature, alongside the universal assumption of urban homogeneity, which disregards the variability between high and low albedo urban land covers obtaining diverse thermal characteristics, has precluded targeted policies in mitigating changes that most influence surface temperature across metropolitan regions (Deilami et al., 2016; Imhoff et al., 2010; Kikon et al., 2016; Li et al., 2011; Tomlinson et al., 2012; Zhang et al., 2013; Zhou et al., 2016, 2015, 2014).

Perth, the state capital city of Western Australia (WA) has observed rapid outward urban land cover expansion of 201.10 km^2 between 2003 and 2013; eclipsing all major Australian, USA and United Kingdom (UK) cities in terms of suburban development (Kelly et al., 2011; MacLachlan et al., 2017a; U.S. Department of Commerce, 2013). In this research, we consequently use the Perth Metropolitan Region (PMR) as a critical case study for assessing the holistic impact of land cover change on temperature; an identified pre-requisite for effective land cover change policy targeting. The aim of this study is to provide a novel investigation into the spatio-temporal characteristics of the UHI at a sub-metropolitan level (i.e., the dynamics of the UHI within the city limits). Specific objectives are to (1) explore the complexities of the UHI effect and (2) identify the associations between land cover and temperature change, both at the intra-urban scale. The former permits quantified evidence for inclusion in future development policies whilst the latter provides a novel approach to spatio-temporally assess the association of individual land cover alterations from various land cover types (e.g. bare earth, grassland and forest) to urban (low and high albedo) on LST. In this paper we document a detailed approach to disentangle the spatial and

temporal intra-urban disparities of the UHI effect. Our findings illustrate the novelty of the analyses undertaken and we demonstrate the transferability of the process to other metropolitan regions globally.

6.3 Study area

The PMR has experienced sustained rapid urban development during the 21st century coinciding with a booming resource sector (ABS, 2015; MacLachlan et al., 2017a). Rapid outward expansion of the PMR has caused sustainability concerns due to large-scale conversion of natural land to impervious surfaces (Dhakal, 2014; Western Australian Planning Commission, 2015a). Changes of this nature alter the energy balance (supplementary section 6.8.1) increasing the storage of long wave radiation compared to surrounding non-urbanised areas forming the UHI effect (Howard, 1988) (Figure 6-1).

The strategic guide for the long term (2050) development of Perth, produced by the Western Australian Planning Commissions (WAPC), specifies sustainability as a key strategy and reducing the UHI as one of sixteen aspirations under the strategy for the Planning Commission, State and Local Government (Western Australian Planning Commission, 2015a). Furthermore, future land rezoning must meet strategic urban planning objectives, rather than in response to individual requests under the key strategy to improve use of existing and proposed urban land supply (Western Australian Planning Commission, 2015a). Other Australian State capitals including Sydney, Melbourne and Adelaide are involved with the Urban Climates Project identifying effects of the UHI for integration into planning and design guidelines (Boland and Philipp, 2013). However, current global UHI methodologies frequently provide singular metropolitan temperature comparison values for cities, which are inappropriate for assessing land-cover temperature change relationships at the intra-urban scale (Kikon et al., 2016; Zhang et al., 2013; Zhao et al., 2017; Zhou et al., 2015, 2014). Such limitations in current UHI measurement approaches prevent effective UHI mitigation and future sustainable rezoning policy formulations required at the sub-metropolitan level, as defined by the State, Planning Commission and Local Government strategies (Western Australian Planning Commission, 2015a).

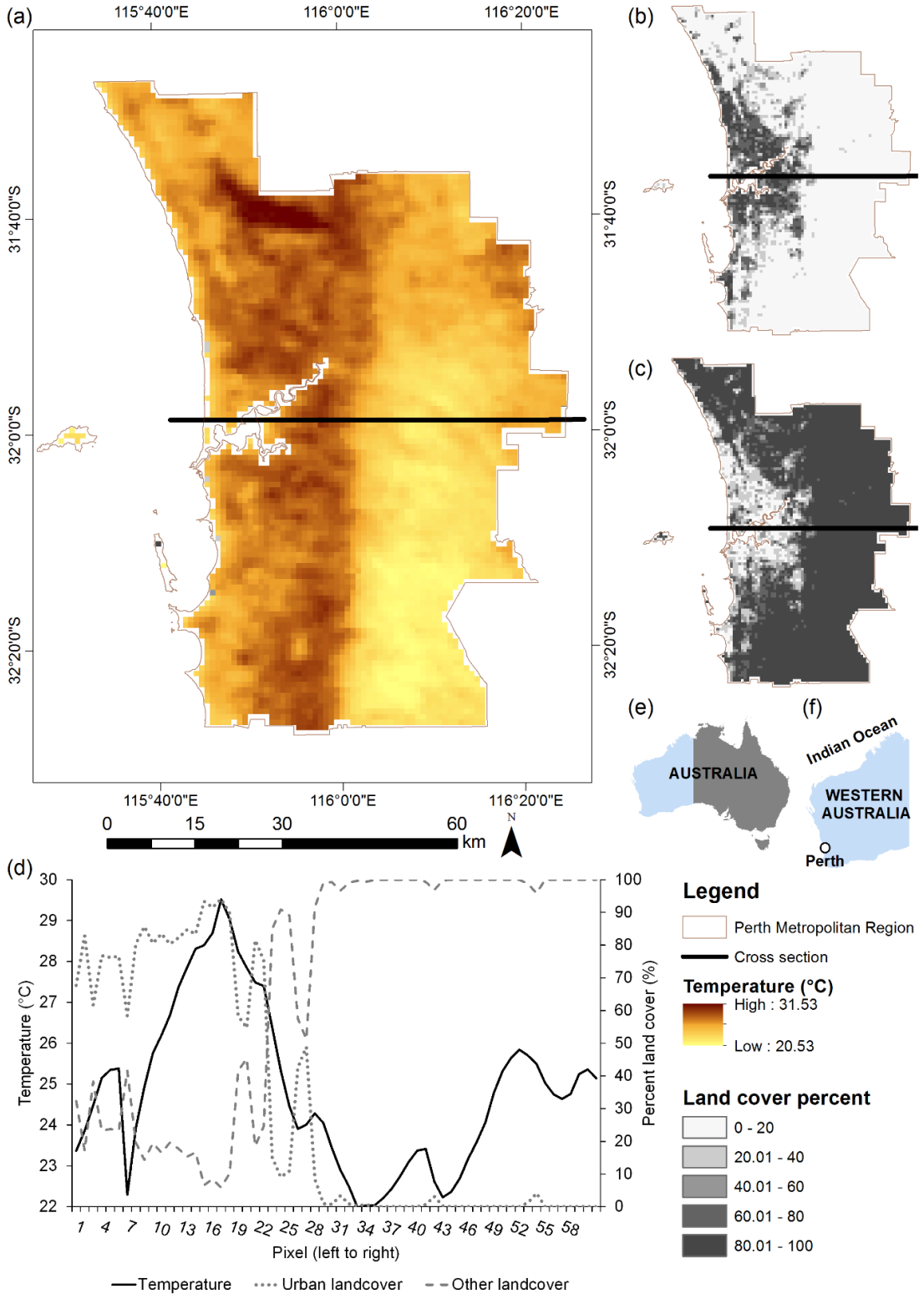

Figure 6-1. A cross section illustrating the UHI effect in Perth, WA, using 2015 average annual daytime temperature derived from MODIS Terra LST product (MOD11A1) (a) in relation to the percent urban (b) and other land cover (c) area, per MODIS pixel based on classified Landsat imagery, graphically displayed (d) with WA identified in (e) and Perth city (f).

Perth currently lacks investigation into the causes and consequences of the UHI effect. Ranked consistently as Australia's fastest growing capital city in terms of population between 2007 and 2014, the majority of urban development occurred as outward low-density suburban expansion (Kelly et al., 2011; MacLachlan et al., 2017a; U.S. Department of Commerce, 2013). Between 1990 and 2015 the urban area of the PMR increased by 45.3% (320.34 km^2), with a 37.4% increase since 2000 (279.80 km^2) (MacLachlan et al., 2017a). Perth's rapid urban expansion can be accredited to Australia's 21st century mineral and energy boom, contributing 95% of the WA's export earnings between 2010 and 2011 with the state's value of mineral and petroleum resources increasing from AUD 4.7 billion in 1996 to a peak of AUD 121.6 billion mid-2013 (Department of Mines and Petroleum, 2015). Given the spatial and temporal dynamics of Perth's changing urban environment, the metropolitan region provides a unique national and globally important case study in spatio-temporally quantifying the intra-urban complexities of rapidly expanding impervious surface areas and the association with LST (Rizwan et al., 2008).

6.4 Data and methodology

6.4.1 Land cover data

Land cover estimates derived from cloud-free Landsat surface reflectance imagery were obtained from MacLachlan et al. (2017b) for the years 2003 (accuracy: 80.33%, kappa coefficient: 0.72) and 2013 (accuracy: 79.00%, kappa coefficient: 0.70) (MacLachlan et al., 2017b). These land cover images were classified by MacLachlan et al. (2017a) into six land cover types; high reflectance urban (e.g. concrete), low reflectance urban (e.g. asphalt), forest, water, grassland and bare earth (MacLachlan et al., 2017a). Two urban land cover classes were defined to reduce spectral confusion between spectrally similar classes and to better represent urban heterogeneity that influences surface thermal properties (MacLachlan et al., 2017a). Unique values were attributed to Landsat (30 × 30 m) land cover types in 2003 and 2013, with subtraction permitting identification of land cover change aggregated to a MODIS pixel. MODIS pixels which obtained a change in land cover greater than all other changes within the pixel and the change to land cover dominated (>50%) the MODIS pixel were identified (Figure 6-2 (a)). A three-year temperature average of selected years (2002–2004 and 2012–2014) reduced natural inter-annual variation (e.g. supplementary section 6.8.3), solely for the land cover change – LST analysis in line with Zhang et al. (2012), Imhoff et al. (2010) and Hu et al. (2015) to create seasonal and annual composite temperature images for 2003 and 2013 (Figure 6-3 (b)).

6.4.2 MODIS temperature data

To assess the association between urban expansion and land cover change on LST within the PMR daily raw MODIS Terra LST data (MOD11A1, collection 5; (Wan, 2006)) were used. MODIS LST data provides both daytime (local time: 10:30 h) and nighttime (local time: 22:30 h) 1 km^2 LST, with the longest consistent record of surface temperature data overcoming temporal and swath restrictions of satellites such as Landsat and the Advanced Spaceborne Thermal Emission and Reflection Radiometer (ASTER) that revisit every 16 days with swaths of 185 km and 60 km respectively providing reduced opportunities for cloud free imagery and precluding complete metropolitan region coverage (Cao et al., 2010; Fu and Weng, 2016). Independent validation has found MODIS LST to obtain an average accuracy of −0.34 K (standard deviation 0.61 K) agreeing with the stated accuracy of 1 K and in most cases 0.5 K (supplementary section 6.8.2) (Wan, 2013). Annual and seasonal; Summer (December–February), Autumn (March–May), Winter (June–August) and Spring (September–November) composites for coincident land cover data of MODIS LST diurnal and nocturnal data were generated on a per pixel basis through consideration of valid pixels only for 2003 and 2013.

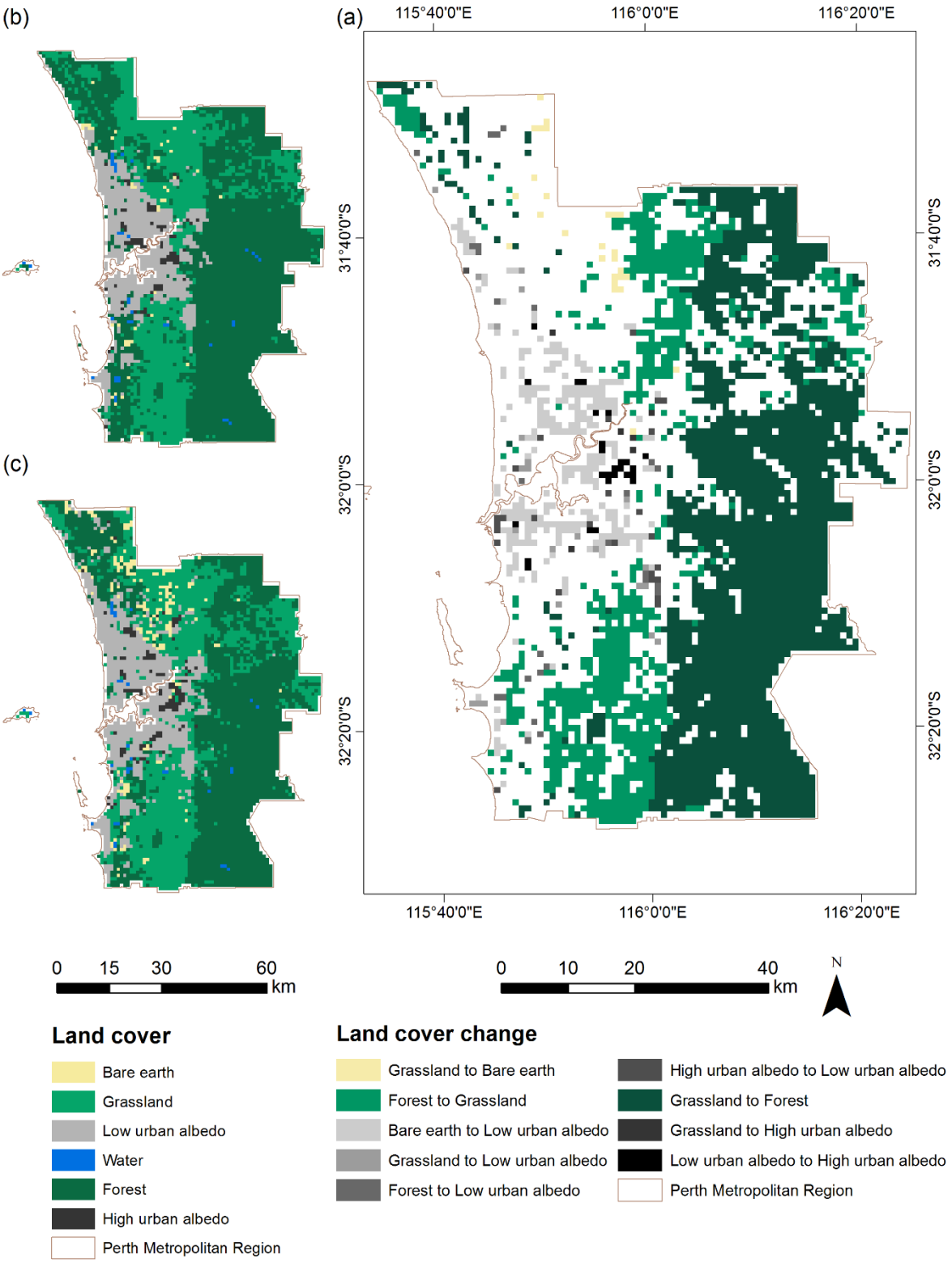

Figure 6-2. Land cover change meeting the criteria of (1) greater than all other changes within a MODIS pixel and (2) the change to land cover dominates (>50%) the 2013 MODIS pixel. Change is derived between 2003 and 2013 from classified Landsat data aggregated to MODIS resolution, where white pixels do not meet the criteria (a), alongside static land cover maps from 2003 (b) and 2013 (c).

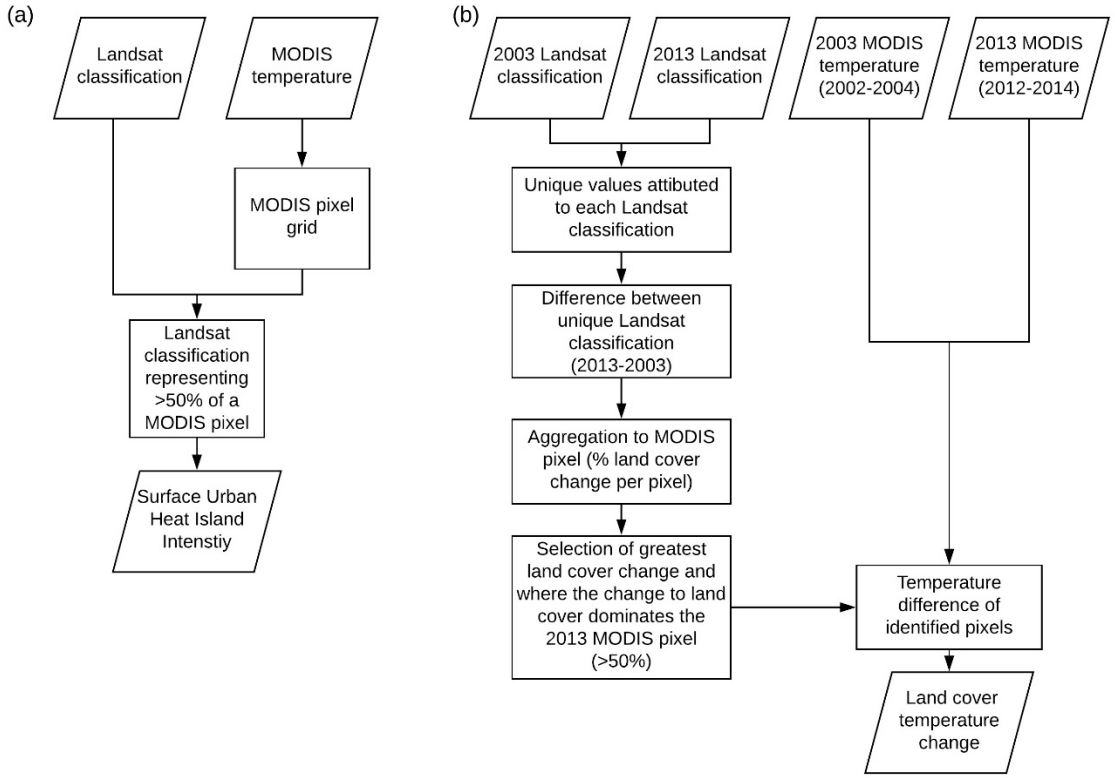

Figure 6-3. Summary of methodological procedures for: (a) SUHII and (b) land cover temperature change.

6.4.3 Establishing a UHI effect

Extraction of the underlying land cover from classified Landsat data per MODIS pixel permitted temperature sub pixel analysis (Hu et al., 2015). Dominant land cover, representing >50% of a MODIS pixel, was compared against MODIS LST (Figure 6-3 (a)).

The association between urban area and LST was established through the Surface UHI Intenisty (SUHII) which compares the temperature of urban surfaces to that of surfaces comprising of different land cover types (Haashemi et al., 2016; Hu et al., 2015; Li et al., 2012; Rizwan et al., 2008):

$$SUHII = LST_{urban} - LST_{other} \quad (6.1)$$

where LST_{urban} is the surface temperature of a MODIS pixel defined as being urban and LST_{other} is the temperature of an alternative land cover type (e.g. forest) to be differenced from urban. This formula can be applied either as a global average or on a per pixel basis. The former takes the average temperature of all urban pixels compared to the average temperature of all comparison land cover pixels (e.g. forest) producing a single output value (e.g. Haashemi et al., 2016). The

latter considers the average temperature of the comparison land cover (e.g. forest) compared to that of each individual urban pixel, permitting a mapped distribution of the SUHII (e.g. Li et al., 2012). In order to identify the mean variation of land cover temperature across the PMR in relation to low urban albedo, the SUHII was calculated as both a static average and between year SUHII difference on a per pixel basis. The former compares the average urban land cover temperature to each land cover type (e.g. urban compared to bare earth) for both 2003 and 2013 consistent with Haashemi et al. (2016) and Wang et al. (2015). The later compares the difference between the SUHII on a per pixel basis between 2003 and 2013, where the SUHII is the difference between individual urban (high and low albedo) and the average forest temperature for both 2003 and 2013, permitting identification of SUHII spatial-temporal variation.

6.5 Results

6.5.1 Spatial and temporal dynamics of the urban heat island

6.5.1.1 Land cover and land surface temperature

A comparison between land cover percentage for four land cover types (bare earth, grassland, low urban albedo and forest) and temperature exhibits the relationship between land cover and annual LST during the daytime (Figure 6-4) and nighttime (Figure 6-5). (Due to the limited number of high albedo urban (91) and water pixels (25) that dominate a MODIS pixel, these land cover types were excluded from this analysis). Land cover percentage per MODIS pixel and temperature values were spatially averaged using a 3 × 3 kernel, with the linear regression trend subsequently calculated (e.g. Hu et al., 2015; Smith, 2003). Annual daytime variation indicates higher temperatures are associated with an increasing percentage of bare earth, grassland and low urban albedo, whilst additional forested percentage per MODIS pixel is associated with lower LST, consistent between 2003 and 2013 (Hu et al., 2015). During nighttime all trends are reversed excluding low urban albedo land cover that is associated with higher LST. Data in 2013 was nocturnally warmer than 2003, however a three year averaging of later land cover-temperature association analysis reduced natural inter-annual variation (e.g. Hu et al., 2015; Imhoff et al., 2010; Zhang et al., 2012).

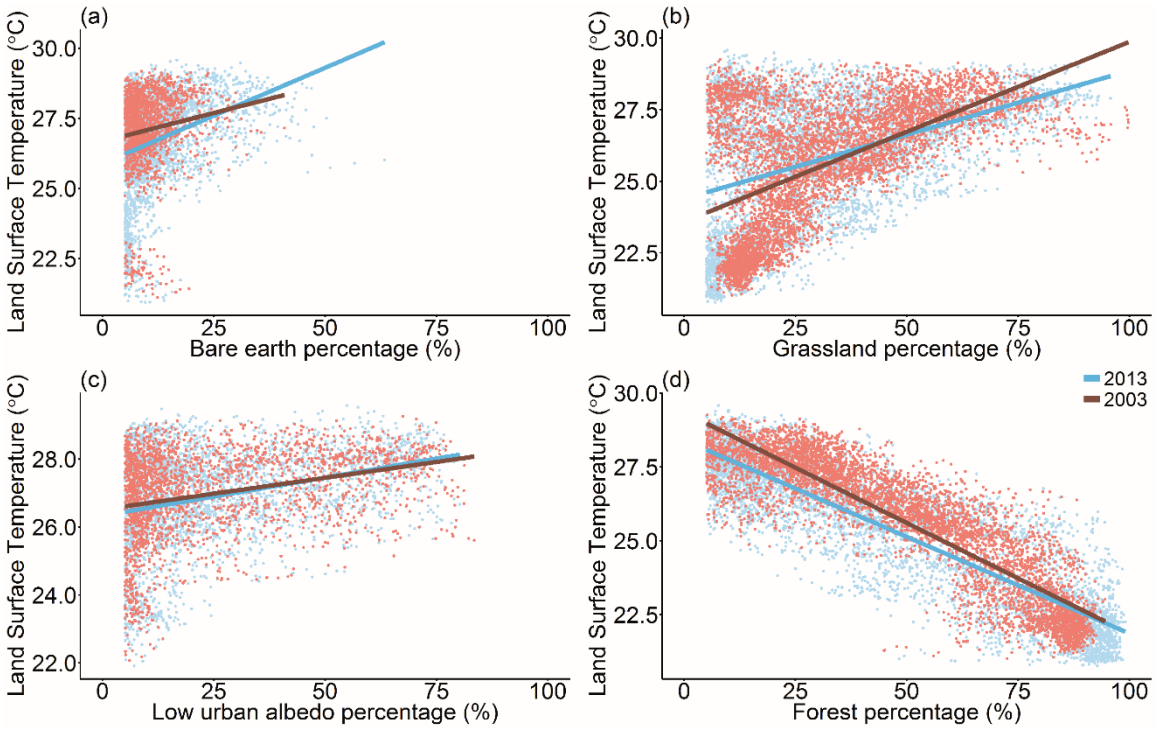

Figure 6-4. The 2003 and 2013 percentage land cover within a MODIS pixel and the average annual daytime LST in 2003 and 2013 for (a) Bare earth (b) Grassland (c) Low urban albedo and (d) Forest, with points (lighter colours) representing individual values of each year. All linear trends are statistically significant at $p < 0.05$.

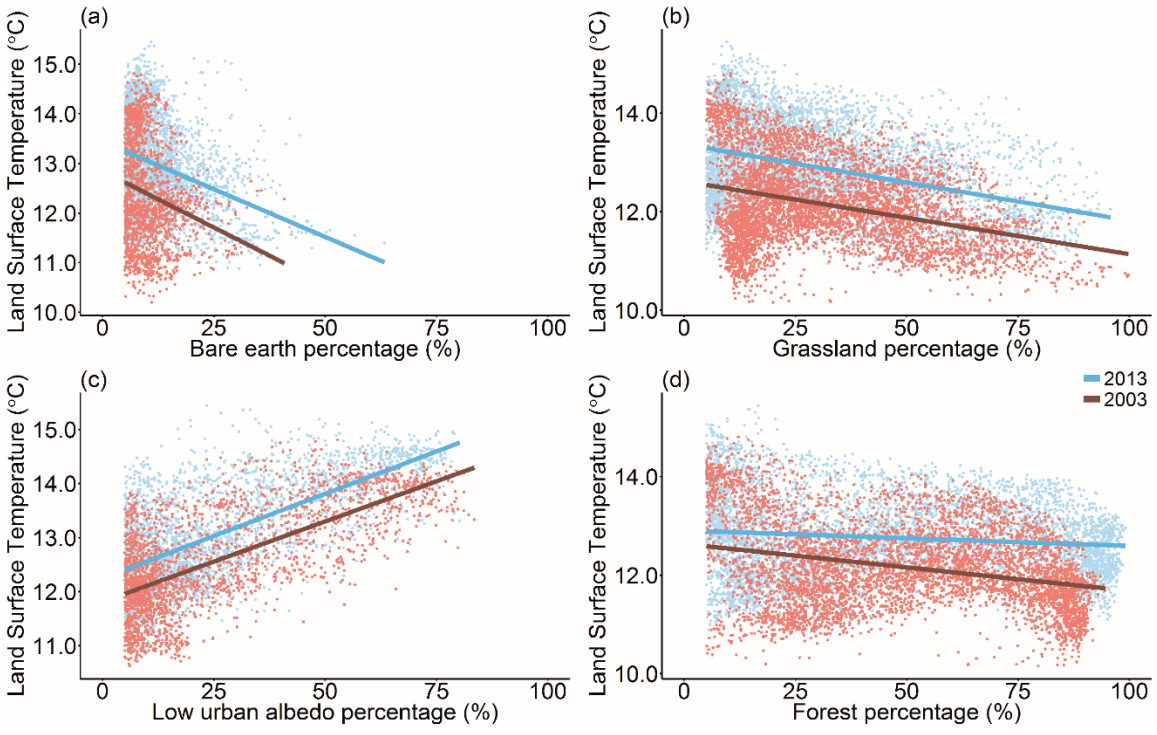

Figure 6-5. The 2003 and 2013 percentage land cover within a MODIS pixel and average annual nighttime LST for 2003 and 2013 for (a) Bare earth (b) Grassland (c) Low urban albedo and (d) Forest, with points (lighter colours) representing individual values of each year. All linear trends are statistically significant at $p < 0.05$.

6.5.1.2 Temporality of the surface urban heat island intensity

To further investigate the association between urban land cover and surface temperature, the average SUHII was computed for classified land cover data for both day and night LST by season and year for 2003 and 2013 (Table 6-1). Diurnal SUHII of low albedo urban was consistently most pronounced in comparison to forest land cover. This is likely due to vegetated areas increasing localised evapotranspiration that cools the local climate resulting in lower LST (Cao et al., 2010) (Table 6-1, Figure 6-4 (d)). However, inter-annual seasonal variations were evident owing to the natural variation of land cover types (supplementary section 6.8.3).

Low urban albedo land cover is representative of suburban locations whilst high urban albedo cover is commonly located within the CBD and industrial sites (MacLachlan et al., 2017d, 2017a). The WAPC specify that the majority of new development within the PMR has occurred as low-density suburban growth, with low urban albedo land cover increasing 20.39 km^2 compared to only 7.59 km^2 of high urban albedo land cover between 2000 and 2015 (Western Australian Planning Commission, 2015a). Diurnal high albedo locations generate additional anthropogenic heat from population movement and economic activity whilst dormant suburban locations

contain greater vegetation cover (associated with higher Normalised Difference Vegetation (NDVI) values) that shades and cools the environment (e.g. Fabrizi et al., 2010; Kennewell and Shaw, 2008). The SUHII is more prominent in spring and summer over autumn and winter across all land covers owing to temperature being tied to the seasonality of climatic factors (e.g. sunlight hours, precipitation and wind) (supplementary section 6.8.3) (Oke, 1982; Xu and Chen, 2017).

Table 6-1. Day and nighttime SUHII and standard deviation (in brackets) between Low Urban albedo (UL) and land cover classes: Bare Earth (BE), Grassland (G), Water (W), Forest (F) and High Urban albedo (UH). Combined urban of both Low and High urban albedo (U) was also separately compared to Forest (F).

Time of day	Season	Year	UL vs. BE (°C)	UL vs. G (°C)	UL vs. W (°C)	UL vs. F (°C)	UL vs. UH (°C)	U vs. F (°C)
Daytime	Summer	2003	-0.29 (1.94)	-2.81 (1.94)	3.26 (1.94)	3.50 (1.94)	-1.10 (1.94)	3.56 (1.92)
		2013	-1.74 (2.02)	-1.98 (2.02)	4.21 (2.02)	3.98 (2.02)	-1.22 (2.02)	4.08 (2.01)
	Autumn	2003	-0.26 (1.10)	-0.88 (1.10)	1.10 (1.10)	2.65 (1.10)	-0.56 (1.10)	2.68 (1.09)
		2013	0.06 (1.05)	-0.16 (1.05)	1.91 (1.05)	3.47 (1.05)	-0.36 (1.05)	3.51 (1.03)
	Winter	2003	0.74 (0.66)	1.06 (0.66)	1.22 (0.66)	2.79 (0.66)	-0.11 (0.66)	2.78 (0.66)
		2013	0.55 (0.62)	0.91 (0.62)	1.41 (0.62)	2.66 (0.62)	0.16 (0.62)	2.65 (0.63)
	Spring	2003	0.93 (1.76)	1.49 (1.76)	3.50 (1.76)	4.43 (1.76)	-1.49 (1.76)	4.53 (1.77)
		2013	0.55 (1.73)	2.02 (1.73)	4.49 (1.73)	5.16 (1.73)	-1.28 (1.73)	5.27 (1.75)
	Annual	2003	0.20 (1.30)	-0.15 (1.30)	2.29 (1.30)	3.32 (1.30)	-0.73 (1.30)	3.36 (1.29)
		2013	-0.04 (1.28)	0.36 (1.28)	2.94 (1.28)	3.86 (1.28)	-0.52 (1.28)	3.91 (1.27)
Nighttime	Summer	2003	1.23 (0.62)	1.88 (0.62)	-0.13 (0.62)	1.09 (0.62)	0.07 (0.62)	1.09 (0.63)
		2013	1.32 (0.64)	1.73 (0.64)	0.05 (0.64)	1.31 (0.64)	0.11 (0.64)	1.30 (0.64)
	Autumn	2003	1.45 (0.75)	1.88 (0.75)	0.67 (0.75)	1.44 (0.75)	0.01 (0.75)	1.44 (0.76)
		2013	1.90 (0.69)	1.87 (0.69)	0.24 (0.69)	1.44 (0.69)	0.21 (0.69)	1.42 (0.70)
	Winter	2003	1.05 (0.68)	1.35 (0.68)	-0.47 (0.68)	1.33 (0.68)	0.21 (0.68)	1.32 (0.69)
		2013	1.58 (0.65)	1.37 (0.65)	-0.31 (0.65)	1.25 (0.65)	0.43 (0.65)	1.21 (0.66)
	Spring	2003	1.62 (0.73)	2.09 (0.73)	-0.63 (0.73)	1.76 (0.73)	0.10 (0.73)	1.76 (0.73)
		2013	1.96 (0.73)	1.75 (0.73)	-0.18 (0.73)	1.82 (0.73)	0.13 (0.73)	1.81 (0.72)
	Annual	2003	1.49 (0.72)	1.92 (0.72)	0.01 (0.72)	1.56 (0.72)	-0.06 (0.72)	1.56 (0.73)
		2013	1.94 (0.67)	1.72 (0.67)	-0.12 (0.67)	1.39 (0.67)	0.16 (0.67)	1.37 (0.67)

In comparison, all land covers (excluding water due to its high heat capacity) are nocturnally cooler than low urban albedo (Table 6-1) (Zhao et al., 2017). During nighttime the absence of solar radiation precludes evaporation and transpiration from vegetation (grassland and forest land covers); the latter due to stomata closure based on the inability to photosynthesize (Daley and Phillips, 2006) (Figure 6-5 (d)). Similarly, the low thermal inertia of bare earth and grassland results in rapid cooling of these land cover types (Weng et al., 2004) (Figure 6-5 (a,b)). However, low urban albedo surfaces are able to absorb and retain a large proportion of the shortwave radiation during the daytime which is re-emitted at long wavelengths at nighttime, and provide the only land cover to consistently increase nocturnal LST with percentage coverage (Figure 6-5 (c)) (Zhao et al., 2016). Contrastingly, high urban albedo surfaces reflect a greater proportion of solar radiation, negating thermal storage and resulting in lower nighttime surface temperatures (Sharifi and Lehmann, 2014). In the absence of direct incoming solar radiation, the surface properties (e.g. heat capacity and thermal conductivity) and low cooling rate subdues the nocturnal effect of seasonality which is consistent with the findings of Peng et al. (2012) and Imhoff et al. (2010) who identified nocturnal seasonal amplitudes of less than 1 °C (Tran et al., 2006).

6.5.1.3 Spatiality of the surface urban heat island intensity

Spatially explicit differences are identified when considering a per pixel methodology in order to identify the change in SUHII between 2003 and 2013. The SUHII was computed for both 2003 and 2013, comparing both low and high urban albedo land cover to the average forest LST on a per pixel basis, with the per pixel SUHII then differenced for annual and seasonal day (Figure 6-6) and night (Figure 6-7) LST. The results indicate that the daytime SUHII difference has increased across the metropolitan region, whilst the nighttime SUHII difference is most pronounced in outer urban pixels associated with land cover change (Figure 6-2). Nevertheless analysis of this nature, commonly seen throughout UHI research (e.g. Li et al., 2012; Shen et al., 2016; Tomlinson et al., 2012) fails in practicality through sole specification of differences in land cover temperature. Consequently planning authorities are currently unable to base development decisions on appropriate land cover change that results in minimal SUHII exacerbation. In this regard the subsequent land cover change methodology permits credible targeted land cover change policies in effective mitigation of land cover change that is most associated with surface temperature.

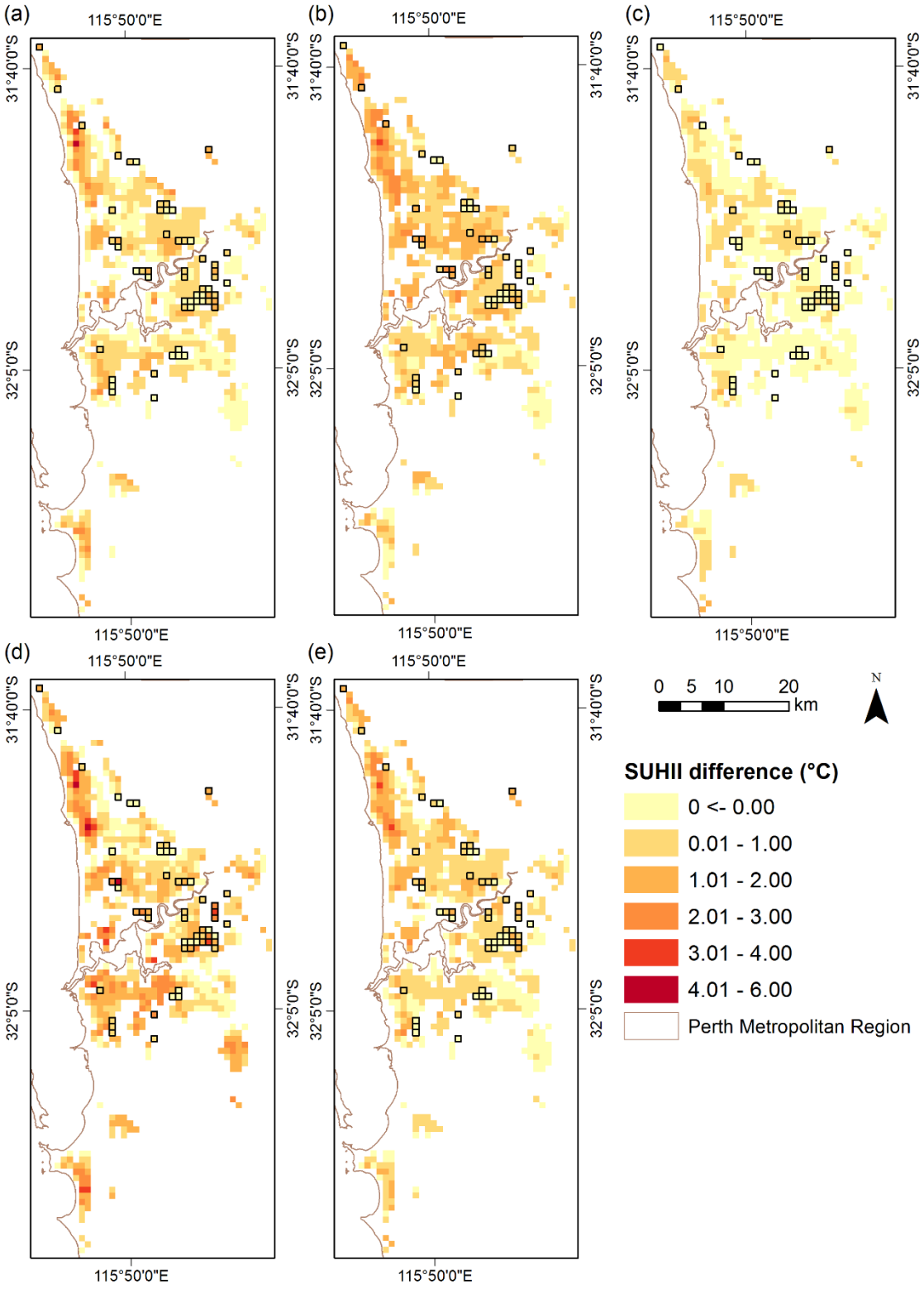

Figure 6-6. The spatial distribution of the difference in daytime SUHII for pixels that remained urban between 2013 and 2003 for: (a) summer (b) autumn (c) winter (d) spring and (e) annual. Urban (low and high albedo) and forest MODIS pixels are identified where a single Landsat land cover class composes >50% of a MODIS pixel. Black outlined MODIS pixels represent high urban albedo.

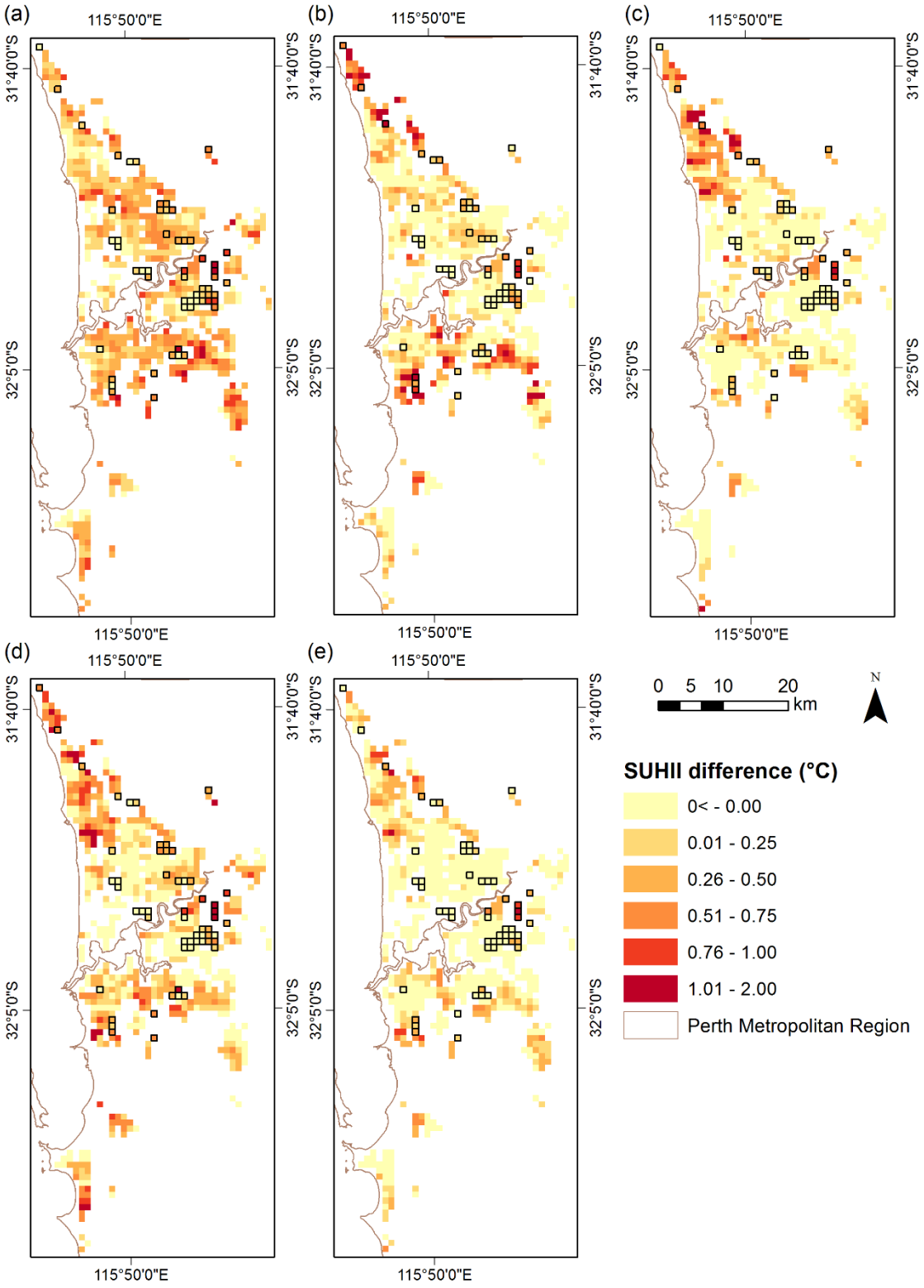

Figure 6-7. The spatial distribution of the difference in nighttime SUHII for pixels that remained urban between 2013 and 2003 for: (a) summer (b) autumn (c) winter (d) spring and (e) annual. Urban (low and high albedo) and forest MODIS pixels are identified where a single Landsat land cover class composed >50% of a MODIS pixel. Black outlined MODIS pixels represent high urban albedo.

6.5.2 Land cover change and land surface temperature

Dominant land cover change from 2003 to 2013 was compared to both the daytime and nighttime LST difference. Of the conversion from all land cover types investigated, forest to low urban albedo and grassland to bare earth produced the most pronounced daytime land cover surface temperature associations (Table 6-2). These observations were replicated with nighttime surface temperature, with the addition of grassland to forest land cover change (Table 6-2). Forest to low urban albedo consistently produced the highest nighttime temperature association (annual: 0.88 °C) across all seasons and that of daytime winter (0.58 °C) and spring (0.85 °C), with only bare earth to low urban albedo in summer (0.31 °C) and autumn (0.72 °C) obtaining higher values.

Figure 6-8 (cross section from Figure 6-1) illustrates a diverse range of land cover changes intersecting the PMR in an applied example. Here, land cover change from forest to low urban albedo produced the largest associated change in both daytime and nighttime temperature of 0.40 °C and 0.37 °C respectively. During daytime, change from bare earth to low urban albedo produced the second most associated temperature change (0.37 °C), whilst during nighttime conversion from grassland produced a marginally higher average value of 0.77 °C (bare earth 0.73 °C). The least overall land cover associated temperature change was from low urban albedo to high urban albedo, with values of 0.19 °C and 0.72 °C for daytime and nighttime respectively.

Table 6-2. Average land cover associated LST change between 2003 and 2013 for the greatest land cover change within a MODIS pixel and the change to land cover that dominates the pixel (>50%). Classes are represented as: Bare Earth (BE), Grassland (G), Forest (F), Low Urban albedo (UL) and High Urban albedo (UH).

Time of day	Season	F to UL (°C)	G to UL (°C)	BE to UL (°C)	UH to UL (°C)	F to G (°C)	G to F (°C)	G to BE (°C)	UL to UH (°C)	G to UH (°C)
Daytime	Summer	0.13	-0.14	0.31	0.11	-0.55	-0.17	0.05	0.20	0.00
	Autumn	0.35	0.32	0.72	0.45	0.19	-0.10	0.65	0.62	0.66
	Winter	0.58	0.46	0.44	0.41	0.51	0.40	0.42	0.35	0.19
	Spring	0.85	0.47	0.39	0.46	0.39	0.12	0.39	0.29	0.51
	Annual	0.40	0.16	0.37	0.19	0.08	0.00	0.44	0.15	-0.05
Nighttime	Summer	1.09	1.09	1.03	1.06	0.94	0.92	0.95	0.86	0.90
	Autumn	0.32	0.25	0.26	0.21	0.15	0.21	0.44	0.19	0.12
	Winter	0.54	0.45	0.27	0.38	0.24	0.65	0.18	0.09	0.04
	Spring	1.13	1.04	0.98	0.96	0.96	0.96	1.00	0.78	0.75
	Annual	0.88	0.77	0.73	0.72	0.70	0.80	0.80	0.58	0.47

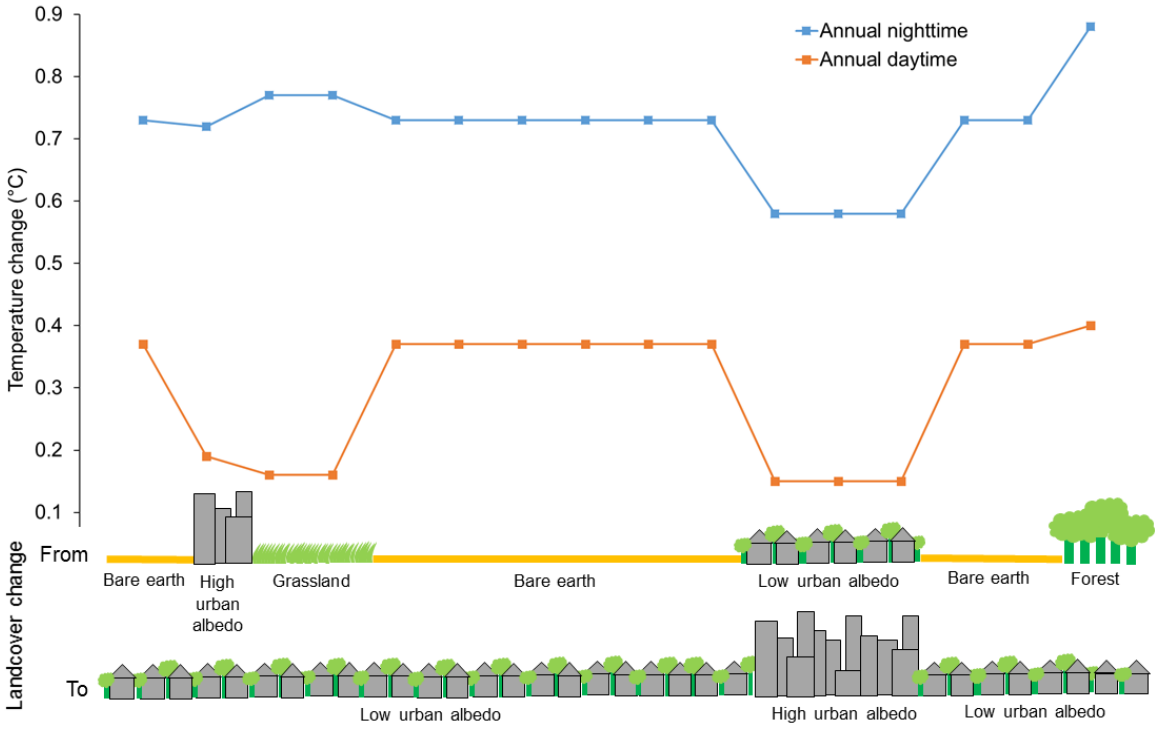

Figure 6-8. Land cover and average annual day and nighttime LST change between 2003 and 2013 for the cross section identified in Figure 6-1, excluding pixels of no change.

6.6 Discussion

Identifying the impact of land cover change on the UHI effect is essential in ensuring sustainable and strategic future planning decisions and alignment with global (e.g. C40 CCLG, 2030 sustainable development goals and CRF), national (e.g. Cooperative Research Centre-Low Carbon Living (CRC-LCL)) and other metropolitan frameworks (e.g. Tokyo, New York and London) (Boland and Philipp, 2013; C40 Cities, 2018; C40 Cities and ARUP, 2011; Governor of Tokyo, 2008; Mayor Bill de Blasio, 2014; Mayor of London, 2016b; Osborn et al., 2015; Revi et al., 2014; Rizwan et al., 2008). In this study, SUHII analysis identified higher low urban albedo daytime temperatures in comparison to water and forest, whilst low urban albedo was persistently warmer at nighttime than all other land covers, consistent with results from Jingjintang, China (AECOM Australia, 2012; Zhou et al., 2015). Our research has advanced UHI analysis to explicitly establish the association between land cover change and LST.

The effects of urbanisation on LST to enhance understanding of the urban climate are commonly investigated as the difference in temperature between land cover types in both temporally static (Li et al., 2011; Tomlinson et al., 2012) and dynamic studies (Kikon et al., 2016; Zhang et al., 2013;

Zhao et al., 2017; Zhou et al., 2015, 2014). Whilst the latter considers changes in urban area over time, both can simplistically divide land cover into urban and non-urban (Shastri et al., 2017). The land cover change methodology implemented here spatially disaggregates metropolitan SUHII values permitting localised intra-urban land cover-temperature associations as opposed to singular (e.g. Table 6-2) and spatially explicit values (e.g. Figure 6-6 and Figure 6-7). The association between land cover change and temperature directly influences policy applications through refinement of future development zones that will minimise exacerbation of the UHI effect. Information of this sort is critical in future land use planning facilitating improved UHI management and future sustainability.

Here we have shown the association between land cover change and LST between 2003 and 2013 across the PMR, with conversion of grassland to bare earth associated with the maximum average annual daytime increase in LST (0.44 °C) based on an average increase of 24.86% per MODIS pixel and 73.87 km^2 over the complete metropolitan region; the largest land cover change type. Of all conversion to low urban albedo land cover originating from forest obtained the largest associated increased in LST whilst conversion from grassland had the lowest overall association for both low and high urban albedo. While the coarse spatial resolution of MODIS LST negates identification of exact and specific land cover associated UHI change, analysis of this nature overcomes temporal and swath limitations of ASTER and Landsat temperature data for complete metropolitan region coverage.

Integration of EO data such as the land cover change approach implemented here permits quantification of areal land cover change that directly influences land surface temperature whilst considering urban heterogeneity (e.g. high and low urban albedo) enabling future sustainable development mitigating negative socio-environmental outcomes of the UHI effect (Burnett et al., 1997; Deilami et al., 2016; Goggins et al., 2012; Goudarzi et al., 2015; Guhathakurta and Gober, 2007; Orru et al., 2013; Smargiassi et al., 2009; Szyszkowicz and Rowe, 2016; USA Environment Protection Agency, 2008). For example, Coutts et al. (2016) advised a local Melbourne municipality on locations of thermal hotspots from EO data for targeted cooling through urban greening. Using EO derived land cover data in this manner aids in understanding the dynamics of the urban environment that alter local and regional climate and increase vulnerability of city systems in line with the CRF (ARUP and The Rockefeller Foundation, 2015). This is particularly important owing to the range of health, energy, water and economic savings that can be attributed to an increase in temperature of only 1 °C; such as an observed monthly increase of 290 gallons in water per single family household in the Phoenix metropolitan area and overall estimated economic expenditure of AUD 300 million per annum by the city of Melbourne in the first global UHI economic quantification (AECOM Australia, 2012; Guhathakurta and Gober, 2007).

As for the PMR, 'Perth and Peel @ 3.5 million', the strategic metropolitan land use planning framework for local planning schemes describes the unprecedented levels of urban expansion within the region (Western Australian Planning Commission, 2015a). Future urban development is guided by Directions 2031 (Western Australian Planning Commission, 2010a) amending the Metropolitan Region Scheme (MRS) and local planning schemes (Western Australian Planning Commission, 2015b, 2015c, 2015d, 2015e). Within these guiding planning documents only 'Perth and Peel @ 3.5 million' lists reduction of the UHI in current urban areas as one of 50 implementing strategies in achieving the Directions 2031 vision themes of a liveable, prosperous, accessible, sustainable and responsible future (Western Australian Planning Commission, 2015a, 2010a). Inclusion of temperature EO data would permit identification of sustainable future urban development locations (e.g. land cover types) that would minimise the UHI impact. The WAPC aims to achieve 47% of future development as infill by 2050, refinement of current or proposed development zones based on land cover change with minimal temperature association such as grassland would mitigate exacerbation of the UHI effect. Consideration of land cover associated temperature change in this manner would contribute to both the sustainability and improvement of current and future land supply key strategies specified within the local Directions 2031 visions whilst aligning with national (CRC-LCL) and international (C40 CCLG, 2030 sustainable development goals and CRF) frameworks (Boland and Philipp, 2013; C40 Cities and ARUP, 2011; Osborn et al., 2015; Western Australian Planning Commission, 2010a).

The freely available EO data and reproducible methodology implemented within this research could be applied to other global cities in credibly mitigating future unsustainable land cover changes which exacerbate temperature differences and associated socio-economic consequences. This is especially pertinent to developing countries that frequently have broader planning considerations including environmental hazards, amenity centres and current infrastructure, permitting improved decision making whilst maximising often limited financial resources (MacLachlan et al., 2017d; Marfai et al., 2014; Suryahadi and Sumarto, 2003).

6.7 Conclusions

Quantification of urbanisation induced land cover change and associated temperature is essential in order to sustainably expand global cities in accommodating the predicted 2.5 billion additional urban dwellers by 2050. Current temperature UHI studies ignore the complexity of surface temperature dynamics producing singular or per pixel values comparing temperature differences between urban and other land cover types for complete metropolitan areas resulting in inappropriate policy incorporation. Landsat data provides the longest time series of medium resolution imagery to monitor urban growth, whilst MODIS obtains the longest time series of daily

surface temperature data covering complete metropolitan regions. In this research, comparison between land cover change and MODIS temperature data for the PMR indicates that change from grassland to bare earth is associated with the greatest overall annual daytime increase in temperature (0.44 °C), whilst conversion from forest to low urban albedo is associated with the greatest nighttime temperature change (0.88 °C) and greatest daytime change (0.40 °C) in conversion to a low urban albedo surface. Whilst these changes may be context specific (to the PMR) the approach presented provides a novel advancement for investigating spatial and temporal intra-urban effects in cities around the world.

Incorporating land cover change UHI considerations into future development decisions is important in order to reduce exacerbation of temperature that has been associated with poor health outcomes, increased energy and water usage and economic expenditure. Recently launched and future EO sensors such as the Visible Infrared Imaging Radiometer Suite (VIIRS) on board the Suomi National Polar-orbiting Partnership (SNPP) satellite will further enhance land cover change analysis. VIIRS will extend the global MODIS LST record through daily data collection at an improved spatial resolution (750 m) permitting further optmisation of land cover change for sustainable city planning in mitigating socio-economic issues associated with poorly planned urban development.

6.8 Supplementary material

This supplementary material sections supports the main chapter and thesis through providing equations and additional material pertaining to concepts raised within chapter 6. The energy balance and Moderate Resolution Imaging Spectroradiometer (MODIS) Land Surface Temperature (LST) data equation are both detailed and explained within this section alongside figures supporting statements regarding the annual natural variation of land cover temperature. A short discussion surrounding other considered approaches and a list of data used within the chapter are also provided to demonstrate the entirety of analytical process.

6.8.1 Urban heat island concept

Contributing Urban Heat Island (UHI) factors are described in the energy balance equation:

$$Q^* + Q_A = Q_H + Q_E + Q_G \quad (6.2)$$

Where Q^* is net radiation; the balance between incoming and outgoing energy at the top of the atmosphere. Q_A depicts anthropogenic heat emitting systems such as air-conditioning and automobiles. Q_H and Q_E are turbulent fluxes of sensible (energy heating the air) and latent heat

(energy used for evaporation) respectively, while Q_G is the surface conductive heat flux (energy heating the ground). In relation to the UHI convection (Q_H) is representative of building thermal properties, evaporation (Q_E) is a function of vegetation coverage and ground storage (Q_G) is dependent on surface albedo (Arnfield, 2003).

6.8.2 MODIS land surface temperature data

The MODIS LST data Version 5 (V5) implements a modified version of the Product Generation Executives (PGE16) code that entails three modules: PGE16A, PGE16B and PGE16C (new compared to version 4). PGE16A obtains LST (T_s) for each clear sky land pixel per five minutes of MODIS data using the generalised-split window algorithm:

$$T_s = C + \left(A_1 + A_2 \frac{1-\varepsilon}{\varepsilon} + A_3 \frac{\Delta\varepsilon}{\varepsilon^2}\right)\frac{T_{31}+T_{32}}{2} + \left(B_1 + B_2 \frac{1-\varepsilon}{\varepsilon} + B_3 \frac{\Delta\varepsilon}{\varepsilon^2}\right)\frac{T_{31}+T_{32}}{2} \quad (6.3)$$

where ε=0.5$(\varepsilon_{31} + \varepsilon_{32})$ and $\Delta\varepsilon = \varepsilon_{31} - \varepsilon_{32}$ represent the mean and difference surface emissivity values from MODIS bands 31 and 32, based on results of estimated land cover types per pixel established using Thermal-Infrared (TIR) Bidirectional Reflectance Distribution Function (BRDF) and emissivity modelling (Snyder et al., 1998; Wan et al., 2002). T_{31} and T_{32} are the brightness temperatures in these split-window bands. Coefficients C, A_i and B_i (i=1,2,3) are provided from interpolation on multi-dimensional look up tables derived using linear regression of simulated MODIS data from radiative transfer calculations (Wan et al., 2002; Wan and Dozier, 1996). Obtained radiance values are converted to either LST day 1 km^2 or LST night 1 km^2 pixels. PGE16B computes LST and emissivity using bands 20, 22, 23, 29 and 31-32 through the day/night LST algorithm to scale atmospheric parameters for optimal LST and emissivity retrieval. PGE16C removes cloud contamination from LST products (Wan, 2013).

Owing to the large spatial extent of MODIS LST (1 km^2) difficulties ensue when attempting validation from point ground based measurements such as weather stations (Wan, 2013). Therefore validation is achieved through Temperature (T) or Radiance (R) based methods. T validation directly compares ground measurements with satellite LST distributed over the MODIS pixel, whilst the R method estimates in situ temperature from MODIS Top Of Atmosphere (TOA) radiance with surface emissivity, atmospheric temperature and water vapour profiles in a radiative transfer code (Coll et al., 2009). In order to globally validate MODIS LST the R methodology is implemented due to the limited spatial coverage of the T methodology (Coll et al., 2009). Across 32 global sites (the most extensive study to date) accuracy was assessed through differencing R derived LST and MODIS LST with an average of -0.34 K and standard deviation of

0.61 K, agreeing with the pre-launch statement that accuracy is better than 1 K and in most cases 0.5 K (Wan, 2013).

6.8.3 Seasonal land cover temperature variation

Seasonal land cover temperature variation was computed using the complete time series (2000, 2003, 2005, 2007, 2013 and 2015) of classified Landsat imagery from MacLachlan et al. (2017a, 2017b) and MODIS Terra LST data (MOD11A1, collection 5; (Wan, 2006)) for daytime (Supplementary Figure 6-9) and nighttime (Supplementary Figure 6-10). Temperature was assigned to a land cover class where it represented more than 50% of a MODIS pixel area of either the coincident year of classified image or future classified image where no coincident land cover data existed.

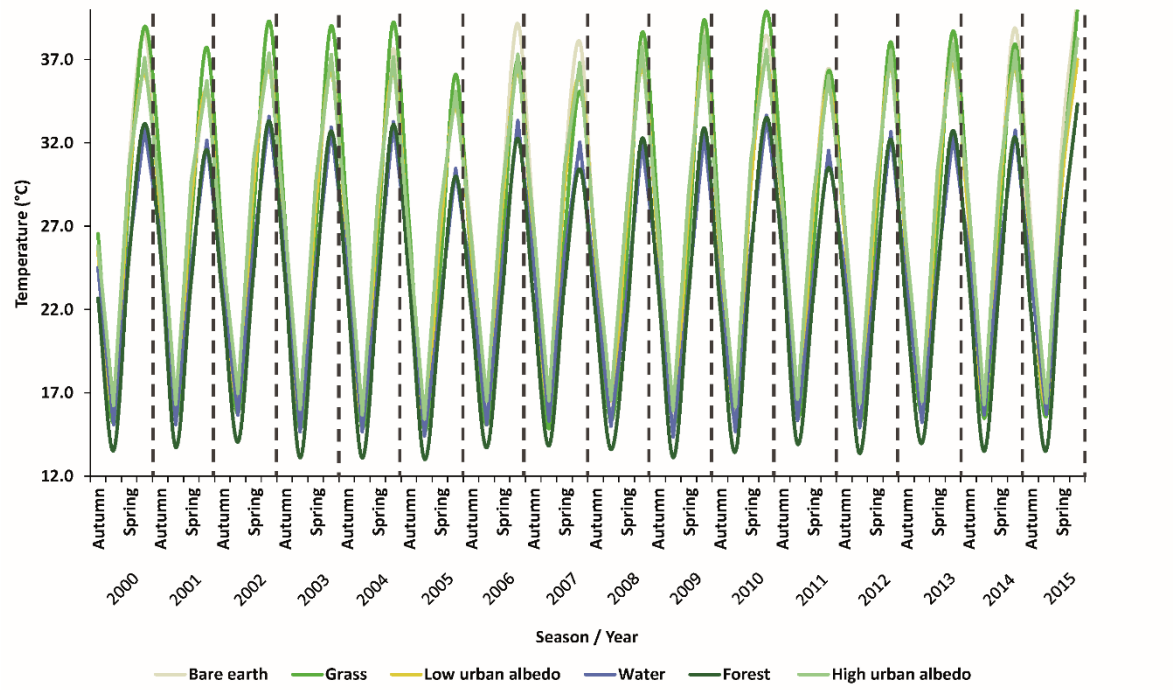

Supplementary Figure 6-9. Seasonal daytime land cover temperature average between 2000 and 2015 from MODIS LST, using coincident or future Landsat land cover classes aggregated to MODIS resolution where it represented more than 50% of a MODIS pixel area.

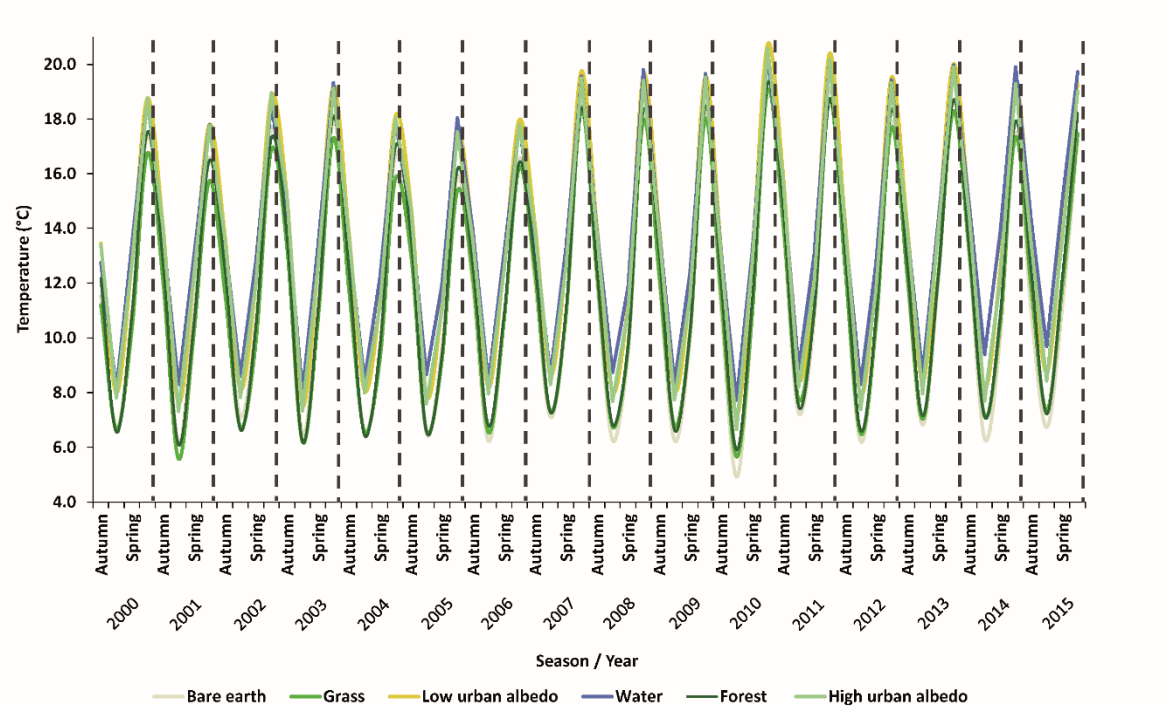

Supplementary Figure 6-10. Seasonal nighttime land cover temperature average between 2000 and 2015 from MODIS LST, using coincident or future Landsat land cover classes aggregated to MODIS resolution where it represented more than 50% of a MODIS pixel area.

6.8.4 Other considered data and approaches

A multitude of alternative land cover and temperature data were considered and tested when undertaking analysis within this chapter. The former includes those datasets mentioned within previous supplementary considerations including: GlobeLand30 (classified Landsat data for 2000 and 2010) (Chen et al., 2015), the European Space Agency's (ESA) Climate Change Initiative (CCI) annual global land cover (300 m) time series (1992-2015) (European Space Agency, 2017) and yearly MODIS land cover products (500 m or 0.05°) (Friedl et al., 2002). However, the lack of a comprehensive record of classified imagery (e.g. GlobeLand30) in coinciding with averaging MODIS temperature data across multiple years to reduce inter-annual variation precluded inclusion. Furthermore, whilst CCI and MODIS land cover products could have provided annual land cover data, their coarser resolution would have reduced the potential in identifying land cover change between years, unable to detect the nuances possible with Landsat data.

In the case of temperature data several other sources were contemplated and computed including that from: Advanced Along-Track Scanning Radiometer (AATSR, on-board the Environmental Satellite) and Thematic Mapper (TM, on board Landsat). However, AATSR was excluded owing to a repeat cycle of 35 days with operational ability between only 2002 and 2012.

Whilst extensive investigation was undertaken with TM in generating LST the lack of compulsory simultaneous in-situ parameters such as atmospheric water content alongside limited data availability (every 16 days assuming cloud free coverage) and the requirement of two images captured over multiple days that resulted in temperature variation unrepresentative solely of land cover prevented effective use. Additionally, the years chosen for the chapter were preselected through weather station temperature analysis to ensure variation that was not influenced by anomalies such as heatwaves. Therefore based on these restrictions and the requirement of daily data, MODIS data from the Terra platform was selected for use within the chapter.

6.8.5 Chapter data list

This section provides an overview of the data presented and analysed within this chapter.

Supplementary Table 6-3. Summary of the data, sources and applications used within chapter 6.

Data	Source	Application
Classified Landsat land cover data between 2000 and 2015 (six images used). Raw data remains the same as that detailed in Supplementary Table 4-3	Chapter 4 or MacLachlan et al. (2017b)	1. Determining land cover temperature relationship (only 2003 and 2013 classified data) 2. Demonstrating land cover inter-annual variation (all data)
Twice daily MODIS data (local WA time: 10:30 and 22:30) from the Terra platform between 2000 and 2015, collection 5, scene identifier h27v12	Online Data Pool, courtesy of the National Aeronautics and Space Administration [Land Processes. Distributed Active Archive Center]	1. Determining land cover temperature relationship (only 2002-2004 and 2012-2014 temperature data) 2. Demonstrating land cover inter-annual variation (all data)

Chapter 7 Earth observation for sustainable city planning

7.1 Abstract

Urban areas are expected to triple by 2030 in order to accommodate 60% of the global population. Anthropogenic landscape modifications expand coverage of impervious surfaces inducing the urban heat island effect; a critical 21st century challenge associated with increased economic expenditure, energy consumption and adverse health impacts. Yet omission of urban heat island measures from global climate models and metropolitan planning methodologies precludes effective sustainable development governance. We present an approach which integrates Earth observation and climate data with three-dimensional urban models to optimise vegetation placement (per m^2) within proposed urban developments to enable more effective localised UHI mitigation. Such data-driven planning decisions will enhance the future sustainability of our cities to align with current global urban development agendas.

7.2 Introduction

The United Nations (UN) New Urban Agenda aims to readdress the way in which cities are planned, designed, financed, developed, governed and managed to sustainably accommodate 60% of the global population by 2030. As one of the 21st century's most transformative trends, urbanisation over this time frame will accommodate approximately 1.024 billion people alongside a tripling of the urban land cover footprint (Seto et al., 2012). Anthropogenic modifications whereby natural land covers are converted to urban surfaces is accepted as the most extreme form of land cover change, often initiating the Urban Heat Island (UHI) effect where temperatures increase over human-made surfaces that can induce adverse socio-economic and environmental consequences (Hu et al., 2015). In the city of Melbourne, the economic implications of the UHI exceed AUD 300 million annually, and in Hong Kong the social repercussions of a 1°C rise in temperature above 29 °C increases mortality rates by 4.1% (Goggins et al., 2012). Environmentally, modelling for the city of Phoenix implies continued unsustainable water consumption where an increase of 0.56°C in daily minimum temperature escalates monthly water consumption by over 1,000 litres per family household (Guhathakurta and Gober, 2007), yet such models fail to account for the UHI effect which is exacerbating water and energy consumption in cities globally (Guhathakurta and Gober, 2007). Sustainable urban management is of vital contemporary importance to cities since the UHI is projected to increase the percentage of Gross

Domestic Product (GDP) lost by 0.71% (in 2050) and 1.04% (in 2100) for the low greenhouse gas (GHG) scenario and 0.80% (in 2050) and 1.79% (in 2100) under the very high GHG scenario (Estrada et al., 2017). Consequently, the UHI effect has been recognised in updated international polices, including the Sendai Framework for Disaster Risk Reduction, the Sustainable Development Goals (SDGs) and City Resilience Framework (CRF) (Supplementary Table 7-1). In response, global cities have implemented UHI reduction activities, categorised into voluntary or policy themes. The *voluntary theme* includes demonstrative projects, education and incentives such as Chicago's exemplar 'green' city hall roof and Baltimore County's 'growing home' campaign offering vouchers for purchasing trees. The *policy theme* incorporates the UHI into metropolitan spatial development strategies such as The London Plan, Perth and Peel @3.5 million and Johannesburg's Spatial Development Framework 2040. However, these policies fail in planning practicality through lacking specificities for combating adverse temperature effects at the local level. Some UHI policy adaptations instigated by local governing authorities are permitting quantifiable planning requirements (e.g. zoning and building codes), such as Seattle's 'Green Factor', Baton Rouge's landscape ordinance and the City of Stirling's Amendment 9 specifying minimum vegetation requirements for developments over a certain size (Supplementary Table 7-1). Yet most modern urban planning designs lack empirical evidence for optimal UHI mitigation strategies with the global state of data-informed governance described as underdeveloped, disparate and marginalised (McPherson, 2016; Michele Acuto, 2018).

Earth Observation (EO) data permits the identification of (un)sustainable urban development in relation to environmental variables (e.g. temperature, elevation) at spatial and temporal scales unattainable from traditional point-based approaches (e.g. static weather station data) (MacLachlan et al., 2017c). Specifically, EO data can produce consistent information necessary for restricting unsustainable development (MacLachlan et al., 2017a) and monitoring UHI effects based on associated land-temperature dynamics (MacLachlan et al., 2017c). To date, EO applications have been frequently restricted to medium-scale spatial resolutions (e.g. 30 m) across complete metropolitan regions, which are inappropriate for determining temperature dynamics across new developments or explicit localised targeted remediation. Consequently, in this paper we build upon previous analyses (MacLachlan et al., 2017c, 2017a) to outline an operational methodology for evidence-based urban planning to optimise localised UHI mitigation through integration of EO data. Our analysis demonstrates the combined power of using remote sensing with open-source spatial modelling to derive temperature characteristics of different development types and determine optimal vegetation placement; we showcase this for a recently proposed redevelopment in the City of Fremantle, a council aiming to become Western Australia's most sustainable local government within the state capital city of Perth.

7.3 Materials and methodology

7.3.1 Outline

The presented spatially explicit modelling approach provides a method for data-informed targeted mitigative action at the pixel level (1 m^2 spatial resolution) to overcome the shortcomings of inconsistent methodologies currently implemented by planning authorities for UHI mitigation, whereby coarse spatio-temporal resolutions and block aggregations can misinform area greening (Supplementary Table 7-1). This resolution was selected to capture localised elevation variations whilst providing an acceptable run time of around 1.5 days when modelling temperature every three hours over three years, coinciding with the data resolution used within both the original and most recent studies respectively proposing and implementing the model (Lindberg et al., 2018, 2008). Remotely sensed elevation data used in conjunction with high spatial resolution land cover data (e.g. aerial surveys), diurnal meteorological data and multi-temporal resolution land cover data (e.g. Landsat) provided the necessary input data for modelling the temporal dynamics of mean radiant temperature (T_{mrt}) and UHI intensity. T_{mrt} defines the average temperatures surrounding a standing human, in this paper we refer to this output as 'temperature' to ease interpretation. We use an open-source temperature model to predict average temperature at a 1 m^2 spatial resolution using three-hourly composite meteorological and shortwave radiation data for the period 2008-2010.

Temperature dynamics of different density urban areas (Figure 7-1 (a)) were compared and optimum vegetative placement based on the average temperature for a proposed redevelopment within the City of Fremantle were determined (Figure 7-1 (b)). For the latter, three scenarios were processed: (1) the current urban footprint, (2) proposed changes to the urban footprint based on a proposed redevelopment, and (3) modelling the proposed redevelopment with no vegetation to redesign vegetation placement to optimise average temperature for the redevelopment footprint under investigation. The proposed site and surrounding city blocks were modelled in all scenarios accounting for influence of neighbouring landscape features (e.g. shadowing).

7.3.2 Materials

7.3.2.1 High resolution aerial imagery

High spatial resolution data were acquired to generate land cover estimates alongside a Digital Surface Model (DSM) and Digital Elevation Model (DEM) to capture the topographical characteristics and dimensions of the urban landscape. Radiometrically calibrated multispectral red (0.58–0.77 μm), green (0.48–0.63 μm), blue (0.41–0.54 μm), and near-infrared (0.69–1.00 μm)

orthophotos were obtained for March 2009 from the Australian Commonwealth Scientific and Industrial Research Organisation (CSIRO) Perth and Peel Urban Monitoring Programme (Caccetta et al., 2012), through the National Environmental Science Program's Clean Air and Landscape Hub. The aerial imagery provided by CSIRO was captured between 10:00 and 14:00 to reduce the effect of shadowing using a Microsoft UltraCAM-D at an altitude of 1300 m producing a spatial resolution of 20 cm. 60% forward and 30% side frame overlap enabled automatic DSM computation using geometric control points provided by Western Australia's land information authority (Landgate). CSIRO's extraction of ground points facilitated derivation of a DEM, with subtraction from the DSM producing a Relative Elevation Model (REM). Due to no data values within the provided Subiaco REM, this was recomputed from the provided DSM and DEM. Vegetation identification by CSIRO was performed though derivation of multiple discriminant functions using canonical variate analysis with rational polynomials (CVAR). Specification of decision boundaries using a hierarchical approach yielded eight spectral classes with the REM determining trees (2 m and above) or grass (below 2 m) processed by CSIRO (Caccetta et al., 2011). Minor manual REM edits were undertaken through digitisation to capture senescent vegetation.

7.3.2.2 Meteorological data

Required meteorological data for temperature modelling included air temperature, relative humidity, barometric pressure, wind speed, and wind direction, obtained from the Perth international airport weather station (YPPH); the most complete temporal record within the Perth Metropolitan Region (PMR). Data were captured by the Australian Bureau of Meteorology (BOM) and freely distributed through the Weather Underground Application Interface (API). Whilst wind speed and direction are classed as 'not needed' by the model implemented here (detailed in the next section), lack of wind has been identified as a contributing factor to increased UHI intensity (Gaffin et al., 2008; Lindberg et al., 2017). In Perth during summer months major land and sea temperature differences induce an onshore wind of up to 40 km hour^{-1} termed the 'Fremantle Doctor' cooling the metropolitan region (Eliot et al., 2006). The continuous meteorological data were used to enable estimation of temperature for each time point (three-hourly) within the model. To achieve this, meteorological variables at hourly time steps in 2008, 2009 and 2010 were temporally matched to three-hourly downward shortwave radiation from the Water and Global Change (WATCH) Forcing Data methodology applied to ERA-interim (WFDEI) data (Uppala et al., 2005; Weedon et al., 2014). WFDEI data are based upon the European Centre for Medium-range Weather Forecasts (ECMEF) ERA-40 reanalysis data at 0.5° spatial resolution, but with inclusion of more extensive satellite, atmospheric and surface observations alongside slight differences in processing and formatting (Uppala et al., 2005; Weedon et al., 2014). WFDEI values were

validated against seven flux tower measurement sites, replicating validation of the WATCH Forcing Data (WFD) (Weedon et al., 2011, 2010) with statistically significant correlations found between all variables at all sites, with the exception of precipitation at Manaus, demonstrating acceptable performance for estimating temperature (Weedon et al., 2014).

7.3.2.3 Open Street Map data

Open street map road data with minor manual digitisation editing to reflect past 2009 road layouts guided three-dimensional modelling of the low (Currambine) and high (Subiaco) density Australian Bureau of Statistics (ABS) defined Level 1 Statistical Areas (SA1) presented in Figure 7-2. Owing to the use of differing subsets compared to chapter 5 and the requirement of detailed digital shapes (e.g. polygons, points and lines) precluded use of previously classified medium resolution EO data (e.g. chapter 4). Therefore open street map data provided an easily integratable, open source and replicable solution in guiding three-dimensional models.

7.3.2.4 Proposed planning application data

Proposed redevelopment plans were used to modify input model parameters for the site and used in conjunction with modelled temperature information to optimise site vegetation placement. The City of Fremantle's planning portal provided the publically distributed proposed redevelopment plans for the Woolstore Shopping Centre and Carpark located at 28 Cantonment Street, Fremantle.

7.3.3 Methodology

7.3.3.1 Temperature modelling

The methodology implements the recently developed UMEP model; an open-source holistic analytic tool for urban climatology and climate sensitive planning applications (Lindberg et al., 2018). UMEP can estimate anthropogenic heat fluxes, urban energy balances, and thermal comfort, over a range of temporal and spatial scales adaptable to multiple data sources and formats (Lindberg et al., 2018). The UMEP permits continuous temperature modelling across complex urban environments, an ideal tool for this analysis. Temperature was estimated at a 1 m^2 spatial resolution and three-hourly intervals using the SOLWEIG (Solar and LongWave Environmental Irradiance Geometry) model. Current metropolitan development procedures often mandate minimum vegetation requirements (e.g. Seattle's 'Green Factor'), yet if inappropriately landscaped, such as exclusive separation of land covers, could result in sub-optimal heat mitigation (Supplementary Table 7-1). Similarly, UHI strategies frequently use temperature extracted from coarse satellite imagery aggregated to city blocks covering inappropriate temporal

periods (e.g. monthly average) that can misguide remediation activities (e.g. Fremantle's 'Urban Forest', Supplementary Table 7-1). Specifically, certain block subdivisions may exacerbate overall temperature yet public land availability can restrict planting to inappropriate sites within the block. Modelling urban temperature at high spatiotemporal resolution enables resource optimisation through refinement of potential sites at 1 m^2 spatial resolution that will most influence overall temperature and determine preferable vegetation distribution within new developments, negating unsustainable designs. With increasing global availability of elevation (e.g. Open Topography), land cover (e.g. GlobeLand30 (Chen et al., 2015)) and meteorological data, our accessible methodological can be replicated within planning procedures to aid the sustainable development and restorative urban design of our cities for localised UHI reduction.

The SOLWEIG model required the following user-determined inputs, modified for each modelled scenario where appropriate: continuous meteorological data, land cover information, building and ground DSM and a vegetation canopy REM (Figure 7-1 (a)). Land cover (excluding trees) was derived from manual digitisation of CSIRO high resolution imagery. CSIRO elevation models and the manually edited vegetation layer were combined to produce the building and ground DSM and vegetation canopy REM. Nearest neighbor resampling of input data to 1 m^2 pixels avoided excessive processing times following the recommended resolution of the UMEP model (Lindberg et al., 2017). Temperature in urban environments is strongly influenced by urban geometry, including building height, aspect and the Sky View Factor (SVF), essential components to human comfort, solar access, and solar energy (Holst and Mayer, 2011; Lau et al., 2015). Within UMEP wall height and aspect were computed using the building and ground DSM, using an edge detection filter for the former (Lindberg et al., 2015b) and a linear filter for the latter (Goodwin et al., 2009; Lindberg et al., 2015a). The SVF, defined by the ratio of radiation received (or emitted) by a planar surface to the radiation emitted (or received) by the entire hemispheric environment, was determined using a shadow casting algorithm using the building and ground DSM and vegetation REM (Lindberg and Grimmond, 2010; Watson and Johnson, 1987). The SOLWEIG model estimates temperature through modelling shortwave and longwave radiation fluxes in six directions: upward, downward and four cardinal points (Lau et al., 2016; Lindberg et al., 2008). Temperature estimates from the SOLWEIG model have been extensively validated for global cities including Shanghai (Chen et al., 2016), Hong Kong (Lau et al., 2016) and Gothenburg (Lindberg and Grimmond, 2011), producing strong correlation between modelled and field measurements (R^2>0.90), with the latter city validation noted as statistically significant. Annual SOLWEIG temperature estimates were averaged over the three modelled years to reduce inter-annual variation (Hu et al., 2015; Imhoff et al., 2010; MacLachlan et al., 2017c; Zhang et al., 2012).

7.3.3.2 Optimising vegetation placement

Fifteen trees, as specified in the original redevelopment plans, were manually distributed according to the highest average annual temperature values, being placed in the centre of a pixel whilst preserving design aspects including: crown radius (2.82 m), spacing (> 7 m) and height (vegetation on street level at 16.41 m and vegetation on buildings at 3.54 m). The new vegetation locations were reflected in an updated vegetation canopy REM achieved through digitisation and new mosaicked raster, re-running the analysis for comparative temperature across the redevelopment site to the original and proposed redevelopment (Figure 7-1).

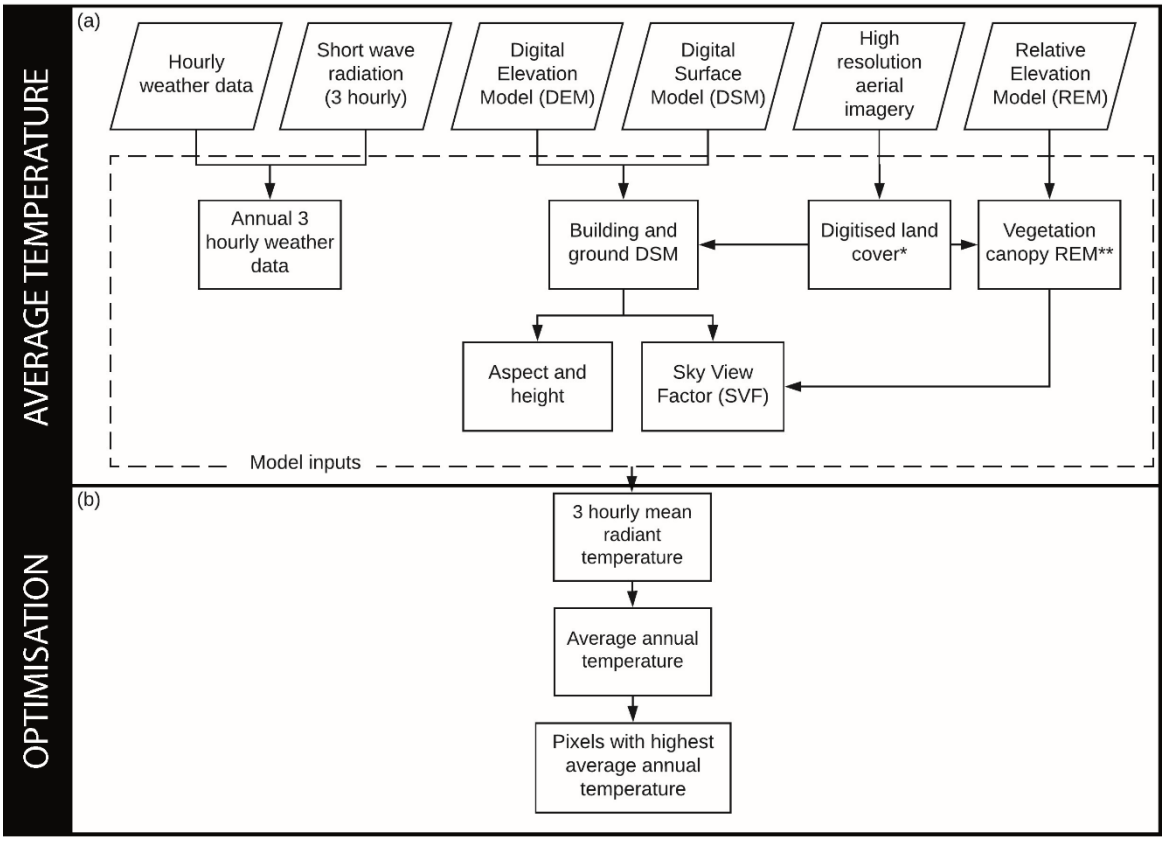

Figure 7-1. Summary of methodological procedures for (a) mean radiant temperature (T_{mrt}) and (b) identifying optimised vegetation locations. * indicates existing development modified using proposed redevelopment plans. **indicates data were modified on three occasions: (1) using proposed redevelopment plans, (2) removing all vegetation across the proposed redevelopment site and (3) using optimised vegetation locations.

7.4 Analysis of Earth observation data

The influence of localised urban development types on temperature dynamics was established through comparison of two census areas within the city of Perth. In addition, the potential for applied mitigative planning UHI action was demonstrated through modelling recently proposed plans for a site redevelopment. As Western Australia's state capital, Perth has experienced rapid and sustained outward low density development since the end of the 20th century in response to a booming resource sector, increasing the urban area by 37.44% (279.80 km^2) between 2000 and 2015 (MacLachlan et al., 2017a). The two ABS SA1s selected for the comparative analysis represent areas which have undergone (i) low density urban fringe green field development (Currambine) and, (ii) high density brownfield infill development (Subiaco). The former area was purely subject to the metropolitan region scheme implementing a master plan to outline provisions for development and use of land, but the latter was superseded by the Subiaco Redevelopment Scheme (SRS) which provided more critical localised development objectives prepared by experts with public consultation (Supplementary Table 7-1). Commencing with similar population density (per 0.1 km^2) values in 2011 (Subiaco: 325, Currambine: 310), by 2015 Subiaco more than doubled in density compared to Currambine (Subiaco: 712, Currambine: 324) (Supplementary Table 7-2). Full details on the study site can be found in the supplementary material, section 7.7.

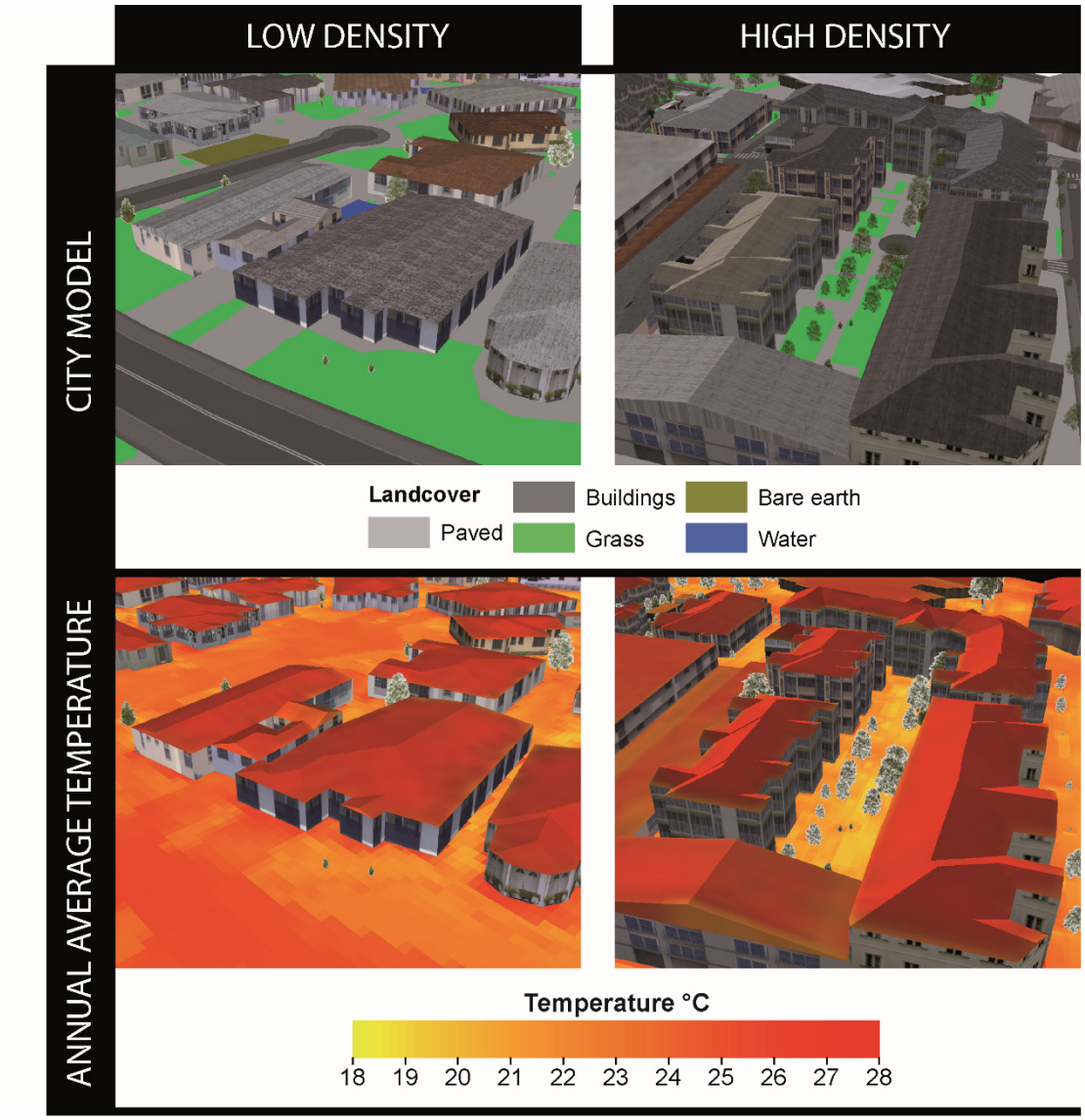

Figure 7-2. Three-dimensional city models (top row) and average annual mean radiant temperature (T_{mrt}) overlays (bottom row) for subsets of two SA1 locations representing low (cul-de-sac in Currambine) and high (infill site in Subiaco) density developments. Two-dimensional renditions for complete SA1 coverage are presented in Supplementary Figure 7-4.

The urban design characteristics of the low density development, such as lower building heights, less dense vegetation and more sprawled layout, produced higher average temperatures of 1.00 °C (paved), 0.90 °C (grass) and 0.60 °C (buildings) compared to that of the high density infill site over the spatial extent of the three-dimensional view area (Figure 7-2). The complete SA1 of Currambine experienced higher temperatures of 0.54 °C (paved), 0.39 °C (grass) and 0.14 °C (buildings) compared to that of Subiaco (Supplementary Figure 7-4). The Western Australia Planning Commission (WAPC) recognise sustainability concerns within the PMR due to the

majority of new development occurring as low density, outward suburban sprawl encroaching into the wildland-urban interface. To combat such apprehensions, the WAPC have detailed infill development strategies alongside UHI reduction aspirations for the long-term (2050) development of the city. Whilst local governments, such as the City of Bayswater and Stirling, have observed population increase with infill development, the tendency towards larger houses on subdivided blocks has significantly declined the level of tree canopy coverage. Consequently low density development and associated canopy reduction are adversely impacting the localised UHI effect (Supplementary Table 7-1).

Reactively, planning initiatives by the City of Fremantle and City of Perth have initiated novel EO data-driven urban forest plans for directing tree planting, whereby medium temporal resolution data (16-day return period) have been used to produce static summer average land surface temperatures aggregated by city block. Such decentralised initiatives are advancing other local schemes, including Pennsylvania's 'Treevitalize', and in Arizona and California where state urban forestry programs aim to increase tree coverage. Urban greening assists in cooling environments through shading and evapotranspiration, reducing the amount of solar radiation reaching the ground and providing ambient heat dissipation respectively (evidence drawn from assessments in Supplementary Table 7-1). Increased neighbourhood green [and blue (Gascon et al., 2017)] space has also been positively associated with better mental health outcomes, such as in Wisconsin (Beyer et al., 2014) and London (Taylor et al., 2016). In terms of relevant enforceable landscape ordinance in Perth, 10% of any gross subdivisible area is required for public open space, normally as a green recreation reserve; a policy which has remained unaltered since the first [Stephenson-Hepburn] metropolitan regional plan was legislated in 1955. These stipulations for open space were based upon population density values, with an assumed number of persons likely to be housed across various residential codes (dwellings per hectare), which ensued to be a gross underestimation for required open space (Grose, 2007). Comparatively, Singapore's 2011 open space provisioning is defined as 4.05 m^2 for every 56.0 m^2 of gross floor area with detailed landscaping requirements such as grass coverage, tree girth, and minimum branches, yet excludes landscape arrangement conditions (Supplementary Table 7-1). Despite such regulations for promoting city open spaces, global policies lack an effective data-driven approach in deriving optimal vegetative placement — particularly for reducing the ever-increasing socio-economic and environmental impacts associated with UHI effects — with current methods restricted by a lack of spatial data and analysis or coarse resolution, block aggregation, limited temporal data collection and outdated open space legislation.

7.5 Applied data-driven vegetation optimisation

Recently published and updated international policies express the importance of UHI reduction due to current exclusion from global climate models, and as a result metropolitan spatial development strategies are having to evolve to reflect these model omissions. Yet modern city development and restorative urban schemes are hampered by a lack of consistent and scientifically valid decisions which can unnecessarily exacerbate the UHI effect (Supplementary Table 7-1). Building on our temperature modelling we illustrate a data-driven approach for optimally placing vegetation for effective planning to locally minimise the UHI. This is demonstrated through modelling the proposed redevelopment plans of the Woolstores shopping centre in the City of Fremantle, from retail to a mixed-use development containing accommodation, commercial property and hotel. The proposed redevelopment will alter land cover from high to low urban reflectance (albedo) which, based on our previous analyses (MacLachlan et al., 2017c, 2017a), represents the optimum urban land cover conversion. At the intra-development scale a data-driven approach can optimise vegetative placement providing evidence to mitigate excess temperatures. Through removing the vegetation of the proposed redevelopment (see Supplementary Figure 7-5) and modelling average temperature per year optimal locations to relocate vegetation were determined. The proposed redevelopment experienced a 1.2 °C reduction in average annual temperature across the site in comparison to the original retail complex. Whilst maintaining proposed building layout and vegetation design characteristics, such as height and spacing, data-driven vegetation placement abated a further 0.8 °C, with a maximum average temperature reduction of 0.9 °C (Figure 7-3). Simplistic and achievable reductions of this nature are especially important due to the range of health, energy, water and economic savings attributable to a 1 °C increase in temperature. For example, an associated 7.5% electricity demand rise in Bangkok (Santamouris et al., 2015) and a 2.1 % increase in respiratory admissions in six Mediterranean cities in relation to maximum apparent temperature (Michelozzi et al., 2009).

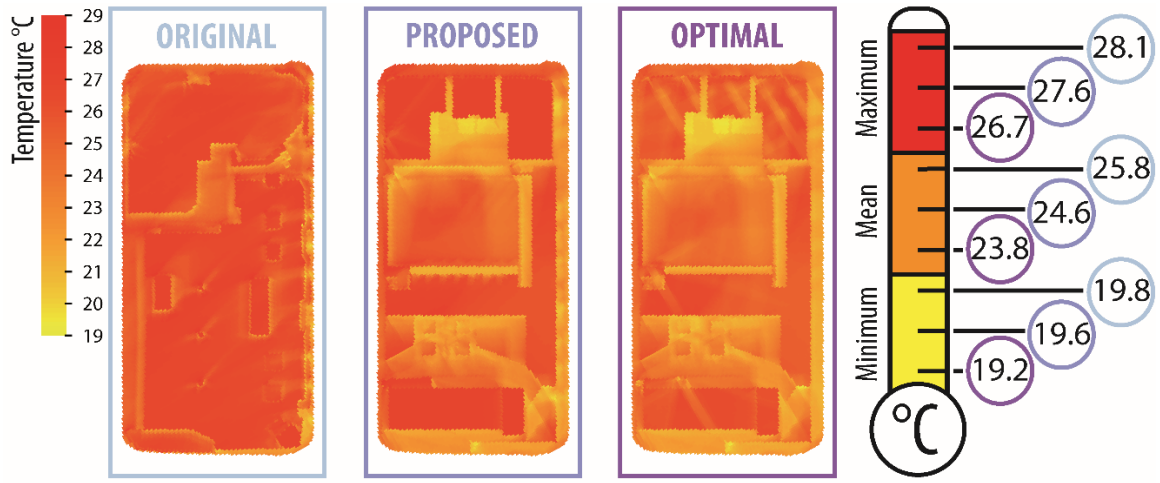

Figure 7-3. Average annual mean radiant temperature (T_{mrt}) using the original urban footprint, proposed redevelopment plans, and proposed plans with optimal vegetation placement. Also indicated are the average annual minimum, mean and maximum mean radiant temperature with colour-coded circles for each urban footprint scenario. The proposed redevelopment constitutes increased building height and variation across the site enlarging shading potential, reducing site mean radiant temperature compared to the original urban area. New vegetation locations and locator maps are exhibited in Supplementary Figure 7-5.

7.6 Global applicability

Urbanised areas are expected to triple by 2030 (2000 baseline of 652,825 km^2) with the Cities and Biodiversity Outlook estimating that 60% of land projected to be urban by 2030 is yet to be built. Current voluntary and policy UHI mitigation policies that aim to increase vegetation coverage frequently fail in location optimisation owing to a lack of spatial data, broad aggregation and selective temporal sampling (Supplementary Table 7-1). Integration of UHI mitigation frameworks, such as the analysis presented here, into international and metropolitan spatial development strategies would overcome the current inconsistent and varied urban planning methodologies exhibited through frequent devolution to local governments, and the incomparability of their results. Upon receipt of development applications, our analysis could be replicated by planning agencies to ensure strategic vegetation placement in reducing overall temperature; a consideration that should be an essential pre-requisite in planning approval for enhancing localised UHI mitigation. Inclusion at the proposal stage would mitigate aforementioned implications and diminish the requirement for extensive urban forest plans and associated financial costs, e.g. estimated at AUD 2.57 million for the complete City of Fremantle

strategy (Supplementary Table 7-1). Similarly, application to existing metropolitan regions could maximise often limited resource investment in optimising restorative urban areas, overcoming the limitations of current methods (e.g. block aggregation). Through scientifically rigorous data-informed governance, metropolitan cities and federations will be able to effectively interact with, and numerically quantify, mitigation actions for meeting international sustainable development policy requirements such as the reduction of environmental costs (e.g. excess temperature) of the UHI specified in the New Urban Agenda (McPherson, 2016). We advocate that the transformation of multi-level policy to incorporate data-driven frameworks, like that proposed here, is an essential requirement for ensuring the future socio-economic and environmental sustainability of our cities.

7.7 Supplementary material

This chapter was originally submitted to Global Environmental Change and provides a concise and straightforward manuscript with the potential for global replicability, in line with journal's requirements. Consequently, the supplementary material presents study area information, relevant urban expansion policies alongside figures and tables which provide further context and support statements within the main chapter and overall thesis. A short discussion surrounding other considered approaches and a list of data used within the chapter are also provided to demonstrate the entirety of analytical process.

7.7.1 Study area

The Perth Metropolitan Region (PMR) has observed sustained low density outward urban expansion since the beginning of the 21st century in response to a rapidly expanding resource sector (Kennewell and Shaw, 2008; MacLachlan et al., 2017a, 2017d). The state's value of mineral and petroleum resources increased from AUD 4.7 billion in 1996 to a peak of AUD 121.6 billion mid-2013, contributing 95% of Western Australia's export earnings between 2010 and 2011 (Department of Mines and Petroleum, 2015). Urban area within the PMR has increased 45.3% (320.33 km^2) between 1990 and 2015, with a 37.44% increase since 2000 (279.80 km^2) (MacLachlan et al., 2017a, 2017b). Perth was consistently considered Australia's fastest growing city between 2007 and 2014, whilst only obtaining a maximum population density (2011) of 3,662 people per km^2; 33.82% and 24.83% lower than Melbourne (10,827) and Sydney (14,747) respectively (ABS, 2015, 2011; MacLachlan et al., 2017a). Low population density has generated demand for dispersed housing in a non-strategic, 'lot-by-lot fashion' founded upon a car-dependent lifestyle (Dhakal, 2014). Due to the large scale conversion from natural land to impervious surfaces, sustainability concerns are specified within the Western Australian Planning

Commissions (WAPC) long-term (2050) development guide. Specifically, land rezoning must meet strategic planning objectives, as opposed to individual requests, with Urban Heat Island (UHI) mitigation listed as one of sixteen aspirations under the city sustainability objective. In response, local governments have devised policies and targets including the City of Fremantle's and City of Perth's Urban Forest Plans that outline greening strategies and deadlines (Supplementary Table 7-1). In determining locations for greening, temporally-specific low resolution imagery and associated satellite land surface temperature data have been used at coarse spatial resolutions (e.g. city blocks) by these planning councils (Supplementary Table 7-1). Such methodologies have potential to provide misinformed, inconsistent and sub-optimal mitigation through consideration of temperature at a singular time of day over a large spatial extent. Nevertheless, other local governments lack any specific UHI policy but recognise the value of maintaining vegetation, for example, Wanneroo's 'street tree' policy and Subiaco's 'plant management' plan (Supplementary Table 7-1).

Supplementary Table 7-1. Relevant influential international, metropolitan and local UHI and urban expansion policies, strategies and assessments (with publication date) referred to in this paper. *Documents lack specific UHI related policy but recognise the value of maintaining vegetation.

International
United Nations The World Cities in 2016 (2016)
United Nations New Urban Agenda (2017)
ARUP City Resilience Framework (2015)
United Nations International Strategy for Disaster Reduction Sendai Framework (2015)
Universal Sustainable Development Goals (2015)
Biological Diversity, Cities and Biodiversity Outlook (2012)

Metropolitan
AECOM Australia, Economic Assessment of the Urban Heat Island Effect, Melbourne (2012)
The Spatial Development Strategy For Greater London (2017)
Western Australia Planning Commission, Perth and Peel @3.5 million (2015)
City of Johannesburg Metropolitan Municipality, Spatial Development Framework 2040 (2016)
Western Australian Planning Commission, Directions 2031 and beyond: metropolitan planning beyond the horizon (2010)
Western Australian Planning Commission, Development Control Policy 2.3 Public Open Space in Residential Areas (2002)
Plan For The Metropolitan Region Perth And Fremantle (1955)
Singapore Government, Open Space Provision (2011)
Western Australian Planning Commission, Metropolitan Region Scheme Text (2006)

Local
USA Environmental Protection Agency, Reducing Urban Heat Islands Compendium of Strategies Trees and Vegetation (2008)
USA Environmental Protection Agency, Reducing Urban Heat Islands Compendium of Strategies Urban Heat Island Basics (2008)
USA Environmental Protection Agency, Reducing Urban Heat Islands, Compendium of Strategies Heat Island Reduction Activities (2008)
City of Stirling, Stirling Urban Forest Community Consultation (2017)
City of Fremantle, One Planet Fremantle Strategy 2014/2015 - 2019/2020, 1–12 (2014)
Metropolitan Redevelopment Authority, Subiaco Redevelopment Scheme (2013)
Metropolitan Redevelopment Authority, Subiaco Redevelopment Scheme 2 (2017)
City of Bayswater, Urban Forest Strategy (2017)
City of Perth, Urban Forest Plan 2016-2036 (2006)
City of Fremantle, City of Fremantle Urban Forest Plan (2017)
City of Fremantle, Annual Budget 2016-17 (2016)
City of Wanneroo, Street Tree Policy (2016)*
City of Subiaco, Plant Pathogen Management Plan (2015)*

Here, the developed methodology was firstly used to compare two Australian Bureau of Statistics (ABS) Level 1 Statistical Areas (SA1), the smallest enumeration unit for which population data is provided within the PMR, representing areas of low (within the suburb of Currambine) and high (within the suburb of Subiaco) density developments. In this paper we refer to these two SA1 areas using the names “Currambine” and “Subiaco” to ease interpretation. The SA1 geographical census enumeration identification numbers for these two areas are provided in Supplementary Figure 7-4. The Metropolitan Redevelopment Authority (MRDA), established in 2011, is responsible for land development within Subiaco, as outlined in version 1 (2013) and version 2 (2017) of the Subiaco Redevelopment Scheme (SRS), which has superseded the Metropolitan Region Scheme (MRS) planning documentation and associated spatial plans (Supplementary Table 7-1). Specifically, the MRDA seeks positive social, economic and environmental development outcomes by transforming underutilised and derelict industrial land through targeted projects. Comparatively, development in Currambine must adhere to the MRS and metropolitan development plan, neither of which directly consider sustainable development or the UHI effect (Supplementary Table 7-1). Secondly, the temperature dynamics of a recently proposed redevelopment for the Woolstores shopping centre in the City of Fremantle were modelled to determine optimal vegetation placement for localised UHI reduction, demonstrating the influence of an applied data-driven planning approach.

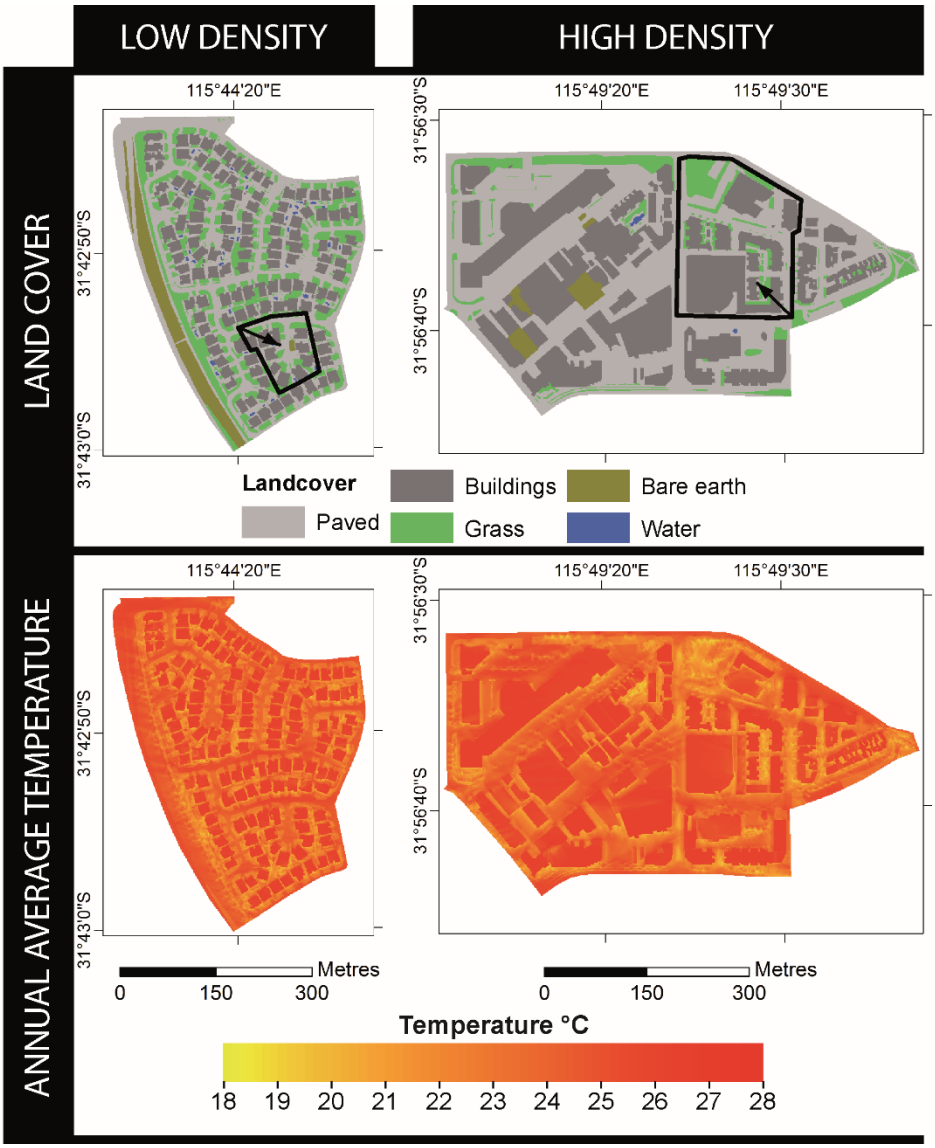

Supplementary Figure 7-4. Land cover (top row) and average annual mean radiant temperature (T_{mrt}) overlays (bottom row) for two SA1s as defined by the ABS representing low (Currambine, SA Level 1 ID: 5107102) and high (Subiaco, SA Level 1 ID: 5104203) density developments. Bold black outline extents with directional arrows denote three-dimensional subsets presented in Figure 7-2.

Supplementary Table 7-2. Total population and population density per 0.1 km^2 between 2011 and 2016 for Subiaco and Currambine SA1s as defined by the ABS. Raw population values are estimated for 2012-2015 and 2017 from ABS Estimated Residential Population (ERP) produced using downscaled SA2 data based on representative indicators for non-census years. 2011 and 2016 values are extracted from ABS census data. Population per 0.1 km^2 was computed from the spatial extent and associated population of each SA1 area.

Statistical Area Level 1		**2011**	**2012**	**2013**	**2014**	**2015**	**2016**	**2017**
Subiaco	Population	625	863	1039	1205	1369	1453	1531
	Per 0.1 km^2	325	449	540	626	712	755	796
Currambine	Population	421	442	455	453	440	406	417
	Per 0.1 km^2	310	326	335	334	324	302	307

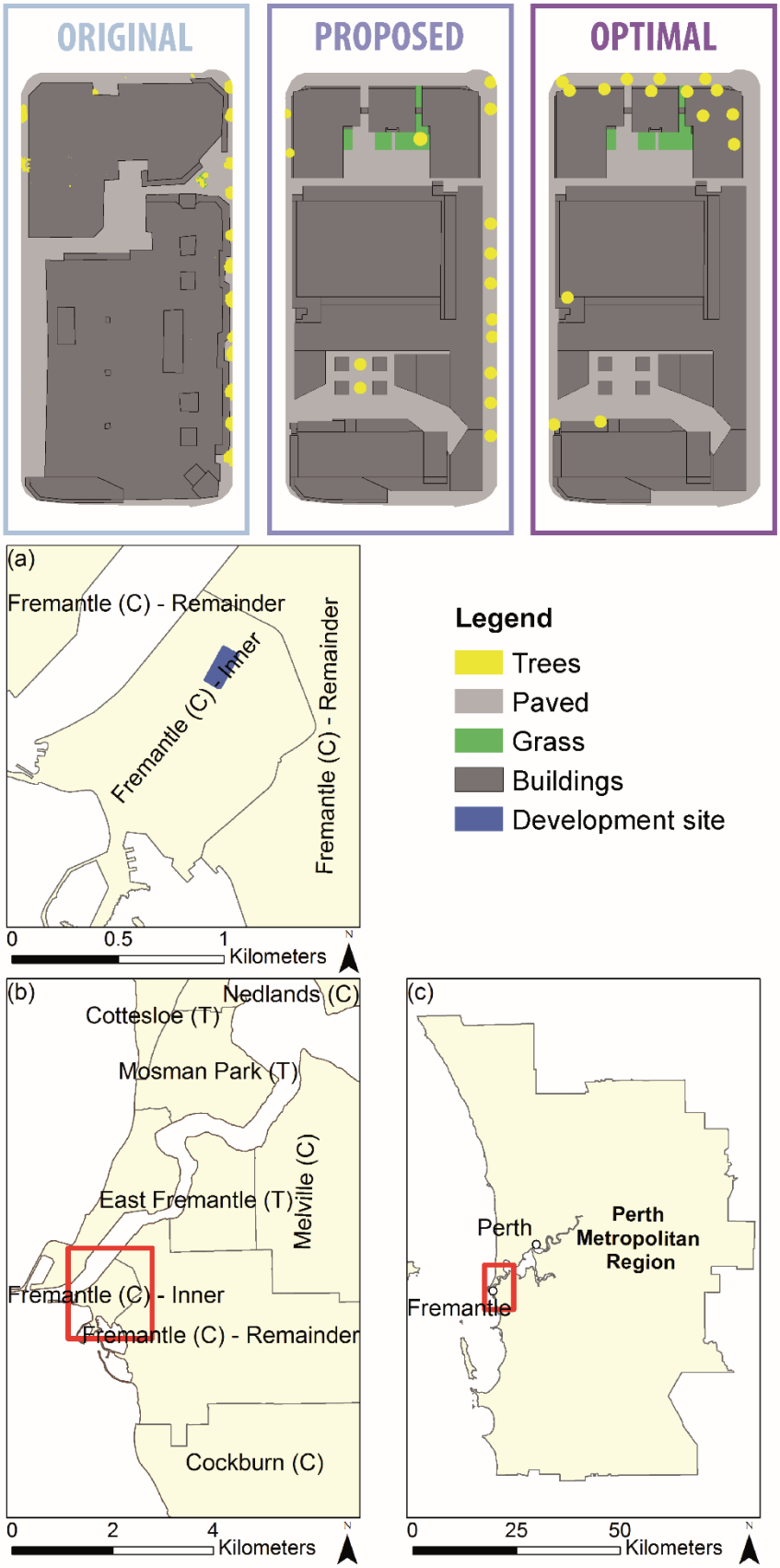

Supplementary Figure 7-5. Building and tree locations within the original, proposed and optimal scenarios in Figure 7-3. Inset maps identify the location of the development within: (a) the Fremantle Local Government Area (LGA), (b) the extent of (a) within the surrounding LGAs and (c) the extent of (b) within the PMR.

7.7.2 Other considered data and approaches

When selecting an appropriate tool to model temperature the DART model for remote sensing images and radiative budget of Earth's surfaces was originally explored (Gastellu-Etchegorry et al., 2004). However, this chapter was designed to be applied and policy focused within the current capabilities of planning departments. Consequently owing to DART's licensing requirements, standalone software nature and lack of a simple and straightforward graphic user interface it was not selected for use.

In terms of further analytical approaches appropriate vegetation locations were originally determined through multiple criteria analysis equally considering temperature and the number of heatwave days per pixel. The latter was computed following the Australian Bureau of Meteorology excess heat factor index (Nairn and Fawcett, 2014). Whilst the number of heatwave days reduced in line with the temperature reductions observed in chapter 7, the number of days identified was particularly high (e.g. between 164 and 140). The excess heat factor establishes a heatwave day in comparison to long term weather station data at ground level. Consequently as a large part of the planning proposal within this chapter was higher than ground level the number of heatwave days was overestimated. Therefore as this analysis could potential cause misinformation pertaining to vegetation placement it was exclude.

7.7.3 Chapter data list

This section provides an overview of the data presented and analysed within this chapter.

Supplementary Table 7-3. Summary of the data, sources and applications used within chapter 7.

Data	Source	Application
High resolution (20cm) orthophotos comprised of four spectral bands, digital surface and elevation models. **Sensor** Microsoft UltraCAM-D **Collection dates** 19 could free days from 14/03/2009	Australian Commonwealth Scientific and Industrial Research Organisation Perth and Peel Urban Monitoring Programme	Mean radiant temperature and three-dimensional modelling
Hourly meteorological data of: air temperature, relative humidity, barometric pressure, wind speed wind direction between 2008 and 2010	Perth international airport weather station (YPPH), captured by the Australian Bureau Of Meteorology and freely distributed through the Weather Underground application interface	Mean radiant temperature modelling
Three-hourly downward shortwave radiation between 2008 and 2010	Water and Global Change Forcing Data methodology applied to ERA-interim (known as WFDEI) data	Mean radiant temperature modelling
Digital road data	Open street map	Three-dimensional modelling
Planning proposal documentation	The City of Fremantle planning website	Applied data-driven vegetative placement in reducing mean radiant temperature

Chapter 8 Discussion

This chapter provides a synthesised discussion of the individual research chapters, the transferability and global applicability of the thesis methodology, and a reflection on the critical challenges identified through this research.

8.1 Research significance

This thesis has provided a holistic practical and applied workflow in monitoring urban areas and presented a methodology which can demonstrably mitigate the Urban Heat Island (UHI) effect through a data-driven approach to enable effective data-informed governance. Specifically the methodologies and outputs exhibited here permit scientifically valid and accurate quantitative comparison to global (e.g. Sustainable Development Goals (SDGs) and the United Nations (UN) Urban Agenda), metropolitan (e.g. The London Plan, Perth and Peel @3.5 million and Johannesburg's Spatial Development Framework 2040) and local (e.g. Fremantle and Perth's Urban Forest programmes) frameworks and targets.

Accurate information on the temporal evolution of urban areas is essential in order to monitor the effect of policy on development and identify potential socio-economic and physical consequences of development, such as air degradation, socio-economic disparities, infrastructural costs, water soil and quality deterioration, the UHI effect, changing water demand and runoff patterns, and reduced biodiversity (Batty et al., 2003; Li et al., 2015; Schneider, 2012; Sexton et al., 2013; Yuan et al., 2005). Paper 1 (chapter 4) provided an operational remote sensing methodology for establishing change in urban area extent for seven sequential Landsat images between 1990 and 2015 for the Perth Metropolitan Region (PMR). This meets the first objective of the PhD research, achieved through consistent classification using the recently developed Import Vector Machine (IVM) classifier, overcoming the current temporal methodological inconsistencies implemented by the Western Australian Planning Commission (WAPC) in monitoring urban areas (e.g. Cadastral valuations, use of multiple urban zones (from 2009) and spatial modelling (from 2010)).

Nevertheless, classified Earth observation (EO) data such as that described in paper 1 (chapter 4) have been found to significantly over or underestimate urban area as a result of spatial constraints (Lu et al., 2011; Wu and Murray, 2003). Resolving errors of this type is a crucial current challenge in the application of EO data in such areas due to the potential for misinforming decision makers (e.g. on future development) whilst also forming the basis of further

environmental studies. For example, Landsat derived urban area estimates have been used within global biogeochemistry and climate models (Zhu and Woodcock, 2014), targeted urban development policies (Hepinstall-Cymerman et al., 2013; Schneider et al., 2005) and UHI studies (Hu et al., 2015), and any over or under estimation of urban area has potential to misinform these applications. Consequently paper 2 (chapter 5) builds on the work presented in paper 1 (chapter 4) through firstly establishing the over estimation of urban area derived using a classified Landsat image (produced in paper 1 (chapter 4)) through comparison to very high resolution (20 cm) aerial imagery. On the basis of this, a correction methodology to calibrate sub-pixel Landsat derived urban area estimates against classified very high resolution data aggregated to Landsat spatial resolution was developed, aligning with the second PhD research objective.

Paper 3 (chapter 6) and paper 4 (chapter 7) undertook analysis in relation to global, metropolitan and local sustainability goals, specifically related to the UHI effect, coinciding with the third and fourth PhD research objectives. Paper 3 (chapter 6) devised a new methodological approach, building on existing research that disregards spatial and temporal land cover change when characterising the impact of urbanism on surface temperature. Previous research often assumes static urban area across multiple years or uses a singular global index such as the Urban Heat Island Intensity (UHII) which is less appropriate for applied planning decisions (Cao et al., 2010; Kikon et al., 2016; Tomlinson et al., 2012). The methodology developed in chapter 6 derived land cover change – temperature associations using Land Surface Temperature (LST) data from the Moderate Resolution Imaging Spectroradiometer (MODIS) between 2003 and 2013 and the previously classified land cover data (derived in paper 1 (chapter 4)). Determination of land cover and temperature relationships of this type permit direct incorporation into future development decisions. For example, this approach could be applied when selecting areas for future rezoning of land for urban development in order to mitigate any unnecessary social, environmental and economic impacts associated with an increase in surface temperature.

Nevertheless, the majority of UHI focused academic research, such as that discussed in paper 3 (chapter 6) has utilised medium (30 m) and coarse (1 km) spatial resolution LST data (Kikon et al., 2016; Tomlinson et al., 2012). Similarly, recent local government initiatives such as those in the City of Fremantle and Perth used Landsat LST from limited temporal observations (e.g. summer) and aggregated results to city block level in guiding urban greening (City of Fremantle, 2017; City of Perth, 2006). Data and analysis of this sort are inappropriate for localised planning decisions at sub-city block levels and can misguide remedial vegetation initiatives. For example, certain sub-block sections may exacerbate overall block temperature, yet available land restricts sites for remedial actions resulting in sub-optimal mitigation and overall investment (City of Fremantle, 2017). Consequently, paper 4 (chapter 7) presented a data-driven approach in optimising

vegetation placement for a proposed redevelopment within the city of Fremantle. The proposed redevelopment constituted a change in land cover from high to low urban albedo obtaining the least overall temperature change based on analysis in paper 3 (chapter 6). Optimal vegetation relocation whilst maintaining design principles reduced average annual mean radiation temperature (T_{mrt}), aligning with the final PhD research objective.

The feasible and easily implemented methods developed in papers 3 and 4 (chapters 6 and 7) enable quantitative engagement with metropolitan and global policies in (i) selecting or refining sustainable future development sites; and (ii) maximising vegetation cooling potential of localised (re)developments, mitigating the requirement for costly and misguided planning, such as the urban forest plans currently being implemented across the Perth Metropolitan Region (PMR).

This thesis has produced the following novel academic research contributions:

- Provided and demonstrated a feasible and policy relevant methodological approach in accurately determining urban area for monitoring infill and density targets proposed by metropolitan development agencies overcoming current temporal inconsistencies and unrepresentative data metrics.
- Developed an approach which mitigates for the over and under estimation of urban area frequently reported using medium spatial resolution EO data. This was achieved by consideration of urban heterogeneity through establishing overestimation differing based upon the type of urban area through a novel spatially explicit approach which may reduce error propagation within future policy or environmental applications.
- Established an innovative approach for determining the association between land cover and temperature change, which overcomes simplification of current academic research that neglects land cover temperature dynamics through singular global metrics and frequent assumption of a singular homogenous urban areas.
- Demonstrated an original localised evidence-based data driven planning method through combining EO data and spatial modelling advancing current restrictions using coarse and temporally limited resolution data.

Combined, these novel academic contributions constitute an applied planning framework for accurately monitoring urban area, determining appropriate land rezoning locations in relation to surface temperature across metropolitan regions and optimising planning (re)developments for locally mitigating the UHI effect.

8.2 Methodological transferability

The methodological approaches implemented within the four paper style chapters presented in this thesis can readily be reproduced across urbanising areas of the Earth's surface. This section outlines the methodological transferability considering alternative study sites, data and personnel expertise for each stage of the applied methods.

The EO preprocessing (e.g. image merging and normalisation) and classification approach presented in chapter 4 required access to licensed remote sensing software including: ENvironment for Visualizing Images (ENVI), Arc Geographic Information Systems (GIS) and the Interactive Data Language (IDL). Due to the PMR covering two Landsat tiles a seamless image mosaic permitting less visible boundaries was produced with subsequent normalisation coded in IDL and classified in the Environmental Mapping and Analysis Program (EnMAP) through the IDL environment (MacLachlan et al., 2017a). Nevertheless, alternative study sites may be located within a single image or could implement a different mosaic methodology, with subsequent normalisation and classification in open source software such as Quantum Geographic Information Systems (QGIS), R statistical software, Python or the more commercially available Arc GIS (Biehl and Landgrebe, 2002). However, as specified in section 2.2, alternative classification procedures may produce different classified land cover accuracies.

For organisations such local governments that might lack remote sensing analysis expertise, freely available global pre-classified data are available including GlobeLand30 (classified Landsat data for 2000 and 2010) (Chen et al., 2015), the European Space Agency's (ESA) Climate Change Initiative (CCI) annual global land cover (300 m) time series (1992-2015) (European Space Agency, 2017) and yearly MODIS land cover products (500 m or 0.05°) (Friedl et al., 2002). However, global methodological classification approaches have the potential for misclassification of underrepresented, geographical or temporal specific attributes. For example, in Perth, high temperatures and low rainfall during the summer months can induce strong spectral similarities between bare earth and urban land cover types (Herold et al., 2002; Lu et al., 2011; Varshney and Rajesh, 2014). In terms of globally accuracy, statistics are often based upon a limited number of testing areas (e.g. Globeland30) that could be unrepresentative of other geographical locations (Chen et al., 2015). Additionally, future analysis (e.g. infill monitoring) would be reliant upon the continued data processing of external organisations. Whilst implementing pre-classified data of this sort would permit a valid approach, localised classifications such as that presented in chapter 4 mitigate study area specific issues, ensure future classification output and provided a localised accuracy assessment.

Chapter 5 required classified medium resolution land cover data (from chapter 4) alongside classified high resolution aerial data, achieved using Object Based Image Analysis (OBIA) within eCognition. Alternative sources of high resolution data include Google Earth, local planning authorities or free satellite imagery request services (e.g. Digital Globe) that can be classified using manual digitisation or free software capable of OBIA such as SPRING or MultiSpec (Biehl and Landgrebe, 2002; Camara et al., 1996). However, the often limited temporal record (e.g. 15 years) of high resolution data in comparison to medium resolution data can restrict application to complete classified collections such as that in chapter 4. Chapter 5 established that, due the range of bias determined from comparison between classified Landsat and high resolution based upon differing urban forms (e.g. Central Business District and older suburban region), the presented correction models were not globally applicable. It is often unfeasible to procure and process high resolution imagery over complete metropolitan regions due to large data sizes (e.g. 8 Terabytes (TB)) for the PMR) and computationally intensive image segmentation routines. Consequently an approach to apply this methodological process across complete metropolitan regions would entail selection of subsets that are representative of localised land cover composition and spatial heterogeneity, such as the four areas presented in chapter 5. Divisions of the metropolitan region (e.g. census units or manually determined) would then be allocated to the most appropriate subset and assigned the associated correction factor. Methodologies of this sort are found within disaster risk fields (e.g. earthquake risk) when limited ground data must be aggregated to metropolitan regions (e.g. Bevington et al., 2012). Replication of this analysis could be undertaken in freely available software such as QGIS, R and Python.

The land cover – temperature association methodology presented in chapter 5 used 2003 and 2013 land cover obtained from chapter 4. Nevertheless, substitution of alternative aforementioned pre-classified data land cover would permit organisations lacking remote sensing classification expertise to replicate analysis. Freely globally distributed daily nighttime and daytime LST data from MODIS Terra (MOD11A1, collection 5 (Wan, 2006)) were used in assessing the association with land cover change. Landsat derived land cover was aggregated to MODIS resolution for both years and a change in land cover determined if (i) the change was greater than all other changes within a MODIS pixel, and (ii) the change to land cover dominated (>50%) the 2013 MODIS pixel. This analysis was achieved in ArcGIS and R statistical software; the former was used to ascribe Landsat land cover to MODIS pixels, whilst the latter established land cover change and assigned temperature difference to qualifying pixels. Substitution of LST from sensors such as Landsat's Thermal Infrared (TIR) sensor and MODIS Terra's Advanced Spaceborne Thermal Emission and Reflection Radiometer (ASTER) is possible, however land cover data must obtain a higher spatial resolution than LST (or sub-pixel land cover if the equivalent resolution) to permit

the from-to change methodological approach (Cao et al., 2010). In this chapter's methodology ArcGIS could easily be replaced with QGIS, Python or R.

Chapter 7 presented a data-driven approach in optimising vegetation placement for a proposed redevelopment. Holistic study area inputs to the model for this analysis were based upon aerial EO data including a building and ground Digital Surface Model (DSM), land cover, and a vegetation canopy Relative Elevation Model (REM). However, the required data layers can be determined from (re)development plans and associated planning applications such as those provided on the City of Fremantle's planning portal using digitisation and raster creation tools within a GIS, if data are not already available in a spatial format. Other data sources including Google Earth, national Light Detection and Ranging (LiDAR) surface model composites (e.g. England and Australia) and freely distributed high resolution datasets such as the State of Indiana's orthophotography, LiDAR and elevation dataset could be also be used in generating the required data layers (Environment Agency, 2016; Intergovernmental Committee On Surveying & Mapping, 2008; The State of Indiana, 2017). Meteorological data from the Weather Underground Application Interface (API) enables access to over 250,000 weather stations in programming languages (e.g. R) which can extract the required parameters of air temperature, relative humidity and barometric pressure for temperature modelling (Lindberg et al., 2017). Downward shortwave radiation is often the restricting factor as it is infrequently monitored by meteorological stations. In chapter 7, this parameter was derived from the freely available 'WATCH Forcing data ERA Interim' providing the most extensive global temporal collection between 1979 (1901 for 20th century data) and 2012 at 3-hourly intervals (Uppala et al., 2005; Weedon et al., 2014). R statistical software was used to match hourly weather station data to 3-hourly downward shortwave measurements, with all datasets then input into the Urban Multi-scale Environmental Predictor (UMEP) model which is available as a free QGIS plugin. Replication of the methodological approach could easily be accomplished using QGIS to enable digitation and accessing freely available data sources.

This section has provided an overview of the methodological transferability for each paper chapter presented in this thesis. Whilst the analyses undertaken often implemented proprietary software and data available through the University of Southampton and University of Western Australia (UWA), replication of all analysis either in individual papers or as holistic project is achievable using freely distrusted data and open source software (Table 8-1).

Table 8-1. Visual representation of the methodological of the thesis transferability using alternative free data sources and software. Acronyms are defined as: Earth Observation (EO), ENvironment for Visualizing Images (ENVI), Interactive Data Language (IDL), Environmental Mapping and Analysis Program (EnMAP), Quantum Geographical Information Systems (QGIS), Geographical Information Systems (GIS), European Space Agency (ESA), Moderate Resolution Imaging Spectroradiometer (MODIS), Support Vector Machine (SVM), Object Based Image Analysis (OBIA), Land Surface Temperature (LST), Light Detection and Ranging (LiDAR), Urban Multi-scale Environmental Predictor (UMEP).

	Data inputs	Alternative inputs	Analysis	Software	Alternative software, methods and data
Paper 1	Landsat surface reflectance (free)	Any other surface reflectance EO data	Classification of normalised imagery	1. ENVI 2. IDL 3. EnMAP 4. Arc GIS	**Software** 1. QGIS 2. R statistical software 3. MultiSpec 4. Arc GIS **Methods** Alternative classifier (e.g. SVM) **Pre classified data** 1. GlobeLand30 2. ESA's annual global land cover (300 m) 3. Annual MODIS LC products (500 m or 0.05°)
Paper 2	1. Classified medium resolution data 2. High resolution data	1. Google Earth 2. Free imagery request services (e.g. Digital Globe) 3. Local planning authorities	1. OBIA 2. Dataset comparison	1. eCogntion 2. Arc GIS 3. Python 4. R statistical software	**Software** 1. SPRING 2. MultiSpec 3. QGIS 4. R statistical software 5. Python **Methods** Manual digitisation of high resolution imagery
Paper 3	1. Classified medium resolution data 2. Daily MODIS LST (free)	1. Alternative land cover products (e.g. pre-classified options mentioned above) 2. Alternative temperature datasets such as Landsat	1. Arc GIS 2. R statistical software	1. Arc GIS 2. R statistical software	**Software** 1. QGIS 2. R statistical software 3. Python **Methods** Any datasets applicable but land cover data must obtain a higher resolution than LST
Paper 4	1. Elevation models 2. High resolution imagery 3. Redevelopment planning proposal (free) 4. Metrological data from Weather Underground (free) 5. Downward shortwave radiation from the WATCH Forcing data ERA Interim dataset (free)	1. Planning documentation 2. Google Earth 3. LiDAR composites 4. Local authority high resolution data	Temperature modelling for: 1. Comparison between low and high density developments 2. Optimising vegetation placement within a proposed redevelopment	1. R statistical software 2. QGIS 3. UMEP	**Software** Analysis was conducted in open source software

8.3 Global applicability

In each paper style chapter the presented results are discussed in relation to relevant local (e.g. Perth and Peel @ 3.5 million) and broad international (e.g. SDGs) policies, aligning analytical findings with specified targets. This section identifies opportunities for methodological integration into international policy in ensuring successful achievement of the SDGs and UN Urban Agenda. Existing global targets and associated monitoring techniques in relation to urban expansion and the UHI effect are firstly described in order to frame idealistic methodological incorporation.

8.3.1 Existing global policies

The UN SDGs are composed of targets with measurable indicators enabling progress monitoring. For example, Goal 11 aims to make cities and human settlements inclusive, safe, resilient and sustainable is composed of ten targets of which three consider urban area (Table 8-2) (Osborn et al., 2015).

Table 8-2. Targets and Indicators in monitoring Sustainable Development Goal 11: make cities and human settlements inclusive, safe, resilient and sustainable. Adapted from United Nations Sustainable Development Goals (2018a).

Target number	**Target text description**	**Monitoring indicator**	**Urban area considered**
11.3	By 2030, enhance inclusive and sustainable urbanisation and capacity for participatory, integrated and sustainable human settlement planning and management in all countries	Ratio of land consumption rate to population growth	Annual amount from local planning authorities
11.6	By 2030, reduce the adverse per capita environmental impact of cities, including by paying special attention to air quality and municipal and other waste management	Annual mean levels of fine Particulate Matter (e.g. $PM_{2.5}$ and PM_{10}) in cities (population weighted)	Average share of the built-up area of cities that is open space for public use for all, by sex, age and persons with disabilities
11.7	By 2030, provide universal access to safe, inclusive and accessible, green and public spaces, in particular for women and children, older persons and persons with disabilities	Average share of the built-up area of cities that is open space for public use for all, by sex, age and persons with disabilities	National governments required to determine land use maps

Each indicator is accompanied by metadata documentation that provides a detailed monitoring methodological procedure. Nevertheless these indicators often fail to either incorporate EO data using local metropolitan derived estimates (e.g. 11.3 and 11.7) or implement global annual estimates (e.g. 11.6) with limitations of these approaches discussed in section 1.2 (Shaddick et al., 2018; United Nations Sustainable Development Goals, 2018b, 2018c; Van Donkelaar et al., 2016).

In contrast to the detailed SDG monitoring indicators, the New Urban Agenda provides only broad standards and principles for planning, construction, development, management and urban

improvement (UN-Habitat III, 2017). In response to the lack of monitoring, the City Prosperity Index (CPI) was formulated by the UN-Habitat to collect urban data (e.g. urban indicators) to form strategic knowledge for evidence-based policies, city visions and long-term action plans in relation to the New Urban Agenda and SDGs (mostly goal 11) (UN-Habitat, 2016). However CPI outputs are chargeable per city, with the three combined outputs — city profiling, state of city report and city action plan — totalling $443,000 over a 3-year period. These implemented methodologies are withheld from publication, lacking peer-review validation from the scientific community and limiting methodological transferability and advancement (Lu et al., 2015).

SDG target 11.3 aims to promote sustainable development and human settlement but excludes measurement or monitoring of the UHI effect. Comparatively, the New Urban Agenda commits UN members to reduce the financial, environmental and public health costs of the UHI effect, yet lacks any monitoring approaches. This is despite heat related mortality rising to the third highest cause of global disaster mortality (Centre for Research on the Epidemiology of Disaster and the United Nations Office for Disaster Risk Reduction, 2016).

8.3.2 Integration of analysis

The lack of urban and UHI methodological guidance often results in metropolitan development agencies producing urban estimates unrepresentative of actual land cover change (e.g. chapter 4) with UHI mitigation devolved to local government (Mayor of London, 2017; Western Australian Planning Commission, 2015a) or omitted from metropolitan consideration (City of Johannesburg Metropolitan Municipality, 2016). Consequently, the absence of global methodological guidance in meeting targets of the New Urban Agenda and SGDs has produced inconsistent, varied and scientifically invalid urban monitoring and UHI informed mitigation plans, with the global state of data-informed governance recently described as underdeveloped, disparate and marginalised (McPherson, 2016; Michele Acuto, 2018). The presented methodologies in this thesis offer the potential to be integrated into the SDGs and New Urban Agenda documents. This is particularly relevant as the latter has no associated methodologies and it is essential to develop a framework for metropolitan areas to follow such as that of the SDGs to provide measurable indicators for targets. Measurement of urban areas currently included in the monitoring indicators of Table 8-2 are derived from a variety of sources and methodologies resulting in an inconsistency across target objectives and the overall SDG 11. In an idealistic scenario inclusion of the approach presented in chapter 4 into the methodology section of the metadata for SDG targets and a New Urban Agenda framework would enable replicable and comparable urban estimates alongside standardisation across targets and international policies.

Similarly, UHI targets should be included under SDG 11 and in relation to the New Urban Agenda for both determining future urban land (chapter 6) and localised remediation (chapter 7). Integration of EO data into SDG metadata methodology is already in existence for certain targets (e.g. Target 11.6). In this case a simplistic methodological overview is provided within the metadata alongside reference to the academic paper for further details. Consequently, in a similar theme metadata documents for targets requiring urban area estimates (e.g. 11.3 and 11.7) could be updated to reflect the published analyses presented within this thesis, alongside distribution of code in ensuring repeatability (Shaddick et al., 2018; United Nations Sustainable Development Goals, 2018d). Metropolitan development agencies responsible for guiding future development at the broad scale would then be able to incorporate land cover-temperature association into selection of future urban development sites (chapter 6), with proposed developments also locally optimised for UHI mitigation (chapter 7) (Table 8-1). Whilst planning requests are often dealt with by local authorities, endorsement of established frameworks by metropolitan agencies would ensure consistent, comparable and measurable UHI mitigation across local (re)developments. Simplistic and achievable alteration of planning proposal requirements such as inclusion of computerised building designs that often are produced to submit paper versions would streamline the analysis process. Incorporation of up-to-date methodological approaches in global policies would prevent consistent devolution of responsibility to metropolitan agencies and local councils whilst ensuring scientifically peer-reviewed data-informed governance in addressing the UN's SDGs and the New Urban Agenda.

8.4 Critical challenges

This thesis has identified current challenges within sustainable urban development and UHI academic EO studies, local and metropolitan government development guidance and international development goals. In summary, current academic research is inappropriate for policy integration as many UHI studies fail to quantify changes in land cover that are associated with temperature change, which are potentially environmentally, socially and economically detrimental (Kikon et al., 2016; Zhang et al., 2013; Zhao et al., 2017; Zhou et al., 2014). Local governments either lack data-driven approaches or are restricted by temporal and spatial resolution constraints (City of Fremantle, 2017; USA Environmental Protection Agency, 2013), whilst metropolitan government urban monitoring for infill attainment is often based upon unrepresentative urban metrics (e.g. land zoned for development) with the potential to misinform development decisions (Western Australian Planning Commission, 2010b). These metropolitan urban estimates are also used within international development goal monitoring and, where methodologies are available, are often incomparable between countries due to differences in the

definition of urban alongside available data (United Nations Sustainable Development Goals, 2018b, 2018c, 2018d). Consequently in order to effectively ensure the future global sustainability of our cities it is essential for greater cohesion between these sectors and for deployment of globally recognised and accepted methodologies across both metropolitan agencies and local governments through the following key recommendations:

1. Transform global sustainable urban policy documents such as the Sustainable Development Goals and New Urban Agenda to include consistent, open and scientifically valid methodologies in monitoring and planning future urban (re)development in relation to environmental factors including the Urban Heat Island effect.
2. Require (a) transparency of current metropolitan agencies in determining future land re-zoning, (b) mandatory uptake of methodologies (proposed in recommendation 1), and (c) accountability for meeting global policy targets as opposed to current devolution to local governments
3. Encourage multi-institutional, applied and policy-integrated research in relation to specific targets of the Sustainable Development Goals and metropolitan development agencies.
4. Effectuate communication between local, metropolitan, national and international governments and the United Nations Sustainable Development Goals and New Urban Agenda in ensuring analytical suitability alongside effective uptake of methodologies proposed in recommendation 1.

8.5 Limitations

Each presented analysis chapter is associated with limiting factors, described within this section. Due to the limited availability of cloud free Landsat satellite imagery that coincided with peak green up (July in Western Australia) in order to maximise spectral contrast between spectrally similar surfaces (e.g. bare earth and urban) analysis was restricted to seven sequential snapshots of data as opposed to annual replication (Chen et al., 2014). Annual replication would enable consistent and up-to date comparison to infill and density targets, as specified by the Western Australian Planning Commission, permitting timely, targeted action to under achieving areas in ensuring attainment. Whilst chapter 5 provided a methodology for refinement of urban area estimations, due to the demanding processing for segmentation of high resolution imagery the analysis was limited to four subsets. Consequently, although this furthered current methodologies (e.g. Lu et al., 2011), application across a complete metropolitan region through an approach descried in section 8.2 could still retain errors in urban estimates due to heterogeneity of urban areas across metropolitan regions. Owing to the requirement of daily LST data, chapter 6 was

limited to using coarse resolution MODIS data, although implemented rules attempted to extract valid land cover – temperature associations small, non-dominant land cover changes within identified pixels could have also influenced changes in temperature between the two time periods. Nevertheless the presented approach overcomes current temporal (e.g. Li et al., 2011; Tomlinson et al., 2012) and spatial restrictions (e.g. Kikon et al., 2016; Zhao et al., 2017) of recent research, being more appropriate for applied policy outcomes. Whilst chapter 7 provided a localised methodology for optimising vegetation locations errors associated with digitisation of planning documentation (e.g. positional or attributable) could further propagate throughout the analysis (Heuvelink, 1999). Although the majority of analysis presented within this thesis only requires freely available remotely sensed data a form of planning redevelopment or proposal is essential for replication of chapter 7 which, based on local legislation could be publically unavailable. In terms global transferability the presented analysis has only considered a developed country and application of these methods to a developing country may present further challenges such as accurate land cover classification owing to the potential for greater diversity of urban characteristics (e.g. slums and informal residential areas). Even with these limitations considered, this body of work still provides substantial contributions to the academic literature.

8.6 Future research

8.6.1 Methodological advancements

In 2018 the UN estimated that 55% of the world's population (7 .6 billion) reside in urban areas and by 2050 this predicted to increase to 68% of the world's 9.8 billion inhabitants (United Nations, 2018). Future data resources will permit refinement of the presented analytical techniques in order to sustainably accommodate the forecast rise in urban dwellers. Free and commercial satellite data available at higher spatial resolution would enable further spatial refinement of analysis presented within chapters 4, 5 and 6. Specifically, in terms of land cover an increase in spatial resolution could provide more homogenous land cover per pixel potentially reducing classification spectral confusion and increasing overall accuracy. Similarly, in terms of LST higher resolution could potentially enable further refinement of specified requirements. For example, the change in land cover must be (i) the greater than all other changes (ii) the change must represent at least 50% of the pixel and (iii) dominate (>50%) the pixel of the final year. Analysis of this sort would further reduce the possibility of erroneous land cover-temperature association, ensuring scientifically valid policy applications. Free surface reflectance data could include that from Sentinel 2 (20 m) with LST data from the Visible Infrared Imaging Radiometer Suite (VIIRS) (750 m) whilst commercial data from companies such as Planet can provide daily high

resolution (1-5 m) imagery with global coverage. However daily high resolution LST products are unavailable, therefore although overall land cover accuracy would reduce the propagation of errors within chapter 6, outputs would remain restricted to the lowest resolution product.

Continuation of novel data combinations alongside further development of land cover classification algorithms will continually aim to improve upon classification outputs. In the case of the former a recently devised methodology automatically identified urban classification training areas from nighttime light data, subsequently used for classification of Landsat imagery in Google Earth Engine (Goldblatt et al., 2018). In the case of the latter the proposed Word ExtrAction for time SEries cLassification + MUltivariate Symbols and dErivatives (WEASEL+MUSE) observed an improved accuracy for rare and difficult land cover classes in comparison to the Random Forest (RF) classifier (Schäfer et al., 2018). Similarly, deep learning is currently the fastest growing trend in big data analysis, characterised by Artificial Neural Networks (ANNs) with more than two hidden layers found to be effective in image recognition (He et al., 2016), object detection (Girshick et al., 2015) and classification (Krizhevsky et al., 2012). Nevertheless the application of deep learning in remote sensing applications is relatively young, with rapid advancement expected in the coming years (Zhu et al., 2017). Implementation of these applications to medium resolution imagery and subsequent validation in comparison to high resolution data (e.g. chapter 5) is essential to establish potential improvements in current over or under estimation of urban area.

Future considerations pertinent to chapter 7 would include digital submissions of proposed (re)developments in order to mitigate errors associated with digitisation and analyst interpretation of proposed planning documentation. This method could easily be upscaled to complete local government or metropolitan areas in determining optimum locations for new vegetation, assuming available digital data such as that from Ordnance Survey's MasterMap (the UK's national mapping agency) OpenStreetMap, or local government spatial databases.

8.6.2 Technological considerations

All analysis presented in this thesis were conducted on a standalone computer, often over extensive time periods. However, recent EO initiatives such as Google Earth Engine and Earth on Amazon's Web Service (AWS) that store multi-petabyte catalogues of publically available datasets (e.g. Landsat and MODIS) significantly reduce local processing requirements permitting up to planetary scale analysis within minutes (Gorelick et al., 2017; Mathieu and Aubrecht, 2018). Due to the built in geoprocessing tools and script sharing functionalities these platforms have the potential to universalise endorsed methodologies for monitoring global targets such as the

indicators of the SDGs, or approaches presented within this thesis. Consequently national, metropolitan and local governments would be able to replicate analysis with extremely limited script modification, such as appropriate selection of local training pixels for image classification (Gorelick et al., 2017). Simplifying complex methodologies in this manner would also overcome potential current barriers such as remote sensing expertise and proprietary software that could prevent uptake by local authorities. Nevertheless these global analytical platforms place reliance upon commercial companies that could reserve the right to withdraw, limit or charge for data processing capabilities, whilst also raising privacy concerns pertaining to unauthorised distribution of analytical results. Idealistically, legislative agreements between these companies, the UN and national governments could ensure the future availability of the analytical platforms in providing simplistic and efficient monitoring based upon complex methodological approaches.

The variety of future EO data sources, new data combinations, novel EO classification algorithms and online big data platforms will permit spatial and temporal processing refinement of methodological approaches and outputs presented within this thesis to inform and monitor local, national and global city development goals in relation to urban induced socio-environmental issues ensuring the future sustainability of our cities.

Chapter 9 Conclusion

Data informed governance is key to ensure the sustainable (re)development of our global cities in accommodating the predicted additional 2.5 billion urban dwellers by 2050. The lack of globally endorsed scientifically valid frameworks, consistent devolution of responsibilities, use of unrepresentative data alongside varied methodological approaches have the potential to misguide future (re)development decisions. The overall thesis aim of demonstrating the application of Earth Observation (EO) data in quantifying urban growth and its impact on the UHI in order to illustrate its potential for informing both global and metropolitan sustainable city development goals was achieved.

The first part of the thesis aim (quantification of urban growth) was established from papers 1 and 2. Specifically, an applied EO methodology was demonstrated over the Perth Metropolitan Region (PMR), which was found to have increased 45% between 1990 and 2015, over 320 km^2. In comparison the Western Australian Planning Commission (WAPC) underestimated overall urban area across the Perth Metropolitan Region (PMR). Nevertheless a comparison between the classified Landsat data and hardened high resolution data (to Landsat pixel area) established that pixels containing <50% urban land cover are largely dominated by vegetation according to the high resolution dataset, whilst Landsat largely identified these pixels as urban. Overestimation of urban area was reiterated when comparing Landsat sub-pixel estimates to the percentage of urban area per Landsat pixel derived from the high resolution classification. The range of bias values over differing development subset types indicated the inappropriateness of applying a single global model in adjusting Landsat estimates. Consequently application of spatially explicit models based on development type reduced moderate resolution urban area over (under) estimation by on an average 55.08% in comparison to the high spatial resolution data set decreasing the average overestimation from 11.86 km^2 per subset to just 0.09 km^2.

The latter part of the thesis aim (quantifying the impact on urban growth on the UHI) was determined from papers 3 and 4. Land cover associated Land Surface Temperature (LST) change across the PMR indicated that conversion from grassland to bare earth was associated with the greatest overall annual daytime increase in temperature (0.44 °C), whilst conversion from forest to low urban albedo was associated with the greatest nighttime temperature change (0.88 °C) and greatest daytime change (0.40 °C) in conversion to a low urban albedo surface. More locally, through combining EO data and spatial models urban development in the form of a low density sprawl (e.g. lower building heights, less dense vegetation and sprawled layout) within the PMR was found to produce higher average annual temperatures of 0.54 °C (paved), 0.39 °C (grass) and

0.14 °C (buildings) compared to that of a high density urban development. An applied application of this methodology was demonstrated using a recently submitted redevelopment proposal. Optimisation of vegetation location was achieved, reducing maximum, mean and minimum average temperatures by 0.9 °C, 0.8 °C and 0.4 °C respectively, whilst maintaining design characteristics such as vegetation height and spacing.

Combined, this PhD research has demonstrated the use of EO data, spatial models and geographic techniques in addressing metropolitan sustainability concerns through overcoming current methodological limitations facilitating the basis for scientifically valid and policy applicable data-informed governance.

Appendix A PhD logistics and further activities

PhD logistics

During the PhD candidature two visits to the University of Western Australia (UWA) were undertaken. During January of the first year (2015) of PhD candidature Andrew MacLachlan undertook a three month visit hosted by Dr Boruff, partly funded by the University of Southampton study abroad scheme. The visit permitted project refinement based on Dr Boruff's localised expertise and identification of pertinent geographic challenges within Perth. During the second year (2016) of candidature the original primary PhD supervisor, Dr Biggs, relocated to UWA taking up the position of Lecturer in Geography at the UWA School of Agriculture and Environment. Subsequently Andrew MacLachlan was sponsored for a training and research visa by Dr Boruff, Dr Biggs and the UWA School of Agriculture and Environment from May 2016 to May 2017, with part funding from the World University Network (WUN) researcher mobility programme. As a consequence of supervisory relocation and University regulations Dr Roberts was listed as the primary supervisor for the remainder of the candidature as Andrew's candidature remained registered at the University of Southampton. Dr Biggs has remained a visiting academic at the University of Southampton throughout the duration of candidature and was the second listed supervisor. However, supervision remained at a 50-50% split. Dr Boruff continued to contribute as an external advisor.

Further PhD activities

Whilst this thesis details the academic requirement of the PhD, throughout the candidature a variety of additional activities have been undertaken, relevant to professional development and the holistic PhD qualification. These include presenting at academic conferences, attainment of further qualifications, successful procurement of additional funding to support research activities alongside teaching and additional research experience detailed below.

Academic conferences

8/4/2018 – 13/04/2018: European Geosciences Union General Assembly, Vienna. Presentation: Earth Observation for Planning Sustainable Cities.

8/12/2017: Economic and Social Research Council Doctoral Training Centre Third Year Conference, University of Southampton. Poster: Urban Dynamics from Space for Sustainable Future Planning.

21/10/2016: Western Australia Surveying and Spatial Science Institute, Perth, University of Western Australia. Presentation: Busting the boom: Implications of Western Australia's economic downturn on urban expansion of the world's most isolated capital city.

28/06/2016 – 01/07/2016: Australian Institute of Geographers, Adelaide. Presentation: Busting the boom: Implications of Western Australia's economic downturn on urban expansion of the world's most isolated capital city.

8/09/2015 – 11/09/2015: UK Remote Sensing and Photogrammetry Society, University of Southampton. Poster: Deconstructing the mixel: a temporal exploration of land use change in Perth.

11/06/2015 – 12/06/2015: Department of Geography and Environment Graduate School Conference, University of Southampton. Poster: Exploration of the current state, pressure and the potential risks of urban expansion in the Greater Perth Region of Western Australia.

Qualifications

11/2015 – 04/2016: Association (Associate Fellow) to the Higher Education Academy (Distinction), through completion of Introduction to Learning and Teaching for Researchers considered the equivalent of the Postgraduate Certificate in Academic Practice module 1.

Teaching

2014 – 2018: Module demonstrator for masters and undergraduate students in Geographical Information Systems and Remote Sensing modules undertaken at the University of Southampton and on field courses in Tenerife and Cambodia.

2016 – 2017: Module tutor for masters and undergraduate students in Geographical Information Systems and Remote Sensing modules at the University of Western Australia.

Tutoring (University of Western Australia)

ENVT4409: Remote Sensing of Environment (around 40, mostly MSc students).

ENVT4411: Geographic Information Systems Applications (around 60, mostly MSc students)

ENVT5511: Advanced Geographic Information Systems for Environmental Management (around 70, mostly MSc students).

Marking (University of Western Australia)

GEOG2201: Geographic Information Systems (around 120 undergraduate students).

Demonstrating (University of Southampton)

GEOG1011: Dangerous World (around 120 undergraduate students).

GEOG2010: Introductory GIS (around 120 undergraduate students).

GEOG2033: Research design, methods and techniques in Physical Geography, Tenerife Field Course 06/03/2016 – 13/03/2016 (around 60 undergraduate students).

GEOG3006: Advanced Geographic Information Systems (around 40 undergraduate students).

GEOG6061: Core Skills in GIS (around 20 MSc students).

GEOG6077: Programming Skills in Remote Sensing (around 10 MSc students).

GEOG3069 (Undergraduate) / GEOG6104 (MSc): Water, People and Environment, Cambodia Field Course 25/01/2018 – 06/02/2018, including designing project material (around 30 students).

Training

13/05/2018 – 14/05/2018: Natural Environment Research Council Airborne Research Facility workshop, British Antarctic Survey, Cambridge.

09/02/2018: Google Earth Engine training: beginner and advanced sessions, Google, London.

09/01/2017 – 20/01/2017: Economic and Social Research Council collaborative exchange: University of Western Australia.

22/03/2016 – 24/03/2016: Economic and Social Research Council Cumberland Lodge residential research training, Cumberland Lodge, Windsor.

11/11/2015 – 27/04/2016: Association (Associate Fellow) to the Higher Education Academy (Distinction) through completion of Introduction to Learning and Teaching for Researchers equivalent to the Postgraduate Certificate in Academic Practice module 1, University of Southampton.

09/12/2014 – 11/12/2014: An Introduction to data handling, exploration, and analysis in Matlab ESRC National Centre for Research Methods, University of Southampton.

Additional research experience

11/06/2017 – 18/06/2018 (Valencia) and 31/07/2018 – 04/08/2018 (New Forest): Contributor in the collection of Valencia, Spain and New Forest, UK fieldwork data for the publication: Brown, L. and Dash, J. Validation of biophysical vegetation products derived from the optical instruments on-board ESA's Sentinel-2 and -3 currently under development, University of Southampton.

13/06/2017 – 23/06/2017: Co-author of Dr Alan Smith's submitted publication: Demonstrating the global potential of a high-resolution spatiotemporal population modelling framework, funded by the World University Network, University of Western Australia and University of Southampton.

04/05/2016: Awarded World University Network researcher mobility funding, University of Southampton

Appendix B Data acknowledgements and copyright statements

The acknowledgement and copyright statements listed here are provided in order of appearance/use throughout this thesis.

Population and digital boundary data were provided courtesy of the Australian Bureau of Statistics under a Creative Commons Attribution 4.0 international license, © Commonwealth of Australia, http://www.abs.gov.au. The latter is now available through https://data.gov.au/.

Natural resource data were provided by the Government of Western Australia, Department of Mines and Petroleum from within their annual statistic digest documentation, © the State of Western Australia.

Landsat data products were retrieved from the United States Geological Survey Earth Explorer system, courtesy of the United States Geological Survey, 12201 Sunrise Valley Drive Reston, VA 20192, USA, https://earthexplorer.usgs.gov.

Google Earth data (read only) used for Landsat validation over the Perth Metropolitan region remains the copyright (©) of Digital Globe and the Centre for Space Studies/Airbus 2018.

The comparison urban estimate data were provided by the Western Australian Planning Commission, with their organisational logo and text supplied on relevant figure acknowledging the licensor as the source of the information, as required by the data license agreement.

Classified Landsat data over the Perth Metropolitan Region (produced and further analysed within this thesis) can be accessed through the PANGAEA data publisher for earth and environmental science under the Creative Commons Attribution 3.0 Unported license, https://www.pangaea.de.

High resolution urban monitor data were provided by the Australian Commonwealth Scientific and Industrial Research Organisation (CSIRO) Perth and Peel Urban Monitoring Programme (Caccetta et al., 2012), through the National Environmental Science Program's Clean Air and Landscape Hub and remains the copyright (©) of CSIRO.

Railway and road vector data were provided by the Shared Location Information Platform delivered by Landgate (Western Australia's land information authority) on behalf of the State of Western Australia. © Western Australian Land Information Authority (Landgate) (2017).

Appendix B

The Moderate Resolution Imaging Spectroradiometer Terra land surface temperature (MOD11A1, collection 5) data were retrieved from the online Data Pool, courtesy of the National Aeronautics and Space Administration [Land Processes. Distributed Active Archive Center, Untied States Geological Survey/Earth Resources Observation and Science Center, Sioux Falls, South Dakota], https://lpdaac.usgs.gov/data_access/data_pool.

Metrological data were retrieved from the Weatherundergound.com website, courtesy of The Weather Company, LLC, 1001 Summit Boulevard, Floor 20, Brookhaven, GA, USA, https://www.wunderground.com.

Downward shortwave radiation data were provided by the European Union Water and Global Change project, specifically the Water and Global Change Forcing Data methodology applied to ERA-interim (known as WFDEI) data, with the required attribution reference to Weedon et al. (2014), http://www.eu-watch.org/data_availability.

Open street map data were provided under the Open Database License (www.openstreetmap.org/copyright), and has the attribution of © OpenStreetMap contributors, https://www.openstreetmap.org.

Planning proposal documentation was accessed from the City of Fremantle planning website courtesy of the city of Fremantle, accessible at https://mysay.fremantle.wa.gov.au. The specific plans used and the concepts they represent are reserved to the Buchan Group – 2006, the authors of the plans, © The Buchan Group 2010.

List of References

ABS, 2017. Australian Statistical Geography Standard (ASGS): Volume 4 - Significant Urban Areas, Urban Centres and Localities, Section of State, Australian Bureau of Statistics. Belconnen, ACT, Australia.

ABS, 2015. Australian National Accounts 1988-2015, Australian Bureau of Statistics. Belconnen, ACT, Australia.

ABS, 2011. Australian Population Grid 2011, Australian Bureau of Statistics. Belconnen, ACT, Australia.

Abutaleb, K., Ngie, A., Darwish, A., Ahmed, M., Arafat, S., Ahmed, F., 2015. Assessment of Urban Heat Island Using Remotely Sensed Imagery over Greater Cairo , Egypt. Adv. Remote Sens. 4, 35–47. doi:10.4236/ars.2015.41004

Adams, J., 1995. Classification of multispectral images based on fractions of endmembers: Application to land-cover change in the Brazilian Amazon. Remote Sens. Environ. 52, 137–154. doi:10.1016/0034-4257(94)00098-8

AECOM Australia, 2012. Economic Assessment of the Urban Heat Island Effect, City of Melbourne. Melbourne, Australia.

Aguilar, M. a, Vicente, R., Aguilar, F.J., Fernández, A., Saldaña, M.., 2012. Optimizing Object-Based Classification in Urban Environments Using Very High Resolution Geoeye-1 Imagery, in: ISPRS Annals of the Photogrammetry, Remote Sensing and Spatial Information Sciences. Melbourne, Australia, pp. 99–104. doi:10.5194/isprsannals-I-7-99-2012

Akbari, H., Rose, S., Taha, H., 2003. Analyzing the land cover of an urban environment using high-resolution orthophotos. Landsc. Urban Plan. 63, 1–14. doi:10.1016/S0169-2046(02)00165-2

Angel, S., Parent, J., Civco, D.L., Blei, A., Potere, D., 2011. The dimensions of global urban expansion: Estimates and projections for all countries, 2000-2050. Prog. Plann. 75, 53–107. doi:10.1016/j.progress.2011.04.001

Angiuli, E., Trianni, G., 2013. Urban Mapping in Landsat Images Based on Normalized Difference Spectral Vector. IEEE Geosci. Remote Sens. Lett. 11, 661–665. doi:10.1109/LGRS.2013.2274327

Arnfield, A.J., 2003. Two decades of urban climate research: A review of turbulence, exchanges of

energy and water, and the urban heat island. Int. J. Climatol. 23, 1–26. doi:10.1002/joc.859

ARUP, The Rockefeller Foundation, 2015. City Resilience Framework—100 Resilient Cities, The Rockefeller Foundation. New York, NY, USA.

Atkinson, P., Cutler, M., Lewis, H.G., 1997. Mapping sub-pixel proportional land cover with AVHRR imagery. Int. J. Remote Sens. 18, 917–935. doi:10.1080/014311697218836

Atkinson, P.M., Lewis, P., 2000. Geostatistical classification for remote sensing: An introduction. Comput. Geosci. 26, 361–371. doi:10.1016/S0098-3004(99)00117-X

Bagan, H., Yamagata, Y., 2014. Land-cover change analysis in 50 global cities by using a combination of Landsat data and analysis of grid cells. Environ. Res. Lett. 9, 1–13. doi:10.1088/1748-9326/9/6/064015

Bagan, H., Yamagata, Y., 2012a. Remote Sensing of Environment Landsat analysis of urban growth : How Tokyo became the world ' s largest megacity during the last 40 years. Remote Sens. Environ. 127, 210–222. doi:10.1016/j.rse.2012.09.011

Bagan, H., Yamagata, Y., 2012b. Landsat analysis of urban growth: How Tokyo became the world's largest megacity during the last 40years. Remote Sens. Environ. 127, 210–222. doi:10.1016/j.rse.2012.09.011

Basu, R., Samet, J.M., 2002. Relation between elevated ambient temperature and mortality: A review of the epidemiologic evidence. Epidemiol. Rev. 24, 190–202. doi:10.1093/epirev/mxf007

Batty, M., Besussi, E., Chin, N., 2003. Traffic, Urban Growth and Suburban Sprawl, Centre for Advanced Spatial Analysis. London.

Bennett, B., 2001. What is a Forest? On the Vagueness of Certain Geographic Concepts. Topoi 20, 189–201. doi:10.1023/A:1017965025666

Bettencourt, L., West, G., 2010. A unified theory of urban living. Nature 467, 9–10. doi:10.1038/467912a

Bevington, J., Eguchi, R., Huyck, C., Dell' Acqua, F., Iannelli, G., Jordan, C., Morley, J., Wieland, M., Parolai, S., Pittore, M., Porter, K., Saito, K., Sarabandi, P., Wright, A., Wyss, M., 2012. Exposure Data Development for the Global Earthquake Model: Inventory Data Capture Tools, in: 15th World Conference on Earthquake Engineering (15WCEE). Lisbon, Portugal.

Beyer, K.M.M., Kaltenbach, A., Szabo, A., Bogar, S., Javier Nieto, F., Malecki, K.M., 2014. Exposure

to neighborhood green space and mental health: Evidence from the survey of the health of wisconsin. Int. J. Environ. Res. Public Health 11, 3453–3472. doi:10.3390/ijerph110303453

Bhatta, B., 2010. Causes and Consequences of Urban Growth and Sprawl, in: Analysis of Urban Growth and Sprawl from Remote Sensing Data. Springer Berlin Heidelberg, Berlin. doi:10.1007/978-3-642-05299-6

Bhatta, B., Saraswati, S., Bandyopadhyay, D., 2010. Urban sprawl measurement from remote sensing data. Appl. Geogr. 30, 731–740. doi:10.1016/j.apgeog.2010.02.002

Bibby, P., Brindley, P., 2013. Urban and Rural Area Definitions for Policy Purposes in England and Wales (v1.0), Government Statistical Service. University of Nottingham.

Biehl, L., Landgrebe, D., 2002. MultiSpec — a tool for multispectral – hyperspectral image data. Comput. Geosci. 28, 1153–1159. doi:10.1016/S0098-3004(02)00033-X

Blasi, M.G., Liuzzi, G., Masiello, G., Serio, C., Telesca, V., Venafra, S., 2016. Surface parameters from seviri observations through a kalman filter approach: Application and evaluation of the scheme to the southern Italy. Tethys 2016, 3–10. doi:10.3369/tethys.2016.13.01

Boland, J., Philipp, C., 2013. Monitoring the Urban Climatic Trends and Impacts, RP2005: Urban Micro Climates. Melbourne, Australia.

Braun, A.C., Weidner, U., Hinz, S., 2012. Classification in high-dimensional feature spaces-assessment using SVM, IVM and RVM with focus on simulated EnMAP data. IEEE J. Sel. Top. Appl. Earth Obs. Remote Sens. 5, 436–443. doi:10.1109/JSTARS.2012.2190266

Braun, A.C., Weidner, U., Hinz, S., 2011. Vector Machines for Hyperspectral Classification - a Comparison, in: 2011 3rd Workshop on Hyperspectral Image and Signal Processing: Evolution in Remote Sensing (WHISPERS). IEEE, Lisbon, Portugal, pp. 1–4. doi:10.1109/WHISPERS.2011.6080861

Breiman, L., 2001. Random forests. Mach. Learn. 45, 5–32. doi:10.1023/A:1010933404324

Breiman, L., 1999. Random forests—random features. Statistics Department, University of California, Berkeley.

Brockerhoff, M.P., 2000. An Urbanizing World. Popul. Bull. 55, 1–44. doi:10.1086/452394

Brown, C.E., 1998. Applied Multivariate Statistics in Geohydrology and Related Sciences. Springer Berlin Heidelberg, Berlin. doi:10.1007/978-3-642-80328-4

Brundtland, G.H., 1987. Our Common Future: Report of the World Commission on Environment and Development, United Nations Commission. Oxford University Press. doi:10.1080/07488008808408783

Buchin, O., Hoelscher, M.-T., Meier, F., Nehls, T., Ziegler, F., 2015. Evaluation of the health-risk reduction potential of countermeasures to urban heat islands. Energy Build. doi:10.1016/j.enbuild.2015.06.038

Buechley, R., Van Bruggen, J., Truppi, L., 1972. Heat Island = Death Island? Environ. Res. 92, 85–92. doi:10.1016/0013-9351(72)90022-9

Bunting, P., 2017. Pre-processing of Remotely Sensed Imagery, in: Díaz-Delgado, R., Lucas, R., Hurford, C. (Eds.), The Roles of Remote Sensing in Nature Conservation: A Practical Guide and Case Studies. Springer International Publishing, Gewerbestrasse, pp. 39–63. doi:10.1007/978-3-319-64332-8_3

Burnett, R.T., Brook, J.R., Yung, W.T., Dales, R.E., Krewski, D., 1997. Association between ozone and hospitalization for respiratory diseases in 16 Canadian cities. Environ. Res. 72, 24–31. doi:10.1006/enrs.1996.3685

C40 Cities, 2018. Good Practice Guide: Cool Cities, C40 Cities Climate Leadership Group. London, UK.

C40 Cities, ARUP, 2011. Climate Action in Megacities: C40 Cities Baseline and Opportunities, C40 Cities Climate Leadership Group. London, UK.

Caccetta, P., Collings, S., Devereux, A., Hingee, K., Mcfarlane, D., Traylen, A., Wu, X., 2012. Urban Monitor: Enabling effective monitoring and management of urban and coastal environments using digital aerial photography Final Report – Transformation of aerial photography into digital raster information products. CSIRO, Australia.

Caccetta, P., Collings, S., Hingee, K., McFarlane, D., Wu, X., 2011. Fine-Scale Monitoring of Complex Environments Using Remotely Sensed Aerial, Satellite, and Other Spatial Data, in: 2011 International Symposium on Image and Data Fusion. IEEE, pp. 1–5. doi:10.1109/ISIDF.2011.6024217

Cai, Y., Zhang, H., Zheng, P., Pan, W., 2016. Quantifying the Impact of Land use/Land Cover Changes on the Urban Heat Island: A Case Study of the Natural Wetlands Distribution Area of Fuzhou City, China. Wetlands 36, 285–298. doi:10.1007/s13157-016-0738-7

Camara, G., Cartaxo, R., Souza, M., Freitas, U.M., Garrido, J., 1996. Spring: Integrating Remote

Sensing and gis by object-oriented data modelling. Comput. Graph. 20, 395–403. doi:10.1016/0097-8493(96)00008-8

Camps-Valls, G., Gómez-Chova, L., Calpe-Maravilla, J., Martín-Guerrero, J.D., Soria-Olivas, E., Alonso-Chordá, L., Moreno, J., 2004. Robust support vector method for hyperspectral data classification and knowledge discovery. IEEE Trans. Geosci. Remote Sens. 42, 1530–1542. doi:10.1109/TGRS.2004.827262

Candade, N., Dixon, B., 2004. Multispectral classification of Landsat images: a comparison of support vector machine and neural network classifiers, in: ASPRS Annual Meeting Proceedings. Denver, CO. Denver, Colorado, USA.

Cao, X., Onishi, A., Chen, J., Imura, H., 2010. Quantifying the cool island intensity of urban parks using ASTER and IKONOS data. Landsc. Urban Plan. 96, 224–231. doi:10.1016/j.landurbplan.2010.03.008

Castrence, M., Nong, D., Tran, C., Young, L., Fox, J., 2014. Mapping Urban Transitions Using Multi-Temporal Landsat and DMSP-OLS Night-Time Lights Imagery of the Red River Delta in Vietnam. Land 3, 148–166. doi:10.3390/land3010148

Centre for Research on the Epidemiology of Disaster and the United Nations Office for Disaster Risk Reduction, 2016. Poverty & Death: Disaster Mortality 1996-2015, United Nations Office for Disaster Risk Reduction. doi:10.1007/s11069-012-0162-0.

Chen, J., Chen, J., Liao, A., Cao, X., Chen, L., Chen, X., He, C., Han, G., Peng, S., Lu, M., Zhang, W., Tong, X., Mills, J., 2015. Global land cover mapping at 30m resolution: A POK-based operational approach. ISPRS J. Photogramm. Remote Sens. 103, 7–27. doi:10.1016/j.isprsjprs.2014.09.002

Chen, L., Yu, B., Yang, F., Mayer, H., 2016. Intra-urban differences of mean radiant temperature in different urban settings in Shanghai and implications for heat stress under heat waves: A GIS-based approach. Energy Build. 130, 829–842. doi:10.1016/j.enbuild.2016.09.014

Chen, T., de Jeu, R.A.M., Liu, Y.Y., van der Werf, G.R., Dolman, A.J., 2014. Using satellite based soil moisture to quantify the water driven variability in NDVI: A case study over mainland Australia. Remote Sens. Environ. 140, 330–338. doi:10.1016/j.rse.2013.08.022

Cheng, G., Han, J., 2016. A survey on object detection in optical remote sensing images. ISPRS J. Photogramm. Remote Sens. 117, 11–28. doi:10.1016/j.isprsjprs.2016.03.014

Cheval, S., Dumitrescu, A., 2014. The summer surface urban heat island of Bucharest (Romania)

retrieved from MODIS images. Theor. Appl. Climatol. 121, 631–640. doi:10.1007/s00704-014-1250-8

Chih-Wei, H., Chih-Chung, C., Chih-Jen, L., 2008. A Practical Guide to Support Vector Classification, Department of Computer Science, National Taiwan University. Taipeo, Taiwan. doi:10.1177/02632760022050997

City of Fremantle, 2017. City of Fremantle Urban Forest Plan. Fremantle, Australia.

City of Johannesburg Metropolitan Municipality, 2016. Spatial Development Framework 2040, City of Johannesburg: Department of Development Planning. Johannesburg, South Africa.

City of Perth, 2006. Urban Forest Plan 2016-2036. City of Perth, Perth, Australia.

Coll, C., Wan, Z., Galve, J.M., 2009. Temperature-based and radiance-based validations of the V5 MODIS land surface temperature product. J. Geophys. Res. Atmos. 114, 1–15. doi:10.1029/2009JD012038

Collings, S., Caccetta, P., Campbell, N., 2011. Empirical Models for Radiometric Calibration of Digital Aerial Frame Mosaics. IEEE Trans. Geosci. Remote Sens. 49, 2573–2588. doi:10.1109/TGRS.2011.2108301

Congalton, R.G., 2001. Accuracy assessment and validation of remotely sensed and other spatial information. Int. J. Wildl. Fire 10, 321–328. doi:10.1071/WF01031

Cortes, C., Vapnik, V., 1995. Support-vector networks. Mach. Learn. 20, 273–297. doi:10.1007/BF00994018

Coutts, A.M., Harris, R.J., Phan, T., Livesley, S.J., Williams, N.S.G., Tapper, N.J., 2016. Thermal infrared remote sensing of urban heat: Hotspots, vegetation, and an assessment of techniques for use in urban planning. Remote Sens. Environ. 186, 637–651. doi:10.1016/j.rse.2016.09.007

Cracknell, M.J., Reading, A.M., 2014. Geological mapping using remote sensing data: A comparison of five machine learning algorithms, their response to variations in the spatial distribution of training data and the use of explicit spatial information. Comput. Geosci. 63, 22–33. doi:10.1016/j.cageo.2013.10.008

Cunningham, S., Rogan, J., Martin, D., DeLauer, V., McCauley, S., Shatz, A., 2015. Mapping land development through periods of economic bubble and bust in Massachusetts using Landsat time series data. GIScience Remote Sens. 52. doi:10.1080/15481603.2015.1045277

Daley, M.J., Phillips, N.G., 2006. Interspecific variation in nighttime transpiration and stomatal conductance in a mixed New England deciduous forest. Tree Physiol. 26, 411–419. doi:10.1093/treephys/26.4.411

Das, S., Mirnalinee, T.T., Varghese, K., 2011. Use of salient features for the design of a multistage framework to extract roads from high-resolution multispectral satellite images. IEEE Trans. Geosci. Remote Sens. 49, 3906–3931. doi:10.1109/TGRS.2011.2136381

De Morsier, F., Tuia, D., Borgeaud, M., Gass, V., Thiran, J.P., 2013. Semi-supervised novelty detection using SVM entire solution path. IEEE Trans. Geosci. Remote Sens. 51, 1939–1950. doi:10.1109/TGRS.2012.2236683

Deilami, K., Kamruzzaman, M., Hayes, J., 2016. Correlation or Causality between Land Cover Patterns and the Urban Heat Island Effect? Evidence from Brisbane, Australia. Remote Sens. 8, 716. doi:10.3390/rs8090716

Dell'Acqua, F., Gamba, P., Lisini, G., 2003. Improvements to urban area characterization using multitemporal and multiangle SAR images. IEEE Trans. Geosci. Remote Sens. 41, 1996–2004. doi:10.1109/TGRS.2003.814631

Department for Communities and Local Government, 2015. English Housing Survey: Housing Stock Report, 2014-2015, English Housing Survey. London, UK. doi:10.1017/CBO9781107415324.004

Department of Mines and Petroleum, 2015. Western Australian mineral and petroleum statistics digest 1984-2015, Perth: Government of Western Australia. Perth, WA, Australia.

Dhakal, S.P., 2014. Glimpses of Sustainability in Perth , Western Australia : Capturing and Communicating the Adaptive Capacity of an Activist Group. Cons. Jounral Sustain. Dev. 11, 167–182. doi:10.7916/D8N879GB

Donnay, J.-P., Unwin, D., 2001. Modelling Geographical Distributions in Urban Areas, in: Donnay, J.-P., Barnsley, M.J., Longley, P.A. (Eds.), Remote Sensing and Urban Analysis. Taylor & Francis, London, UK, pp. 189–207.

Dorais, A., Cardille, J., 2011. Strategies for incorporating high-resolution google earth databases to guide and validate classifications: Understanding deforestation in Borneo. Remote Sens. 3, 1157–1176. doi:10.3390/rs3061157

Downs, A., 2005. Smart Growth: Why We Discuss It More than We Do It. J. Am. Plan. Assoc. 71, 367–378. doi:10.1080/01944360508976707

Du, Y., Teillet, P.M., Cihlar, J., 2002. Radiometric normalization of multitemporal high-resolution satellite images with quality control for land cover change detection. Remote Sens. Environ. 82, 123–134. doi:10.1016/S0034-4257(02)00029-9

Earl, N., Simmonds, I., Tapper, N., 2016. Weekly cycles in peak time temperatures and urban heat island intensity. Environ. Res. Lett 11, 1–10. doi:10.1088/1748-9326/11/7/074003

Eliot, M.J., Travers, A., Eliot, I., 2006. Morphology of a Low-Energy Beach, Como Beach, Western Australia. J. Coast. Res. 221, 63–77. doi:10.2112/05A-0006.1

Environment Agency, 2016. Environment Agency LIDAR data, Environment Agency. Birmingham, UK.

Esposito, F., Malerba, D., Semeraro, G., Kay, J., 1997. A comparative analysis of methods for pruning decision trees. IEEE Trans. Pattern Anal. Mach. Intell. 19, 476–491. doi:10.1109/34.589207

Estrada, F., Botzen, W.J.W., Tol, R.S.J., 2017. A global economic assessment of city policies to reduce climate change impacts. Nat. Clim. Chang. 7, 403–406. doi:10.1038/nclimate3301

European Space Agency, 2017. Land Cover Newsletter, ESA Climate Change Inititave. Paris, France.

Fabrizi, R., Bonafoni, S., Biondi, R., 2010. Satellite and ground-based sensors for the Urban Heat Island analysis in the city of Rome. Remote Sens. 2, 1400–1415. doi:10.3390/rs2051400

Feyisa, G.L., Meilby, H., Darrel Jenerette, G., Pauliet, S., 2016. Locally optimized separability enhancement indices for urban land cover mapping: Exploring thermal environmental consequences of rapid urbanization in Addis Ababa, Ethiopia. Remote Sens. Environ. 175, 14–31. doi:10.1016/j.rse.2015.12.026

Field, A., 2009. Discovering Statistics Using SPSS (Introducing Statistical Methods series), 3rd ed. SAGE Publications Ltd, London, UK.

Flood, N., 2014. Continuity of Reflectance Data between Landsat-7 ETM+ and Landsat-8 OLI, for Both Top-of-Atmosphere and Surface Reflectance: A Study in the Australian Landscape. Remote Sens. 6, 7952–7970. doi:10.3390/rs6097952

Foody, G.M., Mathur, A., 2006. The use of small training sets containing mixed pixels for accurate hard image classification: Training on mixed spectral responses for classification by a SVM. Remote Sens. Environ. 103, 179–189. doi:10.1016/j.rse.2006.04.001

Foody, G.M., Mathur, A., 2004. A relative evaluation of multiclass image classification by support vector machines. IEEE Trans. Geosci. Remote Sens. 42, 1335–1343. doi:10.1109/TGRS.2004.827257

Franke, J., Roberts, D.A., Halligan, K., Menz, G., 2009. Hierarchical Multiple Endmember Spectral Mixture Analysis (MESMA) of hyperspectral imagery for urban environments. Remote Sens. Environ. 113, 1712–1723. doi:10.1016/j.rse.2009.03.018

Franklin, M., Koutrakis, P., Schwartz, J., 2008. The Role of Particle Composition on the Association Between PM2.5 and Mortality. Epidemiology 19, 680–689. doi:10.1111/j.1743-6109.2008.01122.x.Endothelial

Friedl, M.., McIver, D.., Hodges, J.C.., Zhang, X.., Muchoney, D., Strahler, A.., Woodcock, C.., Gopal, S., Schneider, A., Cooper, A., Baccini, A., Gao, F., Schaaf, C., 2002. Global land cover mapping from MODIS: algorithms and early results. Remote Sens. Environ. 83, 287–302. doi:10.1016/S0034-4257(02)00078-0

Friedl, M.A., Sulla-Menashe, D., Tan, B., Schneider, A., Ramankutty, N., Sibley, A., Huang, X., 2010. MODIS Collection 5 global land cover: Algorithm refinements and characterization of new datasets. Remote Sens. Environ. 114, 168–182. doi:10.1016/j.rse.2009.08.016

Frumkin, H., 2002. Urban sprawl and public health. Public Health Rep. 117, 201–217. doi:10.1016/S0033-3549(04)50155-3

Fu, P., Weng, Q., 2016. Consistent land surface temperature data generation from irregularly spaced Landsat imagery. Remote Sens. Environ. 184, 175–187. doi:10.1016/j.rse.2016.06.019

Fuller, R.M., Groom, G.B., Jones, A.R., 1994. The Land Cover Map of Great Britain: an automated classification of Landsat Thematic Mapper data. Photogramm. Eng. Remote Sensing 60, 553–562.

Gaffin, S.R., Rosenzweig, C., Khanbilvardi, R., Parshall, L., Mahani, S., Glickman, H., Goldberg, R., Blake, R., Slosberg, R.B., Hillel, D., 2008. Variations in New York city's urban heat island strength over time and space. Theor. Appl. Climatol. 94, 1–11. doi:10.1007/s00704-007-0368-3

Gallo, K., Xian, G., 2014. Application of spatially gridded temperature and land cover data sets for urban heat island analysis. Urban Clim. 8, 1–10. doi:10.1016/j.uclim.2014.04.005

Galster, G., Hanson, R., Ratcliffe, M.R., Wolman, H., Coleman, S., Freihage, J., 2001. Wrestling

Sprawl to the Ground: Defining and measuring an elusive concept. Hous. Policy Debate 12, 681–717. doi:10.1080/10511482.2001.9521426

Gao, B.-C., 1996. NDWI - a normalized difference water index for remote sensing of vegetation liquid water from space. Remote Sens. Environ. 58, 257–266. doi:10.1016/S0034-4257(96)00067-3

Gascon, M., Zijlema, W., Vert, C., White, M.P., Nieuwenhuijsen, M.J., 2017. Outdoor blue spaces, human health and well-being: A systematic review of quantitative studies. Int. J. Hyg. Environ. Health 220, 1207–1221. doi:10.1016/j.ijheh.2017.08.004

Gashu, K., Egziabher, T.G., 2018. Spatiotemporal trends of urban land use / land cover and green infrastructure change in two Ethiopian cities: Bahir Dar and Hawassa. Environ. Syst. Res. 7, 1–15. doi:10.1186/s40068-018-0111-3

Gastellu-Etchegorry, J.P., Martin, E., Gascon, F., 2004. DART: A 3D model for simulating satellite images and studying surface radiation budget. Int. J. Remote Sens. 25, 73–96. doi:10.1080/0143116031000115166

Geoscience Australia, 2015. Digital Elevation Model (DEM) of Australia Dervied From LiDAR 5 Metre Grid.

Ghimire, B., Rogan, J., Miller, J., 2010. Contextual land-cover classification: incorporating spatial dependence in land-cover classification models using random forests and the Getis statistic. Remote Sens. Lett. 1, 45–54. doi:10.1080/01431160903252327

Giorgio, G.A., Ragosta, M., Telesca, V., 2017. Climate variability and industrial-suburban heat environment in a mediterranean area. Sustain. 9, 1–10. doi:10.3390/su9050775

Girshick, R., Donahue, J., Member, S., Darrell, T., Malik, J., 2015. Region-Based Convolutional Networks for Accurate Object Detection and Segmentation. IEEE Trans. Pattern Anal. Mach. Intell. 38, 142–158. doi:10.1109/TPAMI.2015.2437384

Gislason, P.O., Benediktsson, J.A., Sveinsson, J.R., 2006. Random forests for land cover classification. Pattern Recognit. Lett. 27, 294–300. doi:10.1016/j.patrec.2005.08.011

Goggins, W.B., Chan, E.Y.Y., Ng, E., Ren, C., Chen, L., 2012. Effect modification of the association between short-term meteorological factors and mortality by urban heat islands in Hong Kong. PLoS One 7, 9–14. doi:10.1371/journal.pone.0038551

Goldblatt, R., Stuhlmacher, M.F., Tellman, B., Clinton, N., Hanson, G., Georgescu, M., Wang, C.,

Serrano-Candela, F., Khandelwal, A.K., Cheng, W.H., Balling, R.C., 2018. Using Landsat and nighttime lights for supervised pixel-based image classification of urban land cover. Remote Sens. Environ. 205, 253–275. doi:10.1016/j.rse.2017.11.026

Goodwin, N.R., Coops, N.C., Tooke, T.R., Christen, A., Voogt, J.A., 2009. Characterizing urban surface cover and structure with airborne lidar technology. Can. J. Remote Sens. 35, 297–309. doi:10.5589/m09-015

Gorelick, N., Hancher, M., Dixon, M., Ilyushchenko, S., Thau, D., Moore, R., 2017. Google Earth Engine: Planetary-scale geospatial analysis for everyone. Remote Sens. Environ. 202, 18–27. doi:10.1016/j.rse.2017.06.031

Goudarzi, G., Geravandi, S., Foruozandeh, H., Babaei, A.A. kbar, Alavi, N., Niri, M.V. osoughi, Khodayar, M.J. avad, Salmanzadeh, S., Mohammadi, M.J. avad, 2015. Cardiovascular and respiratory mortality attributed to ground-level ozone in Ahvaz, Iran. Environ. Monit. Assess. 187, 1–9. doi:10.1007/s10661-015-4674-4

Governor of Tokyo, 2008. Tokyo Metropolitan Environmental Master Plan., Tokyo Metropolitan Government. Tokyo, Japan.

Gronlund, C.J., Berrocal, V.J., White-Newsome, J.L., Conlon, K.C., O'Neill, M.S., 2015. Vulnerability to extreme heat by socio-demographic characteristics and area green space among the elderly in Michigan, 1990-2007. Environ. Res. 136, 449–461. doi:10.1016/j.envres.2014.08.042

Grose, M.J., 2007. Perth's Stephenson-Hepburn Plan of 1955. Aust. Plan. 44, 20–21. doi:10.1080/07293682.2007.9982608

Guhathakurta, S., Gober, P., 2007. The impact of the Phoenix Urban Heat Island on residential water use. J. Am. Plan. Assoc. ©American Plan. Assoc. Chicagti. 73, 317–329. doi:10.1080/01944360708977980

Guo, Y., Gasparrini, A., Armstrong, B., Li, S., Tawatsupa, B., Tobias, A., Lavigne, E., de Sousa Zanotti Stagliorio Coelho, M., Leone, M., Pan, X., Tong, S., Tian, L., Kim, H., Hashizume, M., Honda, Y., Guo, Y.-L.L., Wu, C.-F., Punnasiri, K., Yi, S.-M., Michelozzi, P., Saldiva, P.H.N., Williams, G., 2014. Global Variation in the Effects of Ambient Temperature on Mortality. Epidemiology 25, 781–789. doi:10.1097/EDE.0000000000000165

Haashemi, S., Weng, Q., Darvishi, A., Alavipanah, S., 2016. Seasonal Variations of the Surface Urban Heat Island in a Semi-Arid City. Remote Sens. 8, 1–17. doi:10.3390/rs8040352

Hansen, M.C., Loveland, T.R., 2012. A review of large area monitoring of land cover change using Landsat data. Remote Sens. Environ. 122, 66–74. doi:10.1016/j.rse.2011.08.024

Hattis, D., Ogneva-Himmelberger, Y., Ratick, S., 2012. The spatial variability of heat-related mortality in Massachusetts. Appl. Geogr. 33, 45–52. doi:10.1016/j.apgeog.2011.07.008

He, K., Zhang, X., Ren, S., Sun, J., 2016. Deep Residual Learning for Image Recognition, in: Computer Vision and Pattern Recognition. Las Vegas, USA. doi:10.3389/fpsyg.2013.00124

Hepinstall-Cymerman, J., Coe, S., Hutyra, L.R., 2013. Urban growth patterns and growth management boundaries in the Central Puget Sound, Washington, 1986-2007. Urban Ecosyst. 16, 109–129. doi:10.1007/s11252-011-0206-3

Hepinstall, J.A., Alberti, M., Marzluff, J.M., 2008. Predicting land cover change and avian community responses in rapidly urbanizing environments. Landsc. Ecol. 23, 1257–1276. doi:10.1007/s10980-008-9296-6

Herold, M., Gardner, M., Hadley, B., Roberts, D., 2002. The spectral dimension in urban land cover mapping from high-resolution optical remote sensing data, in: Proceedings of the 3rd Symposium on Remote Sensing of Urban Areas. Istanbul, Turkey.

Heuvelink, G.B.M., 1999. Propagation of error in spatial modeling with GIS. Geogr. Inf. Syst. Vol. 1 Princ. Tech. Issues 2, 207–217.

Holst, J., Mayer, H., 2011. Impacts of street design parameters on human-biometeorological variables. Meteorol. Zeitschrift 20, 541–552. doi:10.1127/0941-2948/2011/0254

Homer, C., Huang, C., Yang, L., Wylie, B., Coan, M., 2004. Development of a 2001 national land-cover database for the United States. Photogramm. Eng. Remote Sens. 70, 829–840. doi:10.14358/PERS.70.7.829

Howard, L., 1988. The Climate of London. Cambridge University Press, London, UK.

Hu, L., Brunsell, N.A., 2015. A new perspective to assess the urban heat island through remotely sensed atmospheric profiles. Remote Sens. Environ. 158, 393–406. doi:10.1016/j.rse.2014.10.022

Hu, X., Weng, Q., 2009. Estimating impervious surfaces from medium spatial resolution imagery using the self-organizing map and multi-layer perceptron neural networks. Remote Sens. Environ. 113, 2089–2102. doi:10.1016/j.rse.2009.05.014

Hu, Y., Jia, G., Hou, M., Zhang, X., Zheng, F., Liu, Y., 2015. The cumulative effects of urban

expansion on land surface temperatures in metropolitan Jingjintang, China Yonghong. J. Geophys. Res. Atmos. Res. 9932–9943. doi:doi.org/10.1002/2015JD023653

Huang, C., Davis, L.S., Townshend, J.R.G., 2002. An assessment of support vector machines for land cover classification. Int. J. Remote Sens. 23, 725–749. doi:10.1080/01431160110040323

Imhoff, M.L., Lawrence, W.T., Stutzer, D.C., Elvidge, C.D., 1997. A technique for using composite DMSP/OLS "city lights" satellite data to map urban area. Remote Sens. Environ. 61, 361–370. doi:10.1016/S0034-4257(97)00046-1

Imhoff, M.L., Zhang, P., Wolfe, R.E., Bounoua, L., 2010. Remote sensing of the urban heat island effect across biomes in the continental USA. Remote Sens. Environ. 114, 504–513. doi:10.1016/j.rse.2009.10.008

Immitzer, M., Atzberger, C., Koukal, T., 2012. Tree species classification with Random forest using very high spatial resolution 8-band worldView-2 satellite data. Remote Sens. 4, 2661–2693. doi:10.3390/rs4092661

Intergovernmental Committee On Surveying & Mapping, 2008. ICSM Guidelines for Digital Elevation Data, Geoscience Australia. Symonston, ACT, Australia.

Jensen, J., 2009. Remote sensing of the environment: An earth resource perspective, 2nd ed. Prentice Hall, New Jersey, USA.

Jensen, J., 2005. Introductory digital image processing, 3rd ed. Prentice Hall, New Jersey, USA.

Jimenez-Munoz, J.C., Sobrino, J.A., Skokovic, D., Mattar, C., Cristobal, J., 2014. Land surface temperature retrieval methods from Landsat-8 thermal infrared sensor data. IEEE Geosci. Remote Sens. Lett. 11, 1840–1843. doi:10.1109/LGRS.2014.2312032

Ju, J., Roy, D.P., Vermote, E., Masek, J., Kovalskyy, V., 2012. Continental-scale validation of MODIS-based and LEDAPS Landsat ETM+ atmospheric correction methods. Remote Sens. Environ. 122, 175–184. doi:10.1016/j.rse.2011.12.025

Kalnay, E., Cai, M., 2003. Impact of urbanization and land-use change on climate. Nature 423, 528–531. doi:10.1038/nature01649.1.

Kam Ng, M., Tang, W.-S., 2004. The Role of Planning in the Development of Shenzhen, China: Rhetoric and Realities. Eurasian Geogr. Econ. 45, 190–211. doi:10.2747/1538-7216.45.3.190

Kelly, J.F., Weidmann, B., Walsh, M., 2011. The Housing We'd Choose, Grattan Institute. Melbourne, Australia.

Kennewell, C., Shaw, B.J., 2008. Perth, Western Australia. Cities 25, 243–255. doi:10.1016/j.cities.2008.01.002

Kenward, A., Yawitz, D., Sanford, T., 2014. Slug summer in the city: Hot and getting hotter, Climate Central. New Jersey, USA.

Kikon, N., Singh, P., Singh, S.K., Vyas, A., 2016. Assessment of urban heat islands (UHI) of Noida City, India using multi-temporal satellite data. Sustain. Cities Soc. 22, 19–28. doi:10.1016/j.scs.2016.01.005

Kim, D.-Y., Han, K.-S., 2013. Remotely sensed retrieval of midday air temperature considering atmospheric and surface moisture conditions. Int. J. Remote Sens. 34, 247–263. doi:10.1080/01431161.2012.712235

Knight, S., Smith, C., Roberts, M., 2010. Mapping Manchester's urban heat island. Weather 65, 188–193. doi:10.1002/wea.542

Knorn, J., Rabe, A., Radeloff, V.C., Kuemmerle, T., Kozak, J., Hostert, P., 2009. Land cover mapping of large areas using chain classification of neighboring Landsat satellite images. Remote Sens. Environ. 113, 957–964. doi:10.1016/j.rse.2009.01.010

Kotsiantis, S.B., Zaharakis, I.D., Pintelas, P.E., 2006. Machine learning: A review of classification and combining techniques. Artif. Intell. Rev. 26, 159–190. doi:10.1007/s10462-007-9052-3

Kressler, F.P., Steinnocher, K.T., 2001. Monitoring urban development using satellite images, in: Proceedings of the Second International Symposium on Remote Sensing of Urban Areas. Regensburg, Germany.

Krizhevsky, A., Sutskever, I., Hinton, G.E., 2012. ImageNet Classification with Deep Convolutional Neural Networks, in: Advances In Neural Information Processing Systems. Sacramento, USA.

Lambin, E.F., Turner, B.L., Geist, H.J., Agbola, S.B., Angelsen, A., Folke, C., Bruce, J.W., Coomes, O.T., Dirzo, R., George, P.S., Homewood, K., Imbernon, J., Leemans, R., Li, X., Moran, E.F., Mortimore, M., Ramakrishnan, P.S., Richards, J.F., Steffen, W., Stone, G.D., Svedin, U., Veldkamp, T.A., 2001. The causes of land-use and land-cover change: moving beyond the myths 11, 261–269. doi:10.1016/S0959-3780(01)00007-3

Lau, K.K.-L., Lindberg, F., Rayner, D., Thorsson, S., 2015. The effect of urban geometry on mean radiant temperature under future climate change: a study of three European cities. Int. J. Biometeorol. 59, 799–814. doi:10.1007/s00484-014-0898-1

Lau, K.K.L., Ren, C., Ho, J., Ng, E., 2016. Numerical modelling of mean radiant temperature in high-density sub-tropical urban environment. Energy Build. 114, 80–86. doi:10.1016/j.enbuild.2015.06.035

Li, C., Wang, J., Wang, L., Hu, L., Gong, P., 2014. Comparison of classification algorithms and training sample sizes in urban land classification with landsat thematic mapper imagery. Remote Sens. 6, 964–983. doi:10.3390/rs6020964

Li, J., Song, C., Cao, L., Zhu, F., Meng, X., Wu, J., 2011. Impacts of landscape structure on surface urban heat islands: A case study of Shanghai, China. Remote Sens. Environ. 115, 3249–3263. doi:10.1016/j.rse.2011.07.008

Li, X., Gong, P., Liang, L., 2015. A 30-year (1984–2013) record of annual urban dynamics of Beijing City derived from Landsat data. Remote Sens. Environ. 166, 78–90. doi:10.1016/j.rse.2015.06.007

Li, Y., Zhang, H., Kainz, W., 2012. Monitoring patterns of urban heat islands of the fast-growing Shanghai metropolis, China: Using time-series of Landsat TM/ETM+ data. Int. J. Appl. Earth Obs. Geoinf. 19, 127–138. doi:10.1016/j.jag.2012.05.001

Liang, S., Fang, H., Chen, M., 2001. Atmospheric correction of Landsat ETM+ land surface imagery-Part I: Methods. IEEE Trans. Geosci. Remote Sens. 39, 2490–2498. doi:10.1109/36.964986

Lindberg, F., CSB, G., Gabey, A., Jarvi, L., Kent, C., Krave, N., Sun, T., Wallenberg, N., Ward, H., 2017. Urban Multi-scale Environmental Predictor (UMEP) Manual [WWW Document]. URL https://umep-docs.readthedocs.io/ (accessed 9.5.18).

Lindberg, F., Grimmond, C.S.B., 2011. Nature of vegetation and building morphology characteristics across a city: Influence on shadow patterns and mean radiant temperatures in London. Urban Ecosyst. 14, 617–634. doi:10.1007/s11252-011-0184-5

Lindberg, F., Grimmond, C.S.B., 2010. Continuous sky view factor maps from high resolution urban digital elevation models. Clim. Res. 42, 177–183. doi:10.3354/cr00882

Lindberg, F., Grimmond, C.S.B., Gabey, A., Huang, B., Kent, C.W., Sun, T., Theeuwes, N.E., Järvi, L., Ward, H.C., Capel-Timms, I., Chang, Y., Jonsson, P., Krave, N., Liu, D., Meyer, D., Olofson, K.F.G., Tan, J., Wästberg, D., Xue, L., Zhang, Z., 2018. Urban Multi-scale Environmental Predictor (UMEP): An integrated tool for city-based climate services. Environ. Model. Softw. 99, 70–87. doi:10.1016/j.envsoft.2017.09.020

Lindberg, F., Grimmond, C.S.B., Martilli, A., 2015a. Sunlit fractions on urban facets - Impact of

spatial resolution and approach. Urban Clim. 12, 65–84. doi:10.1016/j.uclim.2014.11.006

Lindberg, F., Holmer, B., Thorsson, S., 2008. SOLWEIG 1.0 - Modelling spatial variations of 3D radiant fluxes and mean radiant temperature in complex urban settings. Int. J. Biometeorol. 52, 697–713. doi:10.1007/s00484-008-0162-7

Lindberg, F., Jonsson, P., Honjo, T., Wästberg, D., 2015b. Solar energy on building envelopes - 3D modelling in a 2D environment. Sol. Energy 115, 369–378. doi:10.1016/j.solener.2015.03.001

Loughnan, M., Tapper, N., Phan, T., Lynch, K., Mcinnes, J., 2013. A spatial vulnerability analysis of urban populations during extreme heat events in Australian capital cities. National Climate Change Adaptation Research Facility, Southport, QLD, Australia.

Lowe, S.A., 2016. An energy and mortality impact assessment of the urban heat island in the US. Environ. Impact Assess. Rev. 56, 139–144. doi:10.1016/j.eiar.2015.10.004

Lu, D., Li, G., Kuang, W., Moran, E., 2014. Methods to extract impervious surface areas from satellite images. Int. J. Digit. Earth 7, 93–112. doi:10.1080/17538947.2013.866173

Lu, D., Moran, E., Hetrick, S., 2011. Detection of impervious surface change with multitemporal Landsat images in an urban-rural frontier. ISPRS J. Photogramm. Remote Sens. 66, 298–306. doi:10.1016/j.isprsjprs.2010.10.010

Lu, D., Weng, Q., 2006. Use of impervious surface in urban land-use classification. Remote Sens. Environ. 102, 146–160. doi:10.1016/j.rse.2006.02.010

Lu, Y., Nakicenovic, N., Visbeck, M., Stevance, A.-S., 2015. Five priorities for the UN Sustainable Development Goals. Nature 520, 432–433. doi:10.1038/520432a

Luo, J., Du, P., Alim, S., Xiangjian Xie, Xue, Z., 2014. Annual Landsat analysis of urban growth of Nanjing City from 1980 to 2013. 2014 Third Int. Work. Earth Obs. Remote Sens. Appl. 357–361. doi:10.1109/EORSA.2014.6927912

MacLachlan, A., Biggs, E., Roberts, G., Boruff, B., 2017a. Urban Growth Dynamics in Perth, Western Australia: Using Applied Remote Sensing for Sustainable Future Planning. Land 1, 1–14. doi:10.3390/land6010009

MacLachlan, A., Biggs, E., Roberts, G., Boruff, B., 2017b. Classified Earth observation data between 1990 and 2015 for the Perth Metropolitan Region, Western Australia using the Import Vector Machine algorithm. Pangaea. doi:10.1594/PANGAEA.871017

MacLachlan, A., Biggs, E., Roberts, G., Boruff, B., 2017c. Urbanisation-Induced Land Cover Temperature Dynamics for Sustainable Future Urban Heat Island Mitigation. Urban Sci. 1, 1–21. doi:10.3390/urbansci1040038

MacLachlan, A., Roberts, G., Biggs, E., Boruff, B., 2017d. Subpixel land-cover classification for improved urban area estimates using Landsat. Int. J. Remote Sens. 38, 5763–5792. doi:10.1080/01431161.2017.1346403

Maiersperger, T.K., Scaramuzza, P.L., Leigh, L., Shrestha, S., Gallo, K.P., Jenkerson, C.B., Dwyer, J.L., 2013. Characterizing LEDAPS surface reflectance products by comparisons with AERONET, field spectrometer, and MODIS data. Remote Sens. Environ. 136, 1–13. doi:10.1016/j.rse.2013.04.007

Malek, S., Bazi, Y., Alajlan, N., AlHichri, H., Melgani, F., 2014. Efficient framework for palm tree detection in UAV images. IEEE J. Sel. Top. Appl. Earth Obs. Remote Sens. 7, 4692–4703. doi:10.1109/JSTARS.2014.2331425

Marfai, M.A., Sekaranom, A.B., Ward, P., 2014. Community responses and adaptation strategies toward flood hazard in Jakarta, Indonesia. Nat. Hazards 75, 1127–1144. doi:10.1007/s11069-014-1365-3

Masek, J.G., Lindsay, F.E., Goward, S.N., 2000. Dynamics of urban growth in the Washington DC metropolitan area, 1973-1996, from Landsat observations. Int. J. Remote Sens. 21, 3473–3486. doi:10.1080/014311600750037507

Masek, J.G., Vermote, E.F., Saleous, N.E., Wolfe, R., Hall, F.G., Huemmrich, K.F., Gao, F., Kutler, J., Lim, T., 2006. A Landsat Surface Reflectance Dataset. IEEE Geosci. Remote Sens. Lett. 3, 68–72. doi:10.1109/LGRS.2005.857030

Mathieu, P., Aubrecht, C., 2018. Earth Observation Open Science and Innovation. Springer, Frascati, Italy and Washington, DC, USA. doi:10.1007/978-3-319-65633-5

Mayor Bill de Blasio, 2014. Transforming New York City's Buildings for a Low-Carbon Future, One City: Built to Last. New York.

Mayor of London, 2017. The Spatial Development Strategy For Greater London Draft For Public Consultation, The London Plan. London, UK.

Mayor of London, 2016a. The Spatial Development Strategy For London Consolidated With Alterations Since 2011, The London Plan. London, UK.

Mayor of London, 2016b. London's response to Climate change, The London Plan. London, UK.

McPherson, T., 2016. Scientists must have a say in the future of cities. Nature 538, 165–166. doi:10.1038/538165a

Melgani, F., Bruzzone, L., 2004. Classification of hyperspectral remote sensing images with support vector machines. IEEE Trans. Geosci. Remote Sens. 42, 1778–1790. doi:10.1109/TGRS.2004.831865

Michele Acuto, 2018. Global science for city policy. Sci. policy forum 359, 165–166. doi:10.1126/science.aao2728

Michelozzi, P., Accetta, G., De Sario, M., D'Ippoliti, D., Marino, C., Baccini, M., Biggeri, A., Anderson, H.R., Katsouyanni, K., Ballester, F., Bisanti, L., Cadum, E., Forsberg, B., Forastiere, F., Goodman, P.G., Hojs, A., Kirchmayer, U., Medina, S., Paldy, A., Schindler, C., Sunyer, J., Perucci, C.A., 2009. High temperature and hospitalizations for cardiovascular and respiratory causes in 12 european cities. Am. J. Respir. Crit. Care Med. 179, 383–389. doi:10.1164/rccm.200802-217OC

Miller, R.B., Small, C., 2003. Cities from space: Potential applications of remote sensing in urban environmental research and policy. Environ. Sci. Policy 6, 129–137. doi:10.1016/S1462-9011(03)00002-9

Møller-Jensen, L., Kofie, R.Y., Yankson, P.W.K., 2005. Large-area urban growth observations—a hierarchical kernel approach based on image texture. Geogr. Tidsskr. J. Geogr. 105, 39–47. doi:10.1080/00167223.2005.10649538

Mountrakis, G., Im, J., Ogole, C., 2011. Support vector machines in remote sensing: A review. ISPRS J. Photogramm. Remote Sens. 66, 247–259. doi:10.1016/j.isprsjprs.2010.11.001

Myint, S.W., Gober, P., Brazel, A., Grossman-Clarke, S., Weng, Q., 2011. Per-pixel vs. object-based classification of urban land cover extraction using high spatial resolution imagery. Remote Sens. Environ. 115, 1145–1161. doi:10.1016/j.rse.2010.12.017

Myneni, R.B., Keeling, C.D., Tucker, C.J., Asrar, G., Nemani, R.R., 1997. Increased plant growth in the northern high latitudes from 1981 to 1991. Nature 386, 698–702. doi:10.1038/386698a0

Nairn, J.R., Fawcett, R.J.B., 2014. The excess heat factor: A metric for heatwave intensity and its use in classifying heatwave severity. Int. J. Environ. Res. Public Health 12, 227–253. doi:10.3390/ijerph120100227

Oke, T.R., 1982. The energetic basis of the urban heat island. Q. J. R. Meteorol. Soc. 108, 1–24. doi:10.1002/qj.49710845502

Okujeni, A., Linden, S. Van Der, Hostert, P., 2015. Remote Sensing of Environment Extending the vegetation – impervious – soil model using simulated EnMAP data and machine learning. Remote Sens. Environ. 158, 69–80. doi:10.1016/j.rse.2014.11.009

Okujeni, A., van der Linden, S., Jakimow, B., Rabe, A., Verrelst, J., Hostert, P., 2014. A comparison of advanced regression algorithms for quantifying urban land cover. Remote Sens. 6, 6324–6346. doi:10.3390/rs6076324

Okujeni, A., van der Linden, S., Tits, L., Somers, B., Hostert, P., 2013. Support vector regression and synthetically mixed training data for quantifying urban land cover. Remote Sens. Environ. 137, 184–197. doi:10.1016/j.rse.2013.06.007

Orru, H., Andersson, C., Ebi, K.L., Langner, J., Åström, C., Forsberg, B., 2013. Impact of climate change on ozone-related mortality and morbidity in Europe. Eur. Respir. J. 41, 285–294. doi:10.1183/09031936.00210411

Osborn, D., Cutter, A., Ullah, F., 2015. Universal Sustainable Development Goals: Understanding the transformational challenge for developed countries, Universal Sustainable Development Goals. Lund, Sweeden.

Otukei, J.R., Blaschke, T., 2010. Land cover change assessment using decision trees, support vector machines and maximum likelihood classification algorithms. Int. J. Appl. Earth Obs. Geoinf. 12, 27–31. doi:10.1016/j.jag.2009.11.002

Pacifici, F., Chini, M., Emery, W.J., 2009. A neural network approach using multi-scale textural metrics from very high-resolution panchromatic imagery for urban land-use classification. Remote Sens. Environ. 113, 1276–1292. doi:10.1016/j.rse.2009.02.014

Pal, M., 2005. Random forest classifier for remote sensing classification. Int. J. Remote Sens. 26, 217–222. doi:10.1080/01431160412331269698

Pal, M., Mather, P.M., 2005. Support vector machines for classification in remote sensing. Int. J. Remote Sens. 26, 1007–1011. doi:10.1080/01431160512331314083

Pal, M., Mather, P.M., 2003. An assessment of the effectiveness of decision tree methods for land cover classification. Remote Sens. Environ. 86, 554–565. doi:10.1016/S0034-4257(03)00132-9

Pan, J., Wang, M., Li, D., Li, J., 2009. Automatic Generation of Seamline Network Using Area Voronoi Diagrams With Overlap. IEEE Trans. Geosci. Remote Sens. 47, 1737–1744. doi:10.1109/TGRS.2008.2009880

Patel, N.N., Angiuli, E., Gamba, P., Gaughan, A., Lisini, G., Stevens, F.R., Tatem, A.J., Trianni, G., 2015. Multitemporal settlement and population mapping from Landsat using Google Earth Engine. Int. J. Appl. Earth Obs. Geoinf. 35, 199–208. doi:10.1016/j.jag.2014.09.005

Patino, J.E., Duque, J.C., 2013. A review of regional science applications of satellite remote sensing in urban settings. Comput. Environ. Urban Syst. 37, 1–17. doi:10.1016/j.compenvurbsys.2012.06.003

Peng, S., Piao, S., Ciais, P., Friedlingstein, P., Ottle, C., Bréon, F.-M., Nan, H., Zhou, L., Myneni, R.B., 2012. Surface urban heat island across 419 global big cities. Environ. Sci. Technol. 46, 696–703. doi:10.1021/es301245j

Perry, M., Rowe, J.E., 2014. Fly-in, fly-out, drive-in, drive-out: The Australian mining boom and its impacts on the local economy. Local Econ. 30, 139–148. doi:10.1177/0269094214564957

Phinn, S., Stanford, M., Scarth, P., Murray, A.T., Shyy, P.T., 2002. Monitoring the composition of urban environments based on the vegetation-impervious surface-soil (VIS) model by subpixel analysis techniques. Int. J. Remote Sens. 23, 4131–4153. doi:10.1080/01431160110114998

Piao, S., Wang, X., Ciais, P., Zhu, B., Wang, T., Liu, J., 2011. Changes in satellite-derived vegetation growth trend in temperate and boreal Eurasia from 1982 to 2006. Glob. Chang. Biol. 17, 3228–3239. doi:10.1111/j.1365-2486.2011.02419.x

Potere, D., Schneider, A., Angel, S., Civco, D., 2009. Mapping urban areas on a global scale: which of the eight maps now available is more accurate? Int. J. Remote Sens. 30, 6531–6558. doi:10.1080/01431160903121134

Powell, R., Roberts, D., 2010. Characterizing Urban Land-Cover Change in Rondônia, Brazil: 1985 to 2000. J. Lat. Am. Geogr. 9, 183–211. doi:10.1353/lag.2010.0028

Powell, R., Roberts, D., 2008. Characterizing variability of the urban physical environment for a suite of cities in Rondônia, Brazil. Earth Interact. 12, 1–32. doi:10.1175/2008EI246.1

Powell, R., Roberts, D., Dennison, P., Hess, L., 2007. Sub-pixel mapping of urban land cover using multiple endmember spectral mixture analysis: Manaus, Brazil. Remote Sens. Environ. 106, 253–267. doi:10.1016/j.rse.2006.09.005

Poznanska, A., Bayer, S., Bucher, T., 2013. Derivation of urban objects and their attributes for large-scale urban areas based on very high resolution UltraCam true orthophotos and nDSM – a case study Berlin , Germany, in: Proceedings of the SPIE. doi:10.1117/12.2030000

Pravitasari, A.E., Saizen, I., Tsutsumida, N., Rustiadi, E., Pribadi, D.O., 2015. Local Spatially Dependent Driving Forces of Urban Expansion in an Emerging Asian Megacity: The Case of Greater Jakarta (Jabodetabek). J. Sustain. Dev. 8, 108–120. doi:10.5539/jsd.v8n1p108

Qian, Y., Zhou, W., Yan, J., Li, W., Han, L., 2014. Comparing Machine Learning Classifiers for Object-Based Land Cover Classification Using Very High Resolution Imagery. Remote Sens. 7, 153–168. doi:10.3390/rs70100153

Quintano, C., Fernández-Manso, A., Roberts, D.A., 2013. Multiple Endmember Spectral Mixture Analysis (MESMA) to map burn severity levels from Landsat images in Mediterranean countries. Remote Sens. Environ. 136, 76–88. doi:10.1016/j.rse.2013.04.017

Ram, T.D., Wang, G., 2013. Probabilistic seismic hazard analysis in Nepal. Earthq. Eng. Eng. Vib. 12, 577–586.

Revi, A., Satterthwaite, D.E., Aragón-Durand, F., Corfee-Morlot, J., Kiunsi, R., Pelling, M., Roberts, D., Solecki, W., 2014. Climate Change 2014: Impacts, Adaptation, and Vulnerability. Part A: Global and Sectoral Aspects. Contribution of Working Group II to the Fifth Assessment Report of the Intergovernmental Panel on Climate Change, in: Field, C.B., Barros, V.R., D.J., D., Mach, K.J., Mastrandrea, M.D., Bilir, T.E., Chatterjee, M., Ebi, K.L., Estrada, Y.O., Genova, R.C., Girma, B., Kissel, E.S., Levy, A.N., MacCracken, S., Mastrandrea, P.R., White, L.L. (Eds.), Climate Change 2014: Impacts, Adaptation, and Vulnerability. Part A: Global and Sectoral Aspects. Contribution of Working Group II to the Fifth Assessment Report of the Intergovernmental Panel on Climate Change. Cambridge University Press, UK and New York, NY, USA, pp. 535–612.

Richter, R., Kellenberger, T., Kaufmann, H., 2009. Comparison of topographic correction methods. Remote Sens. 1, 184–196. doi:10.3390/rs1030184

Ridd, M.K., 1995. Exploring a V-I-S model for urban ecosystem through remote sensing: a comparative ananomy for cities. Int. J. Remote Sens. 16, 2165–2185. doi:10.1080/01431169508954549

Rigg, J., 1998. Rural-urban interactions, agriculture and wealth: a Southeast Asian perspective. Prog. Hum. Geogr. 22, 497–522. doi:10.1191/030913298667432980

Rinner, C., Hussain, M., 2011. Toronto's urban heat island-exploring the relationship between land use and surface temperature. Remote Sens. 3, 1251–1265. doi:10.3390/rs3061251

Rizwan, A.M., Dennis, L.Y.C., Liu, C., 2008. A review on the generation, determination and mitigation of Urban Heat Island. J. Environ. Sci. 20, 120–128. doi:10.1016/S1001-0742(08)60019-4

Rodriguez-Galiano, V.F., Chica-Olmo, M., Abarca-Hernandez, F., Atkinson, P.M., Jeganathan, C., 2012. Random Forest classification of Mediterranean land cover using multi-seasonal imagery and multi-seasonal texture. Remote Sens. Environ. 121, 93–107. doi:10.1016/j.rse.2011.12.003

Roscher, R., Förstner, W., Waske, B., 2012. I2VM: Incremental import vector machines. Image Vis. Comput. 30, 263–278. doi:10.1016/j.imavis.2012.04.004

Roscher, R., Waske, B., Forstner, W., 2010. Kernel discriminative Random fields for land cover classification, in: APR Workshop on Pattern Recognition in Remote Sensing. Istanbul, Turkey. doi:10.1109/PRRS.2010.5742801

Roy, D.P., Kovalskyy, V., Zhang, H.K., Vermote, E.F., Yan, L., Kumar, S.S., Egorov, A., 2016. Characterization of Landsat-7 to Landsat-8 reflective wavelength and normalized difference vegetation index continuity. Remote Sens. Environ. 185, 57–70. doi:10.1016/j.rse.2015.12.024

Santamouris, M., Cartalis, C., Synnefa, A., Kolokotsa, D., 2015. On the impact of urban heat island and global warming on the power demand and electricity consumption of buildings - A review. Energy Build. 98, 119–124. doi:10.1016/j.enbuild.2014.09.052

Sawaya, K.E., Olmanson, L.G., Heinert, N.J., Brezonik, P.L., Bauer, M.E., 2003. Extending satellite remote sensing to local scales: Land and water resource monitoring using high-resolution imagery. Remote Sens. Environ. 88, 144–156. doi:10.1016/j.rse.2003.04.006

Schäfer, P., Pflugmacher, D., Hostert, P., Leser, U., 2018. Classifying land cover from satellite images using time series analytics, in: CEUR Workshop Proceedings. Montreal, Canada.

Schneider, A., 2012. Monitoring land cover change in urban and peri-urban areas using dense time stacks of Landsat satellite data and a data mining approach. Remote Sens. Environ. 124, 689–704. doi:10.1016/j.rse.2012.06.006

Schneider, A., Friedl, M., Potere, D., 2010. Mapping global urban areas using MODIS 500-m data: New methods and datasets based on "urban ecoregions." Remote Sens. Environ. 114, 1733–

1746. doi:10.1016/j.rse.2010.03.003

Schneider, A., Friedl, M.A., Potere, D., 2009. A new map of global urban extent from MODIS satellite data. Environ. Res. Lett. 4, 1–11. doi:10.1088/1748-9326/4/4/044003

Schneider, A., Mertes, C.M., 2014. Expansion and growth in Chinese cities, 1978–2010. Environ. Res. Lett. 9, 024008. doi:10.1088/1748-9326/9/2/024008

Schneider, A., Seto, K., Webster, D., 2005. Urban growth in Chengdu, western China: Application of remote sensing to assess planning and policy outcomes. Environ. Plan. B Plan. Des. 32, 323–345. doi:10.1068/b31142

Schwarz, N., Schlink, U., Franck, U., Großmann, K., 2012. Relationship of land surface and air temperatures and its implications for quantifying urban heat island indicators - An application for the city of Leipzig (Germany). Ecol. Indic. 18, 693–704. doi:10.1016/j.ecolind.2012.01.001

Seto, K., Fragkias, M., Guneralp, B., Reilly, M., 2011. A next-generation approach to the characterization of a non-model plant transcriptome. PLoS One 6, 1–9. doi:10.1371/ journal.pone.0023777

Seto, K.C., Güneralp, B., Hutyra, L.R., 2012. Global forecasts of urban expansion to 2030 and direct impacts on biodiversity and carbon pools. Proc. Natl. Acad. Sci. U. S. A. 109, 16083–8. doi:10.1073/pnas.1211658109

Sexton, J.O., Song, X.-P., Huang, C., Channan, S., Baker, M.E., Townshend, J.R., 2013. Urban growth of the Washington, D.C.–Baltimore, MD metropolitan region from 1984 to 2010 by annual, Landsat-based estimates of impervious cover. Remote Sens. Environ. 129, 42–53. doi:10.1016/j.rse.2012.10.025

Shaddick, G., Thomas, M.L., Green, A., Brauer, M., van Donkelaar, A., Burnett, R., Chang, H.H., Cohen, A., Dingenen, R. Van, Dora, C., Gumy, S., Liu, Y., Martin, R., Waller, L.A., West, J., Zidek, J. V., Prüss-Ustün, A., 2018. Data integration model for air quality: a hierarchical approach to the global estimation of exposures to ambient air pollution. J. R. Stat. Soc. Ser. C Appl. Stat. 67, 231–253. doi:10.1111/rssc.12227

Shalaby, A., Tateishi, R., 2007. Remote sensing and GIS for mapping and monitoring land cover and land-use changes in the Northwestern coastal zone of Egypt. Appl. Geogr. 27, 28–41. doi:10.1016/j.apgeog.2006.09.004

Sharifi, E., Lehmann, S., 2014. Comparative Analysis of Surface Urban Heat Island Effect in Central

Sydney. J. Sustain. Dev. 7, 23–34. doi:10.5539/jsd.v7n3p23

Shastri, H., Barik, B., Ghosh, S., Venkataraman, C., Sadavarte, P., 2017. Flip flop of Day-night and Summer-Winter Surface Urban Heat Island Intensity in India. Sci. Rep. 7, 1–8. doi:10.1038/srep40178

Shen, H., Huang, L., Zhang, L., Wu, P., Zeng, C., 2016. Long-term and fine-scale satellite monitoring of the urban heat island effect by the fusion of multi-temporal and multi-sensor remote sensed data: A 26-year case study of the city of Wuhan in China. Remote Sens. Environ. 172, 109–125. doi:10.1016/j.rse.2015.11.005

Sheng, L., Lu, D., Huang, J., 2015. Impacts of land-cover types on an urban heat island in Hangzhou, China. Int. J. Remote Sens. 36, 1584–1603. doi:10.1080/01431161.2015.1019016

Smargiassi, A., Goldberg, M.S., Plante, C., Fournier, M., Baudouin, Y., Kosatsky, T., 2009. Variation of daily warm season mortality as a function of micro-urban heat islands. J. Epidemiol. Community Health 63, 659–664. doi:10.1136/jech.2008.078147

Smith, S.W., 2003. The Scientist and Engineer's Guide to Digital Signal Processing; Chapter 15 - Moving Average Filters, Digital Signal Processing. California Technical Publishing, San Diego, USA.

Snyder, W.C., Wan, Z., Zhang, Y., Feng, Y.-Z., 1998. Classification-based emissivity for land surface temperature measurement from space. Int. J. Remote Sens. 19, 2753–2774. doi:10.1080/014311698214497

Sobrino, J.A., Jiménez-Muñoz, J.C., Paolini, L., 2004. Land surface temperature retrieval from LANDSAT TM 5. Remote Sens. Environ. 90, 434–440. doi:10.1016/j.rse.2004.02.003

Song, X.-P., Sexton, J.O., Huang, C., Channan, S., Townshend, J.R., 2016. Characterizing the magnitude, timing and duration of urban growth from time series of Landsat-based estimates of impervious cover. Remote Sens. Environ. 175, 1–13. doi:10.1016/j.rse.2015.12.027

Stathakis, D., Perakis, K., Savin, I., 2012. Efficient segmentation of urban areas by the VIBI. Int. J. Remote Sens. 33, 6361–6377. doi:10.1080/01431161.2012.687842

Suarez-Rubio, M., Lookingbill, T.R., Elmore, A.J., 2012. Exurban development derived from Landsat from 1986 to 2009 surrounding the District of Columbia, USA. Remote Sens. Environ. 124, 360–370. doi:10.1016/j.rse.2012.03.029

Suess, S., van der Linden, S., Leitao, P.J., Okujeni, A., Waske, B., Hostert, P., 2014. Import Vector Machines for Quantitative Analysis of Hyperspectral Data. Geosci. Remote Sens. Lett. IEEE 11, 449–453. doi:10.1109/LGRS.2013.2265102

Sun, C., Wu, Z., Lv, Z., Yao, N., Wei, J., 2013. Quantifying different types of urban growth and the change dynamic in Guangzhou using multi-temporal remote sensing data. Int. J. Appl. Earth Obs. Geoinf. 21, 409–417. doi:10.1016/j.jag.2011.12.012

Sun, G., Chen, X., Jia, X., Yao, Y., Wang, Z., 2015. Combinational Build-Up Index (CBI) for Effective Impervious Surface Mapping in Urban Areas. IEEE J. Sel. Top. Appl. Earth Obs. Remote Sens. 1–12. doi:10.1109/JSTARS.2015.2478914

Sundarakumar, K., Harika, M., Begum, S.K.A., Yamini, S., Balakrishna, K., 2012. Land Use And Land Cover Change Detection And Urban Sprawl Analysis Of Vijayawada City Using Multitemporal Landsat. Int. J. Eng. Sci. Technol. 4, 170–178.

Suryahadi, A., Sumarto, S., 2003. Poverty and Vulnerability in Indonesia before and after the Economic Crisis. Asian Econ. J. 17, 45–64. doi:10.1111/1351-3958.00161

Szyszkowicz, M., Rowe, B.H., 2016. Respiratory Health Conditions and Ambient Ozone : A Case-Crossover Study Insights in Chest Diseases. iMedPub Journals 1, 155–161. doi:10.4137/EHI.S40493

Tan, J., Zheng, Y., Tang, X., Guo, C., Li, L., Song, G., Zhen, X., Yuan, D., Kalkstein, A.J., Li, F., Chen, H., 2010. The urban heat island and its impact on heat waves and human health in Shanghai. Int. J. Biometeorol. 54, 75–84. doi:10.1007/s00484-009-0256-x

Tan, K.C., Lim, H.S., MatJafri, M.Z., Abdullah, K., 2009. Landsat data to evaluate urban expansion and determine land use/land cover changes in Penang Island, Malaysia. Environ. Earth Sci. 60, 1509–1521. doi:10.1007/s12665-009-0286-z

Tang, J.X., Deng, C.W., Huang, G.B., Zhao, B.J., 2015. Compressed-Domain Ship Detection on Spaceborne Optical Image Using Deep Neural Network and Extreme Learning Machine. Ieee Trans. Geosci. Remote Sens. 53, 1174–1185. doi:10.1109/tgrs.2014.2335751

Tao, C., Tan, Y., Cai, H., Tian, J., 2011. Airport detection from large IKONOS images using clustered sift keypoints and region information. IEEE Geosci. Remote Sens. Lett. 8, 128–132. doi:10.1109/LGRS.2010.2051792

Taylor, M.S., Wheeler, B.W., White, M.P., Economou, T., Osborne, N.J., 2016. Urban street tree density and antidepressant prescription rates; A cross - sectional study in London, UK.

Landsc. Urban Plan. 136, 174–179. doi:10.1016/j.landurbplan.2014.12.005

The State of Indiana, 2017. 2016-2017 Strategic Plan Update for the Indiana Geographic Information Office, Indiana Geographic Information Office. Indiana, USA.

Thompson, R.J., 2015. A model for the creation and progressive improvement of a digital cadastral data base. Land use policy 49, 565–576. doi:10.1016/j.landusepol.2014.12.016

Tomlinson, C.J., Chapman, L., Thornes, J.E., Baker, C.J., 2012. Derivation of Birmingham's summer surface urban heat island from MODIS satellite images. Int. J. Climatol. 32, 214–224. doi:10.1002/joc.2261

Tomlinson, C.J., Chapman, L., Thornes, J.E., Baker, C.J., 2011. Including the urban heat island in spatial heat health risk assessment strategies: a case study for Birmingham, UK. Int. J. Health Geogr. 10, 1–14. doi:10.1186/1476-072X-10-42

Tran, H., Uchihama, D., Ochi, S., Yasuoka, Y., 2006. Assessment with satellite data of the urban heat island effects in Asian mega cities. Int. J. Appl. Earth Obs. Geoinf. 8, 34–48. doi:10.1016/j.jag.2005.05.003

Turner, B., Lambin, E., Reenberg, A., 2010. The emergence of land change science for global environmental change and sustainability. PNAS 103, 13070–13075. doi:10.1073/pnas.0704119104

U.S. Census Bureau, 2018. United States Census Geography, United States Census Bureau. New York, NY, USA.

U.S. Department of Commerce, 2013. 2013 Housing Profile: United States, U.S. Department of Housing and Uban Development. Washington, USA.

UN-Habitat, 2016. City Prosperity Initiative Steps, City Prosperity Initiative. Nairobi, Kenya.

UN-Habitat III, 2017. New Urban Agenda, Conference on Housing and Sustainable Urban Development (Habitat III). Nairobi, Kenya.

UNISDR, 2015. Sendai Framework for Disaster Risk Reduction 2015 - 2030, in: Third World Conference on Disaster Risk Reduction, Sendai, Japan, 14-18 March 2015. Sendia, Japan.

United Nations, Department of Economic and Social Affairs, P.D., 2014. World Urbanization Prospects: The 2014 Revision, Highlights (ST/ESA/SER.A/352). New York, NY, USA. doi:10.4054/DemRes.2005.12.9

United Nations, 2018. World Urbanization Prospects: The 2018 Revision, Key Facts, United Nations Department of Economic and Social Affairs Population Division. New York, NY, USA.

United Nations, 2016. The World's Cities in 2016: Data Booklet., Economic and social affair. New York, NY, USA.

United Nations Sustainable Development Goals, 2018a. Tier Classification for Global SDG Indicators, United Nations. New York, NY, USA.

United Nations Sustainable Development Goals, 2018b. Target 11.3: By 2030, enhance inclusive and sustainable urbanization and capacity for participatory, integrated and sustainable human settlement planning and management in all countries, metadata, United Nations. New York, NY, USA.

United Nations Sustainable Development Goals, 2018c. Work Plans for Tier III Indicators; 11.7, United Nations. New York, NY, USA.

United Nations Sustainable Development Goals, 2018d. Target 11.6: By 2030, reduce the adverse per capita environmental impact of cities, including by paying special attention to air quality and municipal and other waste management, United Nations. New York, NY, USA.

Uppala, S.M., Kållberg, P.W., Simmons, A.J., Andrae, U., da Costa Bechtold, V., Fiorino, M., Gibson, J.K., Haseler, J., Hernandez, A., Kelly, G.A., Li, X., Onogi, K., Saarinen, S., Sokka, N., Allan, R.P., Andersson, E., Arpe, K., Balmaseda, M.A., Beljaars, A.C.M., van de Berg, L., Bidlot, J., Bormann, N., Caires, S., Chevallier, F., Dethof, A., Dragosavac, M., Fisher, M., Fuentes, M., Hagemann, S., Hólm, E., Hoskins, B.J., Isaksen, L., Janssen, P.A.E.M., Jenne, R., McNally, A.P., Mahfouf, J.F., Morcrette, J.J., Rayner, N.A., Saunders, R.W., Simon, P., Sterl, A., Trenberth, K.E., Untch, A., Vasiljevic, D., Viterbo, P., Woollen, J., 2005. The ERA-40 re-analysis. Q. J. R. Meteorol. Soc. 131, 2961–3012. doi:10.1256/qj.04.176

USA Environment Protection Agency, 2008. Reducing Urban Heat Islands Compendium of Strategies Urban Heat Island Basics, US EPA. U.S. Environmental Protection Agency, Washington, USA.

USA Environmental Protection Agency, 2013. Reducing Urban Heat Islands Compendium of Strategies Heat Island Reduction Activities, US EPA. Washington, USA.

USGS, 2015. Product Guide Provisional Landsat 8 Surface Reflectance Product, Department of the Interior U.S. Geological Survey. Virginia, USA.

Van de Voorde, T., Jacquet, W., Canters, F., 2011. Mapping form and function in urban areas: An

approach based on urban metrics and continuous impervious surface data. Landsc. Urban Plan. 102, 143–155. doi:10.1016/j.landurbplan.2011.03.017

Van Donkelaar, A., Martin, R. V., Brauer, M., Hsu, N.C., Kahn, R.A., Levy, R.C., Lyapustin, A., Sayer, A.M., Winker, D.M., 2016. Global Estimates of Fine Particulate Matter using a Combined Geophysical-Statistical Method with Information from Satellites, Models, and Monitors. Environ. Sci. Technol. 50, 3762–3772. doi:10.1021/acs.est.5b05833

Vapnik, V., Chervonenkis, A., 1971. On the uniform convergence of relative frequencies of events to their probabilities. Theory Probab. Its Appl. XVI, 264–280. doi:10.1007/978-3-319-21852-6_3

Varshney, A., Rajesh, E., 2014. A Comparative Study of Built-up Index Approaches for Automated Extraction of Built-up Regions From Remote Sensing Data. J. Indian Soc. Remote Sens. 42, 1–5. doi:10.1007/s12524-013-0333-9

Verburg, P.H., Crossman, N., Ellis, E.C., Heinimann, A., Hostert, P., Mertz, O., Nagendra, H., Sikor, T., Erb, K., Golubiewski, N., Grau, R., Grove, M., Konaté, S., Meyfroidt, P., Parker, D.C., Roy, R., Shibata, H., Thomson, A., Zhen, L., 2015. Anthropocene Land system science and sustainable development of the earth system: A global land project perspective. Anthropocene 12, 29–41. doi:10.1016/j.ancene.2015.09.004

Vermote, E., Tanre, D., Deuze, J.L., Herman, M., Morcrette, J.J., 1997. Second Simulation of the Satellite Signal in the Solar Spectrum (6S). 6S User Guide Version 2. Appendix III: Description of the subroutines. Maryland, USA.

Vitousek, P., Mooney, H., Lubchenco, J., Melillo, J., 1997. Human Domination of Earth Ecosystems. Science (80-.). 277, 494–498. doi:10.1126/science.277.5325.494

Voogt, J., 2004. Urban heat islands: hotter cities [WWW Document]. Am. Inst. Biol. Sci. URL http://www.actionbioscience.org/environment/voogt.html (accessed 9.3.18).

Voogt, J. a., Oke, T.R., 2003. Thermal remote sensing of urban climates. Remote Sens. Environ. 86, 370–384. doi:10.1016/S0034-4257(03)00079-8

Wan, Z., 2013. New refinements and validation of the collection-6 MODIS land-surface temperature/emissivity product. Remote Sens. Environ. 140, 36–45. doi:10.1016/j.rse.2013.08.027

Wan, Z., 2006. MODIS Land Surface Temperature Products Users' Guide. ICESS, University of California, Santa Barbara, USA.

Wan, Z., Dozier, J., 1996. A Generalized Split-Window Algorithm for Retrieving Land-Surface Temperature from Space. IEEE Trans. Geosci. Remote Sens. 34, 892–905.

Wan, Z., Zhang, Y., Zhang, Q., Li, Z. liang, 2002. Validation of the land-surface temperature products retrieved from terra moderate resolution imaging spectroradiometer data. Remote Sens. Environ. 83, 163–180. doi:10.1016/S0034-4257(02)00093-7

Wang, J., Huang, B., Fu, D., Atkinson, P., 2015. Spatiotemporal Variation in Surface Urban Heat Island Intensity and Associated Determinants across Major Chinese Cities. Remote Sens. 7, 3670–3689. doi:10.3390/rs70403670

Wang, L., Liu, D., Wang, Q., Wang, Y., 2013. Spectral Unmixing Model Based on Least Squares Support Vector Machine With Unmixing Residue Constraints 10, 1592–1596. doi:10.1109/LGRS.2013.2262371

Wanner, W., Li, X., Strahler, a. H., 1995. On the derivation of kernels for kernel-driven models of bidirectional reflectance. J. Geophys. Res. 100, 21,077-21,089. doi:10.1029/95JD02371

Watanachaturaporn, P., Arora, M.K., Varshney, P.K., 2008. Multisource classification using support vector machines: An empirical comparison with decision tree and neural network classifiers. Photogramm. Eng. Remote Sensing 74, 239–246. doi:10.14358/PERS.74.2.239

Watson, I.D., Johnson, G.T., 1987. Graphical estimation of sky view-factors in urban environments. J. Climatol. 7, 193–197. doi:10.1002/joc.3370070210

Weedon, G.P., Balsamo, G., Bellouin, N., Gomes, S., Best, M.J., Viterbo, P., 2014. Data methodology applied to ERA-Interim reanalysis data. Water Resour. Res. 50, 7505–7514. doi:10.1002/2014WR015638

Weedon, G.P., Gomes, S., Adam, J.C., Bellouin, N., Viterbo, P., Bellouin, N., Boucher, O., Best, M., 2010. The Watch Forcing Data 1958-2001: a Meteorological Forcing Dataset for Land Surface-and Hydrological-Models, WATCH Technical Report. Oxford, UK.

Weedon, G.P., Gomes, S., Viterbo, P., Shuttleworth, W.J., Blyth, E., Österle, H., Adam, J.C., Bellouin, N., Boucher, O., Best, M., 2011. Creation of the WATCH Forcing Data and Its Use to Assess Global and Regional Reference Crop Evaporation over Land during the Twentieth Century. J. Hydrometeorol. 12, 823–848. doi:10.1175/2011JHM1369.1

Weeks, J., 2010. Defining Urban Areas, in: Rashed, T., Jürgens, C. (Eds.), Remote Sensing of Urban and S Areas. Springer, Austin, USA and Bochum, Germany.

Weng, F., Pu, R., 2013. Mapping and assessing of urban impervious areas using multiple endmember spectral mixture analysis: a case study in the city of Tampa, Florida. Geocarto Int. 28, 594–615. doi:10.1080/10106049.2013.764355

Weng, Q., 2001. Modeling urban growth effects on surface runoff with the integration of remote sensing and GIS. Environ. Manage. 28, 737–748. doi:10.1007/s002670010258

Weng, Q., Lu, D., Schubring, J., 2004. Estimation of land surface temperature-vegetation abundance relationship for urban heat island studies. Remote Sens. Environ. 89, 467–483. doi:10.1016/j.rse.2003.11.005

Western Australian Planning Commission, 2016a. Western Australian Planning Commission Urban Growth Monitor: Perth Metropolitan, Peel and Greater Bunbury Regions 2016, The Government of Western Australia Department of Planning. Perth, WA, Australia.

Western Australian Planning Commission, 2016b. Draft State Planning Policy 1, State Planning Framework (Variation No. 3), The Government of Western Australia Department of Planning. Perth, WA, Australia.

Western Australian Planning Commission, 2015a. Perth and Peel @ 3.5 million, The Government of Western Australia Department of Planning. Perth, WA, Australia.

Western Australian Planning Commission, 2015b. Central Sub-regional Planning Framework, The Government of Western Australia Department of Planning. Perth, WA, Australia.

Western Australian Planning Commission, 2015c. North-West Sub-regional Planning Framework, The Government of Western Australia Department of Planning. Perth, WA, Australia.

Western Australian Planning Commission, 2015d. North-East Sub-regional Planning Framework, The Government of Western Australia Department of Planning. Perth, WA, Australia.

Western Australian Planning Commission, 2015e. South Metropolitan Peel Planning Framework, The Government of Western Australia Department of Planning. Perth, WA, Australia.

Western Australian Planning Commission, 2014. Delivering Directions 2031 Report Card 2014, The Government of Western Australia Department of Planning. Perth, WA, Australia.

Western Australian Planning Commission, 2013a. The Housing We'd Choose: A study for Perth and Peel, The Government of Western Australia Department of Housing and Department of Planning. Perth,WA, Australia.

Western Australian Planning Commission, 2013b. The Housing We'd Choose: A study for Perth

and Peel summary report, The Government of Western Australia Department of Planning and Housing. Perth, WA, Australia.

Western Australian Planning Commission, 2012. Urban Growth Monitor: Perth Metropolitan, Peel and Greater Bunbury Regions 2012, The Government of Western Australia Department of Planning. Perth, WA, Australia.

Western Australian Planning Commission, 2010a. Directions 2031 and beyond: metropolitan planning beyond the horizon, The Government of Western Australia Department of Planning. Perth, WA, Australia.

Western Australian Planning Commission, 2010b. Urban Growth Monitor: Perth Metropolitan, Peel and Greater Bunbury Regions 2010, The Government of Western Australia Department of Planning. Perth, WA, Australia.

Western Australian Planning Commission, 2010c. Development Control Policy 1.9, The Government of Western Australia Department of Planning. Perth, WA, Australia.

Western Australian Planning Commission, 2009. Urban Growth Monitor: Perth Metropolitan, Peel and Greater Bunbury Regions 2009, The Government of Western Australia Department of Planning. Perth, WA, Australia.

Wilson, E.H., Hurd, J.D., Civco, D.L., Prisloe, M.P., Arnold, C., 2003. Development of a geospatial model to quantify, describe and map urban growth. Remote Sens. Environ. 86, 275–285. doi:10.1016/S0034-4257(03)00074-9

Wong, K. V., Paddon, A., Jimenez, A., 2013. Review of World Urban Heat Islands: Many Linked to Increased Mortality. J. Energy Resour. Technol. 135, 1–11. doi:10.1115/1.4023176

Wu, C., Murray, A.T., 2003. Estimating impervious surface distribution by spectral mixture analysis. Remote Sens. Environ. 84, 493–505. doi:10.1016/S0034-4257(02)00136-0

Xian, G., Homer, C., Bunde, B., Danielson, P., Dewitz, J., Fry, J., Pu, R., 2012. Quantifying urban land cover change between 2001 and 2006 in the Gulf of Mexico region. Geocarto Int. 27, 479–497. doi:10.1080/10106049.2011.652675

Xie, Q., Zhou, Z., 2015. Impact Of Urbanization On Urban Heat Island Effect Based On TM Imagery In Wuhan, China. Environ. Eng. Manag. J. 14, 647–655.

Xie, Q., Zhou, Z., Teng, M., Wang, P., 2012. A multi-temporal Landsat TM data analysis of the impact of land use and land cover changes on the urban heat island effect. J. Food, Agric.

Environ. 10, 803–809. doi:10.1504/IJEP.2014.067693

Xu, D., Chen, R., 2017. Comparison of urban heat island and urban reflection in Nanjing City of China. Sustain. Cities Soc. 31, 26–36. doi:10.1016/j.scs.2017.01.017

Xu, H., 2008. A new index for delineating built-up land features in satellite imagery. Int. J. Remote Sens. 29, 4269–4276. doi:10.1080/01431160802039957

Yang, J., Wang, Z.-H., Kaloush, K.E., 2015. Environmental impacts of reflective materials: Is high albedo a 'silver bullet' for mitigating urban heat island? Renew. Sustain. Energy Rev. 47, 830–843. doi:10.1016/j.rser.2015.03.092

Yang, X., Lo, C.P., 2000. Relative radiometric normalization performance for change detection from multi-date satellite images. Photogramm. Eng. Remote Sensing 66, 967–980.

Yu, W., Vaneckova, P., Mengersen, K., Pan, X., Tong, S., 2010. Is the association between temperature and mortality modified by age, gender and socio-economic status? Sci. Total Environ. 408, 3513–3518. doi:10.1016/j.scitotenv.2010.04.058

Yuan, F., Bauer, M.E., 2007. Comparison of impervious surface area and normalized difference vegetation index as indicators of surface urban heat island effects in Landsat imagery. Remote Sens. Environ. 106, 375–386. doi:10.1016/j.rse.2006.09.003

Yuan, F., Sawaya, K.E., Loeffelholz, B.C., Bauer, M.E., 2005. Land cover classification and change analysis of the Twin Cities (Minnesota) Metropolitan Area by multitemporal Landsat remote sensing. Remote Sens. Environ. 98, 317–328. doi:10.1016/j.rse.2005.08.006

Zha, Y., Gao, J., Ni, S., 2003. Use of normalized difference built-up index in automatically mapping urban areas from TM imagery. Int. J. Remote Sens. 24, 583–594. doi:10.1080/01431160304987

Zhang, H., Qi, Z.F., Ye, X.Y., Cai, Y. Bin, Ma, W.C., Chen, M.N., 2013. Analysis of land use/land cover change, population shift, and their effects on spatiotemporal patterns of urban heat islands in metropolitan Shanghai, China. Appl. Geogr. 44, 121–133. doi:10.1016/j.apgeog.2013.07.021

Zhang, P., Imhoff, M.L., Bounoua, L., Wolfe, R.E., 2012. Exploring the influence of impervious surface density and shape on urban heat islands in the northeast United States using MODIS and Landsat. Can. J. Remote Sens. 38, 441–451. doi:10.5589/m12-036

Zhao, G., Dong, J., Liu, J., Zhai, J., Cui, Y., He, T., Xiao, X., 2017. Different Patterns in Daytime and

Nighttime Thermal Effects of Urbanization in Beijing-Tianjin-Hebei Urban Agglomeration. Remote Sens. 9, 1–15. doi:10.3390/rs9020121

Zhao, S., Zhou, D., Liu, S., 2016. Data concurrency is required for estimating urban heat island intensity. Environ. Pollut. 208, 118–124. doi:10.1016/j.envpol.2015.07.037

Zhou, D., Zhang, L., Hao, L., Sun, G., Liu, Y., Zhu, C., 2016. Spatiotemporal trends of urban heat island effect along the urban development intensity gradient in China. Sci. Total Environ. 544, 617–626. doi:10.1016/j.scitotenv.2015.11.168

Zhou, D., Zhao, S., Liu, S., Zhang, L., Zhu, C., 2014. Surface urban heat island in China's 32 major cities: Spatial patterns and drivers. Remote Sens. Environ. 152, 51–61. doi:10.1016/j.rse.2014.05.017

Zhou, D., Zhao, S., Zhang, L., Sun, G., Liu, Y., 2015. The footprint of urban heat island effect in China. Nat. Sci. reports 5, 1–11. doi:10.1038/srep11160

Zhou, W., Troy, a., 2008. An object-oriented approach for analysing and characterizing urban landscape at the parcel level. Int. J. Remote Sens. 29, 3119–3135. doi:10.1080/01431160701469065

Zhu, G., Blumberg, D.G., 2002. Classification using ASTER data and SVM algorithms; Remote Sens. Environ. 80, 233–240. doi:10.1016/S0034-4257(01)00305-4

Zhu, J., Hastie, T., 2005. Kernel Logistic Regression and the Import Vector Machine. J. Comput. Graph. Stat. 14, 185–205. doi:10.1198/106186005X25619

Zhu, X.X., Tuia, D., Mou, L., Xia, G.S., Zhang, L., Xu, F., Fraundorfer, F., 2017. Deep Learning in Remote Sensing: A Comprehensive Review and List of Resources. IEEE Geosci. Remote Sens. Mag. 5, 8–36. doi:10.1109/MGRS.2017.2762307

Zhu, Z., Woodcock, C.E., 2014. Continuous change detection and classification of land cover using all available Landsat data. Remote Sens. Environ. 144, 152–171. doi:10.1016/j.rse.2014.01.011

Zhu, Z., Woodcock, C.E., Rogan, J., Kellndorfer, J., 2012. Assessment of spectral, polarimetric, temporal, and spatial dimensions for urban and peri-urban land cover classification using Landsat and SAR data. Remote Sens. Environ. 117, 72–82. doi:10.1016/j.rse.2011.07.020